University of Reading

The Role of Post-Tropical Cyclones for European Extreme Weather

---

Elliott M. Sainsbury

A thesis submitted in fulfilment of the requirements for the degree of Doctor of Philosophy

PhD Atmosphere, Oceans and Climate

Department of Meteorology

School of Mathematical, Physical and Computational Sciences

September 2022

University of Reading

Declaration

I confirm that this is my own work and the use of all material from other sources has been properly and fully acknowledged.

Elliott M. Sainsbury

Abstract

Post-tropical cyclones (PTCs) can bring extreme winds and heavy precipitation to Europe. This thesis aims to further our understanding of the hazards posed to Europe by PTCs, and the factors (environmental and cyclone-specific) governing their development, variability, and projected changes.

It is shown that PTCs are disproportionately responsible for windstorm risk over Europe: Despite comprising less than 1% of the cyclones impacting Northern Europe during the North Atlantic hurricane season, approximately 9% of the cyclones impacting the region during the hurricane season with storm-force (>25 m s^{-1}) winds are PTCs.

The interannual variability of recurving North Atlantic tropical cyclones (TCs) – defined as TCs which reach the North Atlantic midlatitudes – is shown to be governed by TC activity in the Main Development Region and subtropical North Atlantic, with interannual variability in the seasonal mean steering flow playing a smaller, secondary role. PTCs which are stronger at their TC lifetime maximum intensity, or which reintensify after ET, are shown to be significantly more likely to reach Europe. Europe-impacting PTCs interact more strongly with an upstream trough in a more baroclinic environment and often reintensify upon crossing a midlatitude jet streak.

Future projections of PTCs in five CMIP6 models are shown to capture many of the observed features of the TC and PTC climatologies in the North Atlantic, and the disproportionate risk associated with Europe-impacting PTCs. No robust 21st century change in Europe-impacting PTC frequency or intensity is found in these models, because two competing factors – a decrease in North Atlantic TC frequency, and an increase in the fraction of TCs reaching Europe – are of the same magnitude. This thesis provides a framework to understand the European PTC climatology and provides evidence of an uncertain future for European PTC risk.

Acknowledgements

Firstly, I would like to thank all of my supervisors: Reinhard Schiemann, Kevin Hodges, Alexander Baker, Len Shaffrey, and Kieran Bhatia. I am extremely thankful for all of the time and guidance that you have given me throughout this project. I am extremely fortunate to have had the opportunity to work with such a fantastic set of mentors. I have learned a great deal from you all and have grown as a scientist as a result.

Thanks also to Ted Shepherd and Oscar-Martinez Alvarado for fruitful discussions and interesting suggestions during my monitoring committee meetings, which helped to steer the project. I am also grateful to Oliver Jones and Matthew Linham at BP for giving me the opportunity to explore the applications of this project. Thank you to my colleagues in Lyle 5 for creating such a friendly and welcoming environment. Also, to the Department of Meteorology in Reading more broadly, for inspiring my passion for meteorology and climate science during my degree, which ultimately led me down the path of research.

Finally, I am most grateful for Aimee and the rest of my family, for always encouraging me to explore my passions and always believing in me.

Authorship of Papers

The framework of this thesis is provided by four lead-author papers. They have been reformatted for inclusion into this thesis, and common sources of data and methodology have been compiled into chapter 2 and repetition removed from the manuscripts. The results are unmodified from the submitted/accepted manuscripts. The first three papers (chapters 3, 4, and 5) have been published in full. The fourth paper (chapter 6) is under review with *Weather and Climate Dynamics*. The candidate's (Elliott M. Sainsbury) estimated contribution for each paper is outlined below.

Sainsbury, E. M., R. K. H. Schiemann, K. I. Hodges, L. C. Shaffrey, A. J. Baker, and K. T. Bhatia, 2020: How Important Are Post-Tropical Cyclones for European Windstorm Risk? *Geophys. Res. Lett.*, **47**, https://doi.org/10.1029/2020GL089853.

Estimated contributions: 85%. E.S. performed all analysis and wrote the manuscript, with input and suggestions from R.S., K.H., A.B., L.S., and K.B. at all stages of the analysis and writing process. Figure 1 of the manuscript is adapted from Figure 1b in Baker et al. (2021). Rein Haarsma and an anonymous reviewer provided comments on an earlier version of this manuscript.

Sainsbury, E. M., R. K. H. Schiemann, K. I. Hodges, A. J. Baker, L. C. Shaffrey, and K. T. Bhatia, 2022b: What Governs the Interannual Variability of Recurving North Atlantic Tropical Cyclones? *J. Clim.*, **35(12)**, 3627–3641, https://doi.org/10.1175/jcli-d-21-0712.1.

Estimated contributions: 85%. E.S. performed all analysis and wrote the manuscript, with input and suggestions from R.S., K.H., A.B., L.S., and K.B. at all stages of the

analysis and writing process. Baoqiang Xiang and two anonymous reviewers provided comments on an earlier version of this manuscript.

Sainsbury, E. M., R. K. H. Schiemann, K. I. Hodges, A. J. Baker, L. C. Shaffrey, and K. T. Bhatia, 2022a: Why do some Post-Tropical Cyclones impact Europe? *Mon. Weather Rev.*, accepted for publication.

Estimated contributions: 85%. E.S. performed all analysis and wrote the manuscript, with input and suggestions from R.S., K.H., A.B., L.S., and K.B. at all stages of the analysis and writing process. Ron McTaggart-Cowan, Rachel Mauk, and two anonymous reviewers provided comments on an earlier version of this manuscript.

Sainsbury, E. M., R. K. H. Schiemann, K. I. Hodges, A. J. Baker, L. C. Shaffrey, K. T. Bhatia, and S. Bourdin, 2022c: Can low-resolution CMIP6 ScenarioMIP models provide insight into future European Post-Tropical Cyclone risk? *Weather Clim. Dyn.*, https://doi.org/https://doi.org/10.5194/wcd-2022-46, accepted for publication.

Estimated contributions: 85%. E.S. performed all analysis and wrote the manuscript, with input and suggestions from R.S., K.H., A.B., L.S., and K.B. at all stages of the analysis and writing process. S.B., Michiel Baatsen, and an anonymous reviewer provided comments on an earlier version of this manuscript.

Table of Contents

List of Acronyms

Acronym	Description
ASO	August, September, October
CMIP6	Coupled Model Intercomparison Project phase 6
CPS	Cyclone Phase Space
ENSO	El Nino Southern Oscillation
ERA5	European-Centre for Medium-Range Weather Forecasting 5th reanalysis
ET	Extratropical Transition
GPI	Genesis Potential Index
HURDAT	HURricane DATabase
IBTrACS	International Best Track Archive for Climate Stewardship
KS	Kolmogorov-Smirnov
LMI	Lifetime Maximum Intensity
MLC	Midlatitude (extratropical) Cyclone
MSLP	Mean Sea Level Pressure
MERRA2	Modern-Era Retrospective analysis for Research and Applications version 2
MDR	Main Development Region
MLR	Multiple Linear Regression
NAO	North Atlantic Oscillation
NASH	North Atlantic Subtropical High
PI	Potential Intensity
PTC	Post-Tropical Cyclone
PV	Potential Vorticity
SLP	Sea Level Pressure
SST	Sea Surface Temperature
US	United States
UK	United Kingdom
VWS	Vertical Wind Shear

Chapter 1

Introduction

1.1. Motivation

Post-tropical cyclones (PTCs) can cause severe weather across Europe in terms of large waves, heavy precipitation, and extreme winds (Evans et al. 2017; Jones et al. 2003; Bieli et al. 2019a). These cyclones arise upon completion of extratropical transition (ET), the process whereby a tropical cyclone (TC) transforms from a warm-core, symmetric system into an extratropical cyclone if it moves poleward and encounters decreasing sea surface temperatures (SSTs), increasing baroclinicity, and increasing wind shear.

Post-tropical cyclones mainly occur in the second half of the North Atlantic hurricane season (September, October, November), and have impacted Europe regularly (but rarely) since records began. Hurricane Debbie impacted Ireland in September 1961 as Ireland's strongest storm on record (in terms of wind speed), with wind gusts reaching 51 m s^{-1} (113 mph), leading to 18 fatalities (Graham and Smart 2021). In 1986, ex-hurricane Charley deposited 200 mm of rain in 24 hours over Kippure, Ireland, setting a new national record for 24-hour precipitation accumulation (Met Éireann 1986). In October 2017, ex-hurricane Ophelia also impacted Ireland with wind gusts as high as 53 m s^{-1} (119 mph) recorded (Stewart 2018). Many more high-impact PTCs have also been documented across Europe, such as ex-hurricane Katia in 2011, which caused approximately £100m in damages upon impacting Scotland (Anfuso et al. 2020; Grams and Blumer 2015), and ex-hurricane Debby in 1982, which caused severe wind damage over Finland (Laurila et al. 2020).

While the above-mentioned Europe-impacting PTCs have many things in common (such as posing hazardous conditions for Europe and their origin in the tropics), there were many aspects of their lifecycle that were different. Ex-hurricane Katia's hazards were aided by strong coupling (known as phase-locking) between the cyclone and the upper-level flow in a strongly baroclinic region of the North Atlantic (Grams and Blumer, 2015). In contrast, ex-hurricane Debby travelled across the North Atlantic as a

diabatic Rossby wave; a self-sustaining shallow cyclone supported by internally-generated moist diabatic processes (Laurila et al. 2020). The relative rarity of Europe-impacting PTCs combined with their large case-to-case variability contributes to the knowledge gaps associated with these cyclones. These will be discussed in more detail in section 1.7.

The response of Europe-impacting PTCs to climate change is uncertain. This is partly because climate models do not have sufficient resolution to accurately simulate TCs (and therefore PTCs) and their climatologies. Even high-resolution climate models are unable to simulate the strongest TCs (Vidale et al. 2021). Europe-impacting PTCs are relatively rare (~2 per year, Baker et al. 2021), and running high-resolution climate models for long enough to sample a sufficient number of PTCs remains challenging. As a result, very few studies exist surrounding the changes to Europe-impacting PTCs. Haarsma et al. (2013) investigated the frequency of hurricane-force (>33 m s^{-1}) PTCs occurring between August and October over four regions of Europe in the present climate and towards the end of the century using a high-resolution (~25 km in the midlatitudes) climate model (EC-Earth). A substantial increase in hurricane-force PTC frequency was found in three of the four regions, including a six-fold increase across the Bay of Biscay and a four-fold increase in the North Sea, highlighting the potential increased risk from PTCs to Europe in the future. Other studies also suggest an increased risk to Europe from PTCs in the future (Liu et al. 2017; Jung and Lackmann 2021), and observational studies have shown a poleward migration of TCs and their hazards in recent decades (Kossin et al. 2014).

There are a number of knowledge gaps related to Europe-impacting PTCs, such as the hazards associated with Europe-impacting PTCs compared to the broader class of midlatitude cyclones, the factors that govern the variability of Europe-impacting PTCs, and the response of Europe-impacting PTCs to climate change. Chapter 3 documents a quantification of the risk associated with PTCs during the North Atlantic hurricane season (June 1st – November 30th). Chapters 4 and 5 contain an analysis on why some TCs reach Europe as PTCs. Chapter 6 provides an assessment of the simulation and projected changes of Europe-impacting PTCs in fully-coupled state of the art climate models (CMIP6, Eyring et al. 2016).

The remainder of chapter 1 contains an overview of the literature related to TCs and PTCs. An overview of TCs with a focus on the North Atlantic basin will be given in section 1.2. Section 1.3 will assess our current understanding of the extratropical transition (ET) process, and section 1.4 discusses the reintensification process associated with PTCs. Section 1.5 documents the existing climatologies and case studies of Europe-impacting PTCs. Section 1.6 contains an assessment of TCs, ET, Europe-impacting PTCs and their response to climate change, and section 1.7 summarises the current knowledge gaps. Aims, research questions and structure are finally addressed in section 1.8.

1.2. North Atlantic Tropical Cyclones and Recurvature

Tropical cyclones (TCs) are among the costliest natural hazards on the planet (Emanuel et al. 2008) and are responsible for large losses of life, economic damages, and structural damages annually. Approximately 80 TCs form globally each year (Emanuel 2003), with approximately 12 of these forming in the North Atlantic. TCs form from seeds and precursors such as African Easterly Waves (AEWs, Thorncroft and Hodges 2001) and mesoscale convective systems, and strengthen due to upwards latent heat transport from the ocean to the atmosphere (wind-induced surface heat exchange (WISHE), Emanuel 1986). For TCs to form, a number of environmental conditions must be met ('Gray conditions', Gray 1975):

1) An initial source of low-level vorticity, such as a pre-existing disturbance or frontal boundary.

2) A sufficient distance (~5 degrees) from the equator (non-zero Coriolis parameter).

3) Weak vertical wind shear (VWS).

4) Sea surface temperatures (SSTs) greater than ~26C accompanied with high ocean heat content.

5) Conditional instability throughout the depth of the troposphere.

6) A moist mid-troposphere.

Conditions 2-6 are regularly met in the tropical North Atlantic through the period June 1st-November 30th (the North Atlantic hurricane season), allowing pre-existing

disturbances the potential to develop into TCs. The interannual variability of North Atlantic TCs is predicted well by large-scale environmental fields and teleconnections related to the Gray conditions. North Atlantic TC activity is strongly correlated with SSTs, VWS, and by other fields which are strongly correlated with SSTs and VWS (such as trade winds, upper-level winds, and temperature, Klotzbach 2014). Interannually, large-scale teleconnections such as ENSO also modulate North Atlantic TC activity (Klotzbach et al. 2019) via changes to VWS and atmospheric stability in the North Atlantic, communicated via the Walker circulation (Gray 1984). The interannual variability of TC activity regionally within the North Atlantic is less well understood (Klotzbach et al. 2019), though skilful regional forecasts of TC activity are possible in some regions, such as for US landfalling major hurricanes (Murakami et al. 2016), and TC activity in the Caribbean Sea (Vecchi et al. 2014).

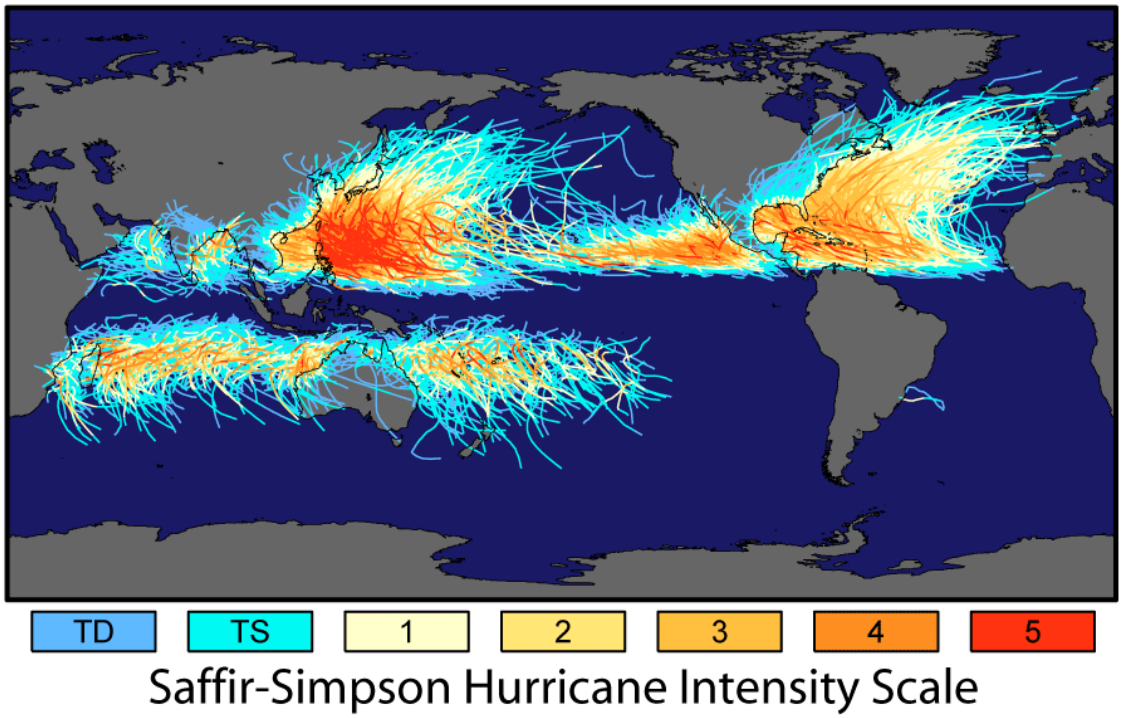

Figure 1.1. Tropical Cyclone tracks from the National Hurricane Centre and Joint Typhoon Warning Centre, 1851-2006. TCs are coloured based on their Saffir-Simpson category. Image courtesy of NASA Earth Observatory, reused with permission.

The track and lifecycle of North Atlantic TCs is in part governed by where in the basin they form, with different teleconnections and environmental conditions controlling TC activity in different parts of the North Atlantic (Kossin et al. 2010; Kozar et al. 2012; Boudreault et al. 2017). Many North Atlantic TCs make landfall in the Caribbean,

Mexico, and the USA. However, a large fraction of North Atlantic TCs instead recurve and enter the midlatitudes (Figure 1.1), where they are often steered by the strong westerly midlatitude flow (Emanuel 2003) and may therefore pose risk to downstream midlatitude regions such as Europe (e.g., Laurila et al. 2020; Rantanen et al. 2020; Baker et al. 2021). While recurvature isn't unique to the North Atlantic, the Pacific and North Atlantic contain the greatest number of recurving TCs, with implications for downstream regions (Bieli et al. 2019a). In particular for recurving TC interannual variability, the roles played by the seasonal mean steering flow and TC activity in the North Atlantic have not been quantified. Quantifying the factors that govern the interannual variability of recurving TCs would provide an improved understanding of the usefulness of seasonal hurricane forecasts for recurving TCs specifically. This question is addressed in chapter 4.

The recurvature of North Atlantic TCs can also lead to landfall along the US East Coast and eastern Canada. This region of the USA is heavily populated, and TCs impacting the US East Coast can cause extensive economic losses and fatalities, such as hurricane Sandy in 2012 (Varlas et al. 2019; Blake et al. 2013). The impacts associated with cyclones like Sandy are in part due to the combined tropical-extratropical hazards associated with the cyclones, which often undergo extratropical transition (ET) as they impact the region.

1.3. Extratropical Transition of Tropical Cyclones

Extratropical transition (ET) is the process whereby a TC loses many of its tropical characteristics – such as its deep warm core and thermally symmetric structure – and develops characteristics associated with extratropical cyclones (Jones et al. 2003; Evans et al. 2017; Keller et al. 2019; Bieli et al. 2019a; Palmén 1958). This occurs as a TC moves poleward from a region favourable for tropical cyclogenesis (warm SSTs, low VWS) to a region characterized by lower SSTs, increasing baroclinicity, wind shear, and Coriolis force (Klein et al. 2000). ET therefore occurs as TCs are steered towards the midlatitudes.

TCs undergoing ET can produce significant wind, wave and precipitation hazards in regions which are rarely affected by TCs. While SSTs typically decrease along the transitioning TCs path, marginal SSTs may still support deep moist convection and

maintenance of latent heat fluxes while the transitioning TC becomes increasingly baroclinically forced (Thorncroft and Jones 2000; Bieli et al. 2019a). This period in the cyclone's lifecycle can be responsible for combined TC and extratropical cyclone hazards (for example, winds of comparable speed to those found in TCs, but enveloping a much larger area around the cyclone than typically seen in TCs). Cyclones impacting land regions during this phase of their lifecycle have the potential to cause significant impacts, such as the extreme precipitation associated with hurricanes Floyd in 1999 (Atallah and Bosart 2003) and Irene in 2011 (Jung and Lackmann 2019), and the combined wind and surge hazards associated with hurricane Sandy in 2012 (Varlas et al. 2019).

1.3.1. Changes to Cyclone Structure

Many structural changes occur during ET, such as an increase in asymmetry, expansion of the wind field, the erosion of the deep warm core and development of a cold core, and the development of a vertical tilt with height (Klein et al. 2000; Evans et al. 2017; Hart 2003; Jones et al. 2003). By investigating satellite imagery of 30 TCs in the Western North Pacific, Klein et al. (2000) identified three distinct phases of the transformation stage of TCs and devised a three-dimensional conceptual model for ET (Figure 1.2). Step 1 is initiated by the interaction between the outer circulation of the TC and a pre-existing baroclinic zone, characterised by large temperature and moisture gradients over cooling SSTs (Ritchie and Elsberry 2001; Klein et al. 2000). During this stage of ET, deep moist convection wanes in the western quadrant due to entrainment of cold, dry air (Fig. 1.2b, step 1). This leads to increasing convective asymmetry, with deep moist convection maintained via warm air advection to the east of the transitioning TC (Klein et al. 2000).

In the second step, increasing vertical wind shear advects the upper-level warm core downstream, producing a noticeable vertical tilt (Fig. 1.2c, step 2). Deep moist convection becomes limited to the cyclone inner core, particularly limited in the southern and western quadrants (Fig. 1.2a, step 2). Cyclone-relative airstreams such as the warm and cold conveyor belts (e.g., Dacre et al. 2012) begin to form in this stage (Evans et al. 2017). During step 3, the cyclone becomes fully embedded in the midlatitude baroclinic zone and convection is completely eroded in the southern and

western eyewall. The TC circulation is confined to the mid and lower troposphere by this stage (Evans et al. 2017; Ritchie and Elsberry 2001). This conceptual model has been qualitatively validated by results from idealised models (Ritchie and Elsberry 2001), and field campaigns (Foerster et al. 2014; Quinting et al. 2014).

Throughout the three stages described in Figure 1.2, the size of the wind field associated with the transitioning TC increases, exposing a considerably larger area to strong winds and large waves. It is often an upper-level trough or pre-existing cyclone that is responsible for providing the initial baroclinicity which prompts the onset of ET (Evans et al. 2017). In such cases, the transitioning TC expands to match the scale of the interacting trough or pre-existing cyclone (Atallah and Bosart 2003). The expansion of the wind field can be associated with the import of angular momentum into the transitioning TC as asymmetry increases, and a weakening of the geopotential height gradient near the centre of the cyclone which causes the radius of maximum winds to move radially outwards (Evans and Hart 2008; Evans et al. 2017).

Ultimately, recurving TCs which reach Europe as PTCs go through ET and undergo many of the structural changes highlighted by Klein et al. (2000). ET can be initiated by a decrease in SSTs, an increase in baroclinicity, or both, and the midlatitude environment into which the recurving TC transitions will determine whether the cyclone undergoes reintensification or decays (Harr et al. 2000a; Keller et al. 2019). The importance of the midlatitude environment (for example, in terms of baroclinicity, strength of the midlatitude jet, location and interaction with upstream troughs) that the TC transitions into, and the characteristics of the incipient TC in determining whether a recurving TC will reach Europe have not previously been quantified and are addressed in chapter 5.

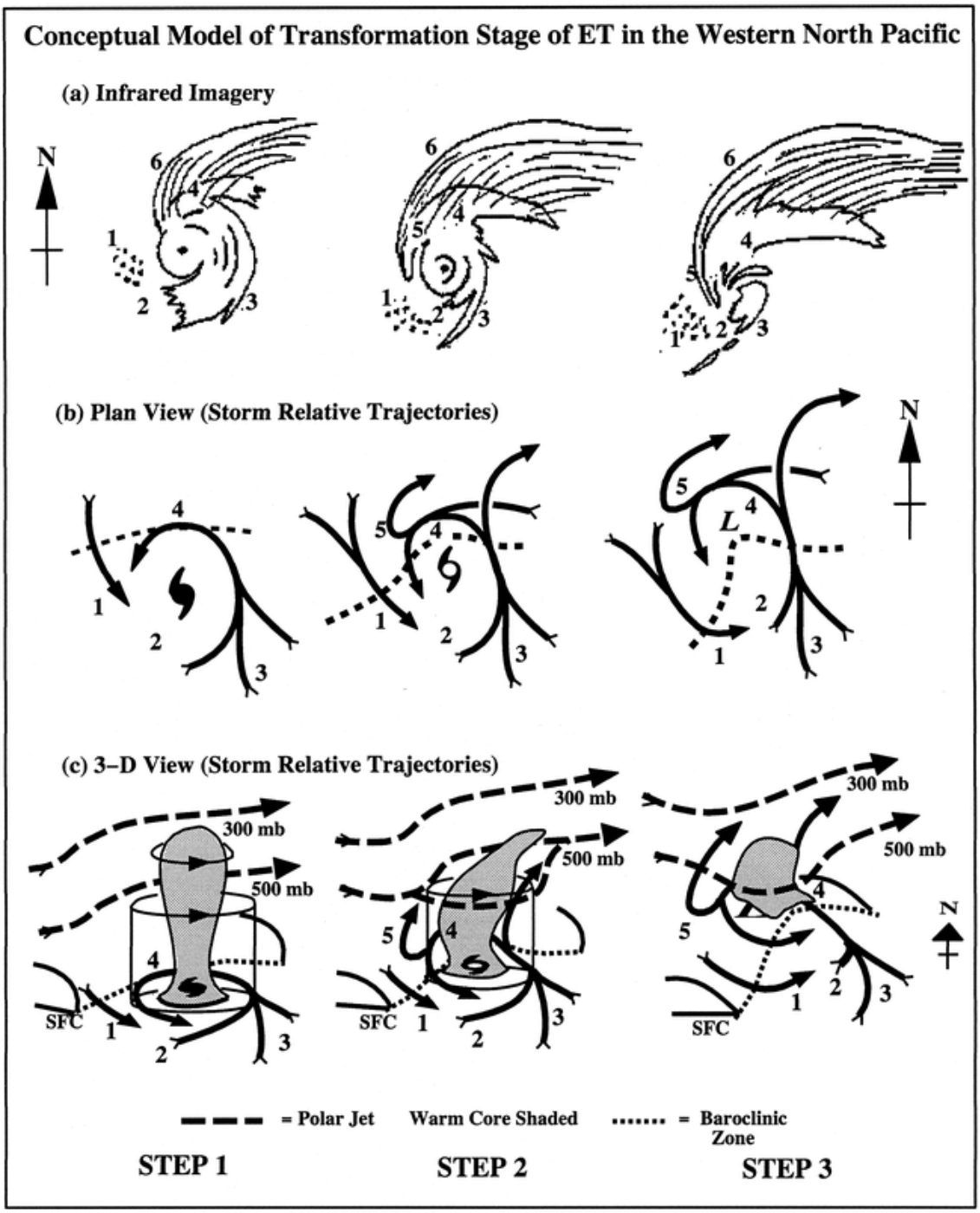

Figure 1.2. Conceptual model for the transformation stage of ET derived from satellite imagery of transitioning TCs in the Western North Pacific. Image from Klein et al. (2000) (Figure 5 therein). Numbers represent different features and processes associated with the composite cyclone, as diagnosed by Klein et al. (2000) (1=equatorward flow of cooler, drier air; 2=decreased tropical convection in the western quadrant; 3=poleward flow of warm, moist air ingested by the TC; 4= ascent of warm, moist inflow along isentropes upon interaction with the baroclinic zone; and 5=ascent, producing cloud bands wrapping westward and equatorward around the cyclone; and 6= cirrus shield). © American Meteorological Society. Used with permission.

1.3.2. North Atlantic ET Climatologies and Identification Methods

A number of climatologies of ET in the North Atlantic (Arnott et al. 2004; Evans and Hart 2003; Hart and Evans 2001), Pacific (Wood and Ritchie 2014; Klein et al. 2000), and worldwide (Bieli et al. 2019a; Studholme et al. 2015) have been constructed using multiple ET identification techniques. In the North Atlantic, Hart and Evans (2001) found that 46% of TCs complete ET, with the majority of TCs doing so between 35 and 45°N. In their study, ET was determined by forecasters at the National Hurricane Center using satellite imagery to subjectively identify TC structural changes consistent with ET (as described in section 1.3.1). However, structural changes can occur slowly in a transitioning TC, and it is often not clear when a TC should be declared 'post-tropical' (Hart and Evans 2001). To identify ET more objectively and to allow for the analysis of ET within climate models, updated climatologies often use automated methods to identify ET.

The most widely used ET identification technique is the cyclone phase space (CPS, Hart 2003). This three-dimensional phase space can be used to quantify the symmetry of a cyclone along with its thermal properties (deep warm core, deep cold core, shallow warm core, etc.). The CPS method has been shown to be in reasonable agreement with subjectively identified ET timings and locations from operational forecasters (Evans and Hart 2003), but model biases in the representation of TCs can result in ET being systematically identified too early in some climate models (Baker et al. 2022). It has been used to construct climatologies of ET in reanalyses (Arnott et al. 2004; Bieli et al. 2019b; Studholme et al. 2015; Wood and Ritchie 2014; Baker et al. 2021) and climate models (Bieli et al. 2020; Liu et al. 2017; Zarzycki et al. 2017; Michaelis and Lackmann 2019; Baker et al. 2022), and has the added benefit of being able to objectively identify the onset and completion of ET. The formulation of the CPS used in this thesis is discussed in section 2.3.3.

Using the CPS method, between 50% (Bieli et al. 2019a) and 68% (Studholme et al. 2015) of North Atlantic TCs are estimated to complete ET, up to 50% of which reintensify and therefore may pose risk downstream (Hart and Evans 2001). There is a distinct difference between tracks of North Atlantic TCs which undergo ET compared with those that do not (Bieli et al. 2019a; Liu et al. 2017; Dekker et al. 2018; Baker et

al. 2021). TCs undergoing ET often recurve and reach the midlatitudes, whereas TCs not undergoing ET typically stay within the tropics (Fig. 1.3) and therefore lack the interaction with baroclinicity which is necessary to start the process. The majority of TCs which complete ET become thermally asymmetric before losing their warm core (as suggested by Klein et al. (2000), Fig 1.2), however a non-negligible fraction of North Atlantic TCs lose their warm core before becoming thermally asymmetric (Bieli et al. 2019a). TCs which lose their warm core before their thermal symmetry are associated with cooler SSTs during ET, and typically complete ET quicker than TCs which become thermally asymmetric first (Bieli et al. 2019a). Cooler SSTs are less able to support deep convection during ET, reducing latent heat fluxes and leading to a quicker erosion of the warm core.

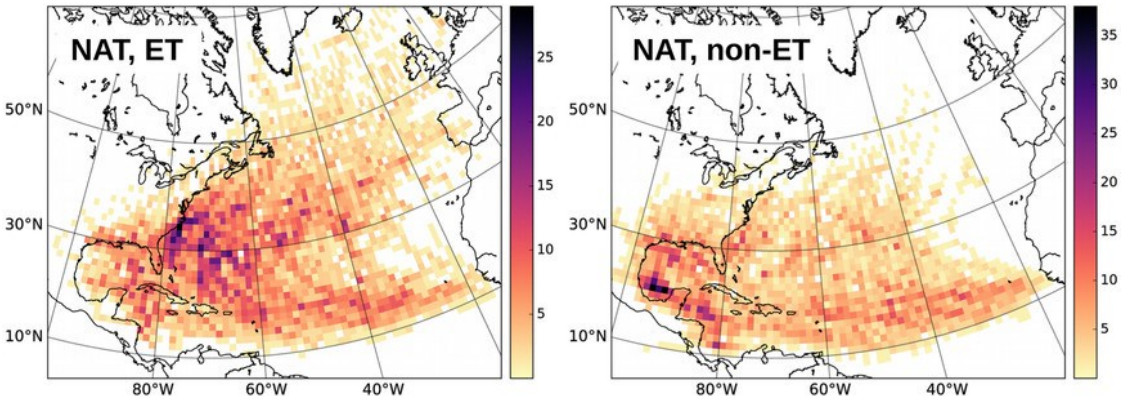

Figure 1.3. Track density for North Atlantic TCs which complete ET (left) and do not complete ET (right) as defined by the CPS using the JRA-55 reanalysis. Track density is shown as the sum of all best track data points falling into 1.25 x 1.25-degree grid boxes, 1979-2017. Figure adapted from Bieli et al. (2019a) (Figure 10 therein). © American Meteorological Society. Used with permission.

There are known issues with the CPS. The method relies on models and reanalyses accurately representing the geopotential height fields around TCs, which is not always a valid assumption due to biases in the representation of TC structure in coarse-resolution gridded datasets (Bieli et al. 2020). For example, observed weak TCs do not always attain a deep warm core in the CPS framework when identified in reanalyses, and therefore are unable to undergo the transition process. In high-resolution models, a low-level warm core may persist, which delays ET completion in the framework of the CPS (Jung and Lackmann 2021). Furthermore, TCs undergoing ET in a baroclinic environment which is favourable for rapid extratropical cyclogenesis may develop a warm seclusion (Shapiro and Keyser 1990). These extratropical cyclones are

characterised by a pocket of warm air near the surface, which in the framework of the CPS can manifest as a low-level warm core. In such cases, ET completion will not be designated by the CPS unless the warm seclusion dissipates, delaying, or potentially missing ET completion identification altogether. Other criteria have been investigated to determine ET, such as the time at which a TC becomes an open wave using the 500 hPa geopotential height (Demirci et al. 2007) and a scalar frontogenesis parameter (Harr et al. 2000a). These methods have been shown to have some success at objectively determining ET onset and completion, but much like the CPS method have limitations. Both the open wave and scalar frontogenesis methods struggle to distinguish between TCs undergoing ET and recurving TCs which do not undergo ET (Kofron et al. 2010).

The existing methods used to identify ET objectively use environmental fields which can indicate extratropical development, which occurs as TCs encounter increasing baroclinicity. This environment can also be conducive to reintensification of the cyclone after ET, and the midlatitude environment into which the cyclone transitions is therefore crucial for the outcome of the TC post-transition (Keller et al. 2019). In particular, the midlatitude environment may be favourable for reintensification of the PTC, extending the hazards associated with the system from the tropics to the midlatitudes (e.g., Evans et al. 2017; Klein et al. 2000; Hart et al. 2006). This is expanded upon in section 1.4.

1.4. Post-ET Reintensification

Upon completion of ET, PTCs have an extratropical cyclone like structure with a large, asymmetric wind field and strong cross-storm temperature gradients separated by frontal zones (Jones et al. 2003). These storms can still pose significant hazards to midlatitude land regions and further intensity changes depend on their interaction with the midlatitude environment; namely phasing with an upstream trough, interaction with a midlatitude jet streak, and environmental baroclinicity (Hart and Evans 2001; Harr et al. 2000a; McTaggart-Cowan et al. 2004). Many previous studies have focussed on case studies of reintensifying PTCs in order to better understand the associated dynamics. These studies highlight a number of different post-ET evolutions. Ex-hurricanes Earl and Danielle in 1998 both underwent ET at the same time in the

North Atlantic but had substantially different post-ET evolutions. Ex-hurricane Danielle reintensified after interaction with the left exit region of an upper-level jet, where latent heat release in deep convection was shown to be paramount to the reintensification process. This contrasts with ex-hurricane Earl, in which interaction with an approaching upper-level upstream trough and associated baroclinicity aided the reintensification (McTaggart-Cowan et al. 2004). An approaching upstream trough has been shown to be crucial to the reintensification of many PTCs (Harr et al. 2000b; Laurila et al. 2020; Agusti-Panareda et al. 2004; Grams et al. 2013b) and in some cases the diabatic forcing within the inner core of the transitioning system, aided by marginal (~26C) SSTs which support continued deep convection, are shown to also be important for the reintensification (Browning 1998; Thorncroft and Jones 2000; Rantanen et al. 2020).

PTCs which interact favourably with the upper-level midlatitude flow can undergo reintensification for a considerable period of time if they become phase-locked with the upper-level midlatitude flow (Haarsma 2021; Riboldi et al. 2019; Brannan and Chagnon 2020). This occurs when potential vorticity advection from the outflow of the transitioning TC acts to amplify the ridge-trough couplet and reduce its phase speed, bringing it closer to the translation speed of the PTC. This can lead to a protracted period of favourable phasing between the cyclone and the environment (Jones et al. 2003; Riemer et al. 2008), leading to a prolonged period of intensification and an overall amplification of the midlatitude waveguide downstream of the cyclone (e.g., Archambault et al. 2013; Riemer et al. 2008; Quinting and Jones 2016) which can cause further high-impact weather downstream (Pohorsky et al. 2019; Grams and Blumer 2015) and a reduction in downstream midlatitude predictability (Anwender et al. 2008; Pantillon et al. 2013).

Climatologies of post-ET reintensification have been derived from TCs in the Western North Pacific (Klein et al. 2000, 2002; Harr et al. 2000a) and North Atlantic (Hart et al. 2006). Harr et al. (2000a) separate transitioning TCs into two groups characterised by the position of the cyclone relative to an upper-level trough. It is found that cyclones in the ‘northwest pattern’ (upstream trough) rapidly reintensify upon completion of ET and move on a north-eastward trajectory, whereas cyclones in the ‘northeast pattern’ (downstream trough/pre-existing cyclone) do not undergo significant reintensification.

TCs in the northeast pattern move rapidly in a zonal direction between the subtropical high and westerly midlatitude flow before dissipating. TCs entering the northwest pattern experience an increase in eddy heat flux post-ET, whereas cyclones in the northeast pattern do not experience this (Harr et al. 2000a). In a trough-relative framework, the tip of the trough therefore acts as a bifurcation point (e.g., Grams et al. 2013a) and is responsible for the large sensitivity the reintensification has to the phasing between the PTC and upper-level trough.

In the North Atlantic, reintensifying TCs post-ET are associated with a negatively tilted upstream trough, whereas TCs which weaken post-ET are associated with a positively tilted trough (Hart et al. 2006). A positively tilted trough is hypothesized to prevent a contraction and intensification of the eddy heat and angular momentum forcings (Fig. 1.4). The first and second columns of Figure 1.4 show the Eliassen-Palm (EP, Eliassen and Palm 1961) flux vectors, used to determine the relative importance of eddy heat and eddy angular momentum fluxes, and their divergence (shading) for the TCs which complete ET over ocean and reintensify (Fig. 1.4e-1.4h) and weaken (Fig. 1.4i-1.4l). Outward pointing arrows represent inward eddy angular momentum flux, and upward pointing arrows represent inward eddy heat flux. The divergence represents eddy potential vorticity flux (Hart et al. 2006). During ET, the strengthening composite is associated with greater inward eddy angular momentum fluxes than the weakening composite. (Fig. 1.4f, g vs Fig. 1.4 j, k). At 24 hours after ET, the strengthening composite is associated with an increase in inward eddy heat flux and a contraction of the region of the highest EP flux divergence towards the cyclone centre (Fig. 1.4h). These changes are consistent with the northwest pattern of Harr et al. (2000a), and do not occur in the weakening composite. However, recent work has suggested that the negative tilt of the upstream trough may be a consequence of strong TC-trough interaction, rather than a predictor of future PTC outcomes (Sarro and Evans 2022).

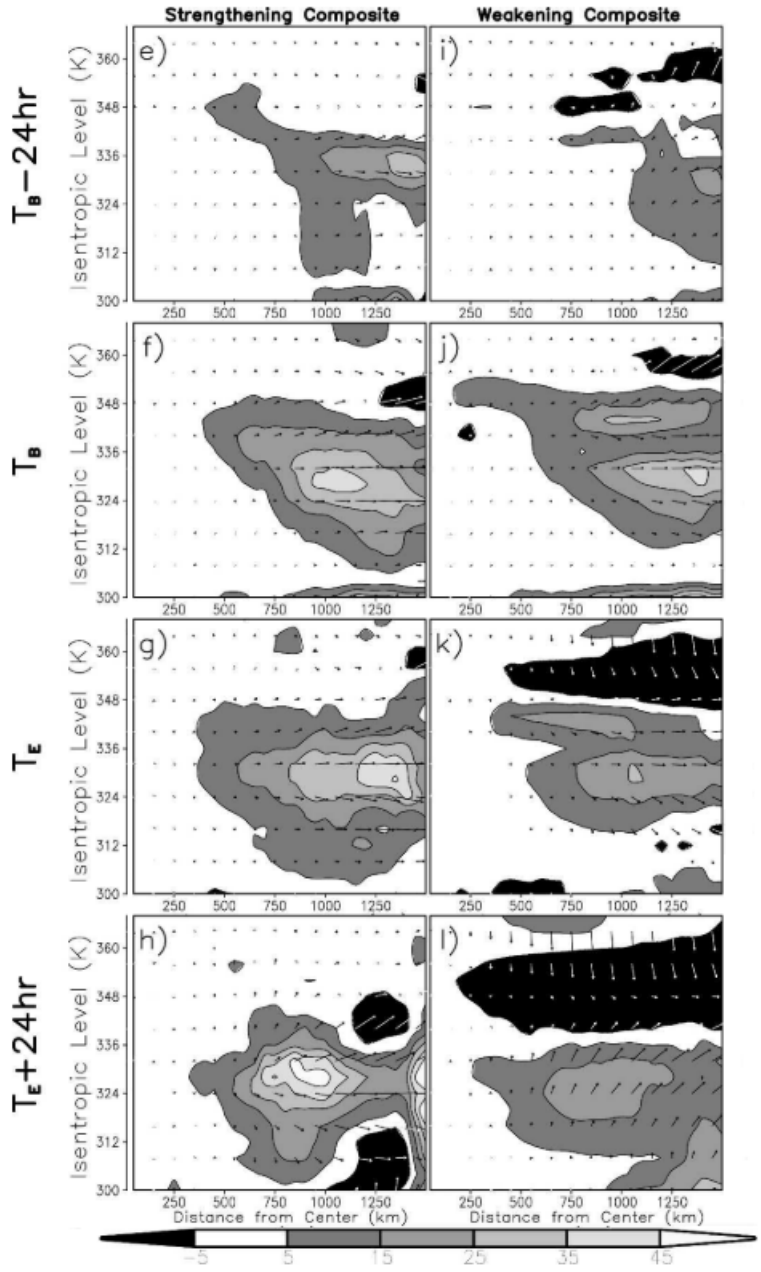

Figure 1.4. Radius-isentropic height cross sections of the Eliassen-Palm flux vectors (arrows) and their divergence (shading, 10^5 Pa m^2 K^{-1} s^{-2}) for post-ET strengthening TCs (complete ET and don't impact land, first column, 6 storms), post-ET weakening TCs (complete ET and don't impact land, second column, 11 storms). Rows represent the time relative to ET (top row = 24 hours before ET onset, second row = ET onset, third row = ET completion, fourth row = 24 hours post-ET completion). Figure adapted from Hart et al. (2006) (Figure 8 therein). © American Meteorological Society. Used with permission.

Despite the climatologies of Harr et al. (2000a) and Hart et al. (2006), many unanswered questions remain, particularly from the perspective of Europe-impacting PTCs. It is unclear whether reintensification of the PTC ultimately determines whether

a PTC will reach Europe, or whether other factors, such as the strength of the incipient TC, are also important. Hart et al. (2006) provides the only climatology on the post-ET evolution of TCs in the North Atlantic, but sample sizes are extremely small (6 reintensifying and 11 weakening cyclones). As a result, there are large uncertainties and a lack of statistical significance, which motivate the need for an updated climatology in the North Atlantic. This is addressed in chapter 5.

1.5. Europe-Impacting PTCs

PTCs are a feature of midlatitude and European storminess during the North Atlantic hurricane season (Baker et al. 2021). They comprise the strongest windstorms on record to impact Ireland (Graham and Smart 2021; Stewart 2018), have been associated with national record precipitation accumulations (such as ex-hurricane Charley in 1986 across Ireland, Met Éireann 1986) and have caused extensive economic damage across parts of Europe (Grams and Blumer 2015; Laurila et al. 2020; Stewart 2012). PTCs have likely impacted Europe for centuries, with reconstructed hurricane trajectories identifying PTCs over Europe as far back as 1680 (Wheeler et al. 2009). This unnamed storm in 1680 likely formed in the Main Development Region and crossed England in August, bringing what was described in logbooks as "*stormy weather that the like has not for several years past been known*" across southern England (Wheeler et al. 2009). In 1961, hurricane Debbie (Met Éireann 1961; Graham and Smart 2021) was one of the strongest storms to ever impact Ireland. At the time, it was responsible for Irelands (joint) highest wind gust of 51 m s^{-1} (113 mph), which has only been surpassed by one storm since: ex-hurricane Ophelia in 2017 (Stewart 2018). However, Ophelia's record measurement was taken at an elevated site. Debbie was associated with sustained hurricane-force winds, with 10-minute mean winds of 39 m s^{-1} (87 mph) recorded at Malin Head (Graham and Smart 2021) and was responsible for significant crop damage and loss of life (Graham and Smart 2021; Met Éireann 1961). Ex-hurricane Charley (Met Éireann 1986) was responsible for rainfall accumulations of over 10 inches (200 mm), setting a new 24-hour record in Ireland and was a 100-year precipitation event across parts of Wales. In 1996, ex-hurricane Lili was responsible for wind gusts of over 40 m s^{-1} (90 mph) along the south coast of England (Lawrence 1996) and produced waves in excess of 12 m in the North Sea,

causing the greatest economic damage associated with a storm across the UK since the great storm of 1987, 9 years prior (Longshore 2008, page 162).

PTC impacts are not limited to western Europe. In 1982, ex-hurricane Debby (Laurila et al. 2020) caused significant wind damage over Northern Finland. Unlike many TCs which reach Europe, Debby did not reintensify after ET straight away, but propagated across the North Atlantic as a diabatic Rossby wave, before rapidly reintensifying over the UK after interacting with an upstream upper-level trough (Laurila et al. 2020). In their study, Laurila et al. (2020) find that the forecast reintensification of Debby is very sensitive to the initial interaction between the remnant TC and the upper-level trough, highlighting the significant reduction in predictability which is often present during the interaction of a TC and the midlatitude environment (Anwender et al. 2008; Harr et al. 2008). The intrinsic lower predictability of the reintensification stage of PTCs can reduce preparation time for PTC impacts, which could be consequential given their high-impact nature.

Alongside numerous case studies of Europe-impacting PTCs (Rantanen et al. 2020; Laurila et al. 2020; Graham and Smart 2021; Moore 2021; Smart and Graham 2021), climatologies have also been constructed from reanalysis and observational data. While not limited to Europe, Hart and Evans (2001) first highlighted the risk associated with PTCs from a climatological perspective using best track data. They estimate 0.5-1 PTC impacts across western Europe per year over the period 1950-1996, noting that this is likely to be a large underestimation (Hart and Evans 2001). More comprehensive analyses of the post-tropical stage of the cyclone lifecycle presented in Baker et al. (2021) found that approximately 2 PTCs reach Europe each year, with good agreement found across seven different reanalyses. Some Europe-impacting PTCs (~20% (Fig. 1.5, Baker et al. 2021) - 50% (Dekker et al. 2018)) of the total Europe-impacting PTCs) reach the region with a warm core/warm seclusion, and these cyclones are typically stronger than their cold-core counterparts. Furthermore, Europe-impacting PTCs tend to reach their maximum intensity ~1-3 days after reaching the region, enhancing their destructive potential (Fig. 8, Baker et al. 2021; Fig. 6, Dekker et al. 2018).

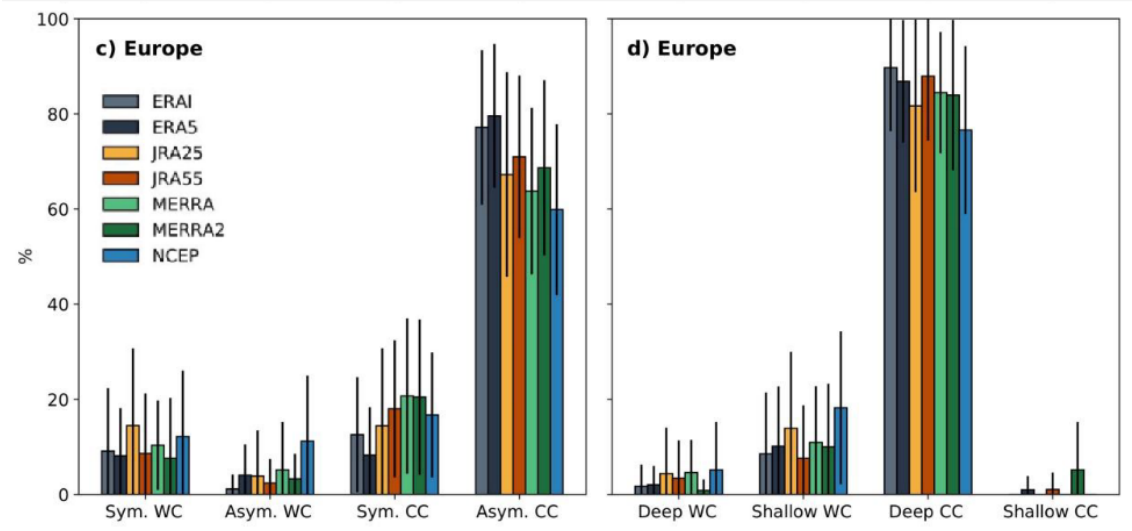

Figure 1.5. Europe-impacting PTC structural characteristics at landfall. Cyclone structure is characterised by position in the cyclone phase space. Error bars show 1 standard deviation of interannual variability. 'Shallow' refers to lower tropospheric core structure, and 'Deep' refers to total (lower and upper) tropospheric core structure. 'Sym.' refers to symmetric/non-frontal structures, 'Asym.' refers to non-symmetric/frontal structures. 'WC' refers to low-level warm core, 'CC' refers to low-level cold core. Y-axis represents the fraction of Europe-impacting cyclones of tropical origin which have each thermal structure. Figure adapted from Baker et al. (2021) (Figure 7 therein), reused with permission.

1.6. Climate Change

Previous studies which investigate the change in Europe-impacting PTCs are limited (in terms of both the number of studies conducted and the sample sizes used within these studies), partly because climate models do not have sufficient resolution to resolve the inner-core structure and full intensity spectrum of TCs (Camargo and Wing 2016; Caron and Jones 2012). Newer generations of high-resolution climate models (e.g., HighResMIP (Roberts et al. 2020a)) have alleviated this problem to some extent (e.g., Manganello et al. 2012), although many deficiencies remain, and almost all climate models still fail to capture the entire distribution of TC intensity (Davis 2018). This section provides an overview of how all stages of a Europe-impacting PTCs lifecycle may change – and in some cases have already changed – due to anthropogenic climate change.

1.6.1. North Atlantic Tropical Cyclones

The response of many aspects of the North Atlantic TC climatology to climate change remain uncertain, but there are some areas in which we have increasing confidence (Knutson et al. 2019; Walsh et al. 2019) due to historically observed trends, a good understanding of the physical mechanism associated with observed (and projected) trends, and robust climate model projections. Since 1950, there has been an observed increase globally in TC related precipitation, the proportion of major hurricanes (category 3+ on the Saffir-Simpson scale), and the frequency of TC rapid intensification, which have been attributed to anthropogenic climate change with 'medium' to 'high' confidence in Working Group 1's contribution to the IPCC AR6 report (Arias et al. 2021). For future projections, there is medium confidence for an increase in TC related precipitation, related to an increased saturation vapour pressure in a warmer climate (Clausius-Clapeyron). It is also likely that the average intensity of North Atlantic TCs will increase (Knutson et al. 2019), which is consistent with the IPCC's global assessment that there is 'high confidence' the proportion of TCs which are intense (category 3+) will increase (Arias et al. 2021). However, confidence remains low regarding the change in the frequency of North Atlantic TCs. Most climate model studies explicitly tracking TCs project either little change or a decrease in North Atlantic TC frequency in the future in low (Villarini and Vecchi 2012; Camargo 2013; Rathman et al. 2014; Bengtsson et al. 2007b) and high (Roberts et al. 2015; Gualdi et al. 2008) resolution climate models (although some predict an increase, e.g., Bhatia et al. 2018). However, the projected changes can be sensitive to the method used to identify the TCs (Roberts et al. 2020a), and many previous studies use different emission scenarios.

Decreases in TC frequency are often found when explicitly tracking TCs in climate models (Knutson et al. 2019), and results are more mixed when other methods are used. For example, statistical-dynamical downscaling of CMIP5/CMIP6 models produces an increase in TC frequency, however this is in part due to the lack of atmosphere-ocean coupling and is dependent on the assumptions that are made regarding TC seeding. Therefore, these results may not be representative of the actual change (Emanuel 2013, 2021a). Further uncertainties in climate projections can come from the representation and projected changes in TC 'seeds' (Vecchi et al. 2019), as changes in their frequency, intensity and likelihood of conversion from seed to TC can

be sensitive to the model used (Vidale et al. 2021). It is hypothesized that future weak TCs may have a larger radius and therefore lower associated vorticity. As a result, identification methods which use fixed vorticity thresholds may fail to identify a larger proportion of weak TCs in the future, introducing an artificial negative trend (Sugi et al. 2020).

Alternative methods to investigate projected TC frequency changes involve the calculation of genesis potential indices (GPIs, e.g., Camargo et al. 2007; Emanuel and Nolan 2004; Emanuel et al. 2008). These are empirical formulae which link environmental variables - which have been shown to be strongly associated with TC genesis historically - with the likelihood of TC formation (Camargo and Wing 2016; Emanuel et al. 2008). This allows us to infer a possible change in TC frequency from the change in the larger scale-environment, which is much better resolved by climate models than individual TCs (Camargo and Wing 2016). GPIs have been shown to match well with the observed locations of TCs (Camargo et al. 2007a), but limitations remain. For example, Camargo et al. (2007b) found that despite two models having a similar GPI climatology, the number of explicitly identified TCs in the models differed by a factor of four, making it difficult to compare models using GPI. Furthermore, GPIs are empirical fits and do not represent the true physical relationship between each environmental field and TC genesis likelihood. Midlevel relative humidity is typically projected to increase in the future (favourable to TC genesis), whereas saturation deficit – the difference between the moist entropy in the mid troposphere and the boundary layer (Emanuel et al. 2008) – is also projected to increase (increasing hostility for TC genesis). GPI metrics using both mid-tropospheric relative humidity (Emanuel and Nolan 2004; Camargo 2013; Vidale et al. 2021; Menkes et al. 2012) and saturation deficit (Emanuel 2010; Jing et al. 2021) fit observational data well and it is not completely clear which should be used in GPI analysis in climate change studies. This can lead to a large sensitivity in projected GPI change depending on the humidity metric used (Jing et al. 2021; Lee et al. 2020), though both formulations show a projected increase in GPI in most studies (Camargo and Wing 2016).

A positive trend in Atlantic hurricane frequency over the last 150 years has been identified, though mostly attributed to natural variability (Emanuel 2021b), but may also be the result of an inhomogeneous data record (Vecchi et al. 2021; Landsea et al.

2010). Of the 141 studies of projected North Atlantic TC changes by the end of the century for 2 C warming, as analysed in Knutson et al. (2019), the median projected change was approximately -15%, but with considerable spread (Fig. 1.6) of approximately -35% to +30% (90% confidence interval). The interannual variability of North Atlantic TCs is larger than the spread in projections, which has contributed to the difficulty robustly identifying trends in the present climate.

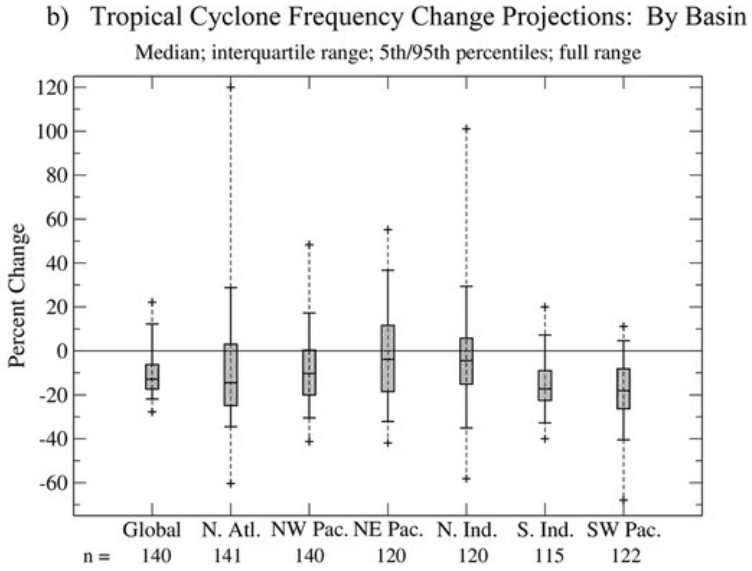

Figure 1.6. Projected change in TC frequency (%) from available studies. Shaded boxes, whiskers, and plus signs denote the interquartile range, 5-95th percentiles, and the maxima and minima. Horizontal lines are the medians. Numbers along the bottom are the number of separate estimates included. Values are scaled to be consistent with a global mean temperature increase of 2 C. Figure adapted from Knutson et al. (2019) (Figure 1b therein). **©** American Meteorological Society. Used with permission.

1.6.2. Extratropical Transition

In an analysis of ET in seven reanalysis products, Baker et al. (2021) found a positive trend in the number and fraction of North Atlantic TCs completing ET from 1980-2018. This trend was significant in 3 reanalyses for the fraction of TCs undergoing ET, and 4 reanalyses for the number of TCs undergoing ET. Coupled with previous studies which show an increase in ET frequency and/or fraction in the North Atlantic in observations (Mokhov et al. 2014), along with observed poleward trends in the location of TC lifetime maximum intensity (LMI, Kossin et al. 2014), the existing literature is in some agreement of an increase in ET related events in the North Atlantic observed over the past few decades.

Even high (~25 km) resolution climate models underestimate the intensity of TCs (e.g., Figs 11 and 12, Baker et al. 2022), and so further work is necessary to understand the impact that these biases have on ET projections from climate models. Furthermore, existing studies use different emission scenarios and model protocols, making it difficult to directly compare studies quantitatively. The projected changes to ET globally and in the North Atlantic have been investigated climatologically using high-resolution climate models (e.g., Baker et al. 2022; Liu et al. 2017; Michaelis and Lackmann 2019) and case study approaches (e.g., Jung and Lackmann 2021; Liu et al. 2020). In the first multi-model study of projected ET changes up to 2050, Baker et al. (2022) find an increase in the latitude of ET in the North Atlantic in fully-coupled and atmosphere-only simulations from an ensemble of HighResMIP-PRIMAVERA models (Haarsma et al. 2016). An increase in ET latitude may be associated with future TCs having a stronger warm core (i.e., more positive thermal wind in the framework of the cyclone phase space), making TCs more resilient to hostile midlatitude conditions in a future climate. This is consistent with Michaelis and Lackmann (2019), who investigated the projected changes in ET in a very high resolution (~15 km) climate model under the SSP5-85 scenario. A significant increase in the latitude of ET was found, associated with a poleward shift in TC lifetime maximum intensity (LMI) in the future under more favourable environmental conditions, characterised by increased potential intensity and decreased vertical wind shear (Michaelis and Lackmann 2019).

Previous studies also find an increase in the fraction (Michaelis and Lackmann 2019) and frequency (Baker et al. 2022; Michaelis and Lackmann 2019) of North Atlantic TCs which complete ET. These findings are consistent with Liu et al. (2017) and Semmler et al. (2008). Liu et al. (2017) find a (non-significant) increase in the frequency of North Atlantic ET events, and a significant (to 90%) increase in the fraction of North Atlantic TCs completing ET in the FLOR (Vecchi et al. 2014) model under RCP4.5 by the end of the century. Semmler et al. (2008) find a small increase in the fraction of North Atlantic ET by the end of the century in a high-resolution regional climate model (RCA3) under the SRES-A2 scenario. The increase in the fraction of TCs completing ET in Michaelis and Lackmann (2019) is associated with more favourable conditions (higher potential intensity, reduced vertical wind shear) in the subtropical North Atlantic, which leads to a larger proportion of TCs surviving the transit between the

region favourable to tropical cyclogenesis and the region favourable for baroclinic development. This region is also characterised by a large (>50%) increase in the frequency of ET events (Figure 1.7).

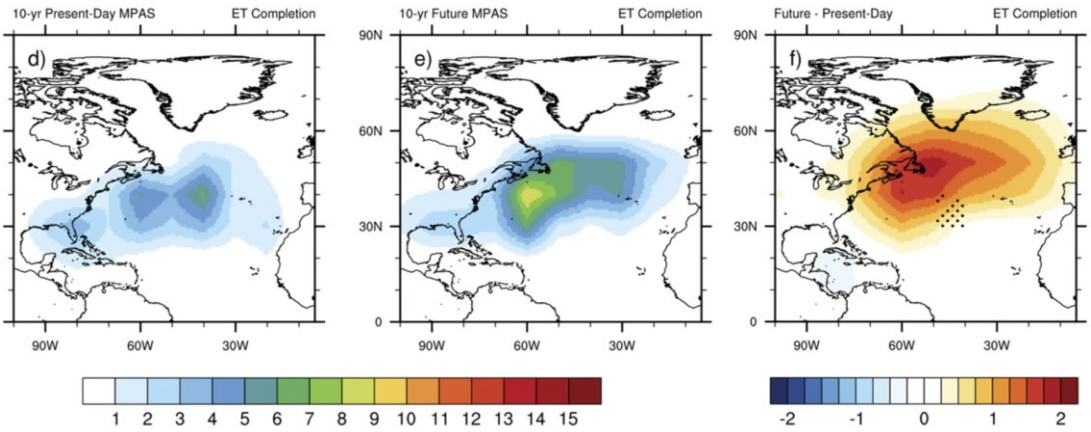

Figure 1.7. ET completion density (number of storms per 10x10 degree box) over 10 simulation years in the North Atlantic using the MPAS-A model with a 15 km grid: Present-day simulations (left), future simulations (middle) and difference (future minus present) (right). Stippling in f indicates where the percentage change is 50% or greater, restricted to regions in which there is at least 1 storm per year. Figure adapted from Michaelis and Lackmann (2019) (Figure 10 therein). **©** American Meteorological Society. Used with permission.

In addition, case study analysis provides a useful insight into how the risk associated with ET events may change in the future. Using a pseudo global warming (PGW) approach, Jung and Lackmann (2021) find that hurricane Irene (which occurred in 2011) would be more intense as a TC and during ET in the future, and that the precipitation associated with Irene increases greater than expected by Clausius-Clapeyron. This is consistent with Liu et al. (2020) which used a similar methodology and found an increase (above Clausius-Clapeyron) of precipitation in the inner-core of Irene, which shifted to the outer rainbands during ET. Using quasi-idealised numerical simulations, Jung and Lackmann (2021) find future ET events have greater intensity, heavier precipitation, and stronger modification of downstream midlatitude conditions in the future when initialised using storm centred-composite fields from previous North Atlantic recurving TCs. Along with projected increases in the frequency/fraction of TCs undergoing ET, these studies highlight the potential increased risk that individual TCs undergoing ET may pose in the future.

1.6.3. Europe-Impacting PTCs

The response of Europe-impacting PTCs to climate change is not completely understood, and only a small number of studies have investigated this question. Haarsma et al. (2013) investigated the frequency of hurricane-force (>33 m s^{-1}) PTCs over four regions of Europe in the present climate and towards the end of the century in a high-resolution (~25 km in the midlatitudes) climate model, EC-Earth. The simulation was atmosphere-only, using prescribed SSTs taken from coupled simulations based on the SRES-A2 emissions scenario (comparable to RCP 4.5). A substantial increase was found in three of the four European regions investigated, including a six-fold increase across the Gulf of Biscay and a four-fold increase in the North Sea (Fig. 1.8). This increase was associated with increasing SSTs in the subtropical North Atlantic (large increase of ~5 K), allowing TCs in the future to form and reside further polewards and eastwards, closer to Europe. A poleward and eastward expansion in the location of TCs may already be occurring. Ophelia (2017) was the easternmost major hurricane (category 3+ on the Saffir-Simpson scale) on record in the North Atlantic, and Lorenzo (2019) was the easternmost category 5 hurricane on record in the North Atlantic.

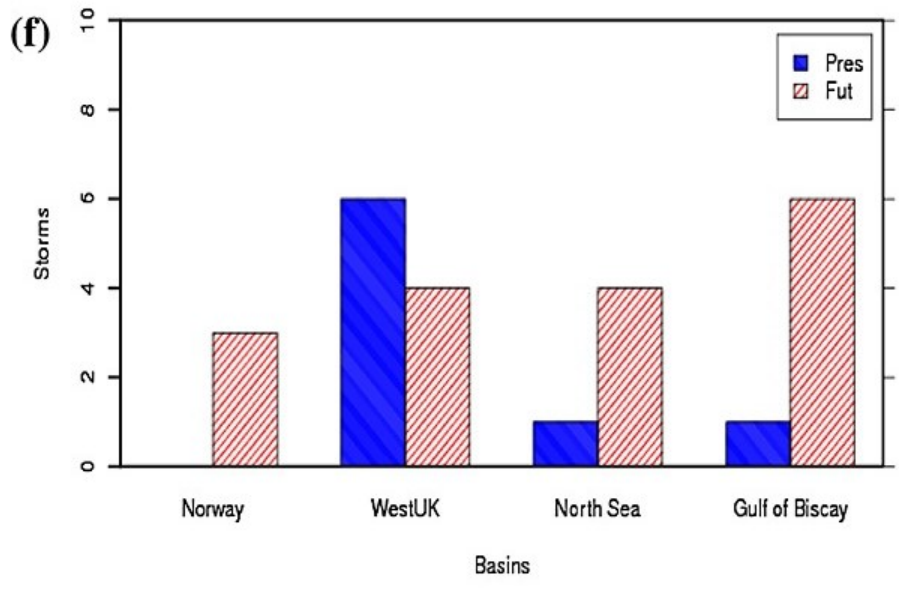

Figure 1.8. Number of hurricane-force storms with tropical origin during August, September, and October in different regions of Europe for the present (blue) and future (red) climates. Figure adapted from Haarsma et al. (2013) (Fig. 2f therein), reused with permission.

Using the same set of simulations, Baatsen et al. (2015) found an increase in the frequency and intensity of PTCs over western Europe. Future Europe-impacting PTCs

were ~8 hPa more intense (Baatsen et al. 2015) and almost always underwent warm-seclusion development. Warm seclusion cyclones have been shown to be more intense than cold-core cyclones in the present climate (Dekker et al. 2018; Baker et al. 2021). Rather than traversing the US East Coast like many Europe-impacting PTCs in the present climate, those simulated in Haarsma et al. (2013) and Baatsen et al. (2015) form in (or north) of the MDR and travel northwards/north-eastwards towards Europe (in both future and present periods), reducing the transit time between ET and Europe impact (Fig 1.9; Fig. 5, Baatsen et al. 2015; Fig 3, Haarsma et al. 2013). These projected PTC tracks are similar to Ophelia (2017) and Debbie (1961), both of which are among the strongest storms on record to impact Ireland (Graham and Smart 2021; Stewart 2018).

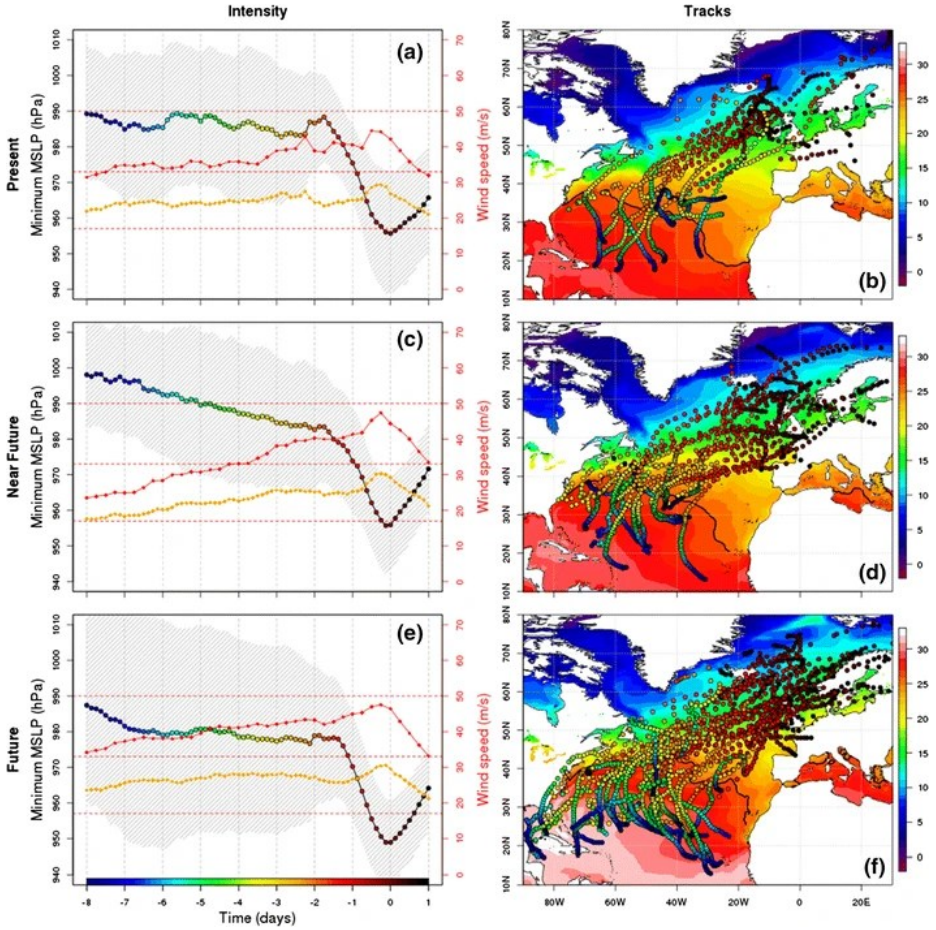

Figure 1.9. Intensity and tracks for present (a, b), near future (c, d) and future (e, f) cyclones, where left panels contain minimum MSLP (black edged circles) and standard deviation (hatching), 10 m wind speed (orange) and 850 hPa wind (red). Right panels show the cyclone trajectories and August-October mean SSTs (degrees Celsius) for the respective periods, and the thick black line indicates the 26 C isotherm. The colour scale of the circles indicates time relative to the first-time step. Figure from Baatsen et al. (2015) (Fig. 3 therein), reused with permission.

While indirectly, many other studies highlight the potential increased PTC risk for Europe in the future. Jung and Lackmann (2021) highlight that future TCs undergoing ET may have enhanced potential for high-impact weather over western Europe due to more intense post-ET cyclones in the future, greater associated precipitation rates, and greater TC-induced perturbation of the downstream waveguide, which can remotely generate high-impact weather downstream (e.g., Grams and Blumer 2015; Pohorsky et al. 2019; Archambault et al. 2013; Quinting and Jones 2016; Michaelis and Lackmann 2019). Michaelis and Lackmann (2019) find post-ET events occur further poleward and are more frequent and intense, indicating increased risk to Europe. Liu et al. (2017) highlight an increase in the number of ET events in the eastern half of the North Atlantic basin, further suggesting an increased risk to Europe. Semmler et al. (2008) highlight a 50% increase in the rate of post-ET reintensification, which may have implications for Europe if reintensification is found to be significantly associated with the likelihood that a PTC will reach Europe. The role of post-ET reintensification for Europe-impact likelihood is investigated in Chapter 5.

Despite previous work, it is currently unknown whether lower-resolution climate models – such as those used in CMIP6 (Eyring et al. 2016) – can capture the climatology of North Atlantic TCs and Europe-impacting PTCs. The response of Europe-impacting PTCs to climate change also remains unknown. Previous studies which explicitly look at Europe-impacting PTC changes use a single climate model with a limited sample size (Haarsma et al. 2013; Baatsen et al. 2015), and previous studies looking at changes to ET more generally do not use consistent emission scenarios, cyclone identification, or model protocols. Additional work is therefore necessary to quantify the uncertainty surrounding projected changes in Europe-impacting PTCs using a multi-model ensemble. This is addressed in chapter 6.

1.7. Current Knowledge Gaps

The previous sections have outlined the current state-of-the-art in terms of our knowledge of PTCs and ET in the North Atlantic basin. This section identifies the knowledge gaps that are addressed in this thesis. While a number of high-impact PTCs have reached Europe over previous decades (e.g., Laurila et al. 2020; Rantanen et al. 2020), the risk associated with Europe-impacting PTCs from a climatological perspective remains unknown. Given the different seasonality, trajectory towards Europe, and origin of PTCs compared to midlatitude cyclones (MLCs), it is necessary to understand how the intensity distribution associated with Europe-impacting PTCs compares to the broader class of cyclones to reach Europe. The existence of numerous high-impact European PTCs over the last four decades (section 1.5), in conjunction with their low climatological frequency (Hart and Evans 2001; Baker et al. 2021) motivates the hypothesis that PTCs may climatologically be more intense over Europe than the broader class of MLCs. This question is of key importance if we aim to understand the potential implications of projected changes in Europe-impacting PTCs and is also important from a risk perspective given the different seasonal characteristics of PTCs compared with MLCs.

Despite the rarity of Europe-impacting PTCs, there is considerable interannual variability associated with their frequency (Fig. 4b, Baker et al. 2021), with Europe impacted by between 0 and 7 PTCs per year since 1979. This interannual variability largely remains unexplored. Given the high-impact nature associated with Europe-impacting PTCs historically, it is crucial to understand what – if anything – controls this variability. This is important from forecasting and climate change perspectives. If an understanding can be developed surrounding the factors that allow TCs to enter the midlatitudes, and the factors that allow TCs which interact with the midlatitudes to reach Europe, it may be possible to identify years where Europe is more or less ‘at risk’ from PTCs.

Many more TCs reach the midlatitudes in the North Atlantic than reach Europe (e.g., Fig. 10, Bieli et al. 2019a; Fig. 6a, Liu et al. 2017) and understanding why some TCs which reach the midlatitudes impact Europe is of large importance. Recent North Atlantic case studies have highlighted the influence of upper-level features (Laurila et al. 2020) and diabatic forcing (Rantanen et al. 2020) for individual PTCs, but a climatological analysis has yet to be undertaken. The conditions associated with

reintensification have previously been investigated (Harr et al. 2000a; Browning 1998; McTaggart-Cowan et al. 2003), however it is not currently known if reintensification is the only factor – or even the most important factor – determining if a midlatitude-entering TC will reach Europe. While a number of climatologies have been constructed looking at the structure and intensity of Europe-impacting PTCs (section 1.5), ET more generally in the North Atlantic (section 1.3.2) and post-ET reintensification (section 1.4), no previous studies have combined this information to investigate why some North Atlantic TCs which undergo ET reach Europe, or investigated the role played by reintensification for such cyclones to reach Europe. Understanding the key factors associated with the cyclones and the surrounding environment which allow some of these cyclones to reach Europe is crucial. An understanding of which factors allow North Atlantic TCs to reach Europe is necessary in order to adequately scrutinise climate model projections of Europe-impacting PTCs, to ensure that climate model climatologies of Europe-impacting PTCs correctly capture these important factors. If there is any consensus regarding how such factors may change in the future, this may inform our understanding of future PTC risk to Europe.

Finally, despite a limited number of previous studies, there are indications that the frequency of high-intensity Europe-impacting PTCs may increase under anthropogenic climate change (Haarsma et al. 2013; Baatsen et al. 2015). However, these studies have a very small sample size and rely on one set of simulations. Further studies have also indicated an increased PTC risk to Europe (e.g., Liu et al. 2017; Michaelis and Lackmann 2019), although these studies also each rely on a single model, and Europe was not their primary focus. Multi-model studies have been conducted on TCs (Roberts et al. 2020b) and ET (Baker et al. 2022) in the North Atlantic, but in such cases, there was not a focus on Europe directly. A multi-model study is necessary to assess the uncertainty in the projected changes in Europe-impacting PTCs, and this is yet to be undertaken. High-resolution climate model ensembles such as HighResMIP (Haarsma et al. 2016) only extend to 2050, and any warming signal and climate change-induced PTC changes may be limited as a result. Some lower resolution climate models, including those in the Coupled Model Intercomparison Project version 5 (CMIP5), have been shown to simulate North Atlantic TCs, although biases remain due to model resolution and biases in large-scale environmental fields important for TCs

(Camargo 2013). While low resolution models will not adequately simulate the structure of TCs, these models are yet to be scrutinised in terms of their European PTC climatologies and it is currently unknown whether models of such resolution can inform our understanding surrounding future changes to European PTC risk.

1.8. Thesis Aim, Research Questions and Structure

The main aim of this thesis is to further our understanding of the hazards posed to Europe by PTCs, and the factors (environmental and cyclone-specific) governing their development, variability, and projected changes. The main research questions that will be answered are as follows:

> **Q1**: How do the intensities of PTCs compare to the intensities associated with the broader class of midlatitude cyclones over Europe?
>
> **Q2**: What factors control the interannual variability in the number of TCs entering the midlatitudes?
>
> **Q3**: Why do some TCs that enter the midlatitudes reach Europe?
>
> **Q4**: How are PTCs represented by CMIP6 climate models, and how is their frequency projected to change in the future?

Research question 1 concerns the risk presented by PTCs in the present climate with reference to the overall population of Europe-impacting cyclones. Research questions 2 and 3 concern the lifecycle of Europe-impacting PTCs, and research question 4 concerns the representation of PTCs in state-of-the-art climate models, and the projected changes in their impacts over Europe in the future.

The remainder of this thesis will be structured as follows:

Chapter 2: In this chapter, datasets used in the following chapters will be introduced and discussed. Methods of TC identification, including tracking, will be discussed.

Chapter 3: This chapter presents a climatological analysis of cyclones (PTCs and midlatitude cyclones, MLCs) over Europe. This includes an investigation into the maximum intensities of PTCs over Europe compared to the broader class of Europe-impacting MLCs and a discussion about the risk posed by PTCs over Europe in the

present climate. This chapter has been published in full in *Geophysical Research Letters* (Sainsbury et al. 2020).

Chapter 4: In this chapter the interannual variability of North Atlantic TCs which reach the midlatitudes – hereafter referred to as 'recurving TCs' – is investigated. The role played by the interannual variabilities of TC frequency in the North Atlantic basin and the seasonal mean steering flow are investigated and quantified using a composite analysis and through the construction of a regression model. This chapter has been published in full in *Journal of Climate* (Sainsbury et al. 2022a).

Chapter 5: Here we investigate why some recurving North Atlantic TCs reach Europe. In particular, the differences in cyclone structure and surrounding environment associated with the recurving TCs which reach Europe are investigated using a composite analysis. Further attention is paid to the roles of TC intensity during and prior to extratropical transition, and reintensification post-ET. This chapter has been accepted for publication in *Monthly Weather Review* (Sainsbury et al. 2022b).

Chapter 6: This chapter presents a critical review of CMIP6 models' ability to simulate TCs and Europe-impacting PTCs, using only those models which simulate the observed TC and PTC climatology reasonably compared to reanalyses. An investigation into the projected changes in Europe-impacting PTCs is undertaken. This chapter is under review with *Weather and Climate Dynamics* (Sainsbury et al. 2022c).

Chapter 7: Here, the main results of the thesis are discussed, and necessary future work is described.

Chapter 2

Datasets and Methods

Chapter 2 contains a description of the datasets and methodology used in this thesis. Section 2.1 contains an overview of observational best track datasets, reanalysis products, and climate models used. Section 2.2 contains a description of the tracking methodology. Section 2.3 describes the TC identification methods which are employed throughout this thesis, including a discussion on their advantages and limitations. Section 2.4 contains an explanation of spatial cyclone statistics calculations.

2.1. Datasets

2.1.1. Reanalyses

A reanalysis is a 'best guess' of previous weather conditions. By making use of a modern dynamical core and assimilation system, a reanalysis allows for the reforecast of the historical state of the atmosphere, constrained by observations, but with modern technologies. Reanalyses are therefore a useful tool to utilise for climatological studies because they provide a gridded dataset which aims to be homogeneous in space and time. However, while the dynamical core and assimilation system used are constant throughout the reanalysis, the assimilated observations in many reanalyses do change over time (including in ERA5 and MERRA2 which are used in this thesis) to make use of increasing observational capabilities.

2.1.1.1. ERA5

The European-Centre for Medium-Range Weather Forecasting (ECMWF) 5th reanalysis (ERA5, Hersbach et al. 2020) is utilised in chapters 3-6. The ERA5 reanalysis has a horizontal resolution of approximately 31 km (spectral resolution of T639) and contains 137 vertical levels (with a model lid at 1hPa), making it one of the highest resolution global reanalyses. ERA5 uses a modern 4-dimensional variational data assimilation scheme (4D-Var) which, along with resolution has previously been shown to drive improvements in the representation of TC location, structure, and intensity in other reanalyses (Hodges et al. 2017; Murakami 2014). ERA5 is based on Cycle 41r2 of the ECMWF's Integrated Forecasting System (IFS), which was operational in 2016.

ERA5's reforecast from 1979 to 2019 has reduced anomaly correlation scores compared to ERA-Interim – ERA5's predecessor – throughout the Northern and Southern hemispheres (Figure 2.1). Observations of radiance, ground-based radar composites, column ozone, surface pressure and aircraft temperature are bias corrected using linear bias correction models within the variational data assimilation system, and other observational data (altimeter, scatterometer and radiosonde) is bias-corrected independently (Hersbach et al. 2020).

While the ERA5 back-extension (ERA5-BE) extends ERA5 back from 1979 to 1950 and is currently available, it has not been utilised in this study. In ERA5 (1979 onwards), tropical cyclone observations from IBTrACS (section 2.1.2) are not assimilated. In ERA5-BE, IBTrACS data were sub-optimally assimilated, giving too much weight to the observations (Bell et al. 2021). The result of this non-optimal assimilation is that some tropical cyclones have simulated surface pressures which are much too low in ERA5-BE. This also introduces a discontinuity between the 1950-1978 period and the 1979- period. For these reasons, ECMWF explicitly state that ERA5-BE should not be used for the analysis of tropical cyclones (Bell et al. 2021). Therefore, the ERA5-BE is not considered in this thesis.

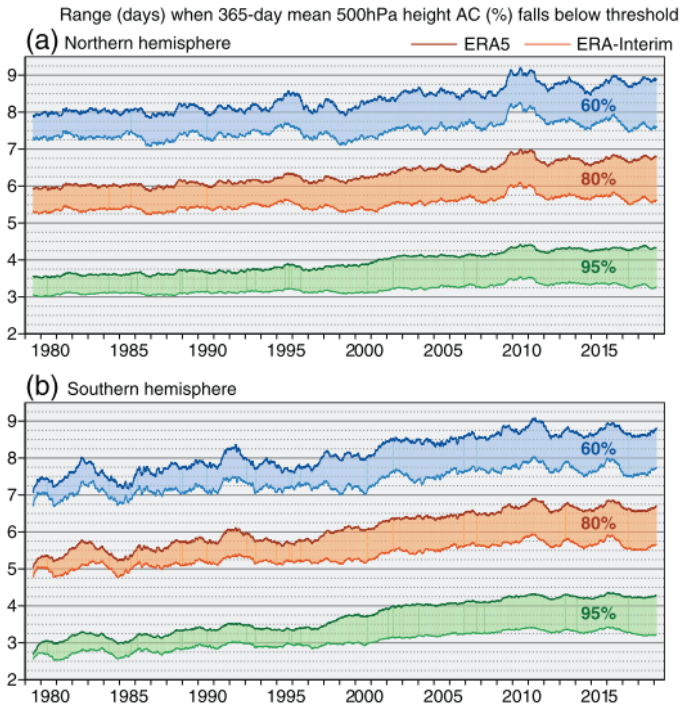

Figure 2.1. Lead time (in days) at which the running 365-day mean anomaly correlations of 500 hPa geopotential height reach 95% (green), 80% (orange) and 60% (blue), for (a) the extratropical Northern and (b) Southern Hemispheres, from 1979 onwards. Thin lines represent ERA-Interim, thicker lines represent ERA5. Shading denotes the improvement found in ERA5 relative to ERA-Interim. Figure and caption adapted from Hersbach et al. (2020) (Figure 1 therein). Reproduced with permission of the licensor through PLSclear.

2.1.1.2. MERRA2

The Modern-Era Retrospective analysis for Research and Applications, version 2 (MERRA2, Molod et al. 2015; Gelaro et al. 2017) is also utilised in this thesis to investigate the uncertainty in results associated with the choice of reanalysis. MERRA2 has a horizontal resolution of approximately 50 km and contains 72 vertical levels (with a model lid of 0.01 hPa). MERRA2 uses the GEOS 5.12.4 3D-Var data assimilation system, which is comprised of the GEOS atmospheric model and GSI analysis scheme. Satellite radiance observations, aerosol optical depth, and aircraft temperature measurements are bias corrected during assimilation (Gelaro et al. 2017). MERRA2 is available from 1980 onwards, providing a large period of overlap for comparison with ERA5 data. Like all reanalyses, tropical cyclone intensity is underestimated in MERRA2 due to the relatively coarse resolution. However, MERRA2 has been shown to capture tropical cyclone characteristics globally to a similar accuracy as other reanalyses (Hodges et al. 2017).

2.1.2. Best Track

Observational best track datasets such as the International Best Track Archive for Climate Stewardship (IBTrACS) version 03r10 (Knapp et al. 2010) and the HURricane DATabase Version 2 (HURDAT2, Landsea and Franklin, 2013) contain information of all observed TCs globally and in the North Atlantic/East Pacific respectively. Information is generally provided 6-hourly and contains position (latitude, longitude), sea level pressure and maximum 1-minute sustained 10 m wind speed associated with all TCs. Position information is obtained using satellite products to identify the location of the low-level centre, and wind speeds are obtained from satellite products or in-situ observations (i.e., dropsondes from reconnaissance missions). HURDAT2 is the North Atlantic/East Pacific contribution to IBTrACS, and so for TC studies in the North Atlantic the two contain the same information. Best track datasets are valuable as they contain

observed TC intensity information, which is often significantly biased in other datasets such as reanalyses.

In the North Atlantic it is the responsibility of the National Hurricane Center (NHC) to record TC position and intensity, which is then used to populate HURDAT2 and IBTrACS. However, operational centres usually only provide this information for the tropical phase of the cyclone's lifecycle. A tropical cyclone is usually not tracked by forecasters after completing extratropical transition unless it poses an immediate risk within the operational centre's region of responsibility. Therefore, HURDAT2 and IBTrACS primarily only contain data for the tropical phase of the cyclones' lifecycle, and best track data alone is therefore of limited use for analysis on the post-tropical stage of the cyclone's life (e.g., Hart and Evans, 2001). In this thesis, this issue is addressed by tracking cyclones in a reanalysis and performing spatiotemporal track matching (section 2.3.1).

HURDAT2 and IBTrACS are inhomogeneous in both space and time due to changes in observational capabilities and analysis techniques (Knapp et al. 2010). HURDAT2 provides TC information from 1850 onwards, but at the start of the record TCs were only identified if they made landfall in a populated region, or if a ship passed through or close by to the cyclone. The HURDAT reanalysis project is currently revisiting the observational data archive and has identified a large number of previously unidentified storms (Hagen et al. 2012; Delgado et al. 2018). For more recent decades in HURDAT2, the issue of inhomogeneity is less significant as satellites allow for coverage of the entire North Atlantic. However even in the post-satellite era, there are inhomogeneities due to policy decisions regarding the inclusion of North Atlantic subtropical cyclones in HURDAT2 and IBTrACS (which were not included from 1987-1995), along with improved forecasting observations and techniques which allow for identification of weak, short-lived TCs (C. Landsea, personal communication). There are also uncertainties associated with TC intensities, as satellite derived intensity estimates are not perfect, and aircraft reconnaissance is not always available (Landsea and Franklin 2013). In addition, the eastern boundary of the NHC area of responsibility was only extended eastward from 35°W to the coasts of Africa and western Europe in 2005 (Rappaport et al. 2009), possibly introducing more inhomogeneities to the observational record for TC tracks.

2.1.3. CMIP6 Models

Data from the Coupled Model Intercomparison Project phase 6 (CMIP6, Eyring et al. 2016) are utilised in chapter 6. The models which are considered have horizontal resolutions ranging from ~50 km (CNRM-CM6-1-HR) to ~200 km (KIOST-ESM) in the atmosphere, and ~0.25° (CNRM-CM6-1-HR, HadGEM3-GC31-MM) to ~1° (MIROC6, IPSL-CM6A-LR) in the ocean. The models have between 32 (KIOST-ESM) and 91 (CNRM-CM6-1-HR) vertical levels in their atmospheric model. Data from the fully-coupled historical simulations between 1984 and 2014 are used. Fully-coupled future simulations under the SSP5-85 scenario are used between 2069 and 2099. These two periods are chosen as they are long enough not to be affected by interannual variability, but short enough to investigate the late-century projected changes, where the climate change signal is largest. These CMIP6 models were chosen for further analysis as they simulate a median North Atlantic TC frequency greater than 6.4 TCs per year, which is the average number of North Atlantic hurricanes (TCs with winds >= 33 m s^{-1}) observed per year in HURDAT2 between 1950 and 2014. Further specifications of the CMIP6 models used in this thesis can be found in Table 2.1.

Model	Reference	Ens. members (Hist/SSP5-85)	Atmosphere model resolution	Ocean model resolution	Vertical levels (+ model lid) (atmos.)	Vertical levels (ocean)
CNRM-CM6-1-HR	(Voldoire et al. 2019)	1/1	~50 km	~0.25°	91 (0.01hPa)	75
HadGEM3-GC31-MM	(Andrews et al. 2020)	1/1	N216 (~60 km)	~0.25°	85 (85km)	75
KIOST-ESM	(Pak et al. 2021)	1/1	~200 km	~100 km	32 (2 hPa)	50
MIROC6	(Tatebe et al. 2018)	10/3	T85 (~1.4°)	~1°	81 (0.004hPa)	63
IPSL-CM6A-LR	(Boucher et al. 2020)	32/1	~157 km	~1°	79 (80km)	75

Table 2.1. Summary of the CMIP6 models used in this study, including model name (column 1), reference to model development (column 2), number of ensemble members used (column 3), atmospheric model resolution (column 4), ocean model resolution (column 5), and number of vertical layers in the atmosphere (column 6) and ocean (column 7) models.

2.2. Cyclone Detection and Tracking

This thesis makes extensive use of TRACK-1.5.2 (Hodges 1994, 1995, 1999), a feature tracking algorithm that allows cyclones to be identified and tracked in gridded datasets such as reanalyses, numerical weather prediction and climate models. In reanalyses, tracking is performed using the 6-hourly spectrally-filtered (T63 resolution, ~200 km in the midlatitudes) relative vorticity (Hodges and Emerton 2015) which has been vertically averaged over the 600-, 700- and 850 hPa levels. Due to a lack of data availability, tracking in CMIP6 models (chapter 6) is performed on the 850 hPa relative vorticity field, spectrally filtered to a T42 (~300 km in the midlatitudes) resolution (Bengtsson et al. 2007a). In all cases, planetary-scale waves (waves with a wavenumber < 6) are removed to isolate the relevant spatial scale for tracking and spectral tapering (Sardeshmukh and Hoskins 1984) is used to suppress noise. Features with a vorticity anomaly exceeding 0.5×10^{-5} s^{-1} are initially identified on the grid, and then refined to find the off-grid locations using B-spline interpolation and maximum ascent optimization (Hodges 1995), which results in smoother tracks. These feature points are then initialised into tracks using a nearest neighbour method. These tracks are then refined by minimising a cost function for track smoothness, forwards and backwards in time, subject to adaptive constraints for track smoothness and displacement distance in a time step (Hodges 1999). Finally, cyclones lasting for longer than 2 days are retained as cyclones for further analysis. Cyclone detection and tracking is performed to identify all cyclone tracks in a gridded dataset, and TC identification (section 2.3) is performed post-tracking.

Additional environmental fields can be sampled along the cyclone tracks and added to the track files. Mean sea level pressure minima are attached to each track at each 6-hourly time step by sampling the full resolution MSLP reanalysis data along the cyclone tracks. The nearest pressure minima within a 5-degree radius (geodesic) spherical cap of the vorticity centre is used, which is determined using B-spline interpolation and

steepest descent minimisation. The maximum 10 m winds in a 6-degree cap of the vorticity centre are identified using a direct grid point search.

TRACK is a widely used tool for detecting and tracking cyclones in gridded datasets such as reanalyses (e.g., Baker et al. 2021; Hodges et al. 2017; Gramcianinov et al. 2020) and climate models (e.g., Studholme et al. 2015; Vidale et al. 2021; Roberts et al. 2020).

2.3. TC Identification Methods

The cyclone detection and tracking methodology described in section 2.2 allows for the identification of all cyclone tracks globally. A second step can then be undertaken to identify the tracks which correspond to TCs. The method of tracking cyclones in gridded datasets and then identifying the TCs post-tracking, rather than identifying and tracking at the same time, is utilised in many studies (e.g., Hodges and Emerton 2015; Feng et al. 2021). It is advantageous as it allows for the identification of the entire lifecycle of the TC without needing to stitch together the precursor, tropical phase and extratropical phase of the cyclone unlike other tracking schemes (e.g., Ullrich et al. 2021). Observational best track datasets often only contain information on the TC during the tropical phase of its life. Cyclone tracking and TC identification therefore allows for studies on the precursor and post-tropical stages of the TCs life to also be undertaken, which is of crucial importance in this thesis. Three methods are used to objectively identify TCs in this thesis, which are explained in further detail below.

2.3.1. Spatiotemporal Track Matching

Spatiotemporal track matching (Hodges et al. 2017) allows for the identification of cyclones which have been tracked in reanalyses and models which correspond to observed TCs. This method is utilised in chapters 3-5. A reanalysis cyclone track matches an observed TC track (for example, a track in HURDAT2) if the mean instantaneous separation distance between the observed TC track and the reanalysis cyclone track is less than 4 geodesic degrees during the period for which the tracks have temporal overlap. If more than one reanalysis cyclone track meets this criterion for an observed TC track, then the reanalysis cyclone track with the smallest mean

separation distance with respect to the observed TC track is identified as the TC track. This method allows for the identification of all observed TCs which are simulated in a reanalysis, without the need for subjective criteria based on intensity or structure. This method of track matching is chosen because it uses the geodesic distance between two tracks and is therefore more suitable when considering global data on a sphere than alternative spatiotemporal distance measures (e.g., Blender and Schubert 2000) which use Euclidian distances.

This method of TC identification works best when used in conjunction with a high-quality observational best track dataset. The benefit of this method is that it allows for the identification of cyclones which have been designated by forecasters as TCs (and therefore are included in best track datasets), and therefore has a low number of 'false positives' – cyclones which have been identified as TCs even though they have not been identified as TCs by forecasters (when treating best track as the 'truth'). The limitations of this TC identification method include the need for high-quality, homogeneous observational TC data, which is not the case in any basin, but may be close in the North Atlantic post-satellite era. This also means that this method cannot be applied to climate models, which do not simulate observed TCs because they are free-running models, unconstrained by observations.

2.3.2. Objective Identification (Warm Core Test)

TCs are also identified in gridded datasets such as reanalyses and climate models using criteria reflecting the known properties of TCs, namely intensity and the presence of a warm core. This method has been applied in chapters 3 and 6 of this thesis. For a cyclone track to be identified as a TC, the following criteria must be met (Hodges et al. 2017):

1) The first point in the cyclone track (genesis) must be equatorward of 30°N
2) The T63 850 hPa relative vorticity must exceed $6x10^{-5}$ s^{-1}
3) The difference in T63 relative vorticity between the 850 hPa and 200 hPa levels must exceed $6x10^{-5}$ s^{-1} to indicate the existence of a warm core via thermal wind balance

4) A T63 relative vorticity signature must exist at each pressure level between 250- and 850 hPa to indicate a coherent vertical structure through the troposphere

Criteria 2-4 must be met for at least 4 consecutive time steps (one day) over the ocean. In chapter 3, reanalyses are used in which there are many available vertical levels for relative vorticity. In this case, criteria 4 is applied to the 850-, 700-, 600-, 500-, 400-, 300- and 250 hPa pressure levels. Less vertical levels are available for CMIP6 models, and so the criteria are only applied to the 850-, 500- and 250 hPa levels.

There are some downsides to this method of TC identification. If best track TC datasets are treated as 'truth', then this method of TC identification does lead to a number of false alarms: cyclones which have been identified as TCs, but which are not present in best track datasets. This may be the result of forecaster subjectivity on what constitutes a TC (and therefore what gets included in best track datasets), and the existence of hybrid cyclones which have some tropical characteristics which are falsely identified as TCs by this method. As with other methods of TC identification, some observed TCs are not identified as TCs using this method (misses), possibly due to poor structural representation in reanalyses. A balance can be found between the hit rate (the number of observed TCs identified by this method) and false alarm rate (the number of identified cyclones which are not present in observational datasets) using the latitude constraint (criteria 1). A threshold of 30°N allows for the identification of most observed TCs, which often form equatorward of 30°N, and limits the number false positives, which often occur in the subtropics and in winter months. However, this presents its own issues. For example, ex-hurricane Ophelia – one of the strongest PTCs to impact Europe in the last 40 years and a great motivation for this thesis – formed at approximately 31°N, and therefore is not identified as a TC using this methodology, unless the latitude constraint is removed. Future poleward expansion of the tropical genesis area (e.g., Haarsma et al. 2013) may allow more TCs to form poleward of 30°N in the future. As a result, a decrease in the fraction of cyclones identified as TCs may occur in the future with warming, and any research focussed on climate trends which use this method of TC identification should test the sensitivity of

results to the latitude constraint. In this thesis, the latitude constraint of 30°N is kept when this method of TC identification is used (chapters 3 and 6).

Despite the limitations which have been outlined, this method allows for TC identification where high-quality observational TC track data is not available and has been shown to be in good agreement with TCs identified using spatiotemporal track matching (section 2.3.1). Bourdin et al. (2022) recently compared this TC identification method with three other TC trackers. This method was found to have the highest hit rate (percent of IBTrACS TCs identified in ERA5), but also has the second highest false alarm rate. The IBTrACS TCs which are missed tend to be weak TCs, which may not be well resolved in reanalyses (Hodges et al. 2017).

2.3.3. Cyclone Phase Space

A third method to identify TCs in gridded datasets is the cyclone phase space (CPS, Hart 2003). This method was originally designed to investigate extratropical transition and has been used in numerous studies to study ET of TCs (e.g., Bieli et al. 2019a, b; Arnott et al. 2004; Wood and Ritchie 2014). The primary use of the CPS in previous studies is to investigate the lifecycle of the thermal structure of transitioning TCs, and CPS is not routinely utilized for TC identification. However, as it allows for cyclones to be classified based on their thermal structure and symmetry, the CPS is investigated in conjunction with track matching (section 2.3.1) and the warm core test (section 2.3.2) for TC identification in chapter 3. The thermal asymmetry, B, upper-level thermal wind, $-V_T^U$, and lower-level thermal wind, $-V_T^L$ can be calculated using the geopotential height fields at 300-, 600- and 900 hPa:

$$B = h\left(\overline{Z_{600} - Z_{900}|}_R - \overline{Z_{600} - Z_{900}|}_L\right), \tag{2.1}$$

$$-V_T^L = \frac{\partial(\triangle Z)}{\partial \ln p}\Big|_{600hPa}^{900hPa}, \tag{2.2}$$

$$-V_T^U = \frac{\partial(\triangle Z)}{\partial \ln p}\Big|_{300hPa}^{600hPa}, \tag{2.3}$$

Where Z is the geopotential height, and overbar denotes the area mean over a semicircle relative to the cyclone's direction of travel (L = to the left; R = to the right), with a radius of 5 degrees (geodesic). h = 1 in the Northern Hemisphere. $\triangle Z =$

$Z_{max} - Z_{min}$ and Z_{max}, Z_{min} are the minimum and maximum respective geopotential heights at a given pressure level within a 5-degree (geodesic) cap about the cyclone center. $-V_T^L$ and $-V_T^U$ can be calculated just using the geopotential height at 300-, 600- and 900 hPa (as in Baker et al. 2021), but if more vertical levels are available, a linear regression of $\triangle Z$ can instead be used between these layers (e.g., Bieli et al. 2019; Hart 2003).

Negative values of $-V_T$ indicates a cold core in the tropospheric region in consideration, and positive values indicate a warm core. TCs have a troposphere-deep warm core (positive thermal wind throughout the troposphere) and are not frontal (low thermal asymmetry). Therefore, cyclones are identified as TCs in this thesis (chapter 3) if $-V_T^U > 0$, $-V_T^L > 0$ and $B \in [-10\ \mathrm{m}, 10\ \mathrm{m}]$ for 4 consecutive time steps (1 day), consistent with the thresholds on CPS parameters used to identify ET in previous studies (Hart 2003; Evans and Hart 2003; Baker et al. 2021). As with the warm core test, there are limitations to using this method. In coarse-resolution datasets (~horizontal resolution of ~100km), many weak, short-lived TCs do not contain an upper-level warm core (Evans and Hart 2003). This is likely due to the datasets having a horizontal resolution which is too low to resolve the inner structure of TCs completely. This leads to an underestimation of TC activity when identifying TCs using the CPS method. Another issue with this method is false positives. Some cyclones which do not form in the tropics (and are not present in observational best track datasets) are identified as being TCs. For example, some warm seclusion cyclones and weak, transient features are identified as being TCs using this method (Hart 2003). To overcome this in chapter 3, additional criteria are applied. The criteria on thermal wind and asymmetry must be met in the domain 120°W-10°W, 0-45°N, and the 925 hPa wind must exceed 17 m s^{-1} for at least one of the 4 consecutive time steps that the upper and lower-level thermal wind, and thermal asymmetry, meet the criteria. This helps to remove many of the spuriously identified TCs.

The benefit of the CPS above the warm core method is that it allows for TCs forming poleward of 30°N – such as Ophelia – to be identified. However, it fails to identify a number of weak TCs and therefore has a lower hit rate than the warm core test when compared to observational TC datasets.

2.4. Spatial Statistics

Spatial statistics related to cyclone tracks - such as track, genesis, and lysis densities - are presented in chapters 3-6. These are calculated using the spherical kernel method of Hodges (1996). This method allows for statistics to be calculated directly on the sphere, without the problems inherent to histogram-type approaches – namely biases, arising due to distortion associated with grid-box binned data on a projection (Hodges 1996). Track density represents the number of cyclones tracking through a unit area per year. Genesis and lysis densities represent the number of cyclones forming and decaying in a unit area per year. In all instances, the unit area is equivalent to a spherical cap with a radius of 5 degrees. A 5-degree cap size is chosen as to smooth the spatial statistics (which can be noisy, especially with a small sample size), but not to the extent that extrema of the densities become significantly damped.

The above-mentioned spatial statistics allow us to investigate the spatial distribution of cyclone tracks as number densities. However, in some instances, it may be of interest to compare cyclone densities in one region with another region, or to look at spatial statistic differences between two sets of cyclone tracks which may have substantially different sample sizes. In such cases, we calculate normalized spatial statistics by dividing the densities by the sample size, i.e., the number of tracked cyclones.

Chapter 3

How Important are Post-Tropical Cyclones for European Windstorm Risk?

Chapter 1 highlights evidence of many high-impact PTCs impacting Europe throughout recent decades. Despite the loss of life, economic damage and national wind records associated with PTCs, their risk to Europe, arising from a combination of occurrence frequency and impact, is not well understood from a climatological perspective. Without this understanding, it is difficult to put future projections of Europe-impacting PTCs (e.g., Haarsma et al. 2013; Baatsen et al. 2015) into perspective. For example, the implications of a 4-6-fold increase in the frequency of hurricane-force PTCs over Europe (Haarsma et al. 2013) depends on their present climate risk. The aim of this chapter is to quantify the wind risk associated with PTCs across Europe by comparing the distribution of PTC wind speeds to the wind speeds associated with cyclones more generally over Europe.

This chapter has been published in *Geophysical Research Letters* under the following reference (Sainsbury et al. 2020):

Sainsbury, E. M., R. K. H. Schiemann, K. I. Hodges, L. C. Shaffrey, A. J. Baker, and K. T. Bhatia, 2020: How Important Are Post-Tropical Cyclones for European Windstorm Risk? *Geophys. Res. Lett.*, **47**, https://doi.org/10.1029/2020GL089853.

Abstract

Post-tropical cyclones (PTCs) extend many hazards associated with tropical cyclones (TCs) to the midlatitudes. Despite recent high-impact cases affecting Europe such as Ophelia, little research has been done to characterize the risk of PTCs. Here we compare the climatologies and intensity distributions of midlatitude cyclones (MLCs) and PTCs in the North Atlantic and Europe by tracking cyclones in the ERA5 reanalysis. Considering hurricane-season cyclones impacting Northern Europe, PTCs show a significantly higher mean maximum intensity than MLCs but make only a small contribution to total windstorm risk. Our results show that a disproportionately large fraction of high-intensity cyclones impacting Europe during hurricane season are PTCs. The fraction of PTCs impacting N Europe with storm-force (>25 m s^{-1}) winds is approximately ten times higher than for MLCs. Less than 1% of cyclones impacting Northern Europe are identified to be PTCs. This rises to 8.8% when considering cyclones which impact with storm-force winds.

3.1. Introduction

The post-tropical stage of a recurving tropical cyclone (TC) can result in hazardous weather such as high winds and heavy precipitation in the midlatitudes, exposing areas which infrequently see such events (Evans et al. 2017; Jones et al. 2003). Recurving TCs and their interaction with the upper-level midlatitude flow can also have severe consequences for downstream predictability of the midlatitude flow (Grams and Blumer 2015; Grams et al. 2015; Keller et al. 2019). They have also been shown to increase the likelihood of downstream extreme weather (Pohorsky et al. 2019), posing challenges for risk management.

Recent papers have investigated how post-tropical cyclone (PTC) impacts and frequency may change as a result of climate change (Baatsen et al. 2015; Haarsma et al. 2013; Liu et al. 2018; Michaelis and Lackmann 2019; Semmler et al. 2008a, 2008b). Baatsen et al. (2015) and Haarsma et al. (2013) show that the number of severe autumn European windstorms is likely to increase in near future and future climates, with most of the increase due to PTCs. Liu et al. (2018) and Semmler et al. (2008a,

2008b) find that the fraction of TCs which undergo extratropical transition is likely to increase in the North Atlantic under RCP 4.5, the SRES-A2 emission scenario, and a 1K increase in SSTs respectively. Michaelis and Lackmann (2019) find that the number of extratropical transition events may increase by 40% by the year 2100 under RCP 8.5. Without an understanding of the risks posed by PTCs for Europe in the current climate, it is difficult to deduce the consequence of a future change in PTC frequency or intensity.

High-impact European events such as the PTCs Debby (Laurila et al. 2020), Floyd (Atallah and Bosart 2003) and Ophelia (Rantanen et al. 2020; Stewart 2018) have revealed the potential risk associated with PTCs in Europe. In particular, Ophelia attracted widespread scientific and public attention after impacting Ireland in October 2017 as Ireland's most damaging storm in over 50 years (Stewart 2018). Climatologies of North Atlantic TCs suggest that between 46% (Hart and Evans 2001) and 68% (Studholme et al. 2015) undergo extratropical transition, with other climatologies falling within this range (Bieli et al. 2019a; Zarzycki et al. 2017). Further to this, Hart and Evans (2001) suggest that over half of these PTCs reintensify in the midlatitudes.

How important PTCs are for European windstorm risk is still an open question. It has been shown that TCs which undergo extratropical transition and develop a warm seclusion obtain the lowest pressure values over Europe of all cyclones which form in the tropics. These cyclones also reach their maximum intensity a day after reaching Europe, increasing the risk that they pose (Dekker et al. 2018). Whilst this result highlights the potential risk tropical-origin systems pose for Europe, these risks also need to be considered in the context of overall European storm risk.

Here we present a systematic comparison between PTCs and midlatitude cyclones (MLCs) for the first time, looking particularly at the risk, in terms of surface winds, that PTCs and MLCs pose for Europe. A more quantitative understanding of the risks associated with PTCs is obtained by investigating both the absolute risk posed by PTCs (such as the frequency of high-impact PTCs compared to high-impact MLCs) and also the relative risk posed by PTCs (i.e., how likely is a given PTC to be impactful, and how does this compare with a given MLC?), paying particular focus to wind speed. The specific questions we answer are:

- How does the intensity distribution of PTCs compare to that of MLCs over Europe?
- Do the intensity distributions vary spatially across the European domain?
- What fraction of high-impact wind events are caused by PTCs?

Section 3.2 contains a description of the data, the cyclone tracking algorithm used to identify the cyclones and a description of the PTC identification procedure. Section 3.3 contains the results of a climatological comparison of PTC and MLC maximum intensities for Europe and section 3.4 contains the discussion and conclusions.

3.2. Datasets and Methodology

3.2.1. Datasets

The ERA5 reanalysis (section 2.1.1.1) is used to provide vorticity fields for tracking, along with the wind and pressure fields. Data from 1979-2017 are used. The 10 m wind speed in cyclones is underestimated in ERA5, even in the midlatitudes (Fig. 3.5). Additional information on the tracks of TCs from the IBTrACS v03r10 (section 2.1.2) best track dataset, a description of which can be found in Knapp et al. (2010), is also used in this study.

3.2.2. Cyclone Detection and Tracking

Cyclone detection and tracking is performed using TRACK-1.5.2. For more information, see section 2.2. For this study, all cyclone tracks which at some point in their lifetime enter a domain defined as 10°W-30°E; 36°N-70°N, hereafter referred to as the European domain, are retained for further analysis.

3.2.3. PTC Identification Methods

Three methods are used to identify PTCs. The first method, and the focus of this paper, identifies PTCs using spatiotemporal matching between the cyclones tracked in the reanalysis and the observed TCs present in the IBTrACS dataset (section 2.3.1). All tracked cyclones not captured in IBTrACS data (and therefore not identified as PTCs) are considered MLCs. Over 95% of all Northern Hemisphere TCs recorded in IBTrACS are found in ERA5 using track matching, comparable to the reanalyses investigated in

Hodges et al (2017). The 5% of cyclones which are not identified tend to be weaker, shorter-lived TCs.

The warm core test (section 2.3.2) and cyclone phase space (CPS, section 2.3.3) are also used to identify the PTCs. In future work we will investigate how PTC impacts may change across Europe using high-resolution climate models. For this, observational data will not be available and objective methods will be utilized. The work presented here is used to verify the effectiveness of these objective methods at tracking and identifying PTCs, and to better understand their limitations. See section 3.5 for more information.

3.2.4. Statistical Maps and Analysis

Cyclone statistics are produced showing the spatial distribution of storm tracks over Europe as described in section 2.4. A 95% confidence interval is constructed and shown in Figure 3.4. This is calculated as

$$p \pm Z\sqrt{\frac{p(1-p)}{n}}, \tag{3.1}$$

where p is the proportion of cyclones in each intensity bin which are identified as PTCs, Z = 1.96 for a 95% confidence interval from a standard normal distribution, and n is the total number of cyclones in the intensity bin (i.e., PTCs + MLCs).

3.3. Results

3.3.1. Cyclone Track Density and Cyclogenesis

In this section we first compare MLCs and PTCs impacting Europe, considering cyclones forming in all months of the year. A large fraction of high-intensity MLCs impact Europe during the winter months and it is therefore necessary not only to compare MLCs and PTCs during the North Atlantic hurricane season (during which the majority of PTCs impact Europe, Fig. 3.6), but also to investigate how PTCs compare to MLCs throughout the year, including during the seasons (autumn and winter) typically associated with the highest risk for Europe. Figure 3.1a shows the track and genesis density for all MLCs impacting Europe in the ERA5 reanalysis from 1979-2017. There are two clear regions of MLC genesis and highest track density: one over the North Sea

and Scandinavia, associated with the midlatitude storm track, and another over the Mediterranean Sea. Cyclone tracks in both regions have different trajectories and associated impacts. Unlike MLCs, PTCs tend to occur in one region over Europe rather than two (Fig. 3.1b). The western side of the European domain, particularly over the UK and Ireland, sees the highest PTC activity. On average, this region experiences 1 or more PTC impacts per year, the highest density over land within the European domain. PTC activity is considerably lower towards the east of the domain.

The highest track density of PTCs occurs inside the Main Development Region for North Atlantic TCs, the region climatologically associated with high TC genesis density. PTC genesis density maxima are close to the west coast of Africa and over the Caribbean. Genesis areas to the west of Africa (and over Africa) are the result of the vorticity-based algorithm tracking the systems in the reanalysis and identifying the genesis of precursor systems (see section 2.2).

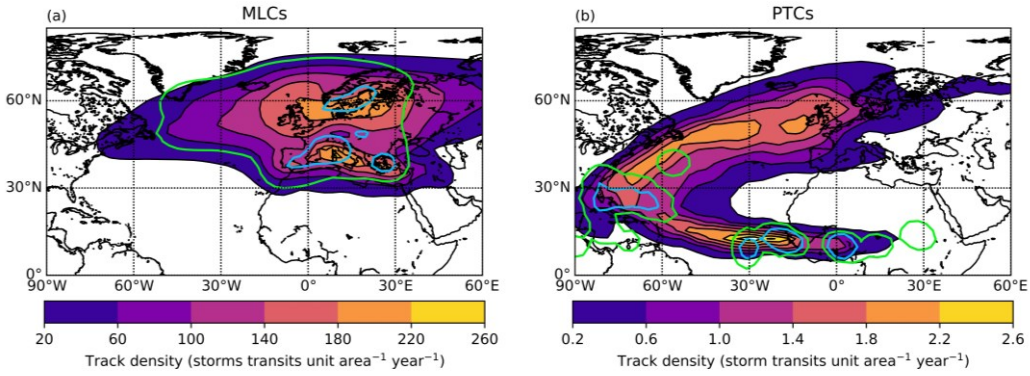

Figure 3.1. Track density (filled contours) and genesis density (open contours) of MLCs (left) and PTCs (right) impacting the European domain (10°W-30°E, 36°N-70°N) tracked in the ERA5 reanalysis from 1979-2017, all year round. Genesis contours are 8 (green) and 32 (blue) MLCs per year (left) and 0.04 (green) and 0.12 (blue) PTCs per year (right). Densities are expressed as the number of cyclones per year in a cap with a 5-degree (geodesic) radius.

3.3.2. Contribution of PTC Intensity to Annual European Windstorm Risk

We split the European domain into two subdomains: The Mediterranean (S Europe), 10°W-30°E, 36°N-48°N, and central and Northern Europe (N Europe) extending from 10°W-30°E, 48°N-70°N. This separation is based on the two centres of maximum MLC track density (Fig. 3.1a) and allows us to investigate the difference in risk associated with PTCs and the MLCs with characteristics specific to each region. N Europe contains

67 PTCs and ~13500 MLCs, and S Europe contains 27 PTCs and 11800 MLCs. Figure 3.2 shows the distributions of all PTCs and MLCs impacting Europe by considering the maximum intensity attained by each system inside the European subdomains, represented by maximum 10 m wind speed, 925 hPa wind speed and minimum MSLP. The distribution of PTCs is skewed towards higher intensities when compared to MLCs, particularly in the N Europe domain (Fig. 3.2d-3.2f). This can be seen for all three intensity metrics. PTCs are also present in high intensity bins in the tail of the distribution, suggesting that some PTCs are amongst the strongest windstorms in the climatology. Taking the mean of all tracked cyclones, PTCs have a maximum 10 m wind speed 2.1 m s^{-1} higher (17.5 m s^{-1} vs 15.4 m s^{-1}), and minimum MSLP 10.2 hPa lower (990.8 hPa vs 1001.0 hPa) than MLCs inside the whole European domain on average. PTCs also have a considerably higher median maximum 10 m wind speed (17.0 m s^{-1} vs 15.0 m s^{-1}) and highest decile intensity (for other specific values, see Table 3.1). A two-sample Kolmogorov-Smirnov (KS) test indicates that the distributions are different, significant to 99.9% for all three intensity metrics used in N Europe, and for MSLP in S Europe (p=0.05 and 0.13 for 10 m and 925 hPa wind speed in S Europe respectively). This may be expected, as MLC's have a shallower structure and generally weaker MSLP in the Mediterranean region. Significant differences are also found between the distributions of PTCs and MLCs when PTCs are instead identified using thresholds on the cyclone phase space (CPS, section 2.3.3) parameters and using T63 relative vorticity fields (warm core test, 2.3.2), with the largest separation between the distributions apparent in N Europe. (Fig. 3.7).

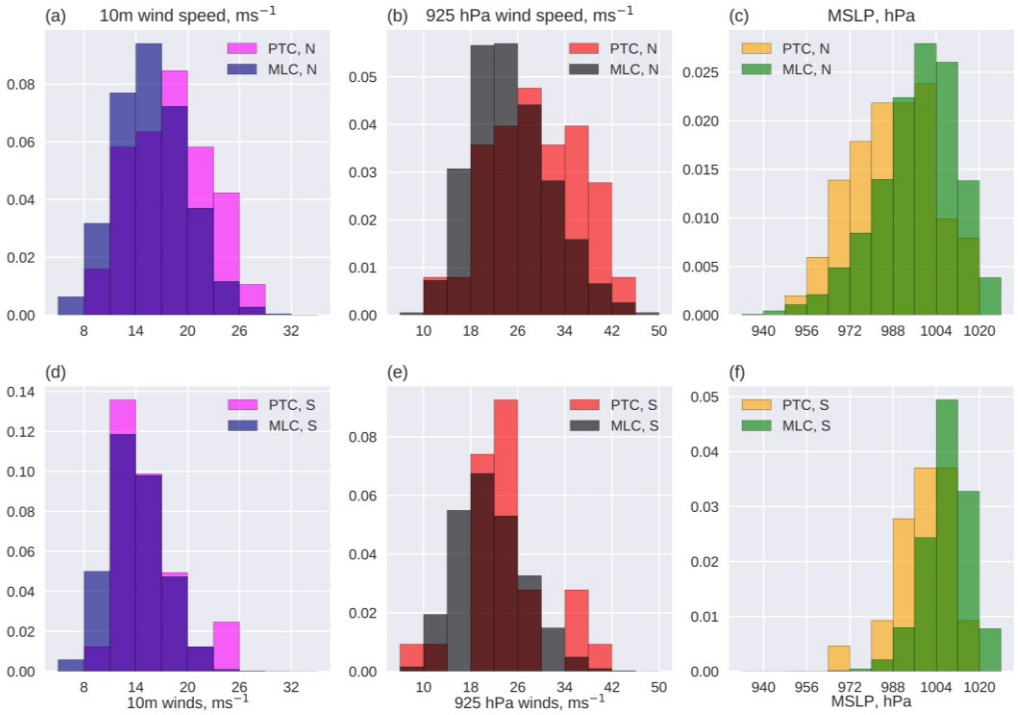

Figure 3.2. Distributions of the maximum intensity (maximum wind speed, minimum MSLP) attained by each PTC and MLC inside (a-c) the North European subdomain (10°W-30°E, 48°N-70°N) and (d-f) the South European subdomain (10°W-30°E, 36°N-48°N), using cyclones tracked through the ERA5 reanalysis all year round, 1979-2017.

3.3.3. Contribution of PTC Intensity to Hurricane-Season European Windstorm Risk

The focus of this section is on cyclones forming during the operationally defined North Atlantic hurricane season (June 1st – Nov 30th). Figure 3.3 also shows that the distribution of PTCs is skewed towards more intense cyclones. This is true for both subdomains, however, results in S Europe should be treated with caution due to a limited sample size of high-intensity PTCs (26 PTCs in total, 7 of which have maximum 10 m wind speeds in excess of 17 m s^{-1}). For N Europe, both the mean and median maximum intensity of PTCs is more than 3 m s^{-1} greater than for MLCs. In S Europe, PTCs have a mean and median maximum intensity 2.3 m s^{-1} and 2.6 m s^{-1} higher than MLCs respectively. The mean maximum wind speeds for the MLC distributions is lower in S Europe and the intensity distribution is narrower than in N Europe, with few cyclones attaining wind speeds exceeding 25 m s^{-1}. The differences between PTC and MLC mean maximum intensity is largest when considering the strongest 10% of

cyclones. The strongest decile of PTCs have 10 m wind speeds 4.2 and 3.9 m s^{-1} higher than the strongest decile of MLCs in N and S Europe respectively. 8.2% of all PTCs impacting N Europe are accompanied by storm-force winds (Beaufort scale 10, >25 m s^{-1}). For MLCs, this fraction is much lower at 0.8%, suggesting that the fraction of PTCs impacting N Europe with storm-force winds is 10.1 times higher than MLCs (95% confidence interval: 1.3-25.6). As with the data used in the construction of Figure 3.2, a two-sample KS test also shows that the distributions are significantly different. The two additional PTC identification methods yield similar results to Figure 3.3, showing a large difference between the PTC and MLC distributions in N Europe and a smaller but still significant difference in S Europe (Fig. 3.8).

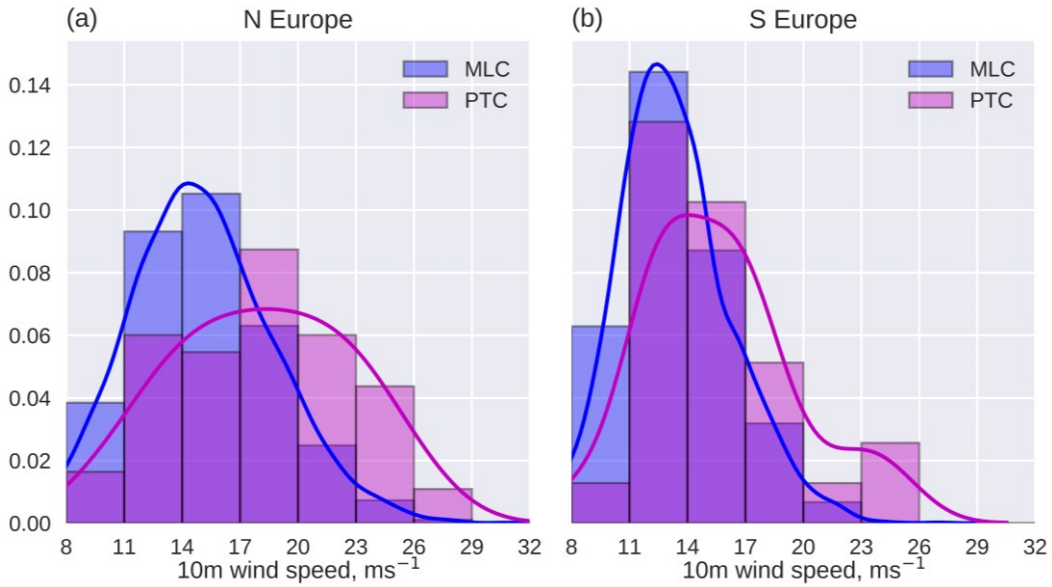

Figure 3.3. Distributions of the maximum intensity attained by each PTC and MLC inside the North Europe subdomain (10°W-30°E, 48°N-70°N) (left) and the South Europe subdomain (10°W-30°E, 36°N-48°N) (right). Gaussian kernel density estimate is overlaid for PTC and MLC distributions in both panels. All cyclone tracks forming during the North Atlantic hurricane season (June 1st – Nov 30th) are used.

Figure 3.4 shows the percentage of wind events occurring in each subdomain which are associated with PTCs. In S Europe, <1% of wind events in the lowest 4 intensity bins are associated with PTCs. This fraction increases to 12% for cyclones with a wind speed > 22 m s^{-1} (shown as the yellow bars). The sample size is small for this bin, with only 25 total cyclones recording windspeeds > 22 m s^{-1} in S Europe between 1979 and 2017, 3 of which are PTCs. This is reflected by the large range of values within the 95%

confidence interval. In N Europe, the fraction clearly varies with maximum cyclone intensity inside the subdomain. Less than 1% of cyclones which form during hurricane season and impact N Europe are PTCs overall, however 8.8% of all hurricane-season-forming cyclones which impact N Europe with storm-force winds are PTCs (Fig. 3.4, red bar at 25 m s^{-1}). The differences between the distribution of PTC and MLC maximum intensities when considering the entire European domain (not shown) is very similar to shown for N Europe for Figures 3.2, 3.3 and 3.4. Despite large uncertainty as shown by the error bars, the lower bound for the 22 m s^{-1} and 25 m s^{-1} intensity bins still exceed the upper bound for the lowest three intensity bins. The results of Figure 3.4 are supported by the alternative PTC identification methods described in section 2.3, which both show that approximately 1% of cyclones impacting N Europe during hurricane season are PTCs, but 7% of storm-force cyclones are PTCs. For S Europe, < 1% of cyclones impacting the subdomain are PTCs for all cyclones with wind speeds below 22 m s^{-1}. This rises to 8% for PTCs identified using thresholds on the cyclone phase space parameters, and to 20% for cyclones identified using T63 vorticity fields (warm core test, Fig 3.9). The variation between the 3 PTC identification methods in S Europe for high-intensity cyclones is an indication of the small sample size; however, all three methods agree that a disproportionately large fraction of high-impact events occurring in Europe during hurricane season are the result of PTCs.

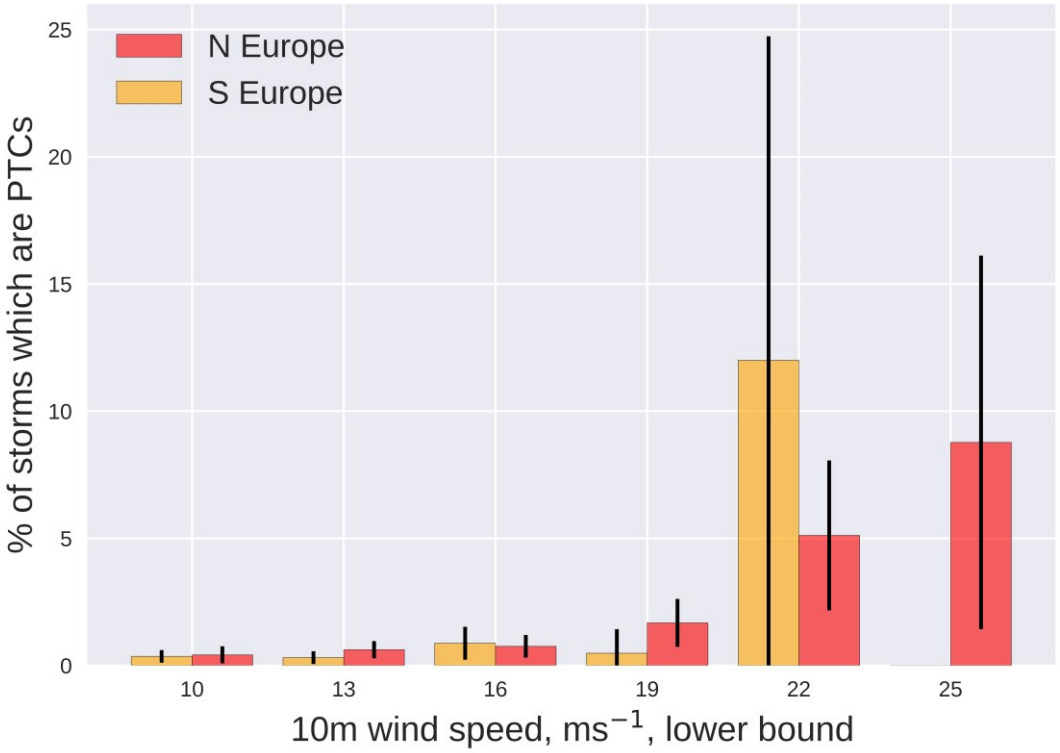

Figure 3.4. The fraction of cyclones impacting Europe which are PTCs as a function of their maximum 10 m wind speed in their respective domain. Lower bound of wind speed shown on x axis, bin width = 3. Error bars show the 95% confidence interval. All cyclone tracks forming during the North Atlantic hurricane season are used.

3.4. Discussion and Conclusions

The aim of this paper was to quantify the importance of PTCs when assessing European windstorm risk. This has been achieved by tracking all cyclones impacting Europe through the ERA5 reanalysis from 1979-2017 and identifying the PTCs using objective track matching with the IBTrACS best track dataset. The main conclusions of this study are:

- At their maximum intensity across Europe, PTCs are on average significantly more intense than MLCs. This holds true when comparing PTCs and MLCs impacting Europe overall, and when comparing cyclones which impact Europe and form during hurricane season.
- 8.2% of all N Europe impacting PTCs which form during hurricane season impact the region with storm-force winds. This fraction is only 0.8% for MLCs,

suggesting that the fraction of PTCs impacting N Europe with storm-force winds is approximately ten times greater than MLCs.

- PTCs are responsible for less than 1% of all cyclones impacting N Europe during hurricane season from 1979-2017. This rises to 8.8% when considering cyclones which impact N Europe with storm-force winds, showing that high-impact wind events during hurricane season are disproportionately caused by PTCs.

The difference in intensity between PTCs and MLCs is largest for N Europe. In this region, the differences between the distributions of PTC and MLC maximum intensities are statistically significant for all three intensity metrics used. For cyclones impacting S Europe, they are significant for the distributions of MSLP when considering all cyclones, and for the distribution of 10 m wind speeds when considering cyclones forming in hurricane season.

This study has used three different methods to identify PTCs, with the results from one method – objective track matching with IBTrACS - presented. Identification methods which use T63 relative vorticity fields and thresholds on the cyclone phase space parameters to identify PTCs support the analysis shown here and yield very similar results, highlighting the robustness of the results presented in this paper. The objective PTC identification methods show statistically significant differences between the maximum intensity distributions of PTCs and MLCs over Europe, with the largest differences between the distributions over N Europe. Both methods show that 7% of all hurricane-season-forming cyclones which impact N Europe with storm-force winds are PTCs, despite PTCs only contributing 1% of the total cyclones to impact the region.

Whilst this paper shows that PTCs are, on average, more intense than MLCs at their maximum intensity over Europe, the question remains as to why this is the case. Warm-seclusion storms (Shapiro and Keyser 1990) post-ET have been shown to have the fastest rates of reintensification (Kofron et al. 2010) and typically have the lowest sea level pressure upon impacting Europe (Dekker et al. 2018). Given the climatological track that PTCs often take over the warm waters of the Gulf stream (Fig. 3.1), along with the contribution of both baroclinic instability and latent heat release for warm-seclusion development (Baatsen et al. 2015), future work will assess whether PTCs are more likely to develop warm-seclusions than the broader class of

MLCs, potentially explaining the disproportionate impacts they cause across Europe. Future work should also investigate whether there are differences in the hazards associated with PTCs and a more 'equal' set of MLCs. For example, by sub-sampling the distribution of MLCs to have the same mean maximum intensity over Europe as the PTC sample would allow for the comparison of tail risk between the two groups while conditioning on mature, high-impact MLCs.

Despite PTCs disproportionately impacting Europe with high intensities, they are a relatively small component of the total cyclone risk in the current climate. However, only small changes are expected in MLC activity. The CMIP5 multi-model mean cyclone number over the North Atlantic basin decreases by 3.6% in DJF and 1.9% in JJA under RCP 4.5 by the end of the century, with a reduction in the number of cyclones attaining wind speeds greater than the present day 90th percentile (Zappa et al. 2013). Conversely, the number of hurricane-force (>33 m s^{-1}) storms impacting Norway, the North Sea and the Gulf of Biscay increases by a factor of 6, virtually all of which originate in the tropics (Haarsma et al. 2013). Whilst the absolute contribution of PTCs to hurricane-season windstorm risk is currently low, PTCs may make an increasingly significant contribution to European windstorm risk in a future climate.

Acknowledgments

The authors thank Rein Haarsma and an anonymous reviewer for their comments which improved the clarity of this manuscript. Thanks also to Ben Bronselaer, Ted Shepherd and Oscar Martinez-Alvarado for useful discussions which improved the quality of the paper. E. M. Sainsbury was funded by the Natural Environment Research Council (NERC) via the SCENARIO Doctoral Training Partnership (grant NE/S007261/1). R. S., K. H., A. B., and L. S. are supported by the U.K. National Centre for Atmospheric Science - Climate (NCAS-Climate) at the University of Reading. A. B. and R. S. also acknowledge PRIMAVERA funding received from the European Commission under grant agreement no. 641727 of the Horizon 2020 research programme.

Data Availability

All ERA5 reanalysis fields used in cyclone tracking (relative vorticity) and analysis (MSLP, 10 m wind speed, 925 hPa wind speed, geopotential) are freely available at the Copernicus C3S Date store (https://www.ecmwf.int/en/forecasts/datasets/reanalysis-datasets/era5). IBTrACS data is available from https://www.ncdc.noaa.gov/ibtracs/index.php?name=ib-v4-access. TRACK is available for use with permission (see http://www.nerc-essc.ac.uk/~kih/TRACK/Track.html, version 1.5.2 used).

3.5. Supporting Information

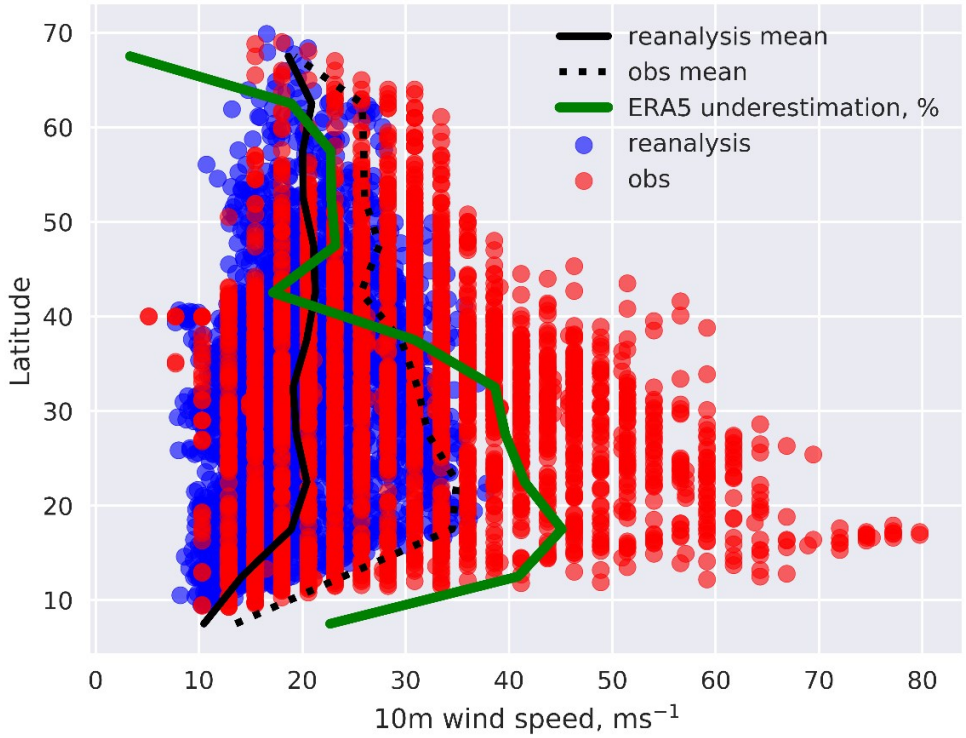

Figure 3.5. Scatterplot of the 10 m wind speed and latitude for each time step in the life of all PTCs impacting the European domain using 10 m wind speed data from the ERA5 reanalysis (blue) and analysis data from IBTrACS (red). Reanalysis storm tracks are truncated to compare the same time steps for which IBTrACS data is present.

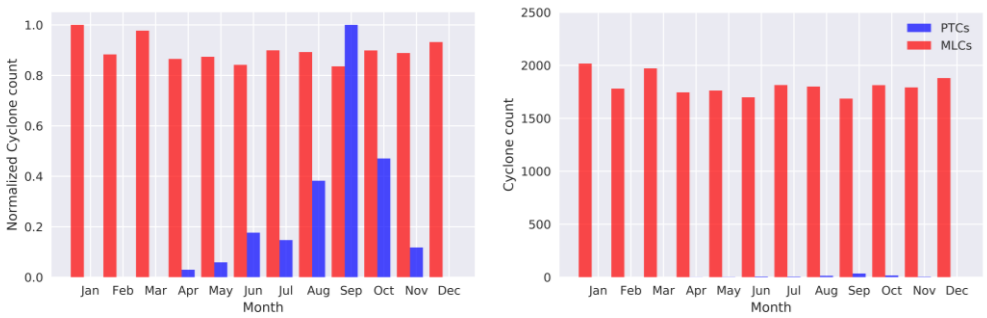

Figure 3.6. Normalized cyclone count of MLCs (red) and PTCs (blue) impacting the European domain (36°-70°N, 10°W-30°E) each month of the year (left), absolute cyclone count of MLCs and PTCs impacting the European domain each month of the year (right). Cyclones are binned by the month of genesis.

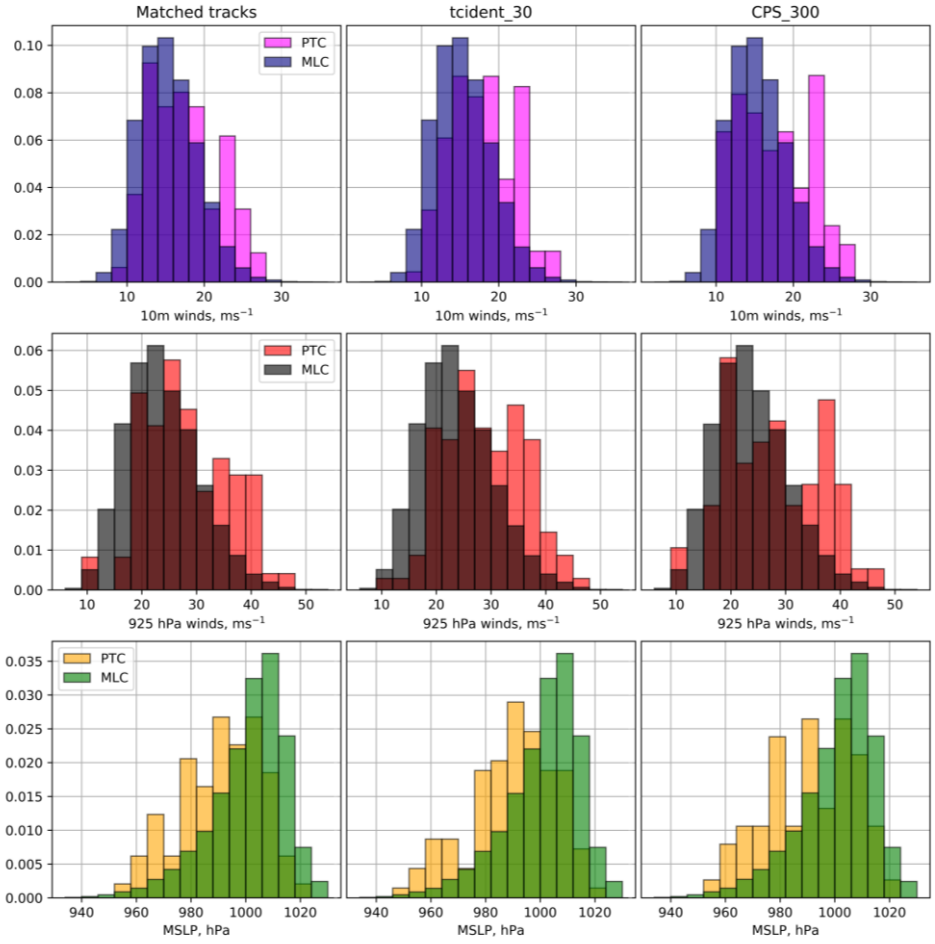

Figure 3.7. Distributions of the maximum intensity attained by each PTC and MLC inside the whole European domain using all storms tracked through the ERA5 reanalysis. tcident_30 represents the storm tracks identified as PTCs using T63 relative vorticity fields. CPS_300 represents the storm tracks identified as PTCs using thresholds on the cyclone phase space parameters.

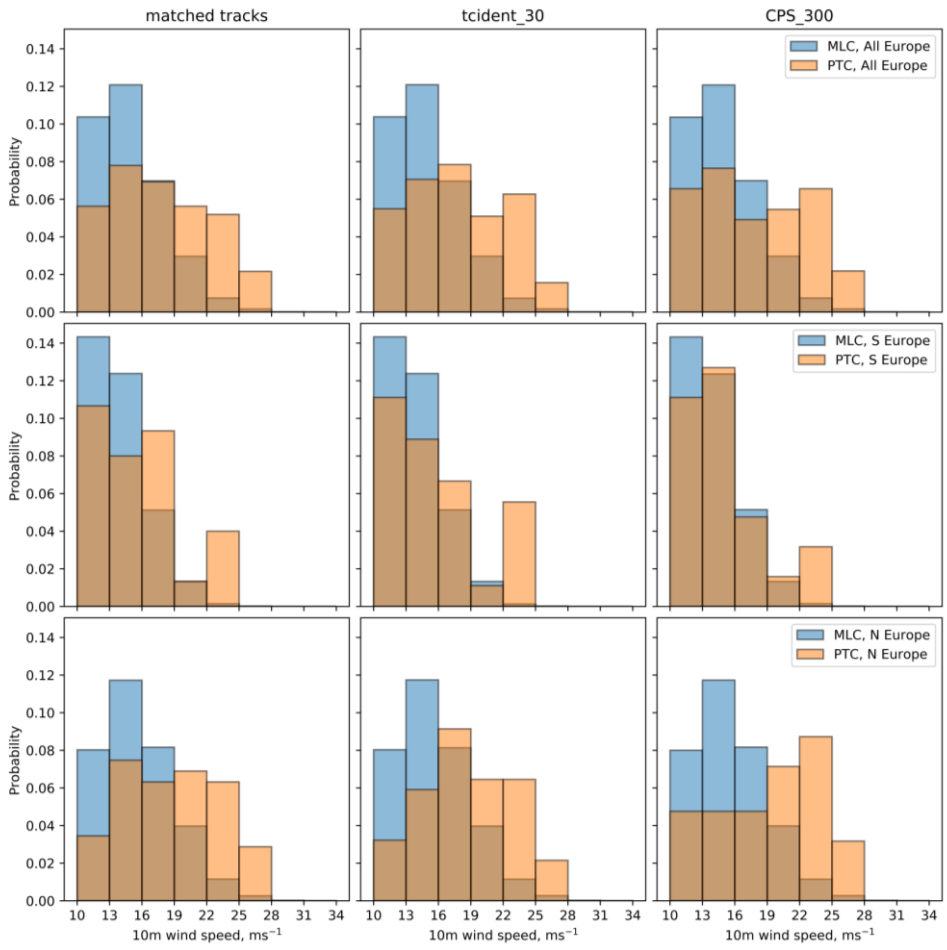

Figure 3.8. Distributions of the maximum intensity attained by each PTC and MLC inside the whole European domain (top), South Europe subdomain (10°W-30°E, 36°N-48°N) (middle) and the North Europe subdomain (10°W-30°E, 48°N-70°N) (bottom). All storm tracks forming during the North Atlantic hurricane season (June 1st – Nov 30th) are used.

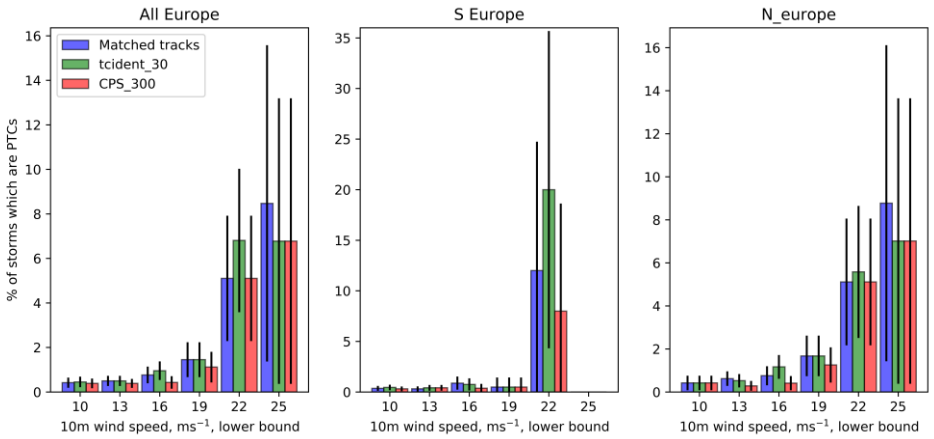

Figure 3.9. The fraction of storms impacting Europe which are PTCs as a function of their maximum 10 m wind speed in their respective domain. Lower bound of wind speed shown on x axis, bin width = 3. All storm tracks forming during the North Atlantic hurricane season are used. Error bars show the 95% confidence interval and are calculated using Equation 3.1 from the main text.

	10 m wind, m s^{-1}		MSLP, hPa	
	PTC	MLC	PTC	MLC
Mean	17.5	15.4	990.8	1001.0
Median	17.0	15.0	992.8	1003.8
0.9 quantile	23.2	20.4	967.2	981.8
St. Deviation	4.3	3.7	15.1	13.9

Table 3.1. Mean, median, standard deviation and 0.9 quantile for the distributions of all PTCs and MLCs inside the whole European domain, using all storms tracked through the ERA5 reanalysis. Sample size for PTCs = 81, sample size for MLCs = 16161.

10m wind, m s^{-1}	N Europe		S Europe		All Europe	
	PTC	MLC	PTC	MLC	PTC	MLC
Mean	18.2	15.0	15.6	13.3	17.6	14.6
Median	18.4	14.8	15.7	13.1	17.0	14.2
0.9 quantile	24.2	20.0	21.2	17.3	23.2	19.2
St. Deviation	4.6	3.8	3.9	2.9	4.3	3.4

Table 3.2. Mean, median, 0.9 quantile and standard deviation of the maximum 10 m wind speed associated with all PTCs and MLCs which impact the European domain and formed during the North Atlantic hurricane season.

Epilogue

Chapter 3 highlights the disproportionate intensity associated with Europe-impacting PTCs compared to the overall European cyclone climatology and discusses the implications that this may have if the climate model simulations of Haarsma et al. (2013) and Baatsen et al. (2015) are realised.

Given the high-impact nature associated with many Europe-impacting PTCs, it is important to understand the factors that govern the variability associated with each stage of their lifecycle. Chapter 4 focusses on the factors that govern the interannual variability of recurving North Atlantic TCs - a pre-requisite of Europe-impacting PTCs – to understand the roles played by TC activity basin-wide, and the seasonal mean steering flow.

Chapter 4

What Governs the Interannual Variability of Recurving North Atlantic Tropical Cyclones?

Chapter 3 shows that despite being relatively rare events, PTCs are disproportionately responsible for European windstorm risk. With this motivation, it is necessary to improve our understanding of the variability associated with Europe-impacting PTCs. PTCs have a long and complex lifecycle, with important roles played by the large-scale tropical environment (for TC genesis and intensity in the tropical phase of their lifecycle), the large-scale tropical and subtropical circulation (which may determine the trajectory of a TC), and the midlatitude environment the potential Europe-impacting PTCs interact with.

There is a large interannual variability in the frequency of North Atlantic TCs which interact with the midlatitudes, in this thesis referred to as recurving TCs. Note that we avoid the term post-tropical cyclone in this chapter as we do not directly examine whether these TCs have undergone ET. The driver(s) of this variability have not previously been investigated on the interannual timescale. Europe-impacting PTCs interact with the midlatitude environment at some point on their approach. In this framework, recurving TCs can be viewed as precursors to potential Europe-impacting PTCs. Given the high-impact nature of Europe-impacting PTCs (chapter 3), understanding the variability of recurving TCs is of high importance.

Chapter 4 investigates the factors that govern the interannual variability of recurving North Atlantic TCs. In particular, the roles played by TC occurrence frequency and large-scale tropical and subtropical circulation (i.e., steering) are investigated.

This chapter has been published in *Journal of Climate* under the following reference (Sainsbury et al. 2022a):

Sainsbury, E. M., R. K. H. Schiemann, K. I. Hodges, A. J. Baker, L. C. Shaffrey, and K. T. Bhatia, 2022b: What Governs the Interannual Variability of Recurving North Atlantic Tropical Cyclones? *J. Clim.*, **35(12)**, 3627–3641,

https://doi.org/10.1175/jcli-d-21-0712.1.

Abstract

Recurving tropical cyclones (TCs) can cause extensive damage along the US East Coast and later in their life cycle over Europe as post-tropical cyclones. While the existing literature attempts to understand the drivers of basin-wide and regional TC variability, less work has been undertaken looking at recurving TCs. The roles played by the interannual variabilities of TC frequency and the steering flow in governing recurving TC interannual variability are investigated in this study. Using a track-matching algorithm, we identify observed TC tracks from the HURricane DATabase version 2 (HURDAT2) in the ERA5 and MERRA2 reanalyses. This allows for detailed analysis of the post-tropical stages of the tracks in the observational TC record, enabling robust identification and separation of TCs that recurve.

We show that over 75% of the interannual variance in annual recurving TC frequency can be explained by just two predictors: the frequency of TCs forming in the subtropical Atlantic, and hurricanes (TCs with wind speeds > 33 m s^{-1}) forming in the Main Development Region. An index describing the seasonal mean meridional steering flow shows a weak, non-significant relationship with recurving TC frequency, supported by composite analysis. These results show that the interannual variability in recurving TC frequency is primarily driven by the seasonal TC activity of the MDR and the subtropical Atlantic, with seasonal anomalies in the steering flow playing a much smaller, secondary role. These results help to quantify the extent to which skilful seasonal forecasts of Atlantic hurricane activity benefit regions vulnerable to recurving TCs.

4.1. Introduction

Recurving North Atlantic tropical cyclones (TCs) can pose extreme hazards to the East Coast of the US, and later in their lifecycle over Europe. For example, hurricane Sandy led to over 200 deaths, many of which were in the north-eastern US, a region which does not often see direct impacts from TCs. At the time, Sandy was the second costliest TC in US history, causing over $65 billion USD in damages (Blake et al. 2013).

The steering flow played a clear role in the unusual track of hurricane Sandy. A ridge over the north-west Atlantic Ocean drove a south-easterly steering flow towards the north-east US. The steering effect of the ridge, along with favourable interaction with an upper-level trough to the north-west, were ultimately responsible for the strength and track of Sandy in the latter stages of its lifecycle. In addition, the interaction between Sandy and the midlatitude waveguide produced downstream ridgebuilding and jet streak acceleration, and the synergistic interaction between Sandy and its environment contributed to the track and intensity of the system (Varlas et al. 2019). For a TC to be classified as recurving using existing methods (such as described in Archambault et al. 2013 and Riboldi et al. 2018), a TC must change its direction of travel from westwards to eastwards while travelling poleward. TCs like Sandy which travelled north-west and then north-east for a time would therefore be classified as recurving TCs, even though they might not traditionally be thought of as recurving TCs (as they do not have the classical "C" shape track). In this study, we are interested in TCs which pose risk to land regions in the North Atlantic midlatitudes (such as the US East Coast and Europe). We therefore define a recurving TC as any North Atlantic TC which enters the North Atlantic midlatitudes in the domain 36-70°N, 82°W-30°E with no requirement for a change in zonal direction of travel.

Recurving TCs can also cause damage across Europe (Dekker et al. 2018; Laurila et al. 2020), particularly in the form of extreme precipitation, strong winds and large waves (Evans et al. 2017; Jones et al. 2003). Ex-hurricane Ophelia was responsible for Ireland's strongest wind gust on record of 119 mph in 2017, and ex-hurricane Charley brought severe flooding to parts of the UK and Ireland in 1986 (Hickney and Connolly-Johnston 2012). Post-tropical cyclones (PTCs) are a robust feature of midlatitude and European storminess during hurricane season (Baker et al. 2021) but are also disproportionately responsible for high-impact windstorm risk. Recent work has shown that, despite accounting for less than 1% of all cyclones to impact Northern Europe during the North Atlantic hurricane season, PTCs represent 9% of all cyclones with storm-force (>25 m s^{-1}) winds (Sainsbury et al. 2020).

Given the risk associated with recurving TCs to the East Coast of the US and later in their lifecycle over Europe, it is crucial to understand what governs the interannual variability of the frequency of recurving TCs. One possible driver of recurving TC

frequency is basin-wide TC frequency. The 2005 North Atlantic hurricane season produced 16 recurving TCs, more than any other year considered in this study (1979-2018). This year also contained the highest number of TCs in the North Atlantic. The greater the number of TCs in the North Atlantic, then the more opportunities there are for TCs to recurve. It is therefore hypothesized that TC frequency is strongly associated with recurving TC frequency.

The physical drivers of basin-wide TC frequency are well understood, with contemporary statistical, dynamical (e.g., Camp et al. 2015; Murakami et al. 2016; Murakami et al. 2016a) and hybrid models now exhibiting good skill at predicting basin-wide TC activity before the onset of peak hurricane season activity (Klotzbach et al. 2019). Forecasts and observations of large-scale environmental fields over the tropical North Atlantic during and prior to hurricane season, which have been shown to have a strong physical link with hurricane season activity (Saunders et al. 2017) explain approximately 60% of the variance in hurricane season activity, allowing for skilful seasonal forecasts from July 1st (Klotzbach 2014).

Boudreault et al. (2017), Kossin et al. (2010) and Kozar et al. (2012) use various clustering techniques to segregate North Atlantic TCs into 4 different groups, in order to understand the drivers of the interannual variability in these groups of TCs. It was found that the frequency with which TCs form in the deep tropics is strongly modulated by the Atlantic Meridional Mode (AMM) – which can modulate the position of the Inter-Tropical Convergence Zone, influencing SSTs and the location of TC precursors forming in the deep tropics - and the El Niño Southern Oscillation (ENSO), which influences wind shear patterns in the North Atlantic due to a Pacific SST-driven shift in the Walker circulation. In contrast, higher latitude TC frequency is modulated by the NAO (Elsner et al. 2000; Kossin et al. 2010). The frequency with which storms form in the Gulf of Mexico is also strongly modulated by ENSO (Boudreault et al. 2017), whereas the frequency with which storms originate in the northern and eastern parts of the basin are modulated by the subtropical high, which influences both the steering flow and the atmospheric stability in the region (Kozar et al. 2012). Much like with TC genesis, the interannual variability of recurving TC frequency may also be modulated by the large-scale environment. Warmer SSTs may facilitate greater intensification (or maintenance of TC intensity), allowing the TC to persist for a greater

amount of time, and reducing the probability of the cyclone decaying before reaching the midlatitudes. Similarly, greater baroclinicity in the northern subtropical Atlantic may facilitate baroclinic growth, offsetting the increasing hostility in the region caused by low SSTs and high vertical wind shear.

While the steering flow on the daily timescale is important for the evolution and track of recurving TCs (such as in the case of Sandy), the role of the steering flow on the seasonal timescale is not as well understood. However, as the mean steering flow may alter the typical trajectory of TC tracks over the hurricane season, it may modulate recurving TC frequency. The seasonal mean steering flow is therefore a second possible driver of recurving TC frequency.

By subsampling the HURDAT database to investigate Main-Development Region (MDR) storms only, Colbert and Soden (2012) investigate the role of the steering flow on North Atlantic hurricane tracks by segregating storms into three categories based on recurvature: straight moving, recurving land and recurving ocean. It was found that recurving ocean storms were associated with a weakening of the North Atlantic subtropical high (NASH) on the timescale of individual storms. On the seasonal timescale, the fraction of storms which ended up in the recurving ocean category was highest during El Niño years and years with a positive AMM. Recent work has also shown that during strong Indian Monsoon years, the strength of the NASH is enhanced, leading to increased landfall probability of MDR TCs (Kelly et al. 2018).

The relative importance of the interannual variabilities in hurricane season activity (TC frequency) and steering flow in the North Atlantic to recurving TCs remains unknown from a climate perspective. In this paper, we investigate the relative importance of both the interannual variabilities of the seasonal mean steering flow and TC frequency in governing recurving TC frequency in the North Atlantic. This is achieved by constructing a statistical model to quantify the variance in recurving TC frequency that can be explained by regional TC activity, and by presenting a composite analysis to investigate the role of the steering flow on the seasonal timescale.

The paper continues in section 4.2 with a description of the data used, along with details of the TC feature-tracking scheme, the spectral filtering technique used to isolate the background flow, and an objective track-matching algorithm used to identify recurvature. Section 4.3 contains an analysis of track and genesis differences

between recurving and non-recurving TCs, a composite analysis to investigate the role of the steering flow, and an analysis of the statistical model. The paper concludes with a summary and discussion in section 4.4.

4.2. Methods and Data

Cyclones are tracked (section 2.2) in two reanalyses. Track matching (section 2.3.1) with HURDAT2 (section 2.1.2) is then employed to identify the TCs. A TC is then classified as either recurving or non-recurving depending on whether the corresponding track in the reanalysis enters a domain in the North Atlantic from 36-70°N, 82°W-30°E. A boundary of 36°N was chosen because almost all (~98%) TC genesis in the North Atlantic occurs equatorward of this latitude band (see Figure 4.1), so for a TC to enter this domain it (almost always) gains latitude. A western boundary of 82°W is used because this allows for all TCs traversing the East Coast to be identified as recurving, along with those that recurve further east in the basin. The sensitivity of the results presented here have been tested on a second domain, extending from 36-70°N, 70°W-30°E, to ensure that results are robust to changes in the definition of recurvature.

4.2.1. Datasets

Two different reanalyses are used to test the sensitivity of our results to the reanalysis product. We use the ERA5 (section 2.1.1.1) and MERRA2 (section 2.1.1.2) reanalyses to provide the 6-hourly relative vorticity fields which are necessary for the cyclone detection and tracking scheme (600-, 700- and 850 hPa, vertically averaged). We also use 6-hourly wind (u and v) fields at 200-, 500-, 700- and 850 hPa pressure levels to construct seasonal mean wind fields for composite analysis and for the construction of a meridional steering flow index. The 6-hourly mean sea level pressure (MSLP) data is also used after removing the TC vortices to construct seasonal means for composite analysis.

The figures presented in this paper contain ERA5 data only, and corresponding figures created using MERRA2 data are available in the supporting information (Figures 4.10-4.13, 4.19). This is done for simplicity and to avoid duplication, because the MERRA2 results are very similar to the results presented in the main manuscript. Observational best track data from HURDAT2 (section 2.1.2) are also used between 1979 and 2018.

4.2.2. Spectral Filtering

Section 4.3.3 contains composite analysis which is used to investigate the large-scale environmental flow during years of high and low recurving TC activity. To ensure that the fields used contain a minimal signature of the recurving TC vortices themselves, the reanalysis data is also spectrally filtered. This is performed on the global, 6-hourly reanalysis fields for MSLP and wind (u and v). The data are truncated to a T11 spectral resolution (approximately 10 x 10 degrees) globally (but output on the original grid), which removes approximately 95% of the circulation associated with the vortices. For further information, see Bhatia et al. (2020). On the seasonal timescale used in this paper the differences between the spectrally filtered flow and the non-filtered flow are relatively small. Some differences exist in the composite plots (Figures 4.4-4.6) depending on whether spectrally filtered data is used or not (Figure 4.18). However, these differences do not alter the interpretation of the figures. For consistency, the spectrally filtered data is used throughout.

4.2.3. Cyclone Detection and Tracking

Cyclone detection and tracking is performed using TRACK (section 2.2). Cyclone detection and tracking is performed for the entire Northern Hemisphere for both reanalyses, and systems which pass through the North Atlantic basin are then selected.

4.2.4. Objective TC Identification

Spatiotemporal track matching (section 2.3.1) is utilized to identify the TCs. A small proportion (~5%) of the TCs in HURDAT2 are not identified in the ERA5 and MERRA2 reanalyses and are excluded from the analysis. These tend to be weak, short-lived systems (Sainsbury et al. 2020) and their exclusion does not affect the results of this study.

4.2.5. Regional Selection and Recurvature Definition

The matched TCs are separated according to 3 regions (shown in Figure 4.1), based on their genesis location in HURDAT2. These 3 regions are the MDR (10-70°W, 6-20°N), Subtropical Atlantic (SUB, 10-82°W, 20-50°N), and the region comprising the Gulf of Mexico and South Caribbean, denoted WEST ((8°N, 70°W), (8°N, 90°W), (16°N, 90°W), (16°N, 100°W), (33°N, 100°W), (33°N, 82°W), (20°N, 82°W) and (20°N, 70°W)). The

choice of 3 regions is subjective, but the regions themselves each have a physical basis. The MDR TCs typically form from African Easterly Waves unlike the TCs in the other two regions (Caron and Jones 2012; Arnault and Roux 2011). In the SUB region, TCs often form under marginal conditions for tropical cyclogenesis. This region also contains TCs which form via tropical transition, with precursors of extratropical origin (Kossin et al. 2010). The TCs forming in region WEST often encounter the most favourable thermodynamic conditions for intensification (for example, see potential intensity map (Figure 3) in Camargo et al. 2013), with the main inhibitor of intensification often being the proximity to land. The 3 regions also have broadly different seasonal mean values of vertical wind shear (e.g., Figure 3, Aiyyer and Thorncroft 2006). The 3 chosen regions therefore allow for a zonal and meridional separation of tracks based on genesis, thermodynamic and dynamic conditions, and precursor type.

The choice is made to group storms into these three regions based on the factors which may be important for recurvature. An obvious factor is proximity to the midlatitudes: a TC forming at higher latitudes is unlikely to be influenced by the strongest easterly trades which steer TCs zonally, and thus may be more likely to recurve. A second justification is the differing thermodynamical and dynamical conditions in the three regions, which largely control the lifetime maximum intensity (LMI) of the TCs. TCs which form in regions climatologically more conducive for intensification will often attain higher intensities, and the resilience associated with stronger TCs is likely key to their longevity and ability to maintain their structure in hostile environments, which may lead to an increased probability of recurvature.

Many studies (e.g., Boudreault et al. 2017; Kossin et al. 2010; Kozar et al. 2012) use clustering methods to group TCs, rather than regional boundaries which are used here and in Colbert and Soden (2012). Despite these differences in methodology, the three TC regions used here can be related to the TC classifications used in other studies. TCs in SUB, WEST and MDR are closely related to clusters 1, 2 and 3 respectively in Kossin et al. (2010) and Kozar et al. (2012). Cluster 4 in these studies mainly relates to TCs forming in the MDR and WEST regions. TCs forming in the SUB and WEST regions are similar to clusters 1 and 2 in Boudreault et al. (2017), with clusters 3 and 4 in this study relating to MDR recurving and MDR non-recurving TCs respectively. These three

previous studies all used a similar clustering technique, which is more readily able to distinguish tracks based on their genesis location than the K-means method used in many other studies of TC clustering (e.g., Harr and Elsberry, 1995).

The TCs in each region are designated as recurving if their ERA5/MERRA2 matched track enters the domain defined as 36-70°N, 82°W-30°E (shaded box, Figure 4.1). This method for identifying recurvature is different to that used by Colbert and Soden (2012), in which the degree of recurvature (either straight moving, recurving-land or recurving-ocean) associated with a TC is determined based on which spatial boundary the HURDAT TC track intersects. Our method of vorticity-based tracking allows us to extrapolate the TC tracks present in HURDAT2, giving us a more robust separation of tracks based on their recurvature.

4.2.6. Multiple Linear Regression Model

We use multiple linear regression to quantify the variability in recurving TC frequency that is associated with TC activity in the North Atlantic. There are several candidates for predictors, including basin wide TC frequency and regional TC frequency in the North Atlantic, with and without intensity constraints. Using the analysis presented in sections 4.3.1 and 4.3.2, a multiple linear regression model is fit using the two most suitable predictors.

$$Rec_{TC} = \beta_0 + \beta_1 x_1 + \beta_2 x_2 + \epsilon, \tag{4.1}$$

where β_0, β_1 and β_2 are coefficients to be fitted, x_1, x_2 are the two chosen predictors, and ϵ represents the residuals.

4.3. Results

4.3.1. Historical TC Recurvature Statistics

Figure 4.1 shows the genesis location for all TCs in HURDAT2 between 1979 and 2018, along with the boundaries for each of the 3 regions that the TCs are separated into. The shaded region represents the domain used to define recurvature. It should be noted that there is an overlap between the SUB region and the recurvature domain, with 12 TCs (<2% of all TCs considered in this study) identified as recurving by virtue of their genesis location. The sensitivity of the results to these overlapping TCs has been tested, and the results remain unchanged whether they are excluded from the analysis

or not. As a result, we include these TCs in the analysis of this paper. The SUB region is the largest spatially and contains the largest number of recurving TCs of any of the 3 regions. It also contains the highest fraction of recurving TCs at 76.6% (Table 4.1). TCs forming in this region form poleward of the strongest easterly trade winds and are also closer to the midlatitude westerly flow. The mean genesis latitude of recurving SUB TCs is 4 degrees further poleward than for the non-recurving TCs (29.5°N and 25.5°N for recurving and non-recurving TCs respectively), and this difference is significant to 95% using a student's t-test.

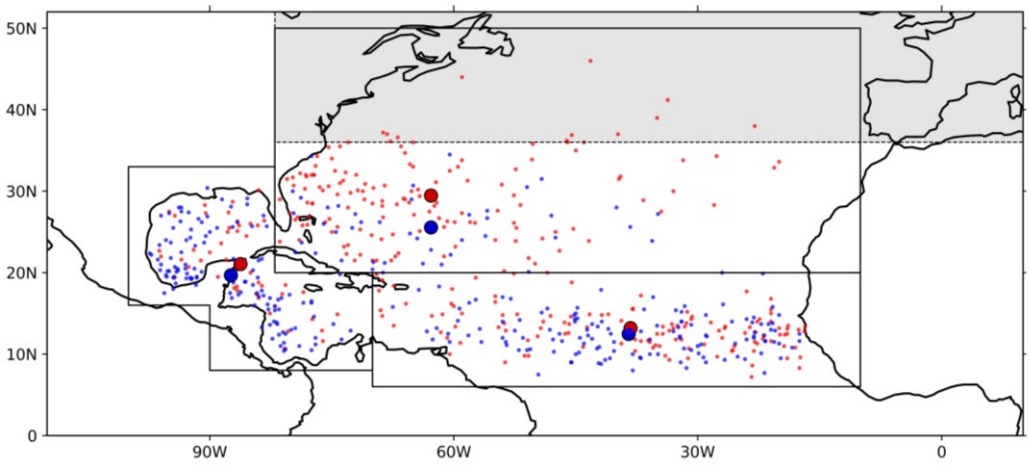

Figure 4.1. Genesis location (HURDAT2) of all recurving (red) and non-recurving (blue) TCs forming in the North Atlantic from 1979-2018. The 3 domains overlaid represent the 3 sampling regions used in this study: MDR (lower right), SUB (upper right), and WEST (left). Shaded region represents the domain used to define recurvature. Larger dots represent the mean genesis location in HURDAT2 for the tracks in the region.

The MDR contains the largest number of TCs of any of the 3 regions, approximately 48% of which recurve. The mean longitude of genesis for TCs in this region is similar for both recurving and non-recurving TCs at 38.3°W and 38.5°W, respectively. Although small, the differences in the mean genesis latitude of recurving and non-recurving TCs in the MDR (13.2°N and 12.5°N) are also statistically significant to 95%.

Only a quarter of TCs forming in the WEST region recurve, and TCs in the WEST region account for only 15% of the overall number of recurving TCs. No significant differences in mean position exist between the recurving and non-recurving TCs in this region. Overall, Figure 4.1 suggests that both the zonal and meridional location of TC genesis are associated with TC recurvature, with TCs forming in regions further polewards and

eastwards in the basin comprising the highest proportion of recurving storms. A summary of this information can be found in Table 4.1.

	MDR	SUB	WEST	Whole North Atlantic
Recurving	121	144	48	313
Non-recurving	130	44	122	296
Total	251	188	170	609
% Recurving	48.2%	76.6%	28.2%	51.4%

Table 4.1. Summary of the number of recurving (second row), non-recurving (third row), and total (fourth row) TCs, along with the % TCs which recurve in each of the 3 sampling regions displayed in Figure 4.1 (fifth row). Right hand column gives the basin-wide statistics.

4.3.2. Regional Historical TC Statistics

4.3.2.1. Historical TC Track and Precursor Genesis Densities

Track and genesis densities are calculated for recurving and non-recurving TCs using the ERA5 reanalysis tracks which have been separated by their region of formation as defined by HURDAT2. Genesis densities outside of each region (which are denoted by the red boxes) are non-zero in some areas. This is because we are assigning storms to a region using HURDAT2 genesis location but calculating genesis and track density using the corresponding ERA5 tracks, where the pre-TC lifecycle stages are identified. Figure 4.2 is therefore showing the TC precursor genesis density. Another reason for the non-zero densities outside of the regions is because the densities are calculated for a unit area using the kernel method, with kernels that spread the influence of a data point depending on their bandwidth. Differencing (recurving minus non-recurving) the track and genesis densities will highlight if there are important differences in genesis within regions and will also indicate where in the TCs lifecycle the trajectories start to differ. In the MDR and SUB regions, the differences in the track density are meridional, with significant negative (lower recurving TC density) differences equatorward, and positive differences (higher recurving track density) poleward. However, in the WEST region the differences are much more zonal, with more recurving TCs in the east of this region (Figure 4.3).

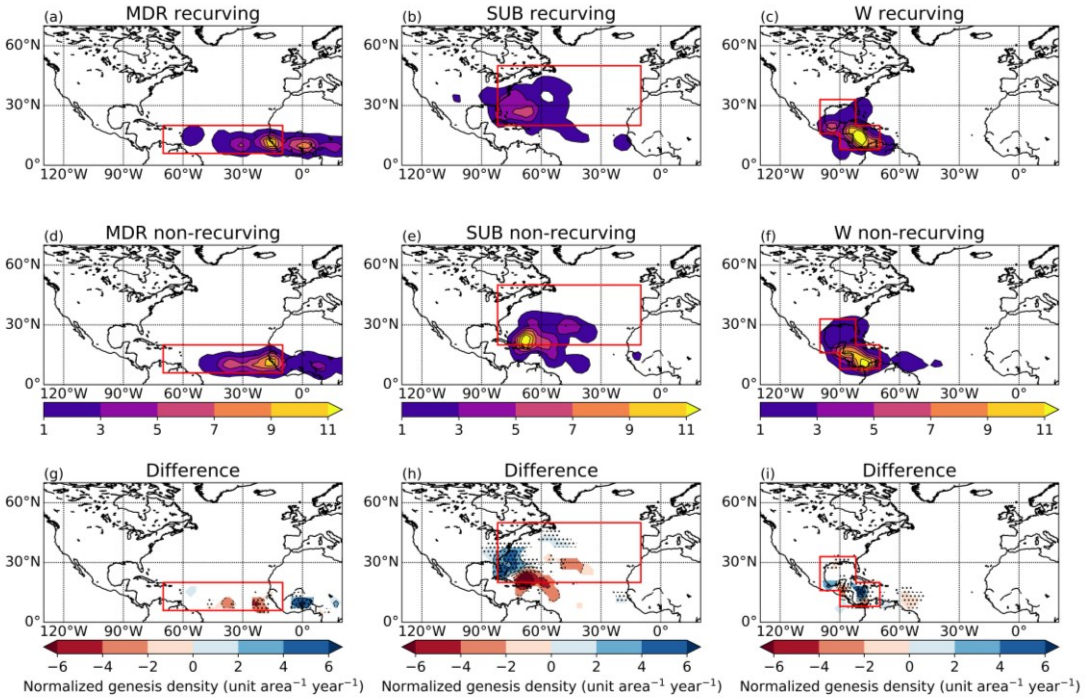

Figure 4.2. Normalized genesis density for the recurving (top) TCs, non-recurving (middle) TCs and recurving minus non-recurving (bottom) in the 3 sampling regions displayed in Figure 4.1. Boundaries for each region are displayed in red. Densities (and differences) less than 1 have been masked for clarity. Stippling denotes significance at the 95% level. Densities are calculated as the number of cyclones per year per unit area, where the area is a 5-degree radius spherical cap. The densities are normalized to account for differences in sample sizes in the different panels (a-f) by dividing by the number of cyclones in the sample.

Most of the recurving TCs forming in the MDR cross the northern boundary of the region, whereas the non-recurving MDR TCs mainly track out of the western edge (Figures 4.3a,d). Track density values for the non-recurving TCs decrease substantially to the west and north of the MDR region, in part due to a broadening of the distribution from east to west, but also because approximately 40% of the non-recurving MDR TCs dissipate before leaving the region. Despite these differences in track density, the difference in precursor genesis density in this region is small (Figure 4.2g).

Significant differences can be seen in the track and genesis densities for TCs forming in the SUB region, with recurving TCs forming further north and west than non-recurving TCs, which form primarily on the border between the MDR and SUB regions (Figures 4.2b,e). This agrees with the significant difference in the genesis latitude of recurving and non-recurving TCs seen in Figure 4.1 and indicates that the location of precursor

genesis is also significantly different for the recurving and non-recurving TCs in the SUB region. The non-recurving TCs in the SUB region gain little latitude and either travel eastwards and decay in the subtropical North Atlantic or reach the Caribbean and southeast US (Figure 4.3e).

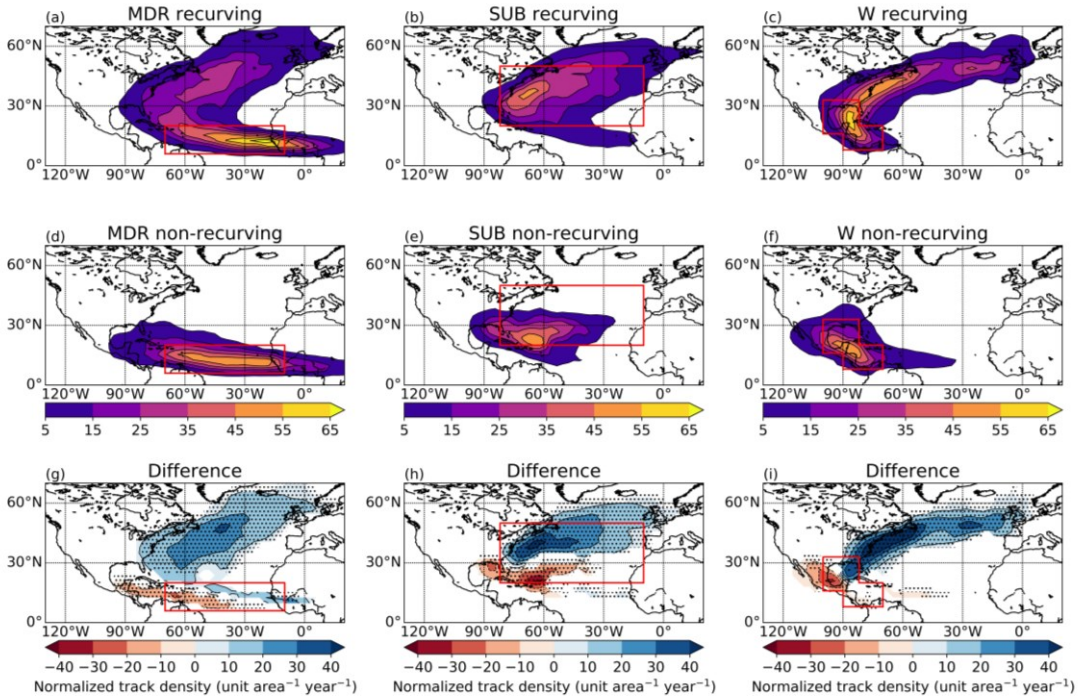

Figure 4.3. Normalized track density for the recurving TCs (top), non-recurving TCs (middle), and difference (recurving – non-recurving) (bottom) TCs in the 3 sampling regions displayed in Figure 4.1. Boundaries for each region are displayed in red. Densities (and differences) less than 5 have been masked for clarity. Stippling denotes significance at the 95% level. Densities are calculated as the number of cyclones per year per unit area, where the area is a 5-degree radius spherical cap. The densities are normalized to account for differences in sample sizes in the different panels (a-f) by dividing by the number of cyclones in the sample.

Few differences exist between the recurving and non-recurving TC genesis densities in the WEST region, but track density differences are seen. The recurving TCs forming in WEST impact the states bordering the eastern side of the Gulf of Mexico, whereas the non-recurving TCs forming in this region often impact Central America. This can be seen in the differenced track density plot for this region (Figure 4.3i).

4.3.2.2. Lifetime Maximum Intensity Distributions

Inherent to TC recurvature is longevity (particularly for storms forming in the MDR). Stronger TCs may be more resilient to hostile environments, and as a result, last

longer. For a MDR TC to recurve, it often must endure less than ideal sea surface temperatures, an environment which may be too hostile for most weak TCs. We therefore investigate the lifetime maximum intensity (LMI) distributions for recurving and non-recurving TCs in the 3 genesis regions used to partition the TCs. These are shown in Figure 4.4. Across much of the North Atlantic basin (WEST and SUB regions), there are small (but statistically significant at 95% by a Kolmogorov-Smirnov test) differences between the LMI distributions of recurving and non-recurving TCs. However, in the MDR there is a large significant difference (Fig. 4.4a). The non-recurving TCs tend to be considerably weaker at their LMI than recurving TCs. 40% of non-recurving TCs which form in the MDR dissipate before leaving the region, attaining a low LMI.

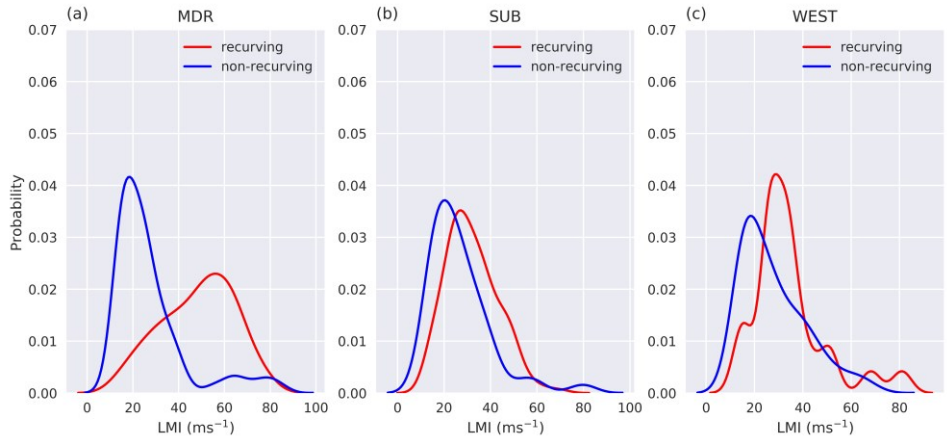

Figure 4.4. Probability distributions of lifetime maximum Intensity (LMI) for all recurving (red) and non-recurving (blue) TCs in the North Atlantic, 1979-2018, for the 3 regions displayed in Figure 4.1. Densities have been calculated using a kernel density estimation.

Recurvature of TCs in the MDR is linked to the strength and westward extent of the North Atlantic subtropical high (NASH) (i.e., the steering flow), with TCs often recurving around the western edge of the high (Colbert and Soden 2012). Some MDR TCs die out before reaching the western edge of the subtropical high and as a result, are classified as non-recurving. Another possible reason that recurving TCs have higher LMI is beta drift (Wang et al. 1998). This drift is usually of the order of a few meters per second (Wang et al. 1997) with stronger TCs drifting poleward out of the easterly trade winds faster than weaker TCs (Colbert and Soden 2012). The recurving TCs also have a longer track over the ocean, potentially allowing those tracking over the warm Gulf Stream to attain greater intensities.

4.3.3. Predictors of Recurving TC Frequency

In this section, we first explore the role of the steering flow in modulating the number of recurving TCs. In section 4.3.3.1. the focus is on TCs forming in the MDR, and in section 4.3.3.2. we investigate TCs forming in the SUB region.

4.3.3.1. The Steering Flow (MDR)

To investigate the role of the seasonal mean steering flow on TC recurvature for storms originating in the MDR, we use the deep-layer flow, $\boldsymbol{V}_{DLS}$ (Equation 4.2), defined previously by Colbert and Soden (2012). The subscripts represent the pressure level (in hPa) at which the flow is used. The MSLP is also used to determine the strength and position of the NASH, the westward extent of which was shown by Colbert and Soden (2012) to modulate TC recurvature from the MDR. In the construction of Figures 4.5 and 4.6, spectral filtering is performed on the MSLP and wind field data as described in section 4.2.2.

$$\boldsymbol{V}_{DLS} = 0.25\boldsymbol{V}_{200} + 0.5\boldsymbol{V}_{500} + 0.25\boldsymbol{V}_{850.} \quad (4.2)$$

Figures 4.5a and 4.6a show the difference in the composite mean August, September, October (ASO) deep layer flow and MSLP respectively, between years which have a very high number and a very low number of recurving TCs originating in the MDR, defined as (number > mean + 1 standard deviation) and (number < mean – 1 standard deviation). Figures 4.5b and 4.6b show the differences between years which have a high (number > mean) and low (number < mean) number of recurving TCs originating in the MDR. Of the 40 years used in our analysis, 9 years have very high activity, 11 years have very low activity, 17 years have high activity and 23 years have low activity.

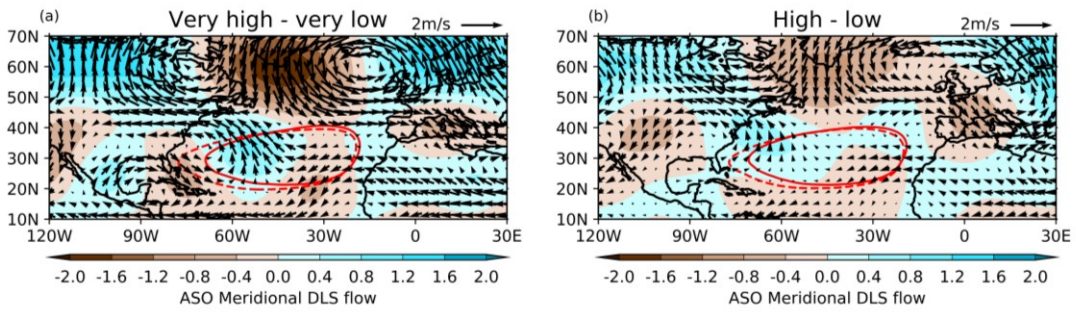

Figure 4.5. Composite differences in the deep layer flow (wind vectors), calculated from T11 spectrally filtered wind fields, based on the number of recurving TCs which form in the MDR. (a): very high minus very low, (b): high minus low. Red lines represent the 1550m contour for the ASO 850 hPa geopotential height during years of very high (solid) and very low (dashed) recurving TC frequency originating in the MDR (4.5a) and during years of high (solid) and low (dashed) recurving TC frequency originating in the MDR (4.5b). Filled contours show the composite difference in the meridional component of the ASO deep layer steering flow.

Figure 4.5a shows anomalously strong south-easterlies over the central Subtropical Atlantic during years where there is a very high number of recurving TCs originating in the MDR. Figure 4.5b also shows the same anomalous meridional flow in the subtropical Atlantic, but this time centred approximately 10 degrees further west. This anomalous flow may steer TCs which formed in the MDR on a poleward trajectory, directing them away from the easterly trade winds before they have tracked to the western side of the basin. This is consistent with Fig. 4.3a, in which the recurving TCs originating in the MDR see an increase in their poleward translation speed in the central Atlantic. At this point in their life cycle, some of the TCs may still be weak. Red contours in Figures 4.5a and b show the 1550 m 850 hPa geopotential height contour for the composites, to illustrate the westward extent of the NASH. During years of high MDR-originating recurving TC frequency, the westward extent of the NASH is reduced (solid lines) compared to years of low frequency (dashed), in agreement with Colbert and Soden (2012).

The sensitivity of the measure used to characterize the steering flow is tested by replicating the composites using a lower level flow (such as described in Chan and Gray 1982). Recreating Figure 4.5 using the 700 hPa flow shows the same anomalous flow pattern as seen in the subtropical Atlantic in Figure 4.5, however in this case the anomalous poleward flow extends further equatorward in to the MDR (Figure 4.16).

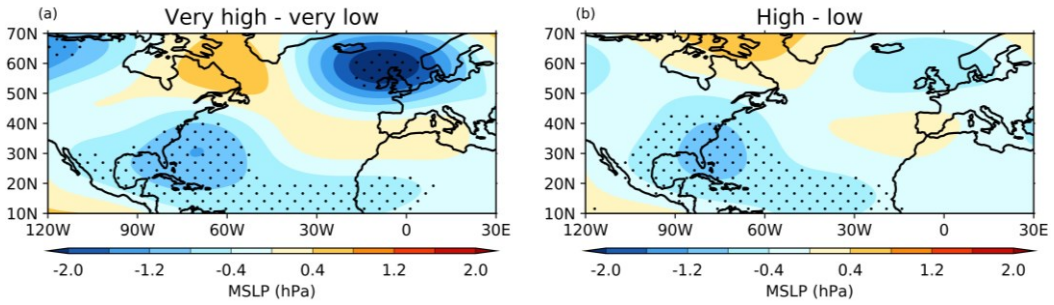

Figure 4.6. Composite differences in the ASO mean MSLP field, constructed from 6-hourly T11 spectrally filtered MSLP data. Composites are based on the number of recurving TCs which form in the MDR. (a): very high minus very low, (b): high minus low. Stippling denotes significance at 95% using a student's t-test.

Both Fig. 4.6a and 4.6b show a significant negative difference in the ASO MSLP field in the tropical Atlantic and the western subtropical North Atlantic towards the east of the south-east US. This suggests that during years when there are a larger number of recurving TCs originating in the MDR, the MSLP in the western subtropical Atlantic is anomalously low. This is physically consistent with the results of Colbert and Soden (2012) and Figure 4.5 and is indicative of higher TC recurvature coinciding with reduced westward extent of the NASH. The anomalously low MSLP in the western subtropical North Atlantic may promote the development of MDR-originating recurving TCs during years of high MDR-originating recurving TC frequency, whilst the anomalously high MSLP in this region suppresses their development and prohibits their northward migration during years of low MDR-originating recurving TC frequency. However, the significant difference between the composites is not confined to the western subtropical Atlantic and can also be seen in the tropical Atlantic and Caribbean. Negative MSLP anomalies in these regions are associated with decreased atmospheric stability (and therefore increased vertical motion), reduced vertical wind shear, and increased midlevel humidity and temperature, leading to higher TC frequency in the MDR (Klotzbach 2007; Knaff 1997; Saunders et al. 2017). Despite compositing based on recurving TC frequency, the difference between the composites could also arise due to differences in the suitability for TC genesis in the MDR, which leads to differences in recurving TC frequency and could indicate a strong association between the TC frequency and recurving TC frequency.

When repeating the analysis in section 4.3.3.1 using MERRA2 spectrally filtered fields (Figures 4.10 and 4.11) instead of ERA5, the results are like those presented here (Figures 4.5 and 4.6), with an anomalous south-easterly flow being present during years which have a high number of recurving TCs. There is a negative difference in MSLP in the western subtropical Atlantic, tropical Atlantic and Caribbean as is shown in Figure 4.6, however the MERRA2 composites have slightly larger differences, and the largest differences are centred more over the Caribbean for the very high minus very low activity composite.

4.3.3.2. The Steering Flow (SUB)

The analysis shown in section 4.3.3.1 is expanded, this time with composites constructed around the number of recurving TCs which form in the SUB region. Composites are comprised of 6 years which have very high and very low activity, 19 years which have high activity, and 21 years which have low activity. As TCs forming in the SUB region often have much lower LMI (Figure 4.4) than those forming in the MDR, they may not extend the entire depth of the troposphere. As a result, the lower tropospheric flow may be a better proxy for their steering flow than the average flow over the entire depth of the troposphere. Figure 4.7 shows the composite mean difference in the ASO 700 hPa flow for years which have been separated based on SUB recurving TC activity. Anomalous cyclonic flow exists in the subtropical Atlantic during years with many recurving TCs originating in the SUB region. This leads to an anomalous north-easterly flow along the coast of eastern Canada and the northeast US. This flow is in the opposite direction to which the recurving TCs forming in the SUB region track (Fig. 4.3a) and as a result, it does not appear that the anomalous flow pattern would aid TC recurvature. It is therefore unlikely that the seasonal mean steering flow plays a direct role in modulating the recurving TC frequency in the SUB region during the 1979-2018 period. Figure 4.7 is repeated using the deep layer flow (Equation 4.2), and the flow pattern is the same (Figure 4.17).

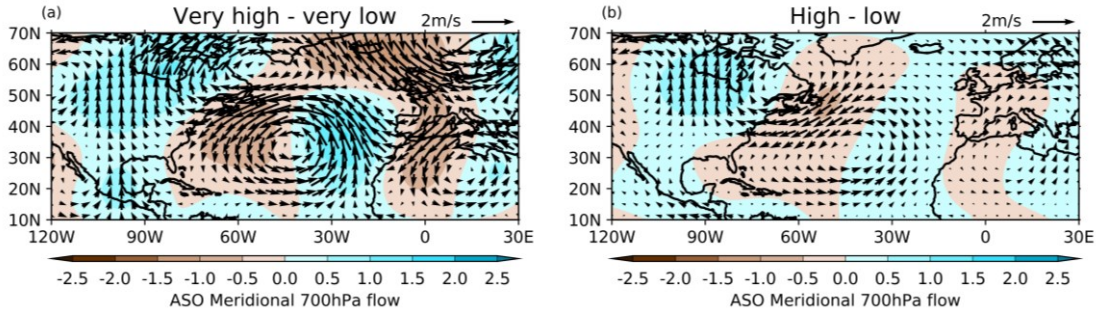

Figure 4.7. Composite differences in the ASO mean 700 hPa wind field (wind vectors), constructed from 6-hourly T11 spectrally filtered 700 hPa (u and v) data (all days in ASO). Composites are based on the number of recurving TCs which form in SUB. (a): very high activity minus very low activity, (b): high activity minus low activity. Filled contours show the composite difference in the meridional component of the ASO 700 hPa flow.

The anomalous cyclonic circulation that exists in the subtropical North Atlantic during years in which there are a high number of recurving SUB TCs is associated with a

reduction in the intensity of the NASH. This may lead to increased TC activity in the SUB region. This contrasts with Figure 4.5, wherein the NASH intensity does not differ between years of high and low MDR-originating recurving TC frequency, but where instead the location of the NASH may be more important. The potential relationship between NASH intensity and SUB TC genesis agrees with Kossin et al. (2010), who suggested that a negative NAO (weaker NASH, higher SLP over Iceland) is associated with a higher TC frequency in the subtropical North Atlantic ('cluster 1' therein). Correlation maps between annual SUB TC frequency and the meridional 700 hPa flow show that whilst correlations do exist in the subtropical North Atlantic between the circulation anomalies and TC activity, these correlations are weak (r~0.3) (Figure 4.15,). Figure 4.7 is not sensitive to the reanalysis used, with the MERRA2 composite supporting the analysis presented here (Figure 4.12).

4.3.3.3. Regional TC Activity

In this section, we explore the association between basin-wide TC frequency and recurving TC frequency. To quantify the variability in recurving TC frequency that is associated with TC activity, a multiple linear regression (MLR) model for recurving TC frequency is constructed using two predictors: The number of hurricanes forming in the MDR each year, and the number of TCs (storms of any intensity if present in HURDAT2) forming in the SUB region each year. These predictors are chosen because 85% of recurving TCs originate in either the MDR or SUB regions (Table 4.1). The majority (81%) of recurving TCs originating in the MDR are of hurricane strength (1-min sustained winds > 33 m s^{-1}) at their LMI (Figure 4.4). Whilst Figure 4.4 indicates that recurving TCs have a statistically significantly higher LMI in all 3 regions, the difference between the distributions is considerably larger in the MDR. While stronger TCs are more likely to recurve, MDR major hurricane frequency is not as strongly associated with recurving TC frequency as MDR hurricane frequency (R^2 of 44.2% and 19.7% for MDR hurricane frequency and MDR major hurricane frequency, respectively). This may be because much of the North Atlantic capable of supporting major hurricanes resides in the western side of the basin, where storms have a higher probability of making landfall and subsequently dying out. As a result, the predictors used are MDR hurricane frequency and SUB TC frequency.

Ordinary least squares assumptions are satisfied – there is no collinearity between MDR hurricane number and SUB TC number. The residuals are approximately normally distributed, tested using a Kolmogorov-Smirnov test, and both predictor terms are significant, each explaining a comparable amount of variance of recurving TCs. The variance in the residuals also does not depend on the value of the predicted variable. The fitted MLR model is shown in Equation 4.3, where Rec_{TC}, MDR_H, $and\ SUB_{TC}$ denote recurving TC frequency, MDR hurricane frequency and SUB TC frequency, respectively.

$$Rec_{TC} = 1.053MDR_H + 0.7539SUB_{TC} + 0.964 + \epsilon \quad (4.3)$$

As this model uses only two predictors, it is unlikely that there is any substantial overfitting. This is tested and confirmed in Figure 4.8b and 4.8c. Using 20 years of data, randomly selected to train the MLR model, the model is then tested on the remaining 20 years of data. This process is iterated 100,000 times to produce the R^2 distribution shown, which has a mean of 75% and a 95% confidence interval of 56-88%, indicating that there is no substantial overfitting and that the model performs well on the test data. Iterating the process gives us approximately 50,000 predictions for the number of recurving TCs for each year, which are used to construct the 95% confidence interval shown by the shading in Figure 4.8.

The resulting MLR model explains 81% of the variance (using all data for the MLR fit) and has an R^2 of 79% when using a leave-one-out cross-validation. Using all data in the regression, the individual R^2 values for the relationship with recurving TC frequency are 33.9% and 42.2% for SUB TC frequency and MDR hurricane frequency, respectively. Figure 4.8 shows that the interannual variability in the recurving TC number is captured extremely well by the model, indicating that activity in the MDR and SUB regions of the North Atlantic explain most of the variance in the interannual variability of recurving TC frequency.

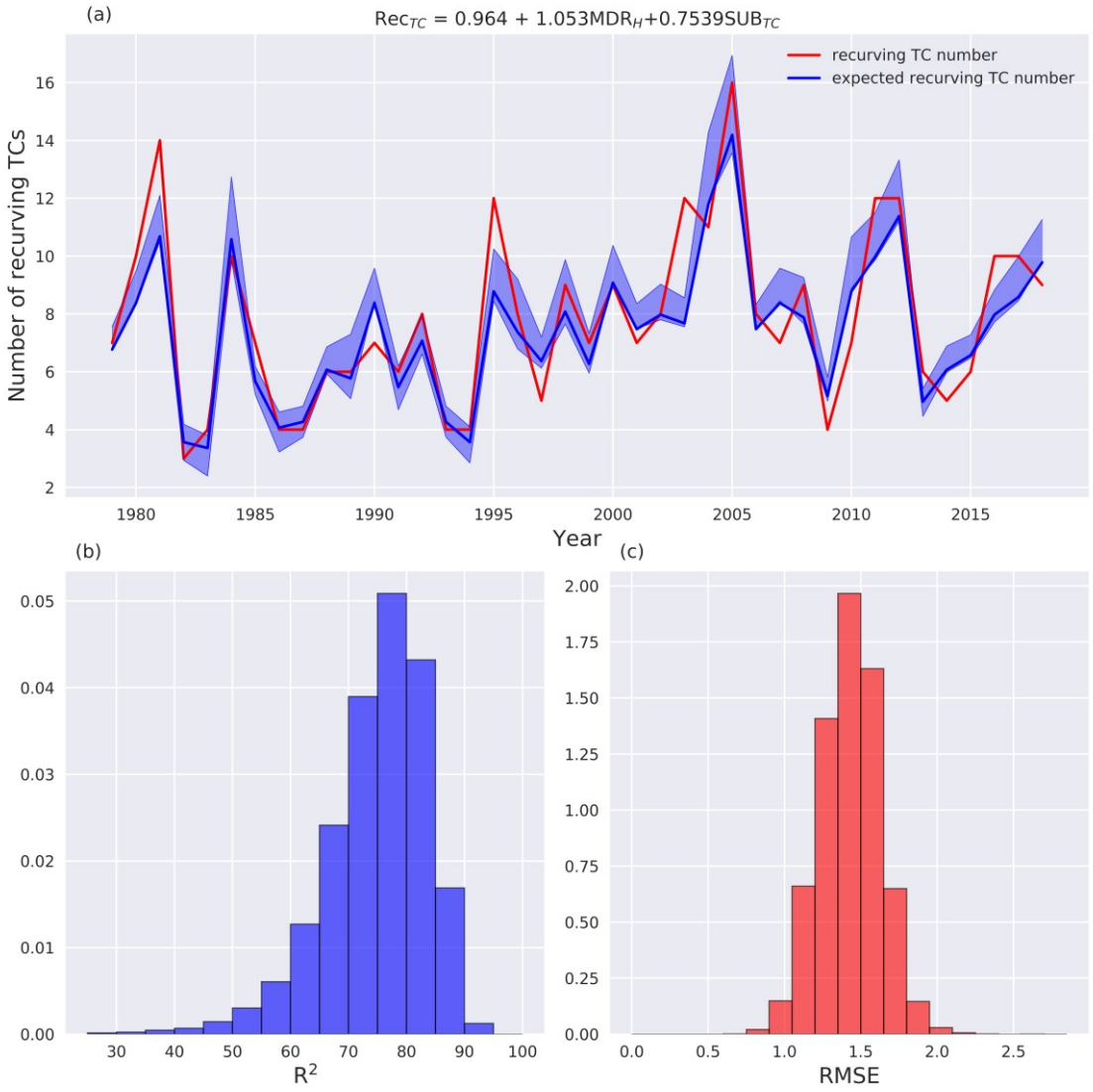

Figure 4.8. (a): Recurving TC frequency in the North Atlantic basin between 1979 and 2018 (red) and expected recurving TC frequency in the North Atlantic basin over the same time period, predicted using the multiple linear regression model described in Equation 4.3 (blue). Probability distributions of R^2 (b) and RMSE (c), calculated using a half-and-half test iterated 100000 times. Shaded region represents the 95% confidence interval, calculated from the half-and-half test.

Poisson regression is often used to investigate the drivers of TC activity (Boudreault et al. 2017; Elsner et al. 2000; Elsner 2003; Elsner et al. 2001; Elsner 1993; Kossin et al. 2010; Kozar et al. 2012; Murakami et al. 2016a) due to the discrete nature of TC counts. To establish robustness, the results presented in Figure 4.8 were also reproduced using a Poisson regression model with a logarithmic link function and the results support the analysis presented in this paper (Figure 4.21).

The sensitivity of the results in Figure 4.8 have been tested extensively by changing the domain used to define TC recurvature (Figure 4.22), changing the reanalysis used to

track the post-tropical stage of the TCs (Figure 4.19), and changing the TCs used in the analysis (all TCs in HURDAT vs named storms only, Figure 4.20). All of these changes lead to a model which has a fit just as good as presented in Figure 4.8.

As TC frequency explains a large fraction of the variance of recurving TC frequency, we investigate the SST anomalies in the North Atlantic during years of high and low MDR hurricane frequency and SUB TC frequency. The SUB TC frequency is not strongly related to tropical Atlantic SSTs and the ENSO state, agreeing with Kossin et al. (2010), however positive SST anomalies exist along the midlatitude US East Coast during high SUB TC frequency years (Figure 4.25). MDR hurricane frequency is highest during La Nina years and years in which there is a positive SST anomaly in the tropical North Atlantic (Figure 4.24), which is anticipated based on previous studies (Klotzbach et al. 2017; Landsea et al. 1999; Vecchi et al. 2011).

While the focus of this study is on recurving TCs, it is sensible to ask whether such a strong relationship is seen between TC activity and non-recurving TC frequency. Separating our 40-year dataset into the 20 years which have a frequency of recurving TCs basin-wide above and below the mean, we find that the ratio (recurving TCs/non-recurving TCs) is over twice as high for years which have a recurving TC frequency greater than the mean (1.7 and 0.8 for years above and below the mean respectively). This indicates that years which have a high recurving TC frequency do not necessarily have a high non-recurving TC frequency. However, the correlation between non-recurving TC frequency and basin-wide TC frequency is extremely high (r~0.8). For recurving TCs, the relationship is with TC activity in the MDR and SUB regions, however for non-recurving TC frequency, we would anticipate the relationship to be with TC activity in the WEST region, in which most TCs do not recurve (Figure 4.1). This would explain why there is a significant relationship between both recurving and non-recurving TC frequency and basin-wide TC frequency, but no significant relationship between recurving and non-recurving TC frequency directly.

4.3.4. Relative Importance of Steering Flow and TC Activity

Figures 4.5 and 4.6 indicate that MSLP and deep layer flow differences exist in the central and western subtropical Atlantic between years associated with high and low recurving TC activity in the MDR, and some of these differences are physically consistent with our understanding of how the westward extent of the NASH

modulates TC recurvature. To quantify the role that the interannual variability of the steering flow plays in modulating recurving TC frequency, we define a steering flow index. This index is created by standardizing the mean ASO meridional component of the deep layer steering flow (Equation 4.2) in a box from 25-35°N, 45-65°W. This region was chosen as it captures the largest meridional flow differences in Figures 4.5 and 4.7 and is the region in which the correlation between recurving MDR TC frequency and ASO meridional deep layer steering flow is highest. It is assumed that the meridional (poleward) component of the flow will determine the poleward propagation of TCs rather than the magnitude of the full (u,v) field. We therefore only consider the meridional component of the flow for the index.

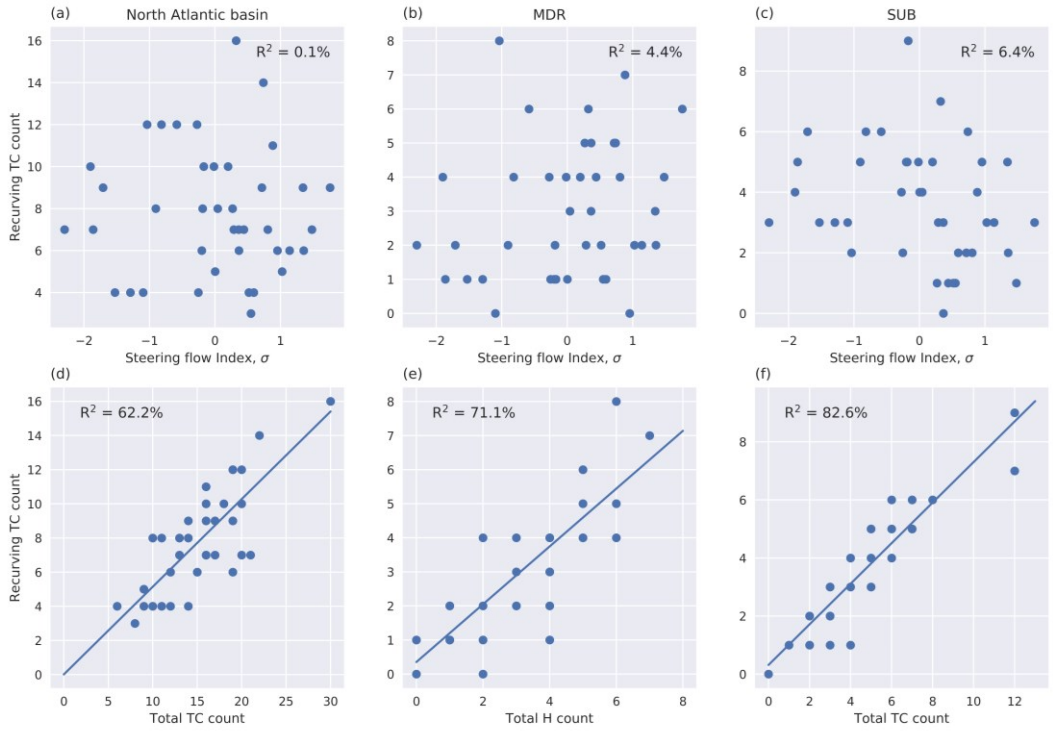

Figure 4.9. Annual recurving TC frequency basin wide (left), originating in the MDR (middle) and originating in the SUB region (right), against the steering flow index (top) and basin-wide TC activity (bottom left), hurricanes originating in the MDR (bottom middle) and TCs originating in the SUB region (bottom right). Meridional component of the deep layer flow in the region 45-65°W, 25-35°N is used to create the steering flow index.

Figures 4.9a, b and c show the relationship between the number of recurving TCs (basin-wide, originating in the MDR, and originating in SUB respectively) and the steering flow index. Basin wide (Figure 4.9a), there is no link between recurving TC frequency and the ASO mean steering flow index. A weak relationship may exist in the

MDR and SUB regions (Figures 4.9b, c), but correlations between the ASO mean steering flow index and recurving TC frequency are not significant at 95%.

In Figure 4.9e, the MDR hurricane frequency is shown instead of MDR TC frequency based on the results of Figure 4.4a, which shows that many weak MDR-originating TCs die out, and as a result, hurricane number is likely a better predictor. Figure 4.9 clearly highlights that the interannual variability of recurving TC frequency is modulated by the frequency with which hurricanes form in the MDR and TCs form in SUB (Figures 4.9e, f), with interannual variability in the seasonal mean steering flow potentially playing a small, secondary role. A second order effect may also come from interannual variability in genesis location, particularly within the SUB region. The result remains unchanged when Figure 4.9 is reproduced using MERRA2 data (Figure 4.13), indicating that it is not sensitive to the reanalysis used.

The TC activity and the seasonal mean steering flow are not completely independent. The NAO index, which in part depends on the strength and location of the NASH is (weakly) associated with TC frequency in the subtropical Atlantic. A weaker NASH may also reduce the pressure gradient between the subtropical Atlantic and the equator, reducing trade wind strength, leading to higher SSTs and enhanced TC frequency. Correlation maps (Figure 4.23) have shown that these correlations are weak (r~0.2-0.3) and not significant, so collinearity between steering and TC activity in the MLR model is unlikely. Interannually, the steering flow is not strongly or significantly associated with basin-wide TC frequency, but TC frequency is strongly and significantly associated with recurving TC frequency.

4.4. Discussion and Conclusions

The aim of this paper is to investigate the relative importance of the interannual variability of TC frequency and the steering flow in governing North Atlantic recurving TC frequency. This is achieved using a track matching algorithm to identify observed TC tracks from HURDAT2 in the ERA5 and MERRA2 reanalyses. This provides extended information about the precursor and post-tropical stages of storms beyond what is available in HURDAT2 alone, which is then used to objectively identify the recurving TCs. We then partition the storms into three sub-regions based on genesis location (Main Development Region (MDR), subtropical North Atlantic (SUB) and the region

comprising of the Gulf of Mexico and south Caribbean (WEST)). The main conclusions of this study are as follows:

- Over 75% of the variance in seasonal North Atlantic recurving TC frequency can be explained by just two predictors: seasonal TC frequency originating in the subtropical Atlantic region, and seasonal hurricane (1 min sustained winds > 33 m s^{-1}) frequency originating in the Main Development Region. The individual R^2 (using all data) are 33.9% for subtropical Atlantic TC frequency and 42.2% for Main Development Region hurricane frequency.
- Only a weak relationship between the meridional component of the seasonal mean deep layer steering flow and recurving TC frequency is found, which is not significant.
- TC frequency explains most of the variability in recurving TC frequency, with interannual variability in the steering flow and genesis latitude potentially playing smaller, secondary roles.

The methods used here are robust to the different reanalyses used to track the TCs, to the boundaries of the domain used to define recurvature, and to the cyclones in HURDAT2 used (all TCs or just those with winds > 17 m s^{-1}).

We are not suggesting that the steering flow is unimportant for TC recurvature; on the timescales of individual TCs, the steering flow is crucial for their steering and evolution. But on the seasonal timescale, the interannual variability in TC frequency is much more strongly associated with the interannual variability of recurving TC frequency than the interannual variability in the steering flow. This result suggests that skilful seasonal forecasts of Atlantic hurricane activity could also increase seasonal forecast skill in regions primarily impacted by recurving TCs, such as the east coasts of the US and Canada, and Europe.

While we have explained a large fraction of variance associated with recurving TC frequency interannually, future work should assess the seasonality of TC recurvature. It could be hypothesized that months which contain the most TCs will feature the most recurving TCs, but this may further be modulated by seasonality in the likelihood that a TC will recurve. This may be controlled by the distance between the region favourable for tropical cyclogenesis (i.e., SSTs > 26C) and the region favourable for

extratropical cyclogenesis (i.e., Eady growth rate > 0.5 day^{-1}) as proposed in Hart et al. (2001).

The results presented here may also help us to understand how recurving TC frequency might change in the future. A small decrease is expected in TC counts in the North Atlantic due to climate change; particularly a decrease in weaker, short lived TCs (Knutson et al. 2019). However, the TCs that do form will likely be more intense at their LMI than in the current climate (Knutson et al. 2019). There already appears to be a poleward migration in the latitude at which TCs attain their LMI (Kossin et al. 2014) and if anthropogenically driven, this will likely persist into the future. Given the poleward shift in LMI and expected increase in the average intensity of TCs (suggesting increased longevity), coupled with the knowledge that weak, short-lived TCs (particularly those forming in the MDR) are unlikely to recurve, the North Atlantic may see more recurving TCs in the future, proportionally and possibly also in terms of absolute counts. Climate model projections should be utilized to further understand how recurving TC frequency and their direct and downstream impacts may change in the future, using high-resolution climate models in particular (such as in Haarsma et al. 2013 and Roberts et al. 2020) which better capture the intensity of TCs.

Acknowledgments

E. Sainsbury was funded by the Natural Environment Research Council (NERC) via the SCENARIO Doctoral Training Partnership (Grant NE/S0077261/1) with additional CASE funding from BP. R. S., K. H., A. B., and L. S. are supported by the U. K. National Centre for Atmospheric Science (NCAS) at the University of Reading. A. B. also acknowledges PRIMAVERA funding received from the European Commission under grant agreement no. 641727 of the Horizon 2020 research program and funding from NERC through the North Atlantic Climate System Integrated Study (ACSIS) grant, reference NE/N018044/1. We thank Baoqiang Xiang and two anonymous reviewers for their comments which greatly improved the quality and clarity of the manuscript.

Data Availability Statement

HURDAT2 data can be downloaded at aoml.noaa.gov/hrd/hurdat/. Reanalysis data used for cyclone tracking and composite analysis can be obtained from https://disc.gsfc.nasa.gov/ (MERRA2) and from the Copernicus C3S Date store (https://www.ecmwf.int/en/forecasts/datasets/reanalysis-datasets/era5) for ERA5. Both reanalyses are freely available. TRACK is available for use with permission (see https://gitlab.act.reading.ac.uk/track/track, version 1.5.2 used).

4.5. Supporting Information

4.5.1. Sensitivity to the Reanalysis

This section contains a repeated analysis of Figures 4.5, 4.6, 4.7 and 4.9 in the main manuscript. In the manuscript, the ERA5 reanalysis (1979-2018) is used. This time we use MERRA2 (1980-2016) data instead. Everything else (spectral filtering methodology) is kept constant.

For Figures 4.10 and 4.11, the sample size for very high, high, low, and very low activity years are 6, 18, 19 and 3 respectively.

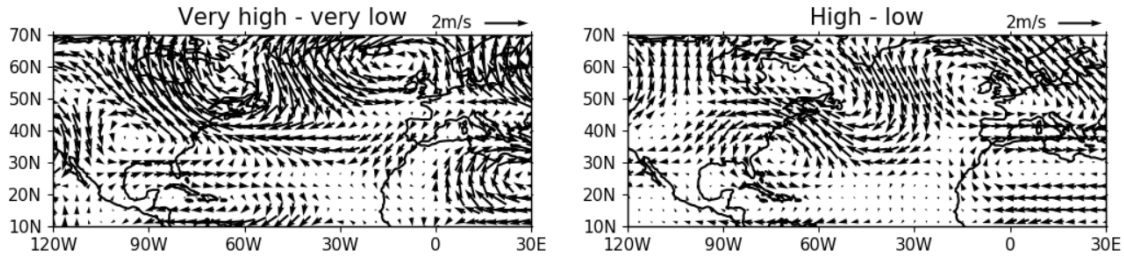

Figure 4.10. As in Figure 4.5 but using spectrally filtered ASO MERRA2 data to calculate the deep layer flow.

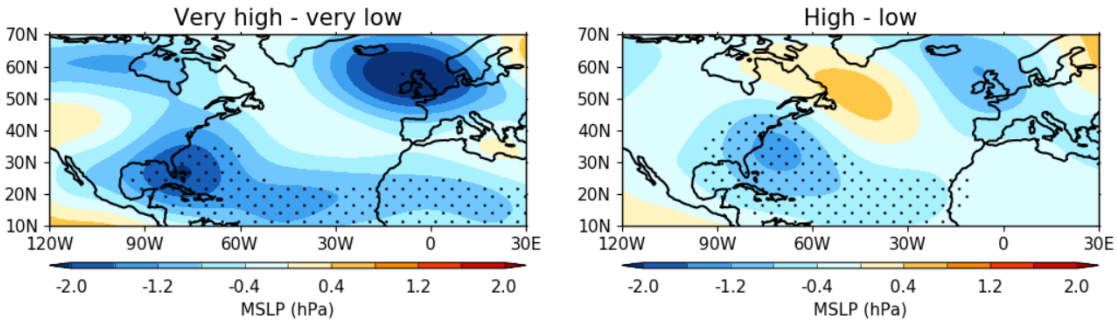

Figure 4.11. As in Figure 4.6 but using spectrally filtered ASO MERRA2 MSLP data.

For Figure 4.12, the sample size for the very high, high, low, and very low composites are 5, 16, 21 and 5 respectively.

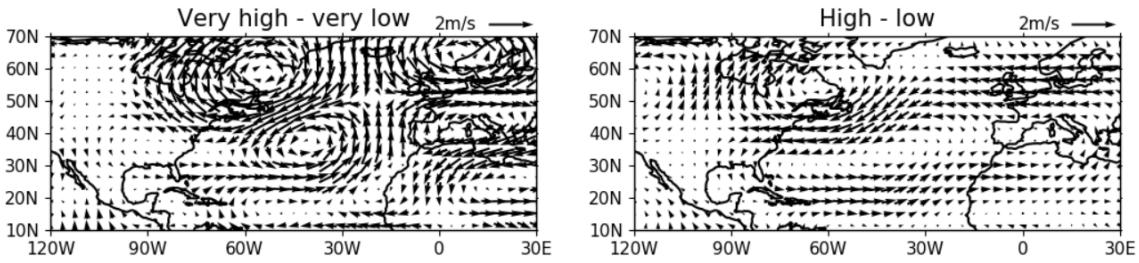

Figure 4.12. As in Figure 4.7 but using spectrally filtered ASO 700 hPa flow data from MERRA2.

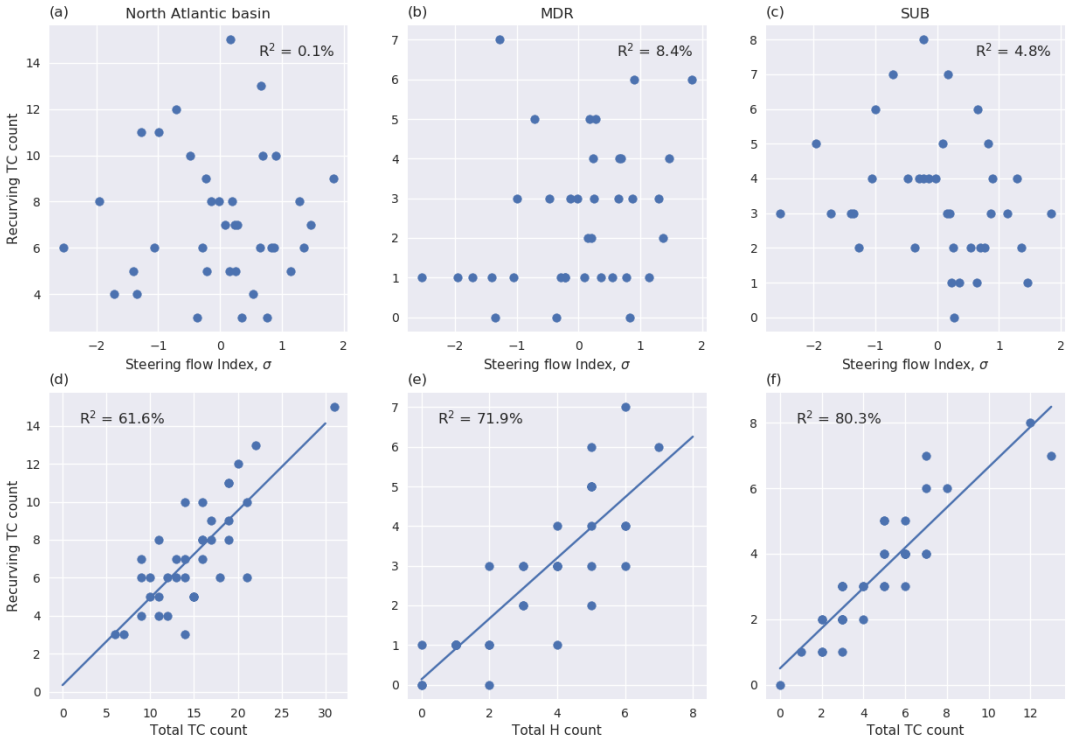

Figure 4.13. As in Figure 4.9, but this time the steering flow index is created from spectrally filtered ASO mean MERRA2 data, instead of ERA5.

4.5.2. Investigation of the Collinearity between the Steering Flow Index and MLR Model Predictors

Figure 4.14 shows the relationship between the steering flow index (as described in the main manuscript), and recurving TC frequency in the MDR and SUB regions. It also shows the relationship between the steering flow index and the two predictor terms of the MLR model, to test that steering and regional hurricane activity are not strongly

correlated. Figure 4.14 shows that the relationship between the steering flow index and the predictor terms in the MLR model are weak and non-significant.

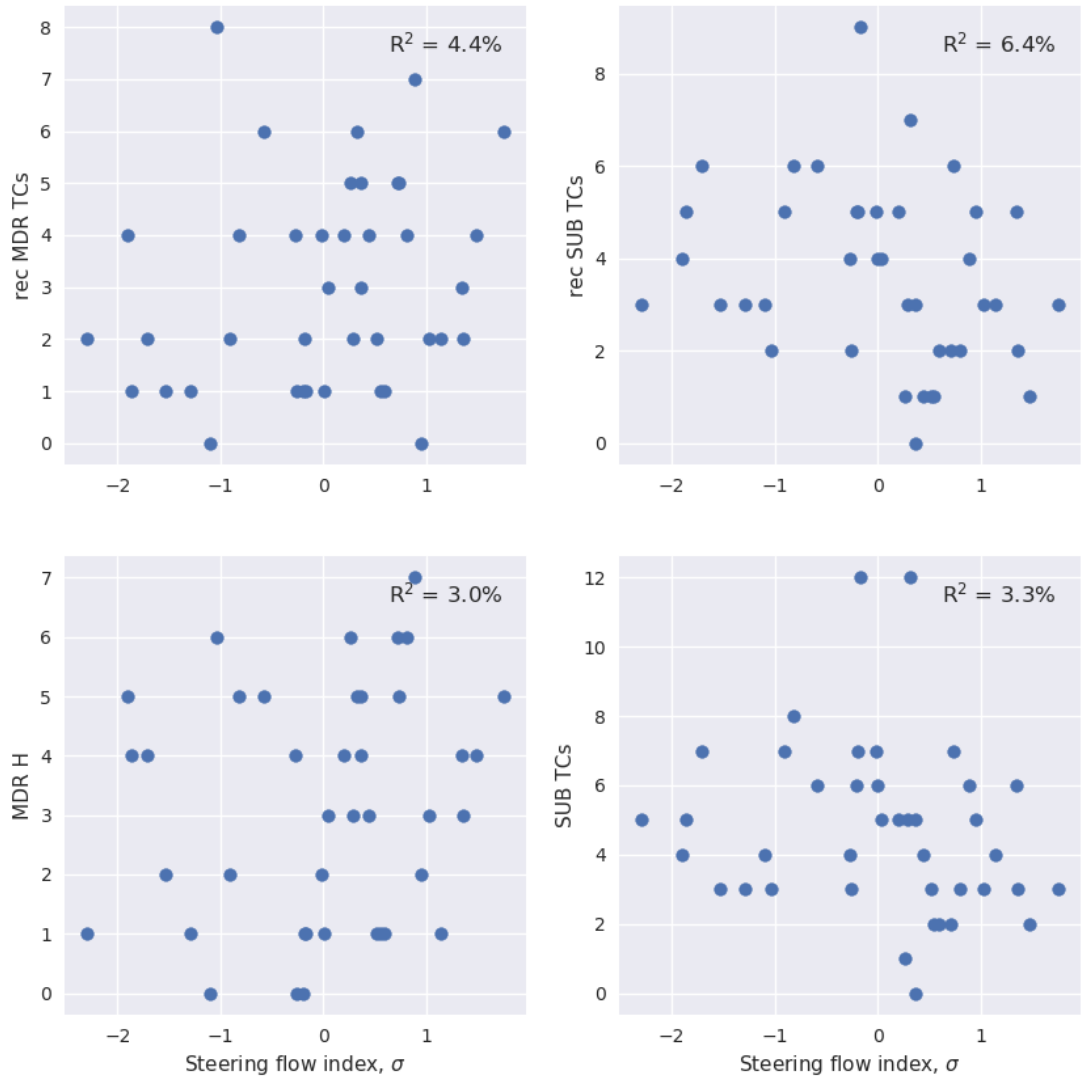

Figure 4.14. Scatterplots of the steering flow index against: (top left) recurving MDR TC frequency, (top right) recurving SUB TC frequency, (bottom left) MDR hurricane frequency, and (bottom right) SUB TC frequency. The steering flow index used here is calculated using ERA5 data as in Figure 4.9 on the main manuscript.

Figure 4.7 in the main manuscript shows that a cyclonic circulation difference exists in the subtropical North Atlantic during years in which there are high number of recurving TCs. This could be due to the relationship between NAO and SUB TC frequency. To investigate the strength of the relationship (SUB TC frequency and 700 hPa flow), a correlation map is constructed and is shown in Figure 4.15. While there

may be some link between SUB TC frequency and the flow, it is relatively weak and non-significant across the majority of the subtropical North Atlantic.

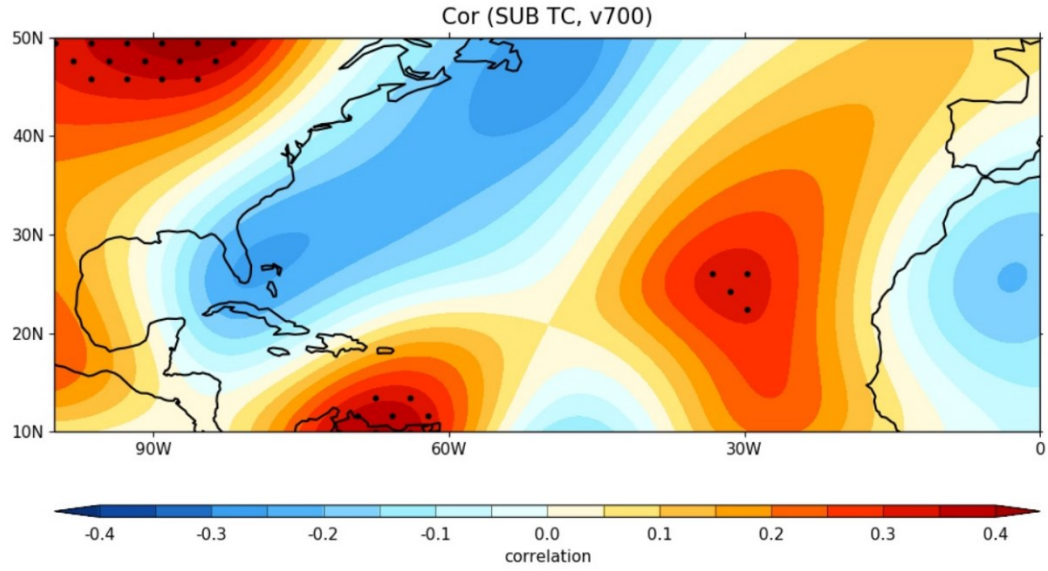

Figure 4.15. Correlation map showing the Pearson's correlation coefficient between SUB TC frequency and the meridional component of the ASO spectrally filtered 700 hPa flow from ERA5. Stippling indicates significance at 95%.

4.5.3. Sensitivity of Figures 4.4 and 4.6 to the Flow Level.

TCs of different intensities extend to different heights in the troposphere and are steered by different levels. Figures 4.16 and 4.17 are recreated versions of Figures 4.5 and 4.7 from the main manuscript, but this time using a different flow level. Figures 4.16 and 4.17 show that there is very little sensitivity of the composites to the flow layer used.

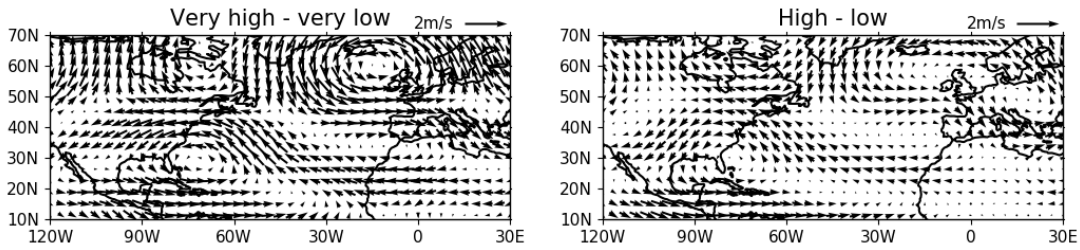

Figure 4.16. As in Figure 4.5 but created using the spectrally filtered ASO mean 700 hPa flow (ERA5).

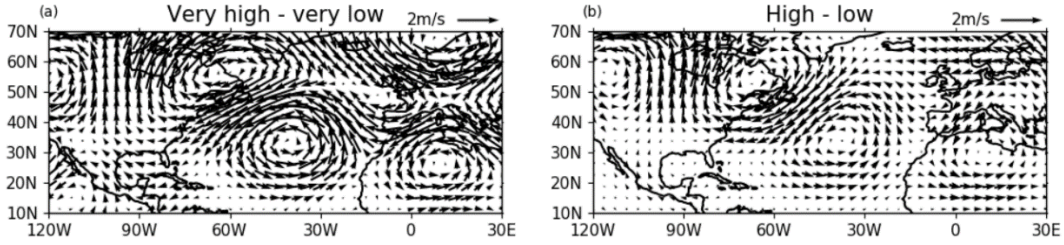

Figure 4.17. As in Figure 4.7 of the main manuscript, but this time using the ASO mean spectrally filtered deep layer steering flow, as defined in the main manuscript.

4.5.4. The Role of Spectral Filtering

In our analysis, we use seasonal mean environmental fields and so it might be expected that the spectral filtering has negligible impact on the seasonal (ASO) timescale. To investigate this, Figure 4.5 from the main manuscript is recreated using the full field data from ERA5. The only difference between Figure 4.18 below, and Figure 4.5 in the main manuscript, is the spectral filtering on the 6-hourly fields before the ASO means are calculated. There are some small differences in the flow between the full field version (Fig. 4.18) and the filtered version (Figure 4.5). This justifies the need to use the spectral filtering so that we are not attributing apparent circulation patterns to the signature of the vortices. Despite some differences between the filtered and non-filtered composites, the large-scale flow is very similar between them.

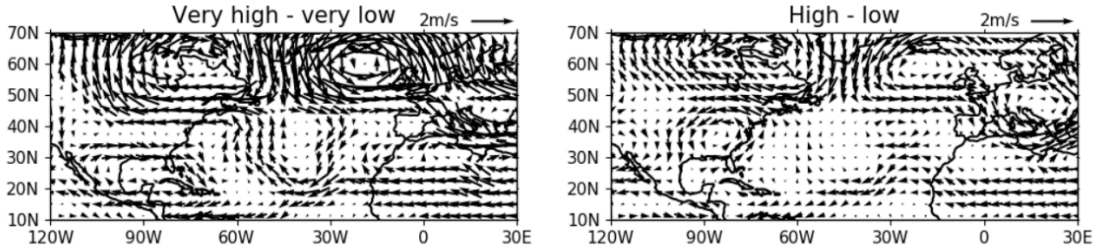

Figure 4.18. As in Figure 4.5 but created using the non-spectrally filtered ERA5 data.

4.5.5. Multiple Linear Regression Model Sensitivity Analysis

In this section, Figure 4.8 from the manuscript is reproduced with several changes to investigate the sensitivity of the MLR fit. Figure 4.19 shows the figure reproduced using MERRA2 matched tracks, Figure 4.20 shows the figure reproduced considering only the cyclones in HURDAT2 which have 10 m winds > 17 m s^{-1} (i.e., named storm strength), Figure 4.21 shows the results reproduced with a Poisson regression model, using a logarithmic link function (more information given directly above Figure 4.21),

and Figure 4.22 shows the results for a different recurvature domain. In all cases, the regression equations are shown in the title of the figures.

Figures 4.19 through 4.22 clearly show that the result is very robust.

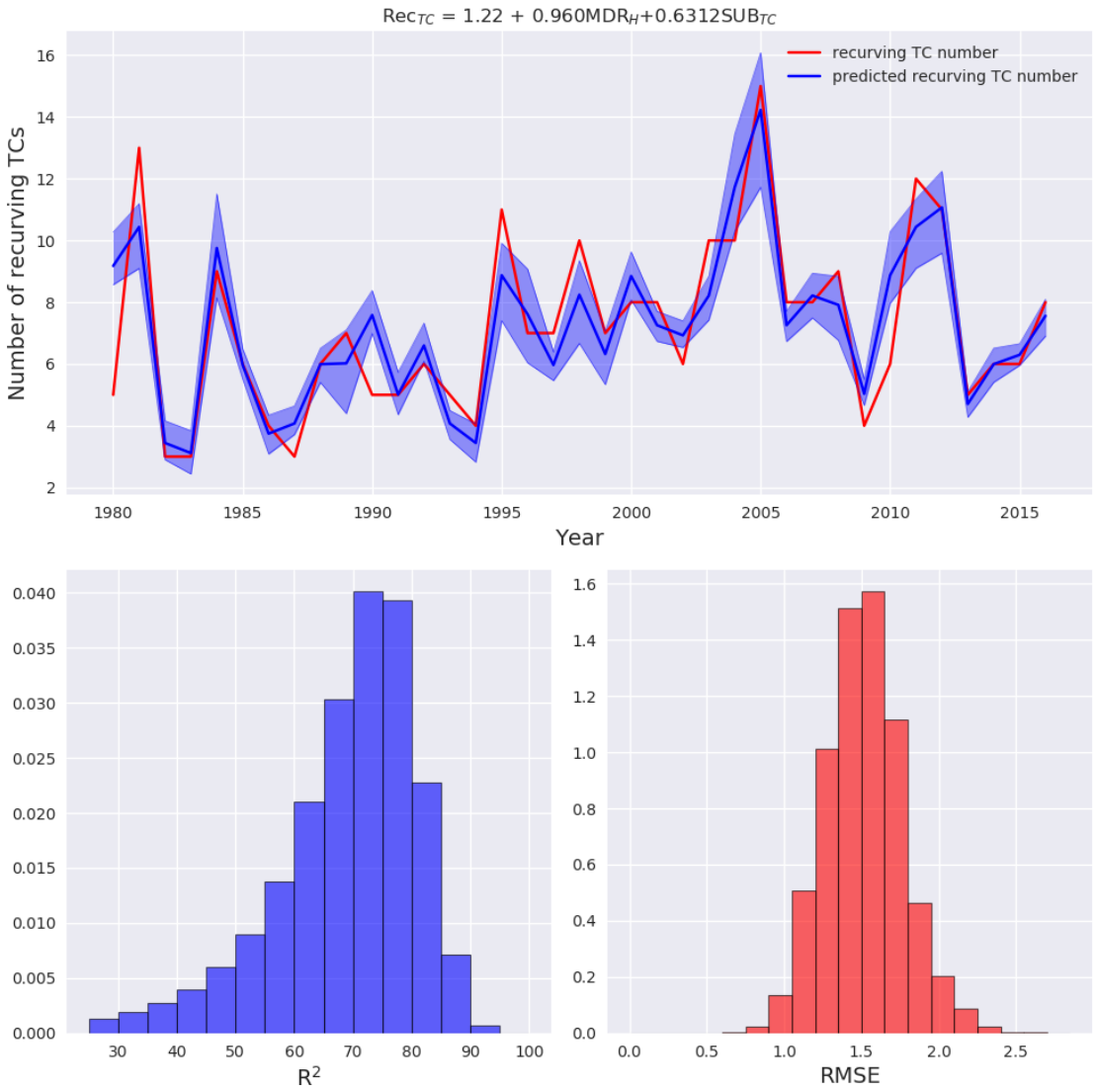

Figure 4.19. As in Figure 4.8 of the main manuscript but using MERRA2 matched tracks instead of ERA5 matched tracks.

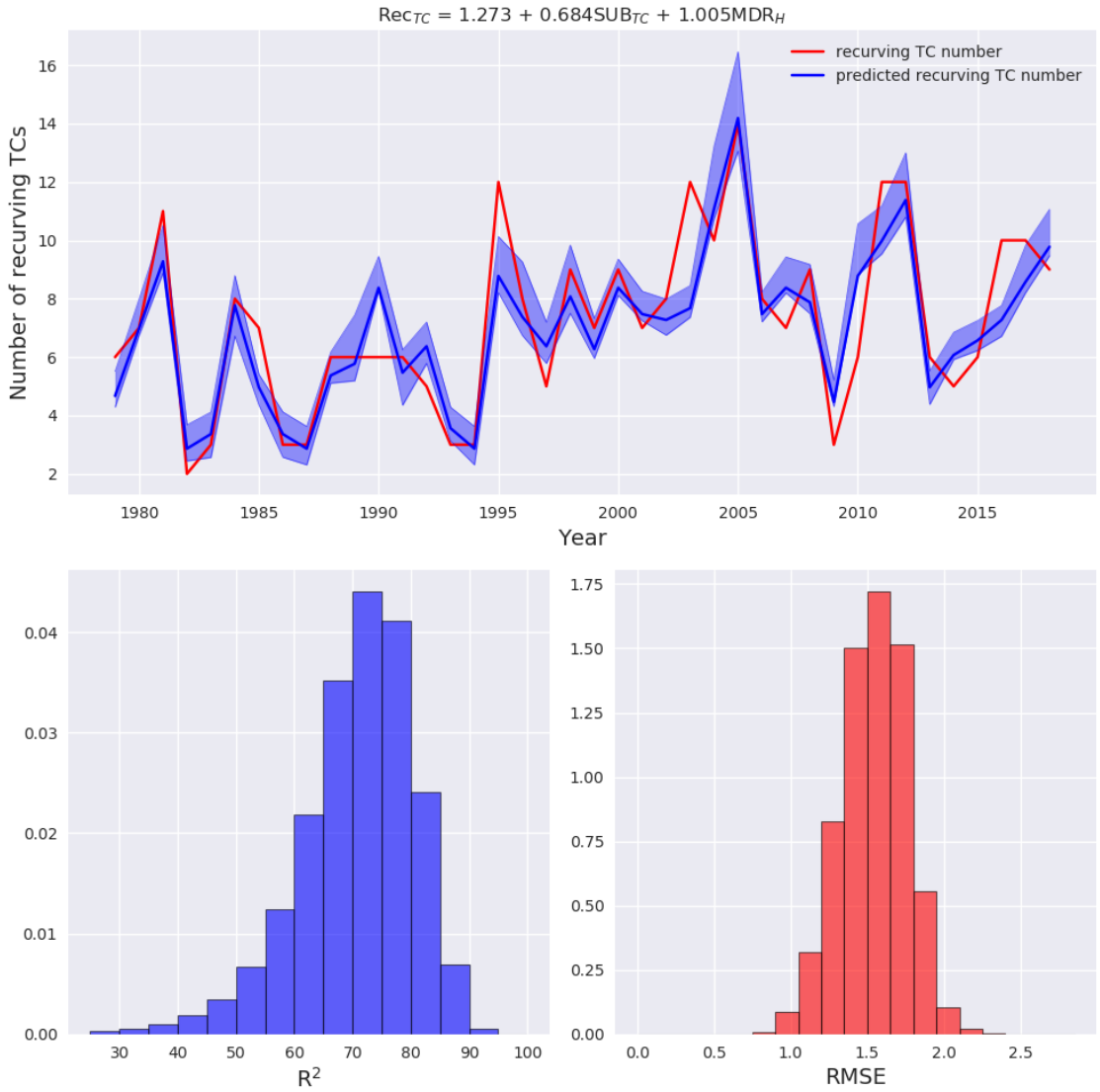

Figure 4.20. As in Figure 4.8 of the main manuscript but considering only TCs which have 10 m winds more than 17 m s^{-1} (i.e., named storm strength storms only).

In many previous studies, Poisson regression is used to model TC statistics. To test the sensitivity of our results to the regression method, a Poisson regression model is constructed using the same predictors (MDR hurricane frequency and SUB TC frequency) and predictand (recurving TC frequency). A model of the form

$$ln(Rec_{TC}) = \beta_0 + \beta_1 MDR_H + \beta_2 SUB_{TC} + \epsilon \quad (4.4)$$

is used.

Figure 4.21b shows that the R^2 distribution is very similar to in Figure 4.8b of the main manuscript, so the relationship between recurving TC frequency and the two predictors is relatively insensitive to the regression model used to explore the relationship.

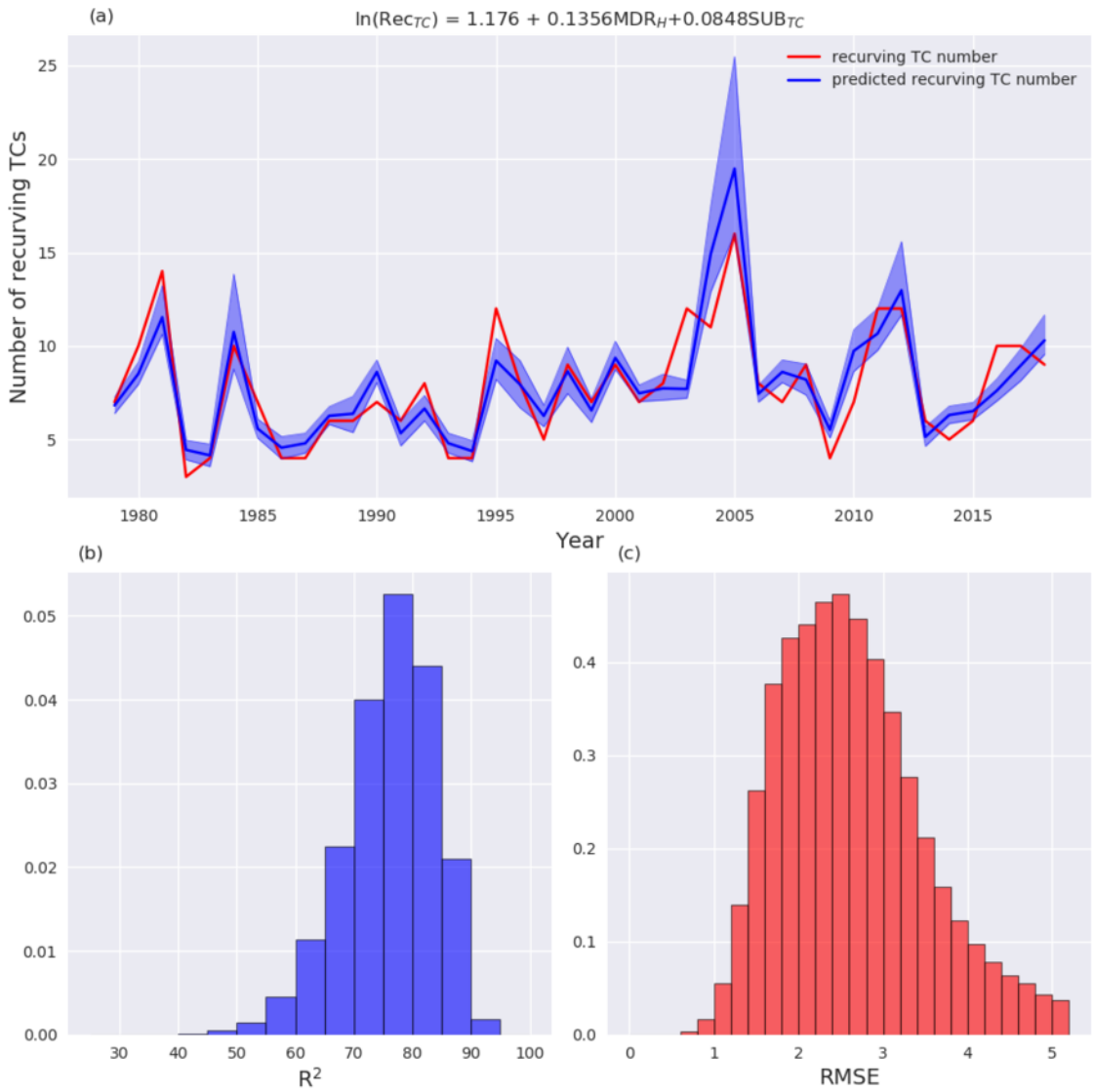

Figure 4.21. As in Figure 4.8 of the main manuscript, but this time the fit is made using a Poisson regression model with a logarithmic link function.

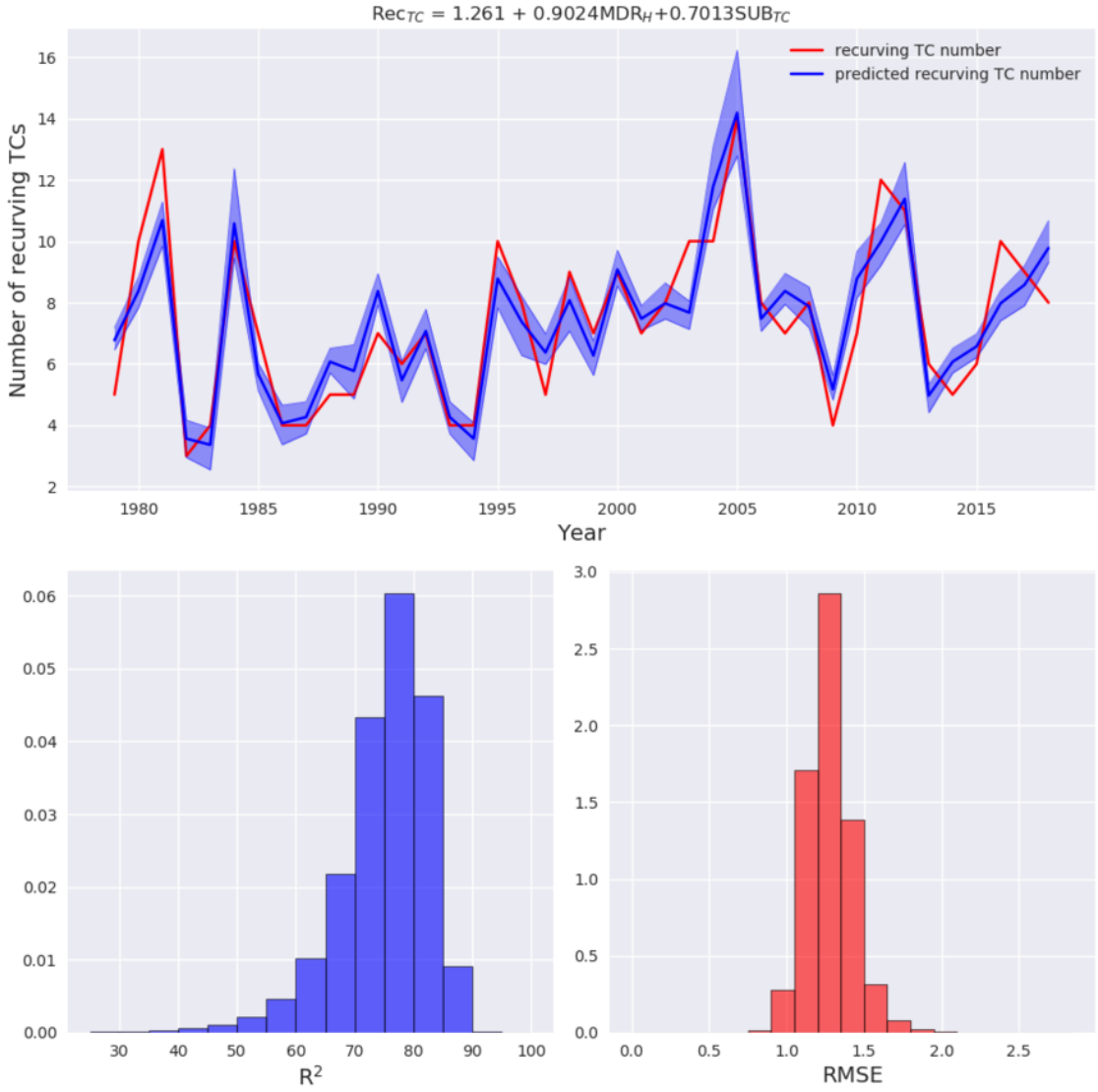

Figure 4.22. As in Figure 4.8 of the main manuscript but using a different recurvature domain: 36-70°N, 70°W-30°E.

4.5.6. Steering Flow Index Derivation

Figure 4.23 shows correlation maps between the recurving TC frequency (MDR and SUB regions) with the meridional deep layer steering flow (ASO) using spectrally filtered ERA5 data. The left-hand panel is used to identify the region to use for the steering flow index, used in Figure 4.9 of the main manuscript.

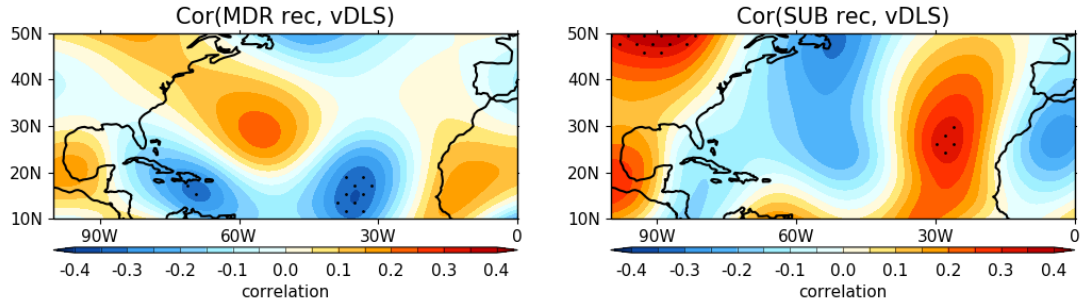

Figure 4.23. Correlation maps showing the Pearson's correlation coefficients between the meridional component of the seasonal mean deep layer flow (using spectrally filtered ERA5 data) and the MDR/SUB recurving TC frequency (left and right panels respectively).

4.5.7. SST Anomaly Analysis

To investigate the role of SST on TC activity in the MDR and SUB regions, we repeat the composite analysis shown in Figures 4.5-4.7, but this time looking at the ASO SST anomalies. ASO SST anomalies for each year are calculated between 1979 and 2018 by subtracting the ASO mean SST from 1979-2018. Linearly detrending the SSTs before compositing does not significantly alter the results, and so is not done in this instance. We separate years of very high, high, low, and very low activity (as defined in section 4.3.3.1), where 'activity' refers to MDR hurricane frequency (Figure 4.24) and SUB TC frequency (Figure 4.25). These activity metrics are chosen because they are the predictors used in the multiple linear regression model and are shown to have a very strong relationship with recurving TC frequency.

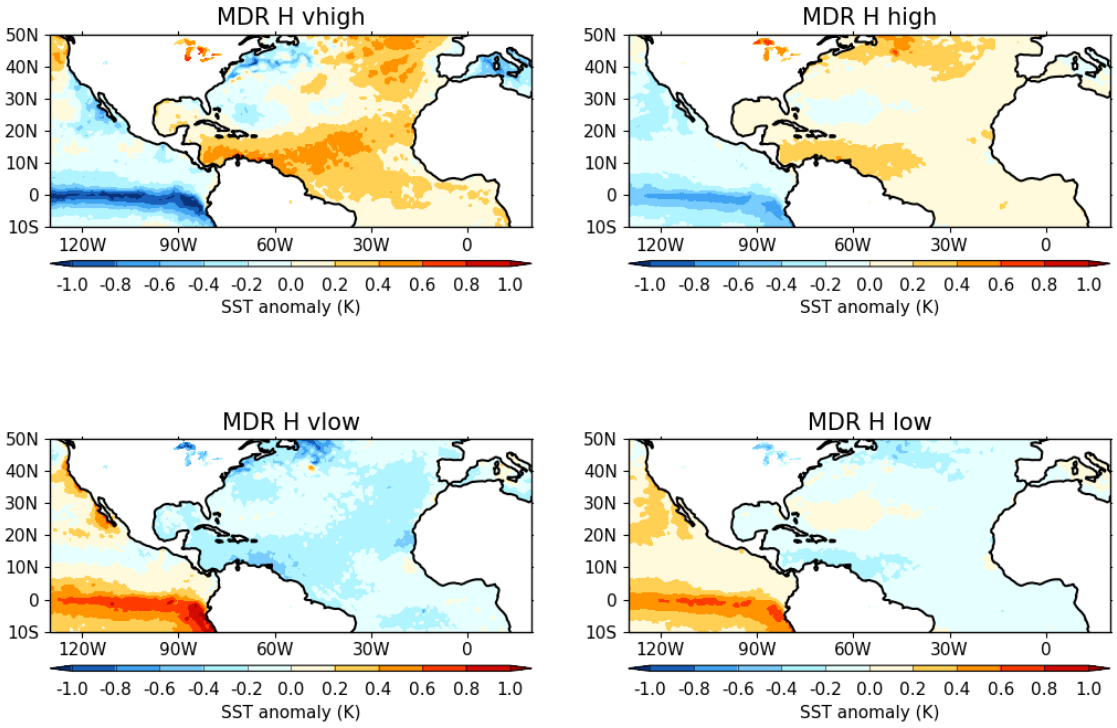

Figure 4.24. Composite differences in the SST anomaly based on the number of hurricanes forming in the MDR. (top left): MDR very high, (top right): MDR high, (bottom left): MDR very low, (bottom right): MDR low. Very high represents years in which the number of recurving TCs originating in the MDR is greater than the mean plus 1 standard deviation. Very low represents years in which the number of recurving TCs originating in the MDR is less than the mean minus 1 standard deviation. High represents years in which the number of recurving TCs originating in the MDR is greater than the mean. Low represents years in which the number of recurving TCs originating in the MDR is less than the mean.

During years which see high MDR hurricane frequency, negative SST anomalies are present in the eastern Pacific and positive SST anomalies are present in the tropical North Atlantic. La Nina conditions and above average SSTs in the tropical North Atlantic are both strongly correlated with TC activity (Landsea et al. 1999). During years of low MDR hurricane frequency, El Nino conditions are present and there is a negative SST anomaly in the tropical North Atlantic.

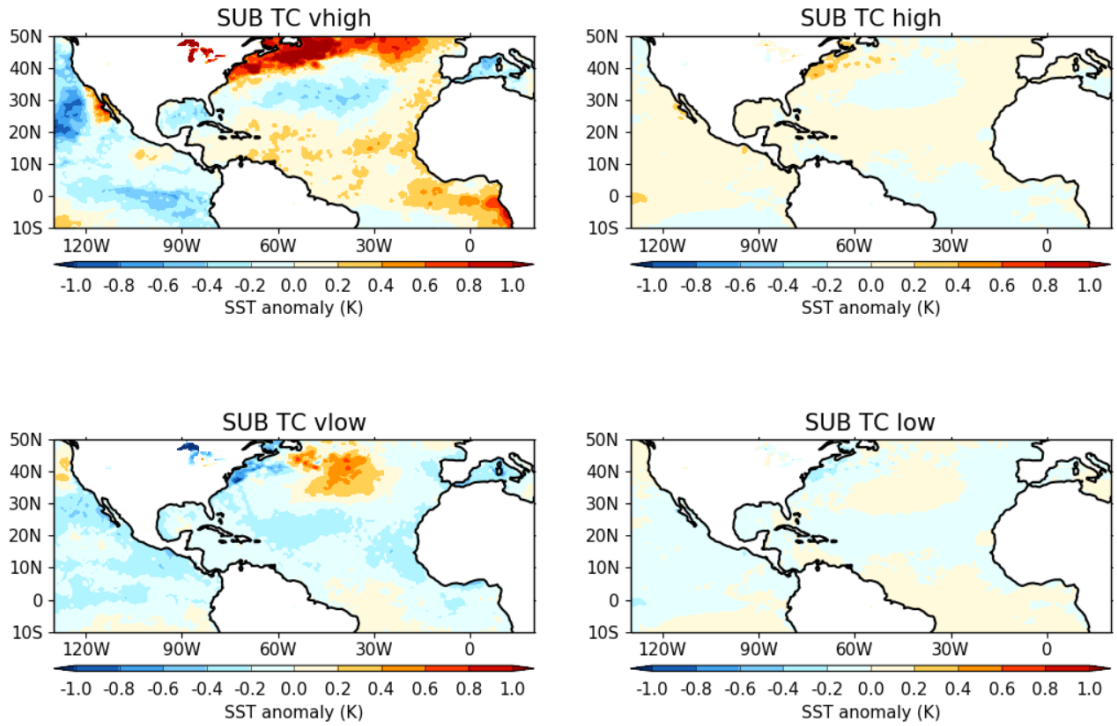

Figure 4.25. As in Figure 4.24, but for SUB TC frequency.

In the SUB region, there does not seem to be a relationship between TC activity and ENSO. This agrees with previous studies which show that, unlike the tropical Atlantic, higher-latitude forming TCs do not have a strong relationship with SSTs (Kossin et al.

2010). However, during years of high SUB TC frequency, positive SST anomalies can be seen along the midlatitude US East coast.

Figures 4.24 and 4.25 have been repeated using MDR recurving TC frequency and SUB recurving TC frequency, and the results are the same as shown in Figures 4.24 and 4.25.

Epilogue

In Chapter 4, is it shown that the interannual variability of recurving North Atlantic TCs is primarily governed by TC activity in the main development region and subtropical North Atlantic, with interannual variability in the seasonal mean steering flow playing a smaller, secondary role. This improves our understanding of the variability associated with TCs which reach the midlatitudes, which is a necessary condition of Europe-impacting PTCs.

In Chapter 5, we explore the variability associated with the second stage of the lifecycle of Europe-impacting PTCs as they traverse the midlatitudes. In particular, we investigate whether stronger TCs, or TCs which reintensify in the midlatitudes, are more likely to reach Europe than TCs which do not.

Chapter 5

Why do some Post-Tropical Cyclones Impact Europe?

Chapter 4 highlights that recurving North Atlantic TC frequency is governed by TC activity in the Main Development Region and the subtropical North Atlantic. As recurving TCs enter the midlatitudes, they often undergo extratropical transition (ET, section 1.3), transforming from TCs to PTCs. Previous studies have highlighted a number of different synoptic environments associated with Europe-impacting PTCs from a case study perspective. For example, ex-hurricane Ophelia (in 2017) was a strong TC (the easternmost major hurricane on record), and despite undergoing significant baroclinic development (Rantanen et al. 2020), the strength of the TC and its direct trajectory towards Europe likely contributed to the hazards associated with Ophelia. Conversely, ex-hurricane Debbie (in 1982) traversed the North Atlantic as a shallow, weak cyclone before rapidly re-intensified near Europe (Laurila et al. 2020), with the midlatitude environment playing a significant role in the hazards associated with Debbie. The relative importance of TC intensity and the favourability of the midlatitude environment for extratropical reintensification have not been investigated on a climatological timescale and are the focus of this chapter.

On the interannual timescale, the relationship between recurving TC frequency and Europe-impacting PTC frequency is relatively weak (r~0.36, Fig. 5.0). The focus in chapter 5 is therefore on the factors which may allow PTCs – defined here as recurving TCs which complete ET - to reach Europe on a storm-by-storm basis.

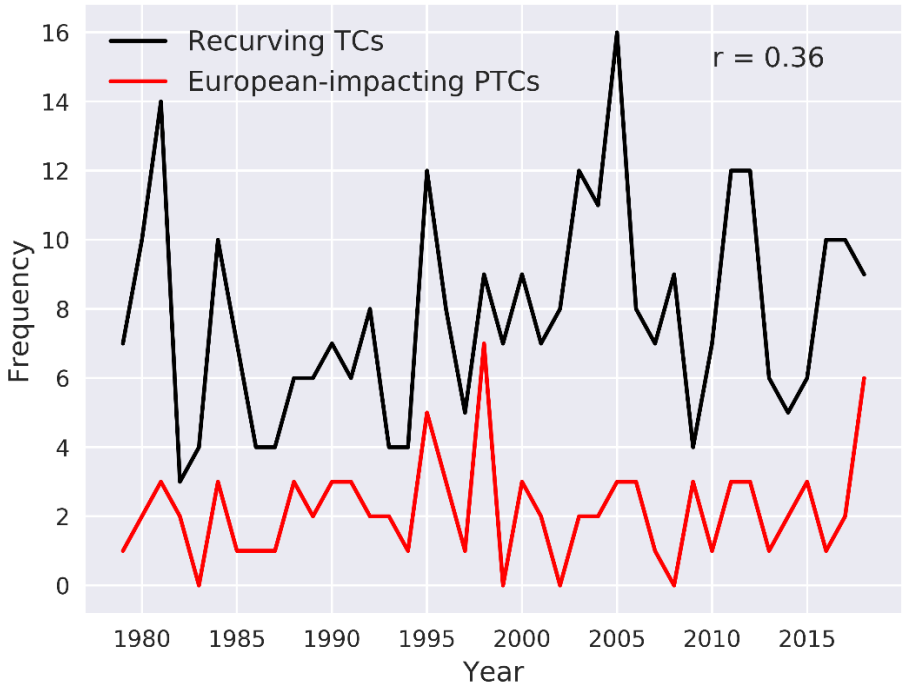

Figure 5.0. Time series of recurving TC frequency (black) and Europe-impacting PTC frequency (red). Recurving TCs and Europe-impacting PTCs are defined as in section 5.2.3.

This chapter has been accepted for publication in *Monthly Weather Review* (Sainsbury et al. 2022b)*:*

Sainsbury, E. M., R. K. H. Schiemann, K. I. Hodges, A. J. Baker, L. C. Shaffrey, and K. T. Bhatia, 2022a: Why do some Post-Tropical Cyclones impact Europe? *Mon. Weather Rev.*, accepted for publication.

Abstract

Post-tropical cyclones (PTCs) can bring high winds and extreme precipitation to Europe. Although the structure and intensity of observed Europe-impacting PTCs has been investigated in previous studies, a quantitative understanding of the factors important for PTCs to reach Europe has not been established. By tracking and identifying the full lifecycle of tropical cyclones (TCs) in the ERA5 reanalysis, we investigate why some PTCs impact Europe and why others do not, using a composite analysis. We show that PTCs which impact Europe are typically ~4-6 m s^{-1} stronger at

their lifetime maximum intensity and throughout the extratropical transition process. They are also twice as likely to reintensify in the midlatitudes. During ET, the Europe impacting PTCs interact more strongly with an upstream upper-level trough in a significantly more baroclinic environment. The Europe impacting PTCs are steered on a more poleward trajectory across a midlatitude jet streak. It is during the crossing of the jet that these cyclones often undergo their reintensification. We also find differences in ET latitude and seasonality, which may be associated with the distinct difference in TC intensity and midlatitude environment surrounding the two composites.

Using contingency table analysis, TC lifetime maximum intensity and whether post-ET reintensification occurs are shown to be significantly associated with the odds that a PTC reaches Europe. This supports our composite analysis and further indicates that TC intensity and reintensification both modulate the likelihood that a PTC will impact Europe.

5.1. Introduction

Tropical cyclones (TCs) which enter the midlatitudes often transition from symmetric, warm-core systems into cold-core, asymmetric extratropical cyclones during a process known as extratropical transition (ET). After ET, these post-tropical cyclones (PTCs) can bring extreme wind, precipitation and waves to regions far removed from the tropics (Evans et al. 2017; Jones et al. 2003). Ex-hurricanes Debbie (in 1961) (Graham and Smart 2021) and Ophelia (in 2017) (Stewart 2018; Rantanen et al. 2020) both set national wind speed records in Ireland. Across Scotland in 2011, ex-hurricane Katia (Grams and Blumer 2015) was responsible for over £100 million in damages due to extreme winds, and further east across Europe, ex-hurricane Debby caused severe damage over northern Finland in 1982 (Laurila et al. 2020). PTCs are also climatologically associated with higher intensities over Europe than midlatitude cyclones. PTCs impacting Northern Europe are typically 3.5 m s^{-1} stronger in terms of their maximum 10 m wind speed, and 10 hPa deeper, than the midlatitude cyclones that impact the region during the hurricane season (Sainsbury et al. 2020).

Climatological assessments of PTCs and their impacts over Europe have been documented in previous studies. Baker et al. (2021) show that approximately 10% of cyclones with tropical Atlantic origin impact Europe, and those retaining or redeveloping warm-core characteristics often have higher windspeeds over Europe. These cyclones often attain their lowest sea level pressure a day after impacting Europe, enhancing their destructive potential (Dekker et al. 2018). These studies improve our understanding of the characteristics and impacts associated with PTCs across Europe and are a crucial addition to the ET climatologies constructed for the North Atlantic more broadly (e.g., Hart and Evans 2001; Bieli et al. 2019; Studholme et al. 2015). However, their focus is not on why, or how, these PTCs reach Europe. A quantitative understanding of the factors important for these systems to reach Europe has not been established and is addressed in this study.

Many previous studies investigate the TC-midlatitude flow interaction associated with the downstream impacts of ET, and this interaction also has implications for the transitioning cyclone itself (Jones et al. 2003; Keller et al. 2019). If the transitioning TC recurves relative to an upstream trough, the advection of anticyclonic potential vorticity by the divergent outflow of the cyclone can lead to local jet streak development, downstream ridgebuilding, and the amplification of a downstream Rossby wave packet (Riemer et al. 2008; Riemer and Jones 2010; Archambault et al. 2013; Riboldi et al. 2019; Keller 2017). Climatologically, ET-related flow amplification is greater in the western North Pacific than in the North Atlantic (Torn and Hakim 2015; Quinting and Jones 2016), however North Atlantic ET events have also been associated with downstream high-impact weather (Grams and Blumer 2015; Pohorsky et al. 2019), downstream flow amplification (Quinting and Jones 2016; Brannan and Chagnon 2020) and a reduction in downstream predictability (Anwender et al. 2008; Pantillon et al. 2013, 2015, 2016). Advection of midlatitude potential vorticity by the outflow anticyclone associated with a transitioning TC can lead to a local deceleration of the upstream trough (Agusti-Panareda et al. 2004; Archambault et al. 2015; Keller et al. 2019), leading to a prolonged period of favourable phasing (phase-locking) between the transitioning TC and the midlatitude waveguide and additional downstream flow amplification.

The TC-trough interaction conducive for downstream amplification also favours reintensification of the transitioning TC (Klein et al. 2000; Keller et al. 2019; Grams et al. 2013a,b). TCs which recurve relative to an upstream trough (the northwest pattern, Harr et al. 2000) are typically steered on a more poleward trajectory and are much more likely to undergo reintensification in the midlatitudes, with reintensification enhanced by increases in eddy heat flux (Harr et al. 2000a). In the North Atlantic, an association has previously been found between reintensification post-ET and interaction with a negatively tilted (north-west to south-east) trough. The negative tilt permits the cyclone a closer approach to the trough and is associated with a contraction and increase in eddy potential vorticity towards the centre of the transitioning TC (Hart et al. 2006), although more recent work suggests that the negative tilt may be a consequence of strong TC-trough interaction, rather than a predictor for future PTC outcomes (Sarro and Evans 2022). Many climatological studies of PTC evolution are focused around TCs in the Western North Pacific (e.g., Harr et al. 2000; Klein et al. 2000, 2002), with much focus on case studies in the North Atlantic (e.g., McTaggart-Cowan et al. 2001, 2003, 2004; Agusti-Panareda et al. 2004). As far as the authors are aware, Hart et al. (2006) is the only published study on the climatological factors determining post-ET evolution of PTCs. However, it uses a very small sample size, with 6 reintensifying cyclones and 11 weakening cyclones. To generalize the results from case studies, an updated climatology for the North Atlantic basin is necessary.

Not only are PTCs disproportionately responsible for high-impact windstorm risk in the current climate (Sainsbury et al. 2020), their frequency and intensity across Europe may also increase in the future due to climate change (Haarsma et al. 2013; Baatsen et al. 2015). However, accurately simulating PTCs can be challenging for CMIP-class climate models due to their coarse resolution (Davis 2018). Many climate models are unable to accurately simulate TC genesis and intensity, which are likely to be important for simulating PTC statistics. Even high-resolution climate models, such as used in Haarsma et al. (2013) are not sufficient to simulate the strongest TCs (Vidale et al. 2021). If a good physical understanding can be established surrounding the factors which are important for PTCs to reach Europe, and how these factors will change because of climate change, then this information can be used to inform future modelling studies on projected changes of Europe-impacting PTCs.

Europe-impacting PTCs generally recurve near the US East Coast (i.e., Figure 5.1b in Baker et al. 2021) and often travel across the entire North Atlantic before they reach Europe. Longevity is therefore key to their ability to reach Europe. We hypothesize two influences for PTC longevity, related to 1) the tropical environment in which the storm originates and resides as a TC, and 2) the midlatitude environment that the TC transitions into. On point 1), a very strong TC which recurves into the midlatitudes will have a stronger warm-core structure, which may be consistent with increased resilience to hostile midlatitude conditions. This could potentially allow the TC to survive longer and reach Europe. Previous studies have highlighted that stronger North Atlantic TCs are able to endure hostile conditions for longer. Hart and Evans (2001) show that weak TCs only tend to reintensify post-ET if they have a transit time of less than 20 hours between a region favourable for tropical cyclogenesis (potential intensity < 960 hPa) and a region favourable for extratropical cyclogenesis (Eady growth rate > 0.25 day^{-1}). However, two thirds of strong TCs (minimum sea level pressure < 970 hPa) which reintensify endured more than 20 hours of transit time. On point 2), if the midlatitude environment into which the TC recurves and transitions is favourable for reintensification, then the PTC will likely reintensify, extending the length of the PTC's life. We therefore hypothesize that PTCs which originate or travel through an environment characterised by warm SSTs and low wind shear (favourable for TC intensification), and PTCs which interact strongly with an upstream trough in a baroclinic environment (favourable for reintensification; e.g., Klein et al. 2000; Harr et al. 2000; Riboldi et al. 2019) will be more likely to reach Europe.

In this paper, we investigate whether there are differences in cyclone and environmental characteristics between PTCs which do, and do not, reach Europe. This is achieved by creating an updated climatology of PTCs. By separating PTCs based on whether they impact Europe, we can use a composite analysis to investigate whether Europe-impacting PTCs are more intense in the tropical phase of their lifecycle, or reintensify more post-ET, than PTCs which don't reach Europe.

The paper continues in section 5.2 with a description of the data and methodology. Section 5.3 contains a composite analysis of PTCs which do and do not impact Europe, along with an evaluation of which factors may be important for a PTC to impact Europe. The paper concludes with a discussion in section 5.4.

5.2. Data and Methods

5.2.1. Data

The ERA5 (Hersbach et al. 2020) reanalysis provides the environmental fields for analysis and the geopotential height fields used for cyclone phase space (CPS, Hart 2003) parameter calculation (300-, 600-, 900 hPa). Relative vorticity fields from 600-850 hPa are also used for cyclone tracking. All data used are 6-hourly. For more information, see section 2.1.1.1.

Observational best track TC data from HURDAT2 (section 2.1.2) are used for objective track matching and to provide realistic wind and pressure data for the tropical phase of the cyclones, as reanalyses underestimate the intensity of TCs due to their insufficient horizontal resolution (Hodges et al. 2017).

5.2.2. Cyclone Detection and Tracking

We use TRACK (Hodges et al. 2017) to track the cyclones through the ERA5 reanalysis. For more information, see section 2.2.

5.2.3. Objective Track Matching

To identify which of the tracked cyclones correspond to the observed TCs, we employ objective track matching (section 2.3.1). TCs tracked through ERA5 are identified as PTCs if they enter a region in the North Atlantic midlatitudes between 36-70°N, 70°W-30°E and complete ET (section 5.2.4). PTCs are further designated as 'Europe PTCs' if they enter the domain 36-70°N, 10°W-30°E, or 'NoEurope PTCs' if they enter the PTC domain and complete ET, but do not impact the 'Europe' region. These regions are constructed such that all Europe-impacting PTCs are defined as PTCs, as the European domain is wholly contained within the PTC domain. These domains have been overlaid on Figure 5.1 (black box for the PTC domain, red box for the Europe domain). During our analysis period (1979-2018), there are 60 PTCs which reach Europe, and 120 PTCs which do not. To ensure the results are robust to this difference in sample sizes, bootstrap resampling was used to generate samples of size 60 for the PTCs which do not reach Europe. This process was iterated 1000 times, and the composites reproduced for the resampled mean. The results were not sensitive to the difference in sample size (not shown).

5.2.4. Extratropical Transition

TCs entering the midlatitudes often undergo extratropical transition, a process whereby the vertically stacked, symmetric cyclone loses its deep warm core and becomes asymmetric as it develops frontal features. This process can be captured objectively using the cyclone phase space (CPS) parameters described in Hart (2003). More information is available in section 2.3.3. The beginning of transition, ET onset, is defined as the time at which the cyclone loses its lower-level warm core or becomes thermally asymmetric (B > 10 m or $-|V_T^L|$ < 0). ET completion is then defined when both criteria are met, i.e., the low-level thermal wind becomes negative, and B exceeds 10 m.

Note that some TCs, particularly very weak ones, never attain a symmetric, deep warm-core structure in the reanalyses ($-|V_T^L|$ and $-|V_T^U|$ never both > 0, B never < 10). As these TCs never meet the CPS criteria for a TC to begin with, they cannot start, or complete ET. Therefore, these cyclones are excluded from the analysis. While tropical depressions and subtropical cyclones are not strictly excluded from our analysis, they rarely meet the CPS criteria, and therefore cannot complete ET and are also excluded. Table 5.1 documents the sample size for PTCs (TCs which both enter the PTC domain and complete ET in ERA5). Data from the 3rd column are used for the intensity analysis of section 5.3.2 and in Figure 5.10b, and data from the 2nd column are used for all other analysis presented.

5.2.5. Storm-Centred Composite Methodology

To investigate the midlatitude environment around PTCs which do and do not impact Europe, a storm centred composite methodology is used. This is the same method as used in Bengtsson et al. (2007), Catto et al. (2010) and Dacre et al. (2012). Data in a cap of pre-specified radius around the cyclone is extracted from the full field onto a radial co-ordinate system which is centred on the cyclone (initially centred on the pole and then rotated to the storm centre). This is done to avoid problems associated with changes in grid spacing across the sphere. In section 5.3.3.1, storms are oriented based on their propagation direction, however in sections 5.3.3.2 and 5.3.4, they are not. This is because in section 5.3.3.1 we focus our analysis on the cyclone structure, whereas in sections 5.3.3.2 and 5.3.4 we are interested in the environment

surrounding the cyclones. For more information on this storm-centred composite method, see the appendix of Bengtsson et al. (2007).

5.2.6. Statistical Significance

Significance of results is calculated using a two-sample Kolmogorov-Smirnov test to compare the distributions of the Europe and NoEurope PTCs. In order to account for spatial correlations in Figures 5.3, 5.4 and 5.7, the methodology of Wilks (2016) is also employed to account for the False Discovery Rate, using α_{FDR} = 0.05. This leads to the null hypothesis (no difference between Europe and NoEurope PTCs) being rejected less frequently than when simply assuming significance if the p-value for the null hypothesis is less than 0.05.

5.2.7. Eady Growth Rate and Potential Vorticity Diagnostics

To investigate whether there are differences in the baroclinicity surrounding the two PTC composites, the Eady growth rate (Hoskins and Valdes 1990), σ, is calculated as in previous studies (Liu et al. 2017; Baker et al. 2022). Eady growth rate is defined as

$$\sigma = 0.31 \frac{f}{N} \frac{\partial U}{\partial Z}, \tag{5.1}$$

where f is the Coriolis parameter, N is the Brunt-Vaisala frequency, $U = U(u, v)$ is the zonal and meridional components of the horizontal wind, and Z is the isobaric height. Vertical derivatives for Z and the horizontal wind are calculated between the 250- and 850 hPa isobaric height surfaces using 6-hourly ERA5 data.

The interaction between a transitioning TC and an upper-level trough is associated with downstream ridgebuilding and jet streak amplification (e.g., Keller et al. 2019), which is largely the result of negative PV advection associated with the TC's divergent outflow (Riemer et al. 2008; Grams et al. 2013b; Pantillon et al. 2013). TC-trough interaction also plays a crucial role in whether the transitioning TC subsequently reintensifies after ET (Hart et al. 2006; Harr et al. 2000a; Riboldi et al. 2019). To quantify the interaction between transitioning TCs and upstream troughs, the negative potential vorticity advection by the irrotational wind (Archambault et al. 2013),

$$PV_{irrot} = \overrightarrow{-V_\chi} \cdot \nabla_P PV, \tag{5.2}$$

is calculated using 6-hourly ERA5 data. Potential vorticity and horizontal winds are averaged between 250- and 350 hPa. The wind is decomposed into irrotational and rotational components using a Helmholtz partition as in previous studies (Quinting and Jones 2016; Riemer et al. 2008). Both σ and PV_{irrot} are averaged in a 15-degree cap centered on the cyclone during ET for comparison between the composites.

5.3. Results

Here we present a composite analysis of the Europe-impacting PTCs (hereafter referred to as 'Europe PTCs'), and the PTCs which do not impact Europe (hereafter called 'NoEurope PTCs'). We first investigate differences in the composite mean TC trajectories and the role of TC intensity, followed by differences in the cyclones and environment about the point of extratropical transition (ET). Analysis centred about the point of extratropical reintensification post-ET is then presented, followed by analysis of the relative importance of the differences between the composites.

5.3.1. Cyclone Trajectory

The composite trajectories for the Europe and NoEurope PTCs are first plotted to investigate whether there are differences in the location of recurvature, and to understand how the trajectories differ in the midlatitudes. The composite trajectories are constructed using the average location of all Europe and NoEurope PTCs at each time step, centred about the point of ET completion. This is presented in Figure 5.1a. A one day running mean is used to smooth the cyclone tracks before compositing, and the composite trajectory is only shown for the time steps for which there are at least 10 TCs still present.

Both the Europe and NoEurope PTCs tend to start in similar locations over W Africa, where the seeds for many strong TCs exist as African Easterly Waves (Landsea 1993; Russell et al. 2017; Thorncroft and Hodges 2001). TC variability in the Main Development Region, where African Easterly Waves propagate to and often become TCs, is largely controlled by the large-scale tropical environment and is discussed in greater detail in section 4.1. The Europe PTCs recurve and enter the PTC domain approximately 5 degrees further east in the basin. The largest differences between the composites are the position of ET completion, and the post-ET trajectory of the composites. The NoEurope PTCs travel north-eastwards in the midlatitudes after

entering the PTC domain, attaining an average maximum latitude of approximately 45°N. The Europe PTCs continue to gain latitude as they cross the Atlantic, reaching ~55°N whilst over Europe. This may allow the Europe PTCs to enter a more baroclinic environment, aiding extratropical reintensification as the cyclones recurve and travel towards Europe. Genesis densities show no difference in the genesis location of the PTCs which do, and do not impact Europe.

The Europe PTCs complete ET significantly (95%, Kolmogorov-Smirnov test) further poleward and significantly further eastwards (15 degrees further east and 4.4 degrees further poleward) than the NoEurope PTCs. However, the difference between composite locations of ET onset is much smaller, indicating that the Europe PTCs travel a greater distance during ET, possibly indicating that the westerlies in the vicinity of the Europe PTCs are stronger than for NoEurope PTCs. The Europe PTCs undergo greater acceleration during ET than NoEurope PTCs (Fig. 5.1b), consistent with the stronger temperature gradients shown in Figure 5.3. There is also a distinct difference in seasonality of the Europe and NoEurope composites. Only 15% of PTCs which complete ET in June reach Europe, however 50% of PTCs completing ET in November reach Europe (Fig. 5.12). There is no significant difference in the length of ET between the composites (2.1 and 2.0 days for Europe, NoEurope PTCs respectively).

The NoEurope PTCs have a shorter lifespan in the midlatitudes, and as a result, do not make it as far east as the Europe PTCs. This confirms that longevity is crucial in determining whether a PTC will impact Europe, as the NoEurope PTCs dissipate on approach. The mean midlatitude translation speed, averaged over the cyclone's whole lifecycle post-ET, is similar and differences are non-significant between both composites (12.5 and 11.7 m s^{-1} for Europe and NoEurope PTCs respectively). However, the maximum midlatitude translation speeds differ significantly at the 95% level (23.2 and 19.5 m s^{-1} for Europe and NoEurope PTCs respectively). This may indicate that Europe PTCs are more likely to rapidly propagate eastwards in the presence of a jet streak and is consistent with Figure 5.6.

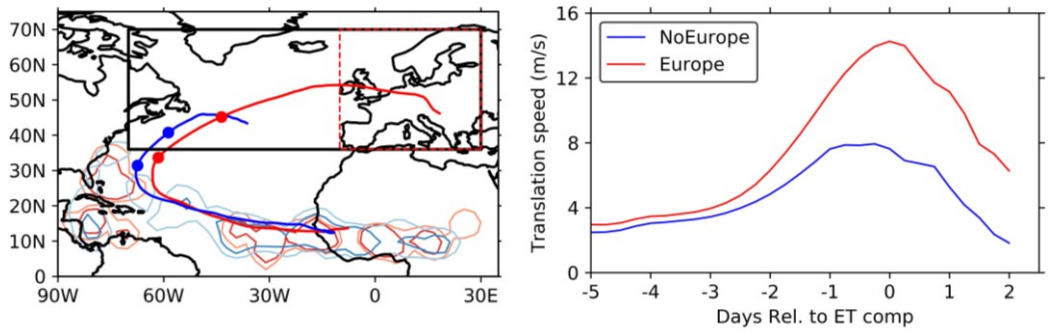

Figure 5.1. (a) Composite trajectory of the Europe PTCs (red) and the NoEurope PTCs (blue), centred on ET completion. Dots represent the composite mean location of ET onset (dots outside the PTC domain) and completion (dots inside the PTC domain). Open contours represent the genesis density (contours shown for 1 and 2 TCs per unit area per year, where the unit area is equal to a 5-degree radius cap). Black box shows the PTC domain, and the red dashed box shows the European domain. (b) shows the composite mean translation speed for the two composites centred on ET completion.

5.3.2. The Association Between TC Intensity and Europe Impact Likelihood

To investigate which factors may influence the likelihood that a PTC will impact Europe, we first analyse the tropical phase of the cyclones. In this section, we compare the intensity of the Europe and NoEurope PTCs. Figure 5.2 shows the composite intensity as a function of time for the Europe (red) and NoEurope (blue) PTCs, centred about ET completion. The bottom panel shows the number of cyclones (Europe and NoEurope) which go into the composites at each time step. We use intensity data (MSLP and 10 m wind) from HURDAT2 and ERA5.

The Europe PTCs are significantly more intense (10 m wind and sea level pressure) than the NoEurope PTCs. This may be consistent with the Europe PTCs having a more resilient structure, capable of withstanding the structural changes through ET for longer as baroclinicity and shear increase, and SSTs decrease. This significant difference persists from before the time of composite mean maximum intensity until several days after ET has completed, however the sample size decreases rapidly from the time step of ET completion onwards (Fig. 5.2c). Overall, the significant difference persists for greater than 7 days. At the composite mean maximum intensity (Figure 5.2a) and actual TC lifetime maximum intensity, the Europe PTCs are more than 5 m s^{-1} stronger than the NoEurope PTCs, and this difference increases to almost 10 m s^{-1} by two days' post-ET completion. Figure 5.2 also shows a secondary peak in intensity

after ET completion for the Europe PTCs, in agreement with Baker et al. (2021) (Figure 8 therein), indicating that this post-ET intensity increase is seen across reanalyses. Furthermore, this suggests that there may be greater reintensification associated with the Europe PTCs than is associated with the NoEurope PTCs. Europe PTCs appear to reintensify more when considering the SLP (Fig. 5.2b) than when considering wind (Fig. 5.2a). This may be the result of the Europe PTCs gaining more latitude than the NoEurope PTCs, entering a region of lower climatological background pressure. However, as there are indications of reintensification in the wind data (Fig. 5.2a), it is likely that the Europe PTCs are undergoing some reintensification, which is confirmed in sections 5.3.4 and 5.3.5. Intensity estimates from ERA5 (dashed lines, Figs. 5.2a and b) before ET completion should be treated with caution, as reanalyses do not have sufficient resolution to capture the structure and intensity of TCs (Hodges et al. 2017). ERA5 is included to check whether there is agreement with observational HURDAT2 data post-ET completion, which is necessary if we wish to rely on ERA5 for cyclone analysis in section 5.3.3 onwards. We see qualitative agreement with HURDAT2, with ERA5 data indicating that Europe PTCs are significantly more intense than the NoEurope PTCs throughout their lifecycle, with further signs of possible reintensification of Europe PTCs in Fig. 5.2b.

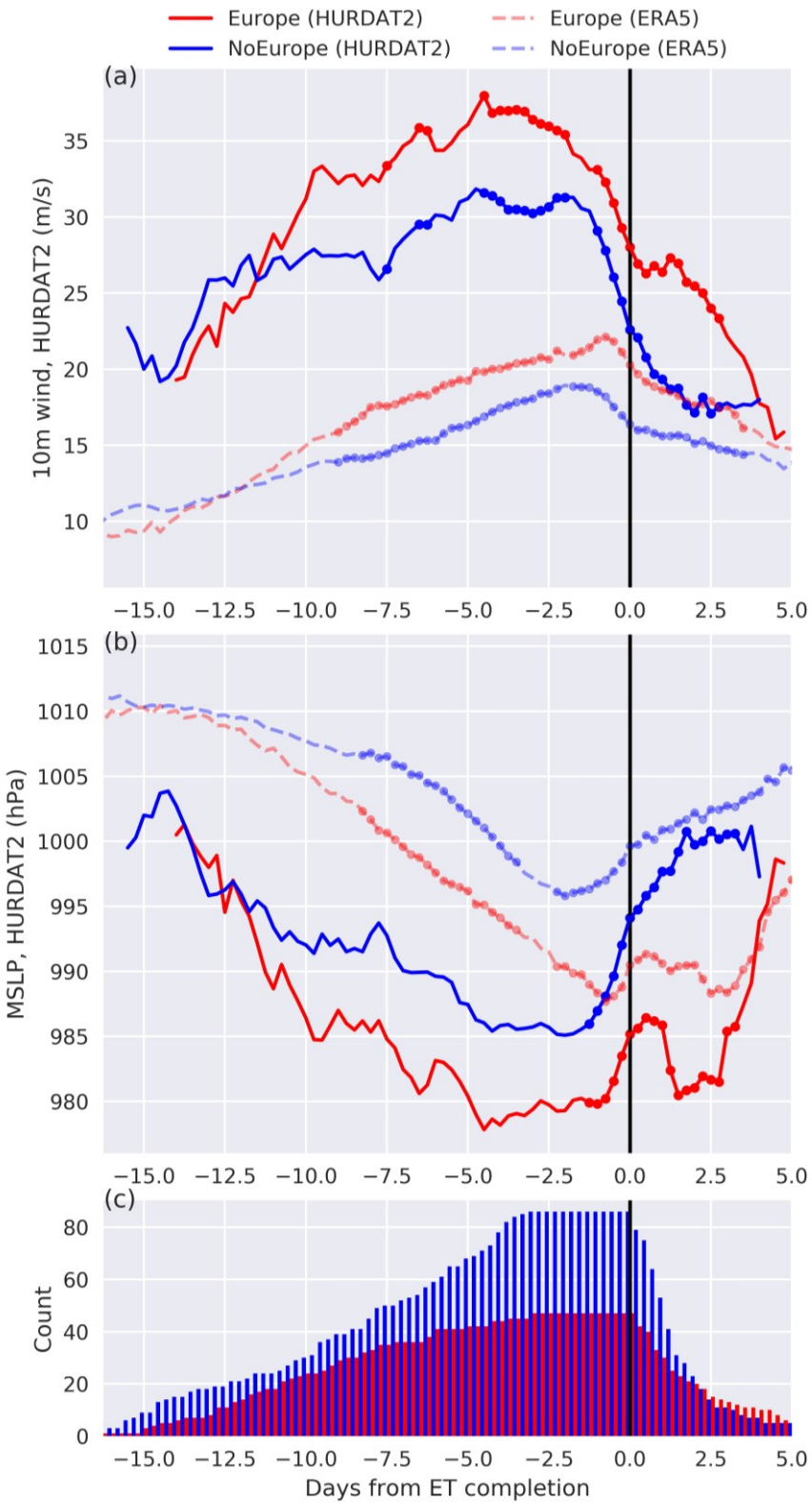

Figure 5.2. Composite lifecycle of the intensity of the Europe (red) and NoEurope PTCs (blue): (a) for 10 m wind, (b) for MSLP for HURDAT2 (solid lines) and ERA5 (dashed lines). (c) shows the sample sizes for the HURDAT2 data. Dots overlaid represent the time steps at which the difference in the intensities is significant to 95%.

	PTCs	HURDAT2 obs. available at designated ET completion time
Europe	60	47
NoEurope	120	87
Total	180	134

Table 5.1. Sample sizes for the Europe (second row), NoEurope (third row), and total (Europe + NoEurope) PTCs (bottom row) considering: all storms tracked in the ERA5 reanalysis with a matching TC in HURDAT2 which complete ET in ERA5 and enter the PTC domain (black box in Figure 5.1) (2nd column), and those which at the time step of ET completion in the reanalysis still have observational data available in HURDAT2 (3rd column, which is the basis for Figure 5.2).

5.3.3. Composite Evolution of Storm Structure and Surrounding Environment

5.3.3.1. Evolution of Storm Structure

In this section we investigate the structure of the cyclone-centred composites of the Europe and NoEurope PTCs. This analysis aims to assess whether differences in cyclone characteristics exist, and if they do exist, whether they are consistent with our hypothesis that PTCs which reintensify are more likely to reach Europe. Figure 5.3 shows a 48-hour evolution of the 850 hPa temperature in a 20-degree cap around the cyclones, centred on the completion of ET. For each cyclone, the anomaly is calculated by subtracting the mean 850 hPa temperature over the 20-degree cap before the compositing is applied. The cyclones are oriented based on their propagation direction, such that the cyclones are moving west to east in the composite.

During the 48-hour period centred on ET completion, the composite mean temperature gradient is much larger for the Europe PTCs than the NoEurope PTCs. The 850 hPa temperature range in a 10-degree cap about the cyclone centre is 74%, 27% and 54% greater for the Europe PTCs than the NoEurope PTCs at 24 hours prior to ET completion, at ET completion, and 24 hours after ET completion, respectively. This may be associated with the difference in location of the Europe and NoEurope PTCs throughout this stage in the cyclone's lifecycle shown in Figure 5.1. A second factor influencing the composites may be their distinct difference in seasonality (Fig. 5.12); most of the Europe PTCs occur later in the season than NoEurope PTCs, and hence interact with a midlatitude environment which is climatologically more baroclinic.

Differencing (Europe minus NoEurope) the cyclone composites highlights significant differences (Figure 5.3 g-i). The Europe PTCs are associated with statistically significantly cooler 850 hPa temperatures to the left of the cyclone's propagation direction than the NoEurope PTCs. These cyclones mainly travel from west to east (or south-west to north-east), and so the area above the cyclone centre in Figure 5.3 is likely to represent the region poleward of the cyclones. Considering the absolute 850 hPa temperatures, the Europe PTCs have significantly colder temperatures to the left of their propagation direction, but similar temperatures in the warm sector, despite the Europe PTCs being ~5 degrees further poleward (not shown). This suggests that Europe PTCs are associated with considerably stronger warm air advection, and highlights that the enhanced temperature gradient accompanying the Europe PTCs is likely associated with the differences in position (Fig. 5.1a) and seasonality (Fig. 5.12) between the composites.

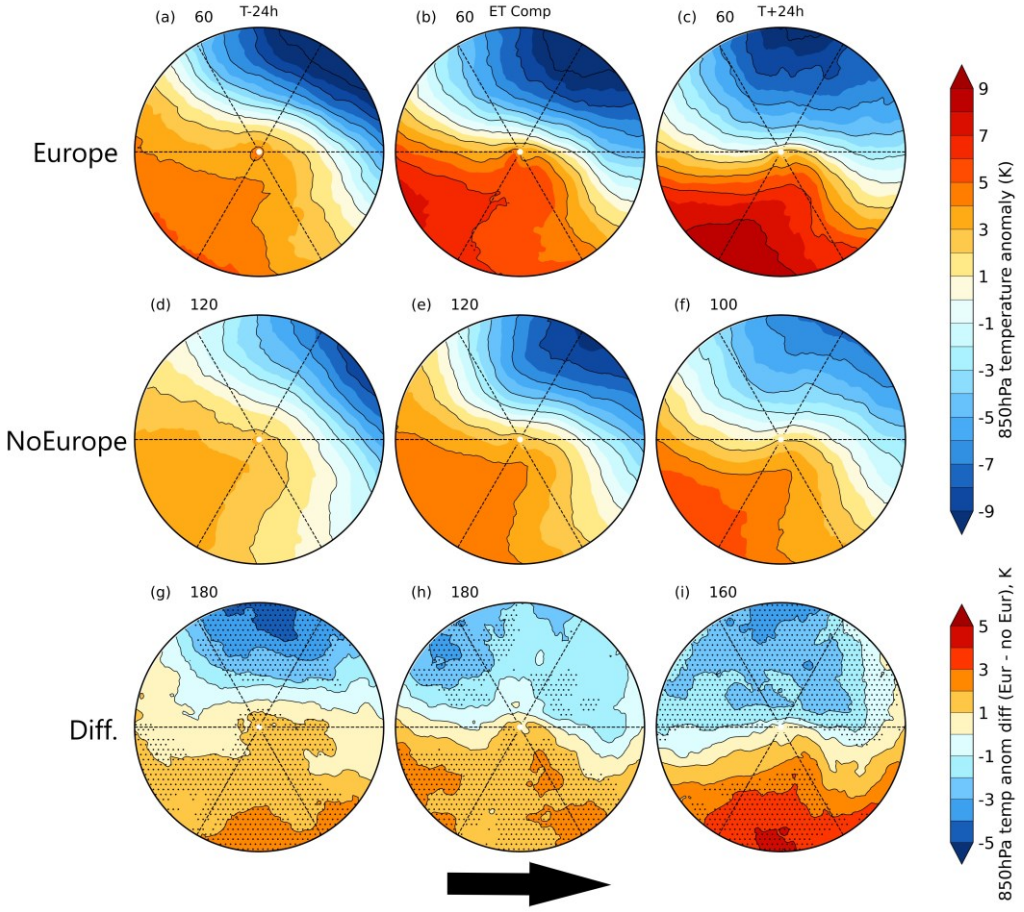

Figure 5.3. Storm centred composite (20-degree cap) of the 850 hPa temperature anomaly (850 hPa temperature minus the 20-degree cap radial mean 850 hPa temperature) for the Europe PTCs (a-c) and the NoEurope PTCs (d-f), and the difference (g-i, Europe minus NoEurope). Plots show a 48-hour evolution, centred about the point of ET completion. Cyclones are aligned according to their direction of travel before compositing, so that they move from west to east in the composite. For panels' g-i, stippling denotes the regions in which the differences are significant to 95%. Large arrow shows the direction of storm propagation. Sample size is shown to the upper-left of each panel.

Figure 5.4 is equivalent to Figure 5.3 but instead shows the 850 hPa cyclone-relative wind magnitude and direction. As with Figure 5.3, cyclones are oriented based on their propagation direction before compositing. Cyclone relative wind magnitude and direction are calculated by subtracting the translation velocity from the Earth-relative winds.

The features of ET established in recent studies (e.g., Evans et al. 2017) can be seen. Over the 48-hour period centred on ET completion, the wind field expands considerably, and asymmetry in the wind field grows as the cyclones in the composites lose their warm core and begin to develop frontal features in the presence of increasing shear and decreasing SSTs (Evans et al. 2017). The strongest winds are to the left of the cyclones (relative to propagation direction) from ET completion onwards, indicative of the cold conveyor belt of extratropical cyclones (Catto et al. 2010).

During ET, the Europe PTCs are associated with significantly higher 850 hPa wind speeds than the NoEurope PTCs. This difference is significant, at 95% (indicated by the stippling), close to the cyclone centre, extending further from the centre in the upper-left section of the composite cyclone (Figure 5.4g-h), where the strongest winds exist. In Figure 5.4i, p-values are less than 0.05 around and above the cyclone, but these values are non-significant when accounting for spatial correlations between grid points using the false discovery rate. The Europe PTCs have maximum 850 hPa winds 21%, 32% and 42% higher than the NoEurope PTCs 24 hours prior to ET completion, at ET completion and 24 hours after ET completion respectively. This indicates that the Europe composite contains stronger cyclones than the NoEurope composite. The area covered by with gale-force (Beaufort scale 8, > 17 m s^{-1}) winds is considerably larger for the Europe PTCs than the NoEurope PTCs, and the percentage difference increases

from 24 hours prior to ET completion until 24 hours post-ET completion. Table 5.2 contains a summary of the maximum wind magnitude, gale-force wind area, and strong gale-force wind area (along with differences) for the composites.

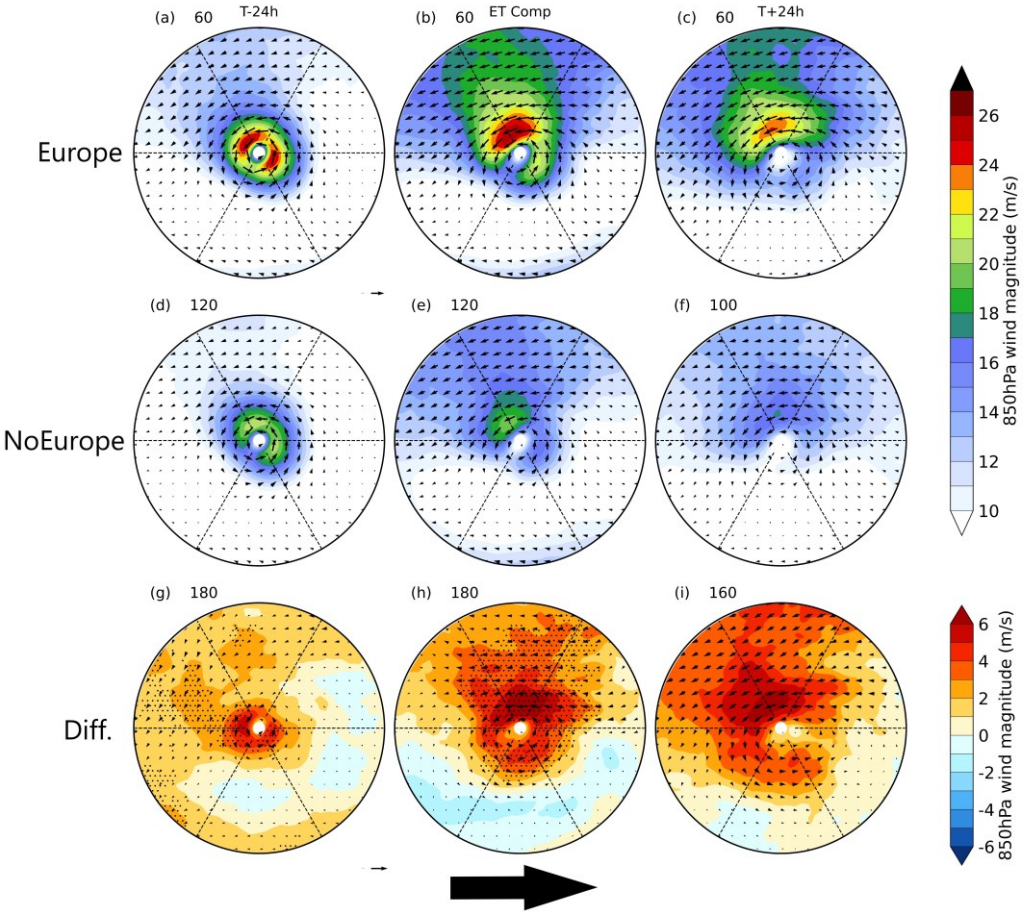

Figure 5.4. As in Figure 5.3, but for the storm-relative 850 hPa wind magnitude (and direction). A 10-degree cap is used. Storm-relative winds are calculated by subtracting the translation velocity from the Earth-relative winds. Key length is equal to 20 m s^{-1} for 5.4a-f and 10 m s^{-1} for 5.4g-i. In panels' g-i, stippling indicates the region in which the difference in the composite means is significant to 95%. Cyclones are aligned according to their direction of travel before compositing, so that they move from west to east in the composite. Large arrow shows the direction of storm propagation. Sample size is shown to the upper-left of each panel.

	Maximum wind mag.			Area > 17 m s^{-1}			Area > 21 m s^{-1}		
	T-24	ET	T+24	T-24	ET	T+24	T-24	ET	T+24
Europe	25.2	26.1	24.2	296	1089	896	130	186	126
NoEurope	20.8	19.8	17.1	166	139	4	0	0	0
Difference	21%	32%	42%	78%	683%	N/A	N/A	N/A	N/A

Table 5.2. A summary of the composite mean maximum intensity (left), gale force wind area (>17 m s^{-1}, Beaufort scale 8, middle) and strong gale area (>21 m s^{-1}, Beaufort scale 9, right) for the Europe PTCs (second row), NoEurope PTCs (third row) and the percentage differences (bottom row). Areas are expressed as $x10^3$ km^2. Values within a 10-degree cap of the cyclone centre are considered. Percentage differences in area of strong winds are only calculated where there is sufficient area in both composites to produce a reliable percentage difference.

The evolution of the thermal structure of the two composites is investigated by analysing the trajectory through the CPS. This is shown in Figure 5.5. The composite trajectories through the phase space are created by centring the cyclones about the point of ET completion and applying a 2-day running mean to smooth the trajectory. This is longer than the running mean used in Figure 5.1 but is necessary because the data comprising Figure 5.5 is noisier than the position information used in Figure 5.1.

A large difference between the composites is found in the B parameter. The Europe PTCs (red line) have a maximum thermal asymmetry (B) value which is ~70% larger than for the NoEurope PTCs (Fig. 5.5a). The difference in B at ET completion is statistically significant to 95%. This suggests that the Europe PTCs develop stronger frontal features than the NoEurope PTCs. The significantly larger B parameter associated with Europe PTCs could also indicate that the Europe PTCs are embedded in a region of higher baroclinicity than the NoEurope PTCs, highlighting the importance of the composite mean differences in cyclone location (Fig. 5.1a) and seasonality (Fig. 5.12). The Europe PTCs attain higher values for the lower and upper-level thermal wind at their maximum intensity, though the difference is not statistically significant (Fig. 5.5b). Larger upper and lower-level thermal wind values suggests a stronger deep warm core, indicating a stronger TC. Consistent with Figure 5.4, which shows that the Europe TCs have stronger winds after ET, the CPS trajectories indicate that the Europe TCs undergo more extratropical reintensification in the mid latitudes. This extratropical reintensification may be the cause of the longer post-ET lifecycle of Europe TCs (6.25 and 3.75 days for Europe and NoEurope PTCs respectively), potentially allowing the cyclones to reach Europe.

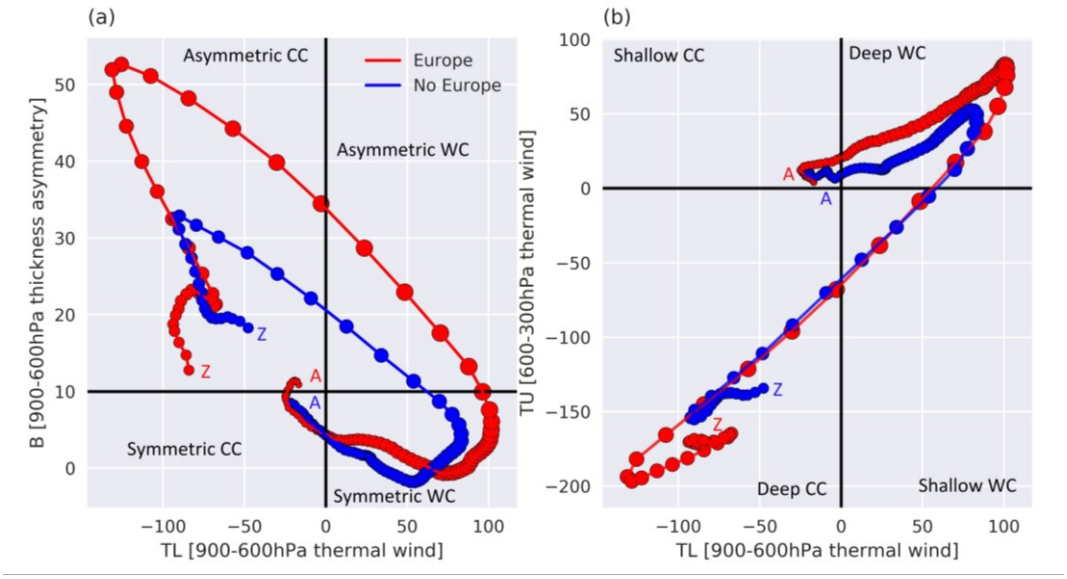

Figure 5.5. Composite lifecycle through the cyclone phase space planes for the Europe (red) and NoEurope (blue) PTCs. Composites are centred about the point of ET completion. A and Z represent the phase space location of the composites at the beginning and end of their lifecycle respectively. Composite mean 10 m wind speed at each time step from ERA5 is illustrated using the size of the markers.

5.3.3.2. Evolution of Local Environment

The analysis of section 5.3.3.1 suggests that Europe PTCs are more intense than NoEurope PTCs, and reintensify more than NoEurope PTCs post-ET. In this section, we investigate the environment surrounding the Europe and NoEurope PTCs to understand why these differences in reintensification exist. As we are looking at the environment around the cyclones, we do not align cyclones along their propagation directions in the construction of the composites in this section.

Figure 5.6 shows the storm-centred composite of the 300 hPa Earth-relative wind magnitude (the approximate level of the jet) and 500 hPa geopotential height in a 20-degree cap around the cyclone centre over a 48-hour period centred on ET completion. At 24 hours prior to ET completion, the Europe PTCs are situated closer to the closely-grouped contours on the eastern flank of an upstream trough than the NoEurope PTCs. At this time, negative PV advection by the irrotational wind (Archambault et al. 2013, 2015) is significantly higher for the Europe PTCs than the NoEurope PTCs, indicating a stronger interaction between the Europe composite and the upstream trough (Table 5.3). Negative PV advection by the irrotational wind is also associated with downstream Rossby wave amplification (Archambault et al. 2013;

Grams and Blumer 2015). This is not visible in Figure 5.6, and a follow up composite study centred on the time of maximum TC-trough interaction would be necessary to understand whether Europe PTCs are more likely to trigger downstream ridgebuilding, jet streak amplification and downstream high-impact weather (e.g., Keller et al. 2019).

The Europe PTCs are also situated in a region of uniformly greater geopotential height gradients than the NoEurope PTCs, signalling stronger baroclinicity in the region of the Europe PTCs related to differences in the location and seasonality of the composites. This is also confirmed by Table 5.3, which shows that the Europe PTCs are in a region of significantly higher (95% level) Eady growth rate throughout ET completion than NoEurope PTCs. The closer approach to (and greater interaction with) the trough may steer the cyclones on a more poleward trajectory, with the cyclones recurving relative to the trough. The poleward steering of the cyclones enables the Europe PTCs to directly interact with the midlatitude jet streak on the eastward flank of the trough. This is consistent with previous studies which highlight the importance of the TC-trough interaction for post-ET reintensification and downstream impacts (Hart et al. 2006; Keller et al. 2019). It is also very similar to the northwest pattern (Harr et al. 2000a; Klein et al. 2000), in which transitioning cyclones in the presence of an amplified upstream trough gain latitude as they undergo rapid extratropical reintensification. The tip of the upstream trough acts as a bifurcation point (Grams et al. 2013a; Riemer and Jones 2014), with cyclones to the east of the tip recurving relative to the trough and gaining latitude. These cyclones often undergo substantial extratropical reintensification, in contrast to cyclones which do not recurve relative to the trough.

The NoEurope PTCs also recurve in the presence of an upstream trough but do not approach the trough as closely as the Europe PTCs. They also remain in a region of weaker geopotential height gradients and lower Eady growth rates than the Europe PTCs. The trough remains poleward of the cyclone, and weaker TC-trough interaction occurs compared to the Europe PTCs. In the NoEurope composite, the cyclones are not steered poleward, and do not interact with the jet streak. This is consistent with the northeast pattern described in Harr et al. (2000), in which the cyclones do not undergo substantial extratropical reintensification. It is described therein that the strong zonal flow between the subtropical high and the midlatitudes prevents a coupling with a

midlatitude baroclinic zone. The Europe PTCs exhibit similar behaviour in terms of jet interaction as the TC-decelerating trough composite in Riboldi et al. (2019), in which the PTC interacts with and subsequently crosses the jet streak situated on the eastern flank of the upstream trough in the 2 days following ET completion. Conversely, the PTCs comprising the TC-accelerating trough composite of Riboldi et al. (2019) do not interact with and cross the jet streak, similar to the NoEurope PTCs presented in Figure 5.6. However, differences in meridional deflection of the jet and extent of downstream ridgebuilding are also found between the accelerating and decelerating trough composites, which are not clearly visible in Figure 5.6.

Hart et al. (2006) found that cyclones which reintensify post-ET are associated with a negatively tilted trough (oriented from north-west to south-east), whereas the post-ET weakening storms are associated with a positively tilted trough. The PTCs in the PTC-decelerating trough composite of Riboldi et al. (2019), which subsequently cross a midlatitude jet streak, also appear to be associated with a negatively tilted trough. However, Figure 5.6 of our analysis shows that the tilt of the trough may not be important for the post-ET reintensification of PTCs, as the troughs in the Europe and NoEurope composites have a very similar orientation. Further work would be necessary to confirm this. In Hart et al. (2006), it is hypothesized that the negative tilt of the upstream trough permits the cyclone a closer approach to the trough, leading to a contraction and intensification of the eddy potential vorticity flux. Recent work suggests that the negative tilt may be the result of strong TC-trough interaction, rather than a predictor of future PTC intensity (Sarro and Evans 2022).

	Europe	NoEurope	Diff
σ (T-24h)	0.41	0.36	**0.05**
σ (ET Comp)	0.53	0.45	**0.08**
σ (T+24h)	0.58	0.49	**0.09**
PV_{irrot} (T-24h)	0.85	0.76	**0.09**
PV_{irrot} (ET Comp)	1.20	1.03	0.17
PV_{irrot} (T+24h)	0.99	0.94	0.05

Table 5.3. Eady growth rate, σ, (rows 2-4, units = day^{-1}) and negative PV advection by the irrotational wind, PV_{irrot} (rows 5-7, units = PVU day^{-1}) averaged in a 15-degree cap around the center of each cyclone at 24 hours prior to ET completion (rows 2, 5), ET completion (rows 3, 6) and 24 hours post-ET completion (rows 4, 7) for Europe PTCs (column 2) and NoEurope PTCs (column 3). Differences (Europe minus NoEurope) are shown in column 4 and bold values are significant at the 95% level using a Kolmogorov-Smirnov test.

In addition to more directly interacting with the jet, the Europe PTCs are associated with a jet which is significantly more intense than the jet associated with the NoEurope PTCs. At each time step shown in Figure 5.6, the maximum jet speed within 10 degrees of the Europe PTCs is significantly (~7 m s^{-1}) higher than for the NoEurope PTCs. Maximum 300 hPa winds in the composite mean jet streak are approximately 10 m s^{-1} higher for the Europe PTCs than the NoEurope PTCs (Figure 5.7). This may indicate that Europe PTCs interact with a more baroclinic midlatitude environment (as suggested by the higher Eady growth rates). However, the difference in jet speeds could also result from local jet streak amplification resulting from negative potential vorticity advection from the divergent outflow of the TC (Riboldi et al. 2019; Keller et al. 2019), which may also be expected given the greater PV advection by the irrotational wind associated with Europe PTCs at 24 hours prior to ET completion.

The difference in baroclinicity surrounding the Europe and NoEurope PTCs motivates an investigation into the seasonality of the two composites. The fraction of PTCs which reach Europe increases throughout the hurricane season, from ~15% for TCs completing ET in July to 50% for TCs completing ET in November (Figure 5.12).

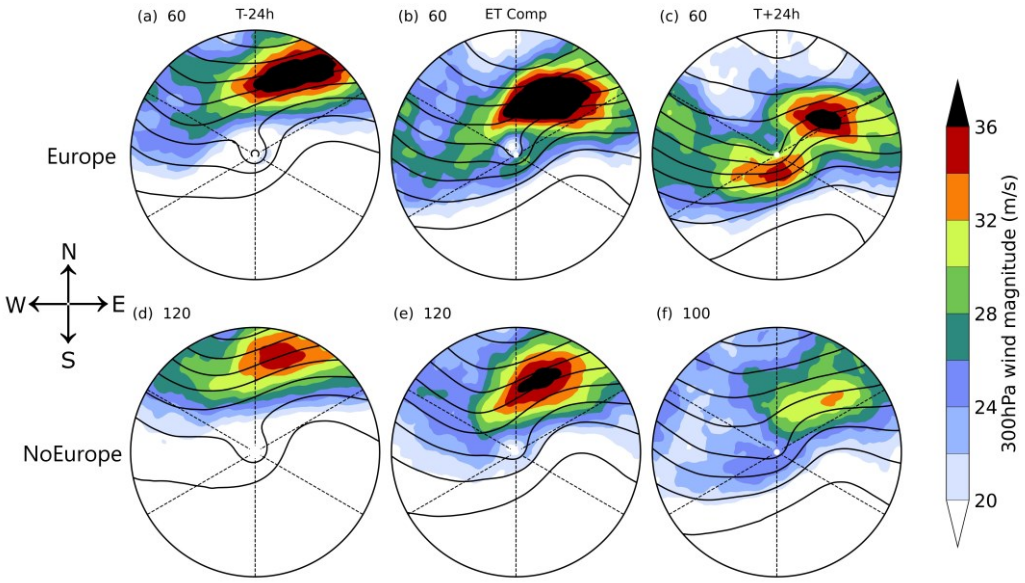

Figure 5.6. Storm-centred composites (20-degree cap) of the 300 hPa wind magnitude (filled contours) and 500 hPa geopotential height (black open contours) for the Europe (a-c) and NoEurope (d-f) PTCs. 48-hour evolution centred about the point of ET completion. Cyclones are not aligned based on their direction of travel. Sample size is shown to the upper-left of each panel.

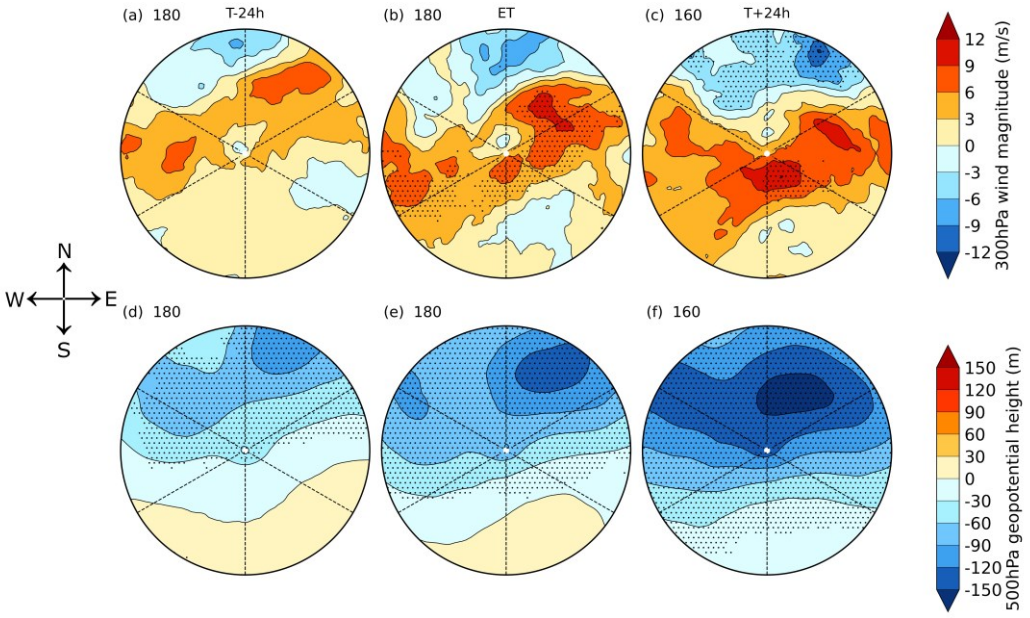

Figure 5.7. Difference (Europe minus NoEurope) of the composite mean (20-degree cap) cyclone-relative 300 hPa wind magnitude (a-c) and 500 hPa geopotential height (d-f) at 24 hours prior to ET completion (a, d), ET completion (b, e) and 24 hours post-ET completion (c, f). Cyclones are not aligned based on their direction of travel. Stippling represents areas in which the composite mean wind magnitudes are significantly different (95%). Sample size is shown to the upper-left of each panel.

5.3.4. The Association Between Extratropical Reintensification and Europe-Impact Likelihood

We have shown that PTCs which impact Europe tend to transition into i) a more favourable environment for reintensification, and ii) develop characteristics associated with a reintensifying cyclone. In this section we test the hypothesis that PTCs which reintensify after ET are more likely to reach Europe. This is achieved by separating the Europe and NoEurope PTCs which reintensify from those that do not. The proportion of PTCs in both composites which reintensify, along with the mean reintensification in each composite, can then be investigated. We then re-composite the reintensifying cyclones about the point of reintensification to investigate the features of the midlatitude circulation which are associated with reintensification.

Figure 5.8 shows the composite lifecycle of the Europe PTCs (red) and NoEurope PTCs (blue), based on whether they reintensify in the midlatitudes or not. PTCs are designated as reintensifying if at some point post-ET, they undergo an increase in 850 hPa T63 spectrally filtered relative vorticity (the field used for cyclone tracking) of $3x10^{-5}$ s^{-1} or larger, where the 6-hourly T63 relative vorticity fields have been smoothed using a 5-point running mean to remove high-frequency variability in intensity. A 5-time step running mean is chosen as it is long enough to sufficiently smooth out high frequency variability within the data without significantly dampening robust changes in vorticity due to reintensification. Overlaid crosses are the time steps at which there is a significant (95% level) difference between the mean 850 hPa T63 relative vorticity for the Europe/NoEurope reintensifiers, and the Europe/NoEurope weakeners.

The Europe PTCs have a much higher T63 relative vorticity at ET completion than the NoEurope PTCs. This is particularly clear for the Europe weakening composite. This indicates that the strength of the TC may be important in modulating the likelihood that a PTC will reach Europe. The NoEurope PTCs which reintensify appear to intensify more than the Europe intensifiers, however this is due to a large spread in the time relative to ET at which the cyclones undergo reintensification. On average, the reintensification amounts are 8.8 and $6.8x10^{-5}$ s^{-1} for the Europe and NoEurope reintensifiers respectively, although this difference is not statistically significant ($p=0.12$). A larger proportion of the Europe PTCs are identified as reintensifying (42%)

compared to NoEurope PTCs (21%). This highlights the importance of both TC intensity and the midlatitude environment into which the TC transitions in determining whether the PTC will reach Europe.

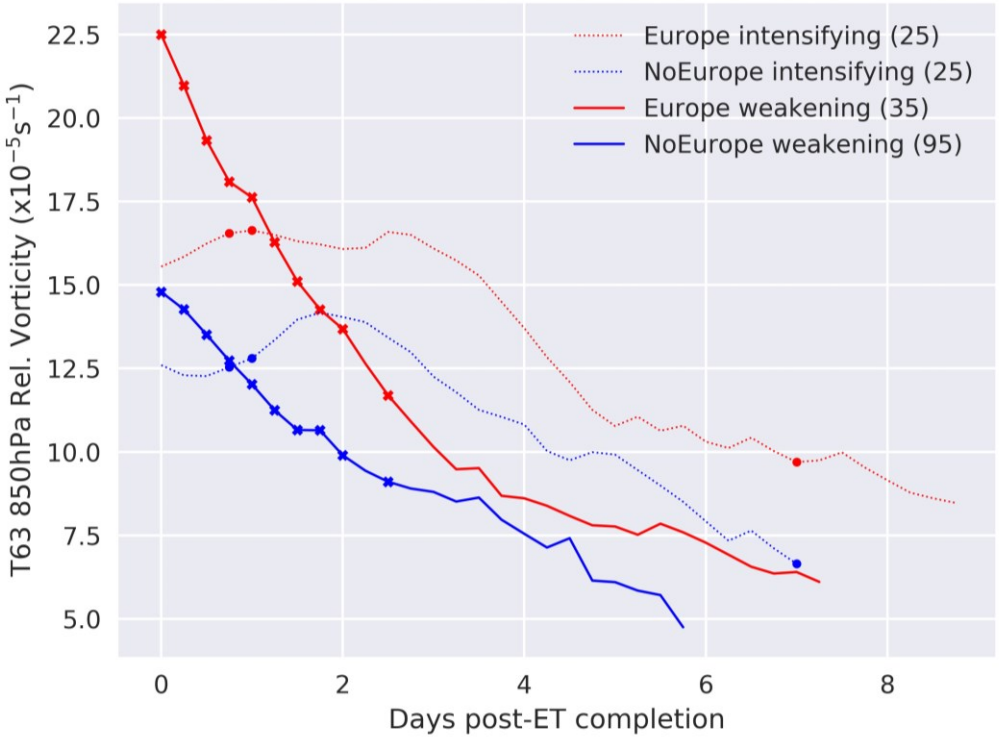

Figure 5.8. Composite lifecycle of the 850 hPa relative vorticity, spectrally filtered to a T63 spectral resolution, for the Europe (red) and NoEurope PTCs (blue) centred on ET completion and separated based on whether they reintensify (dashed) or weaken (solid) post-ET. Data from ERA5 is used, and all TCs which complete ET in ERA5 (180) are included in the composite. Crosses and dots represent the time steps at which the difference in the composite means are significant to 95% using a Kolmogorov-Smirnov test (comparing Europe reintensifiers with NoEurope reintensifiers (dots), and Europe weakeners with NoEurope weakeners (crosses)). The sample size in each composite is shown in the legend.

Figure 5.9 shows the storm centred composites for the Europe reintensifiers and the NoEurope reintensifiers. Instead of centring the composites about ET completion, we now centre them about the onset of reintensification (left), time of max reintensification rate (middle) and maximum post-ET intensity (right). The onset of reintensification is the time step after ET completion at which the T63 relative vorticity begins to increase. The time of maximum intensification rate is the time step at which the max 6 hourly T63 relative vorticity increase occurs between reintensification onset

and maximum intensity. Max post-ET intensity is the time step of the maximum T63 relative vorticity post-ET.

The PTCs in both composites begin reintensification as they begin to interact with the right entrance of the jet streak. They reach their maximum rate of reintensification when superposed with the jet maximum and attain their maximum intensity when they have exited the jet and are situated by the left exit region. The right entrance and left exit regions of the jet are regions of enhanced upper-level divergence (Klein et al. 2002) which may act to aid the reintensification process. The Europe reintensifiers cross a stronger composite mean jet than the NoEurope reintensifiers and undergo more intensification.

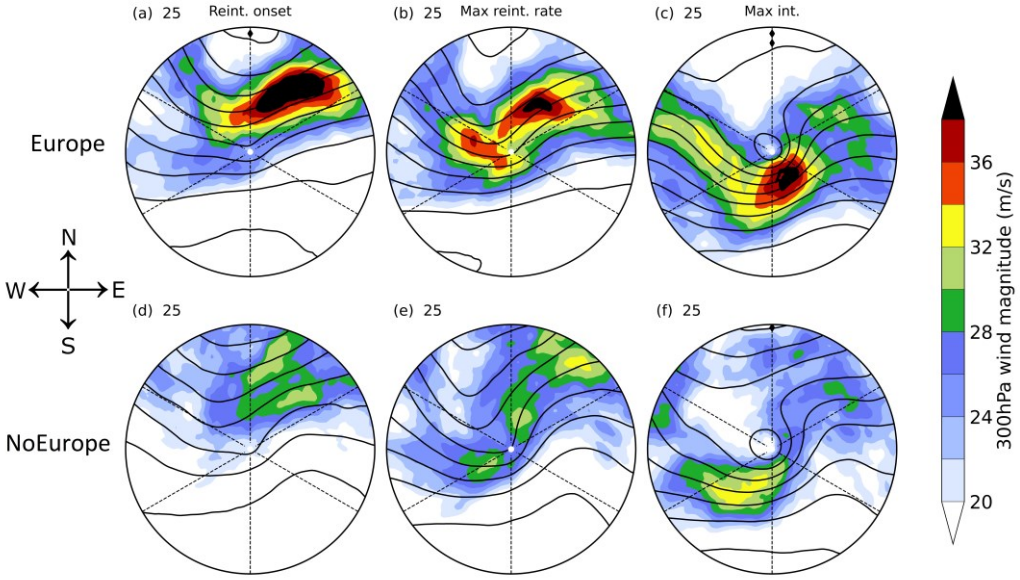

Figure 5.9. Storm centred composites (20-degree cap) showing the 300 hPa wind magnitude (filled contours) and 500 hPa geopotential height (black open contours) for the Europe PTCs which reintensify (a-c) and the NoEurope PTCs which reintensify (d-f). Composites are centred about the point of post-ET reintensification onset (left), post-ET max intensification rate (middle) and post-ET maximum intensity (right). Cyclones are not aligned based on their direction of travel. Sample size is shown to the upper-left of each panel.

5.3.5. Relative Importance of TC Intensity and Reintensification

The analysis presented in sections 5.3.2 and 5.3.4 suggest that there is a strong association between the likelihood that a PTC will impact Europe and a) the intensity of the TC, both at the lifetime maximum intensity of the storm and as it begins ET, and b) whether the cyclone reintensifies after ET. In this section, we investigate the

association between each factor and the likelihood that a cyclone will impact Europe in more detail and investigate the relative importance of both factors.

Figure 5.10 shows the conditional probability that a PTC will impact Europe based on its intensity at TC lifetime maximum intensity, intensity at ET onset, and the amount of reintensification that the cyclone undergoes post-ET. TC lifetime maximum intensity and reintensification are chosen because there are significant differences in these metrics when comparing the Europe and NoEurope PTCs (Figures 5.2 and 5.8 respectively). TC lifetime maximum intensity is defined as the maximum wind speed associated with a TC in HURDAT2 up to the point of ET completion, as determined using the ERA5 cyclone phase space analysis. Intensity at ET onset is investigated because it better represents the intensity that the TC has when it begins interacting with the midlatitude environment than TC lifetime maximum intensity. However, we have less data available for this metric (see columns 2 and 3 of Table 5.1 for sample sizes of TC lifetime maximum intensity and ET onset intensity, respectively). As a result, the number of storms going into Fig. 5.10b is smaller than Fig. 5.10a and c. Bin edges used for 5.10a-b are (from left to right) < 20th percentile, 20-40th percentile, 40-60th percentile, 60-80th percentile and > 80th percentile of the combined distribution. For reintensification (5.10c), the bin percentiles are <40th percentile, 40-55th percentile, 55-70th percentile, 70-85th percentile and > 85th percentile. It was necessary to choose different percentiles to bin storms based on reintensification because more than 20% of storms do not reintensify at all. The combined distribution is comprised of all the Europe and NoEurope PTCs, and the percentile bin edges are used to ensure a consistent sample size across bins.

There is a clear increasing trend in Figures 5.10a-c. For TC lifetime maximum intensity, only ~22% of the weakest PTCs impact Europe, compared to almost 50% for the strongest 20%. Only 10% of the weakest PTCs at ET onset impact Europe, compared to over 50% for the strongest 20%, indicating a strong association between the intensity of the TC at the beginning of ET and whether the cyclone reaches Europe. For reintensification there is also a trend. Approximately 20% of storms which do not reintensify at all (Bin 1) make it to Europe, compared to ~60% for the storms which undergo the most reintensification. Figure 5.10 highlights that both the midlatitude

environment, which largely facilitates reintensification, and TC intensity, are strongly associated with Europe-impact likelihood.

Figure 5.10d shows the relationship between the TC lifetime maximum intensity and the reintensification post-ET. The correlation between TC lifetime maximum intensity and reintensification post-ET is weak but significant, with a Pearson's correlation coefficient of -0.2. The lack of a strong association between reintensification and TC intensity combined with Figures 5.10a and c, which show that stronger TCs (at TC lifetime maximum intensity) and storms which reintensify are more likely to impact Europe, indicate that both factors are associated with whether a PTC will impact Europe. The lack of association between reintensification and TC intensity also suggests that while both factors are important in modulating the likelihood that a PTC will reach Europe, they may not both be important for the same PTC. This suggests that there may be two pathways through which a PTC can reach Europe: a strong TC which gradually weakens on approach, or a TC (which may not necessarily be a strong TC) that undergoes substantial reintensification in a favourable midlatitude environment after ET. Furthermore, the lack of association between TC intensity and reintensification is consistent with previous studies which suggest that TC intensity is not a primary factor determining whether a favourable phase-locked configuration will exist between the transitioning TC and the upstream trough (Archambault et al. 2013; Brannan and Chagnon 2020).

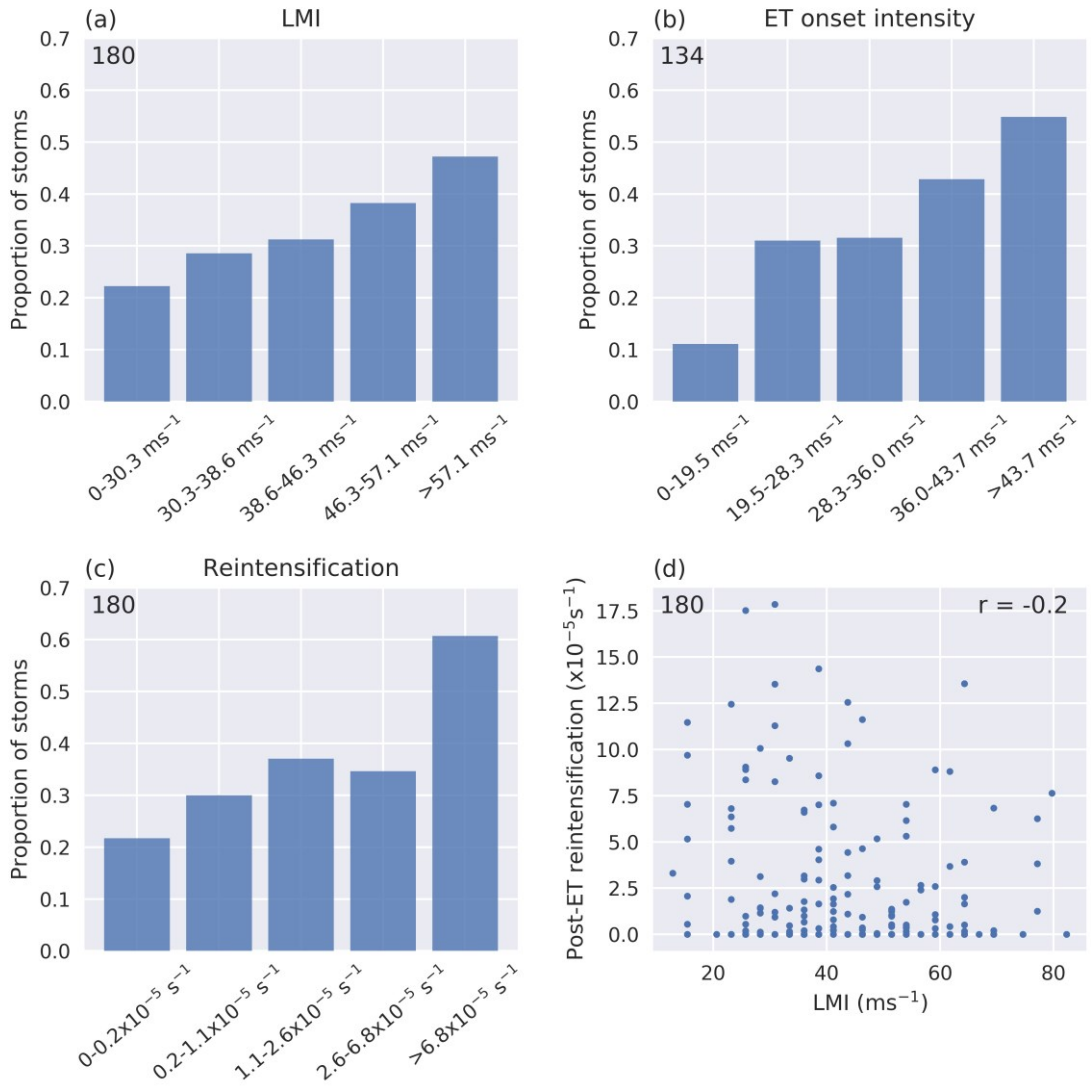

Figure 5.10. Conditional probability that a PTC will impact Europe based on the TC lifetime maximum intensity (a), intensity at ET onset (b), and T63 relative vorticity increase post-ET (c). (d) a scatterplot of TC lifetime maximum intensity and T63 relative vorticity increase post-ET for all Europe and NoEurope PTCs. Sample size is shown to the upper left of each panel.

Table 5.4 shows a joint contingency table to further investigate the association that TC intensity and reintensification have with PTCs reaching Europe, with the Odds ratios displayed in Figure 5.11. TC lifetime maximum intensity and reintensification have odds ratios of 2.38 and 2.71 respectively. In both cases, the lower bound 95% confidence interval (brackets, Figure 5.11) are greater than 1, indicating a significant association between TC lifetime maximum intensity, reintensification, and whether a PTC reaches Europe. Odds ratios for reintensification conditioned on TC lifetime maximum intensity, Odds(Europe$|_{R,MH}$)/Odds(Europe$|_{W,MH}$) and Odds(Europe$|_{R,NON-MH}$)/Odds(Europe$|_{W,NON-MH}$), are 3.1 (non-significant) and 3.45 (significant) respectively.

Similarly, odds ratios for TC lifetime maximum intensity conditioned on reintensification, Odds(Europe|$_{MH,R}$)/Odds(Europe|$_{NON\text{-}MH,R}$) and Odds(Europe|$_{MH,W}$)/Odds(Europe|$_{NON\text{-}MH,W}$) are 2.47 (non-significant) and 2.75 (significant). When only considering weak TCs the role of reintensification appears larger, and when only considering weakening storms post-ET the role of TC lifetime maximum intensity is larger (higher odds ratios). This shows that PTCs usually need at least one of these factors in order to reach Europe, however having both factors doesn't further increase the odds of reaching Europe significantly compared to just one factor (95% confidence interval includes 1).

A small fraction of NoEurope PTCs were major hurricanes and reintensified post-ET (4/120). Of these 4 cyclones, 3 made landfall across the continental US and travelled north-eastward across north-eastern Canada, undergoing brief reintensification before dissipating. The fourth PTC travelled poleward towards Greenland after ET. Similarly, there are some Europe PTCs which neither reintensify nor were major hurricanes (15/60). This subgroup of Europe PTCs recurves further east in the basin, with 10/15 completing ET east of 30°W (Figure 5.13). When considering all PTCs, there is also a significant association between the longitude of ET completion and the odds of reaching Europe (Fig. 5.11) when using a threshold of 70°W.

	TC lifetime max intensity ≥ 50 m s^{-1} (major hurricane)			TC lifetime max intensity < 50 m s^{-1} (non-major hurricane)		
	Europe	NoEurope	Total	Europe	NoEurope	Total
Reintensify post-ET	8	4	12	17	21	38
Weaken post-ET	20	31	51	15	64	79
Total	28	35	63	32	85	117

Table 5.4. Joint contingency table for PTCs separated based on whether they reintensify or weaken post-ET, were a major hurricane at their lifetime maximum intensity, and whether they impact Europe.

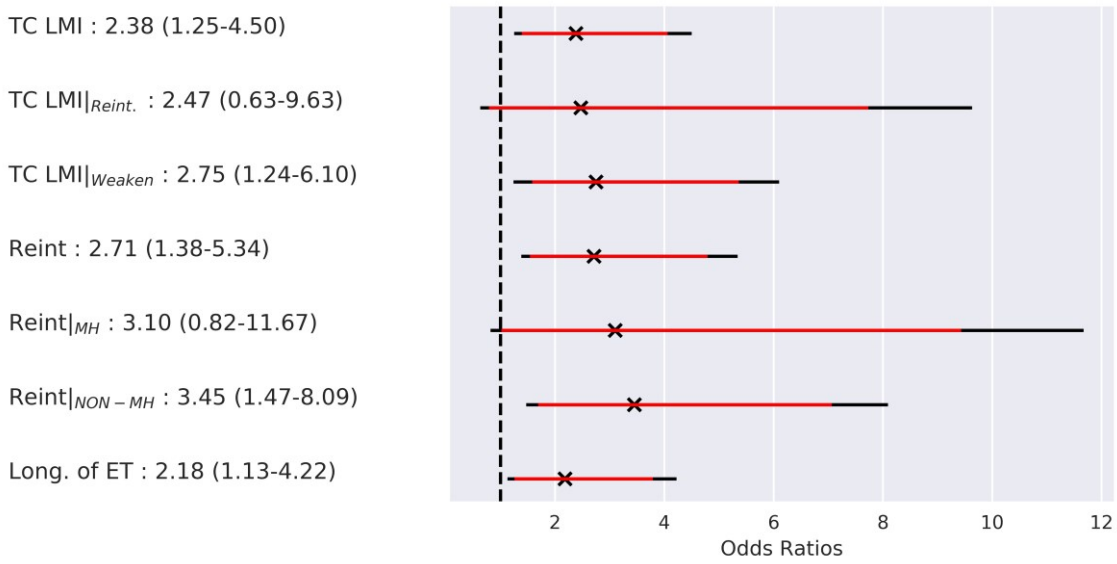

Figure 5.11. Odds ratios (black crosses) and associated 95% (black horizontal lines) and 90% (red horizontal lines) confidence intervals for TC intensity, reintensification, and longitude of ET completion. Vertical dashed black line indicates an odds ratio of 1. Numbers and brackets to the left of the panel show the odds ratios and the associated 95% confidence interval.

5.4. Summary and Conclusions

PTCs can bring severe weather to Europe in terms of extreme precipitation, high winds, and large waves. These PTCs have been associated with national record wind gusts across Ireland as well as large economic losses across Europe. However, many PTCs never make it to Europe at all. In this study, we try to understand the factors which determine whether a PTC will impact Europe. This is achieved by identifying the observed PTCs in the ERA5 reanalysis using a feature tracking scheme, allowing us to undertake detailed analysis of the post-tropical stage of these storms.

Using a composite analysis, we show that PTCs which impact Europe are much more likely to undergo extratropical reintensification than PTCs which do not impact Europe (NoEurope). By quantifying the area-averaged negative potential vorticity advection by the irrotational wind in the vicinity of the PTCs (Archambault et al. 2013), the Europe PTCs are shown to interact more strongly with an upstream trough at a much closer distance to the storm centre during extratropical transition (ET) than the NoEurope PTCs. This is consistent with previous studies which highlight the importance of TC-trough interactions for PTC reintensification and downstream flow amplification (Hart et al. 2006; Keller et al. 2019; Riboldi et al. 2019). During ET, the baroclinicity, characterized by the Eady growth rate, is significantly higher in the vicinity of Europe

PTCs than NoEurope PTCs. Baroclinicity generally increases throughout hurricane season, and TCs completing ET in October and November are more likely to reach Europe than those completing ET earlier in the season. The Europe PTCs travel on a more poleward trajectory, allowing them to interact with a midlatitude jet streak. The jet streak associated with the Europe PTCs is also stronger, signalling a more favourable environment for reintensification, which may be the result of a more favourable background state in the midlatitudes, or locally produced via interaction between the TC outflow and the upper-level waveguide. It is during interaction with the midlatitude jet streak that many of the Europe PTCs undergo reintensification. The NoEurope PTCs travel less polewards after ET, and the composite mean does not directly interact with a midlatitude jet streak. The NoEurope PTCs are also less likely to reintensify.

The Europe PTCs also have a substantially higher intensity in their TC phase, both at their lifetime maximum intensity and as they begin ET as they enter the midlatitudes. Contingency table analysis suggests that both TC intensity and whether reintensification occurs post-ET modulate the likelihood that the storm will impact Europe, although these factors may not be important for the same PTC. Our results indicate that the mid latitude environment into which the TCs recurve and the strength of the TCs are key to understanding why some PTCs impact Europe. The importance of TC intensity is consistent with previous studies, which suggest that PTCs may retain some 'memory' of the tropical phase of their lifecycle during, and potentially after, ET (Datt et al. 2022). All results presented in this paper have been verified using a second reanalysis, MERRA2 (Gelaro et al. 2017; Molod et al. 2015), and results very similar to ERA5 (not shown).

This paper has focused on the characteristics of the cyclones themselves and the surrounding environment. An investigation of the larger scale atmospheric circulation, such as the phase of the NAO, may also provide some insight into why some PTCs reach Europe. It could be hypothesized that positive NAO conditions may lead to greater longevity, faster translation, or a higher likelihood of reintensification, and therefore may have implications for the probability that a PTC will reach Europe. This will be investigated in future work.

In the context of climate change, our results highlight the challenges of projecting PTC impacts over Europe in a future climate, as has been highlighted for ET more generally in the North Atlantic basin (Zarzycki et al. 2017). In this study, we have shown that TC intensity and post-ET reintensification are key metrics of model fidelity. Some climate model projections indicate a poleward shift in the jet (Harvey et al. 2020), possibly signalling less opportunity for PTCs to interact with the jet, leading to less extratropical reintensification. However, SSTs are projected to warm, and TC lifetime maximum intensity may increase as a result. Previous studies suggest that this may already be occurring (Kossin et al. 2020). If the change in TC intensity outweighs any potential poleward shift in the jet, then in the future a larger proportion of PTCs may reach Europe.

Acknowledgments

The authors thank Ron McTaggart-Cowan, Rachel Mauk, and two anonymous reviewers for their comments which greatly improved the quality and clarity of this manuscript. E. Sainsbury was funded by the Natural Environment Research Council (NERC) via the SCENARIO Doctoral Training Partnership (Grant NE/S0077261/1), with additional CASE funding from BP. R. S., K. H., A. B., and L. S. are supported by the U. K. National Centre for Atmospheric Science (NCAS) at the University of Reading. A. B. acknowledges European Commission funding through the PRIMAVERA project under grant agreement no. 641727 of the Horizon 2020 research program, and NERC funding through The North Atlantic Climate System Integrated Study (ACSIS) grant, reference NE/N018044/1.

Data Availability Statement

HURDAT2 data is available from aoml.noaa.gov/hrd/hurdat/. ERA5 reanalysis data can be obtained from the Copernicus C3S Date store (https://www.ecmwf.int/en/forecasts/datasets/reanalysis-datasets/era5). ERA5 data are freely available. TRACK-1.5.2 is available at https://gitlab.act.reading.ac.uk/track/track.

5.5. Supporting Information

Europe PTCs are associated with a significantly more baroclinic environment (characterised by higher Eady growth rates) than the NoEurope PTCs. This motivates the question of whether the two composites exhibit different seasonality. PTCs forming earlier in the season are less likely to reach Europe, and approximately 50% of PTCs which complete ET in November reach Europe (Figure 5.12).

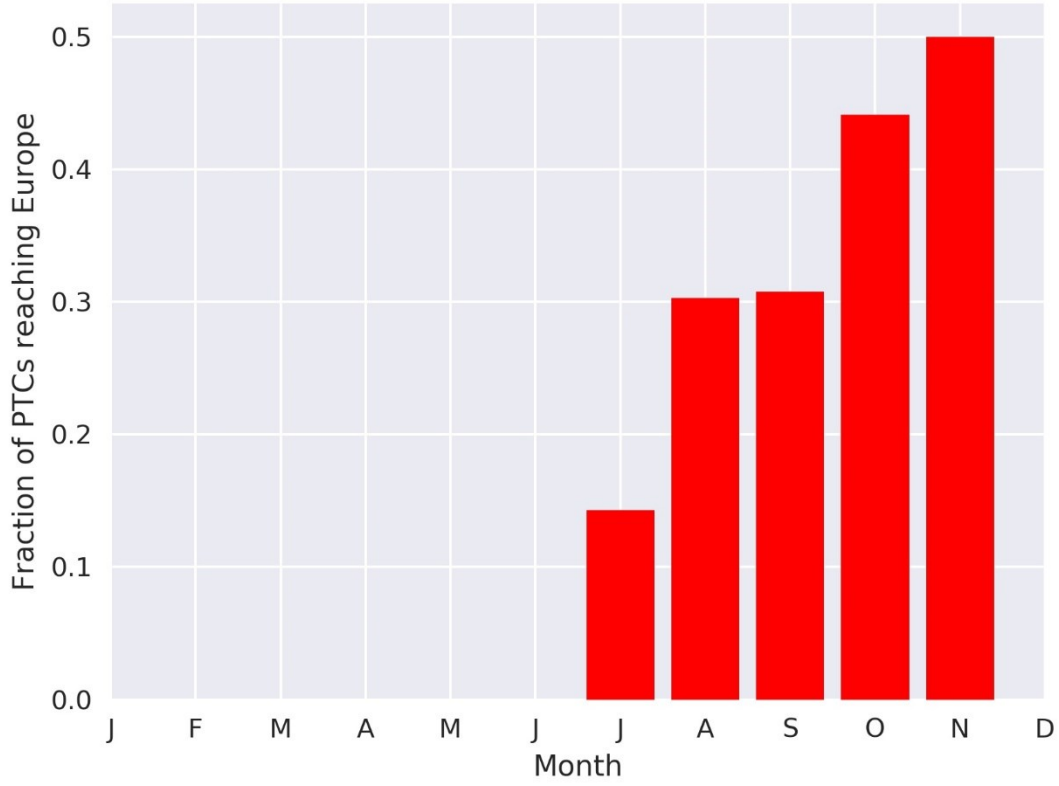

Figure 5.12. Fraction of PTCs that reach Europe, where PTCs have been separated based on the month during which they complete extratropical transition. Months which contain less than 10 PTCs (over the analysis period of 1979-2018) are masked to remove noise associated with small sample sizes.

Figure 5.13 shows the tracks for the Europe PTCs which were non major hurricanes (TC lifetime maximum intensity < 50 m s^{-1}) and weakened post-ET (left), and the tracks for the NoEurope PTCs which were major hurricanes and reintensified post-ET (right).

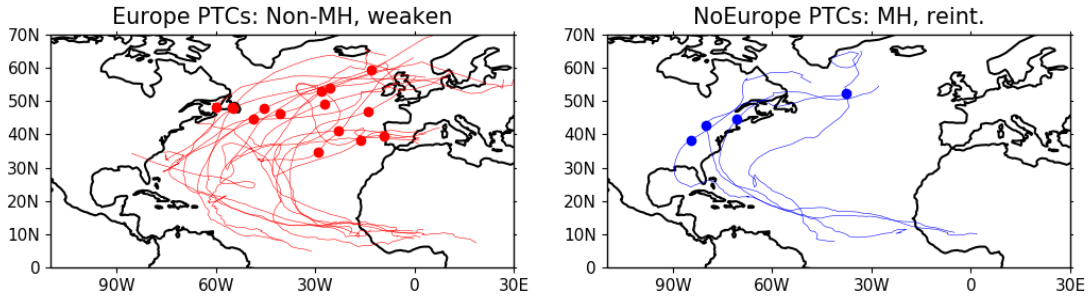

Figure 5.13. Tracks for the 15 Europe PTCs which were not major hurricanes, and did not reintensify post-ET (left), and tracks for the 4 NoEurope PTCs which were major hurricanes and did reintensify post-ET (right). Dots represent the locations of ET completion for the tracks.

Epilogue

So far in this thesis, we have demonstrated that Europe-impacting PTCs are disproportionately responsible for windstorm risk over Europe; that TC activity in the main development region and subtropical North Atlantic explain much of the variance in North Atlantic TC frequency; and have demonstrated that TC intensity, and interaction with the midlatitude environment (i.e., whether a storm reintensifies) modulate the likelihood that a PTC will reach Europe.

Chapter 6 attempts to bring these new pieces of knowledge together to investigate whether CMIP6 models adequately represent the TC and PTC climatology, and to investigate their projected changes. An understanding of how the PTC intensity distribution compares to the overall cyclone distribution across Europe (from Chapter 3) is used to investigate the ability of these models to simulate PTCs and their hazards. The relationship between TC frequency and recurving TC frequency (Chapter 4) is used to understand the extent to which CMIP6 models capture the drivers of variability in recurving TC frequency. Finally, the results from Chapter 5 are used to formulate hypotheses of how we may expect Europe-impacting PTC statistics to change in a warmer climate.

Chapter 6

Can Low-Resolution CMIP6 ScenarioMIP Models Provide Insight into Future European Post-Tropical Cyclone Risk?

PTCs are disproportionately responsible for windstorm risk over Europe in the current climate (chapter 3), motivating the study of whether Europe-impacting PTCs may become more frequent or intense in the future due to climate change. Previous studies concerning future PTC risk to Europe use only a single climate model (Baatsen et al. 2015; Haarsma et al. 2013), and a multi-model study is therefore necessary. Chapter 6 investigates whether global climate models from the Coupled Model Intercomparison Project phase 6 (CMIP6) capture key features of the TC and Europe-impacting PTC climatologies. The projected change in Europe-impacting PTCs is investigated using factors known to be associated with TC recurvature (chapter 4), the cyclone and environmental conditions which allow PTCs to reach Europe (chapter 5), and the simulated TCs and PTCs in an ensemble of 5 selected CMIP6 models.

This chapter has been submitted for publication in *Weather and Climate Dynamics* (Sainsbury et al. 2022c):

Sainsbury, E. M., R. K. H. Schiemann, K. I. Hodges, A. J. Baker, L. C. Shaffrey, K. T. Bhatia, and S. Bourdin, 2022c: Can low-resolution CMIP6 ScenarioMIP models provide insight into future European Post-Tropical Cyclone risk? *Weather Clim. Dyn.*, https://doi.org/https://doi.org/10.5194/wcd-2022-46, under review

Abstract

Post-Tropical Cyclones (PTCs) can cause extensive damage across Europe through extreme winds and heavy precipitation. With increasing sea surface temperatures, tropical cyclones (TCs) may form and travel further polewards and eastwards than observed historically. Recent work has suggested that the frequency of intense Europe-impacting PTCs may increase substantially in the future.

Using an objective feature tracking scheme and TC identification method, we track and identify the full lifecycle of TCs in the North Atlantic in five CMIP6 climate models in the historical (1984-2014) period and in the future under the SSP5-85 scenario (2069-2099). These five models are selected based on their ability to simulate TC frequency similar to observed in the North Atlantic, although model deficiencies remain.

We find no robust changes in Europe-impacting PTC frequency or intensity in the future. This is because two competing factors – a significant decrease in TC frequency of 30-60%, and an increase in the proportion of TCs reaching Europe – are approximately the same size. The projected increase in the proportion of TCs reaching Europe is largely driven by an increase in the likelihood of recurvature and is consistent with projected decreases in vertical wind shear and increases in potential intensity along the US East Coast in the future. The projected increased likelihood of recurvature is also associated with a shift in TC genesis away from the Main Development Region, where model biases cause very few TCs to recurve. This study indicates that large uncertainties surround future Europe-impacting PTCs and provides a framework for evaluating PTCs in future generations of climate models.

6.1. Introduction

Post-Tropical Cyclones (PTCs) can bring Europe hazardous weather such as extreme precipitation, high winds, and large waves (Bieli et al. 2019a; Evans et al. 2017; Jones et al. 2003). Compared to the overall European cyclone climatology, PTCs are disproportionately responsible for the most intense windstorms to impact Europe during hurricane season (Sainsbury et al. 2020), and often attain their maximum intensity a couple of days after impacting the region, enhancing their destructive potential (Baker et al. 2021; Dekker et al. 2018).

In 2017, hurricane Ophelia (Rantanen et al. 2020) became the easternmost major hurricane on record (Stewart 2018), and in 2019 hurricane Lorenzo became the easternmost category 5 hurricane on record. Both cyclones later impacted Europe as PTCs, and Ophelia was responsible for Ireland's highest-recorded wind gust of 53 m s^{-1} (119 mph). Projected increases in sea surface temperature (SST) and the range of latitudes occupied by TCs (Studholme et al. 2022), combined with the observed trend in TC lifetime maximum intensity latitude (Kossin et al. 2014) opens the possibility for more cyclones to form– and attain high intensities- further polewards and eastwards in the basin, closer to Europe (Baker et al. 2022; Haarsma et al. 2013; Haarsma 2021). Additionally, as TCs attain greater intensities they may become more resilient to hostile environmental conditions such as decreasing SSTs and increasing wind shear (Baker et al. 2022; Michaelis and Lackmann 2019), increasing their likelihood of both recurving (Sainsbury et al. 2022a), and reaching Europe (Sainsbury et al. 2022b). Diabatic processes have also been shown to be important in case studies of high-impact PTCs (Rantanen et al. 2020), implying a future increased PTC risk in a warmer atmosphere which is capable of holding a larger amount of moisture (Haarsma 2021).

Few studies have investigated the projected changes of Europe-impacting PTCs, and those that do only considered storm-force (Baatsen et al. 2015) and hurricane-force (Haarsma et al. 2013) PTCs. Using a high resolution (~25 km in midlatitudes) climate model with prescribed SSTs, Haarsma et al. (2013) found large increases in hurricane-force PTC frequency over Norway, the North Sea, and the Bay of Biscay by the end of the 21st century under the IPCC Representative Concentration Pathway 4.5 (RCP 4.5) scenario, but based on a small sample size. The projected increase was associated with an increase in SSTs, extending the TC genesis region poleward and eastwards and therefore allowing more TCs to reach the baroclinic midlatitudes before dissipating. When considering storm-force Europe-impacting PTCs in the same simulations, the minimum sea level pressure that the cyclones attained was found to be 8 hPa lower at the end of the 21st century (Baatsen et al. 2015).

Liu et al. (2017) considered North Atlantic TCs undergoing extratropical transition (ET) more generally and found an increase in TC density in the eastern North Atlantic under the RCP 4.5 emission scenario by the end of the century in a flux-adjusted version of the FLOR model (Vecchi et al. 2014), indicating an increase in TC-related risks for

Europe. A statistically significant increase in the fraction of TCs undergoing ET is also found in the future (Liu et al. 2017). This trend has also been found in several (but not all) reanalyses (Baker et al. 2021), and mixed results have been found in climate model studies (Michaelis and Lackmann 2019; Bieli et al. 2020). Using a pseudo global warming (PGW) approach to dynamical downscaling, Jung and Lackmann (2019) found that hurricane Irene (Avila and Cangialosi 2011) would be considerably stronger (> 20 hPa deeper) in a future climate under the RCP 8.5 scenario and would undergo extratropical transition for considerably (18 hours) longer, extending TC-like conditions further poleward than in the present climate. Further PGW case studies also show increases in precipitation during the ET phase (Liu et al. 2020) and an increase in TC strength during the ET process (Jung and Lackmann 2021), further highlighting the potential future increase in TC-related hazards to midlatitude regions. Finally, Baker et al. (2022) find an increase in the frequency of ET events in the North Atlantic along with a poleward shift in ET location by 2050 in HighResMIP models under the RCP 8.5 scenario. While this is the first multi-model study of projected changes in ET in an ensemble of high-resolution climate models, it does not have a European focus. Additionally, projections are limited to 2050, by which time forced changes may not have fully emerged.

Given the potential for an increased PTC risk to Europe in the future, a multi-model study with a focus on Europe is necessary to quantify the associated model uncertainty and to assess whether lower resolution models can provide insight into future PTC changes. Many lower-resolution climate models do not simulate a realistic TC frequency (e.g., Camargo 2013), and even high-resolution climate models are unable to capture the strongest TCs (e.g., Walsh et al. 2015; Vidale et al. 2021; Roberts et al. 2020a). In this paper we investigate the projected changes in Europe-impacting PTCs in an ensemble of five CMIP6 models which are shown to simulate a realistic North Atlantic TC frequency compared to observations. Some of these models have a lower horizontal resolution than previous studies (e.g., Baker et al. 2022; Haarsma et al. 2013), and thus simulated TCs are expected to be weaker. However, a multi-model study using models containing multiple ensemble members allows for a greater sample size, and greater uncertainty quantification. It is unknown whether low-resolution CMIP6 models can give insight into projected changes in TC and PTC

statistics despite their deficiencies and biases. This is investigated in this study. As far as the authors are aware, a multi-model study with a focus particularly on Europe-impacting PTCs has never been undertaken.

This paper aims to answer the following questions:

- To what extent can CMIP6 models capture the characteristics of the North Atlantic TC climatology?
- How well do CMIP6 models capture the disproportionate intensity associated with Europe-impacting PTCs relative to the overall cyclone climatology?
- Are there any areas of model consensus regarding projected changes in PTC frequency over Europe?

In section 6.2, we describe the cyclone detection and tracking scheme, TC identification procedure, and CMIP6 models included in this study. Section 6.3 contains an overview of the TC climatologies in the selected CMIP6 models, the projected changes in the frequency and intensity of Europe-impacting PTCs, and further analysis to investigate the cause of the projected changes. The paper concludes with a discussion in section 6.4.

6.2. Methods

6.2.1. Data

For this study, we use data from the fully-coupled historical and SSP5-85 model simulations from phase 6 of the Coupled Model Intercomparison Project (CMIP6, Eyring et al. 2016). Although many CMIP6 models have a resolution too low to simulate the observed structure and intensity of TCs, low-resolution climate models can still often simulate TC-like vortices (Haarsma et al. 1993). On average, there are 6.4 North Atlantic hurricanes (wind speeds >= 33 m s^{-1}) per year in observations (HURDAT2) between 1950 and 2014. Climate models tend to underestimate TC frequency, therefore models which simulate a median TC frequency > 6.4 $year^{-1}$ during the North Atlantic hurricane season (June 1st – Nov 30th), averaged over the entire historical run, are selected. This threshold is chosen to ensure we focus on CMIP6 models which simulate North Atlantic TC frequency reasonably compared to observations, and to ensure the selected models have a sufficient sample size of TCs

and Europe-impacting PTCs for meaningful statistical analysis. More information on TC identification can be found in section 2.3.2, and additional information on CMIP6 model selection can be found in the supporting information (Figure 6.11).

The chosen 5 models are: CNRM-CM6-1-HR (CNRM hereafter), HadGEM3-GC31-MM (HadGEM hereafter), KIOST-ESM (KIOST hereafter), MIROC6 (MIROC hereafter) and IPSL-CM6A-LR (IPSL hereafter). CNRM and HadGEM have a higher horizontal resolution in the atmosphere and ocean than the other selected models (Table 2.1). While CNRM and HadGEM also have HighResMIP simulations available, they use a different experimental protocol (e.g., different aerosol forcing and land surface scheme) and only run out to the year 2050. In this study we focus on the ScenarioMIP simulations for consistency with the other selected models. The period 1984-2014 is used for the historical run, and 2069-2099 for the SSP5-85 scenario, giving an 85-year difference between the mid points of the two time periods considered in this study. More information can be found in Table 2.1. Key results have been reproduced using only ensemble members which are available for both the historical and SSP5-85 scenario simulations and are shown in the supporting information (Figure 6.17, Table 6.5). The 6-hourly wind components are utilised at 850-, 500- and 250 hPa for calculation of the vorticity fields necessary for TC identification (more information in section 2.3.2). The 6-hourly mean sea level pressure and 10 m wind data are also used to investigate the intensity of the cyclones. Monthly mean temperature and specific humidity profiles are utilised to calculate potential intensity (PI), and monthly mean relative humidity, wind, and SSTs to construct the genesis potential index (Emanuel and Nolan 2004).

Using the same tracking and TC identification scheme as CMIP6 models, the European Centre for Medium Range Weather Forecasts 5th reanalysis (ERA5, Hersbach et al. 2020) is used for verification of model TC climatologies from 1984-2014. The 6-hourly relative vorticity fields from ERA5 are used for cyclone tracking and TC identification, and 6-hourly sea level pressure and 10 m winds from ERA5 to investigate cyclone intensity.

6-hourly position, 10 m wind speed and sea level pressure data from the HURricane DATabase version 2 (HURDAT2, Landsea and Franklin 2013) is used between 1984 and

2014 in section 6.3.1 to compare TC intensity and spatial distribution with those simulated in ERA5 and CMIP6.

6.2.2. Cyclone Tracking

Cyclone detection and tracking is performed using the objective feature tracking scheme, TRACK (Hodges 1994, 1995, 1999), configured for TCs. The tracking is performed on the spectrally filtered (T63 resolution) relative vorticity fields vertically averaged (600-850 hPa) for ERA5, and at 850 hPa (spectrally filtered to T42) for CMIP6 due to data availability. For more information on the tracking scheme, see Hodges et al. (2017) and section 2.2.

The spatial distribution of TC track and genesis densities are calculated from the cyclone tracks using the spherical kernel method described in Hodges (1996). Densities are expressed as cyclones per year per unit area, where the unit area is equivalent to a spherical cap with a radius of 5 degrees (Figures 6.1 and 6.2).

6.2.3. Objective TC Identification

TCs are identified from the larger sample of tracked cyclones using the methodology described in section 2.3.2. Only tracks which form in the North Atlantic hurricane season (June 1st – November 30th) are considered in this study. The TC identification criteria are applied to the vorticity fields at the 850-, 700-, 600-, 500-, 400-, 300- and 250 hPa pressure levels for ERA5, but only to the 850-, 500- and 250 hPa levels for CMIP6 models due to data availability. Previous (unpublished) work found little sensitivity on cyclone statistics to this difference in data and methodology for tracking and TC identification (not shown). The SSTs are expected to increase as a result of climate change, and so the poleward extent of TC genesis may move polewards, potentially beyond 30°N (which is the latitude constraint placed on genesis of TCs in Hodges et al. 2017). To ensure that our TC identification method is suitable, we first check that there is no robust projected increase in TC genesis poleward of 30°N. This is achieved by modifying the TC identification method by relaxing the latitude constraint for genesis to 45°N, then re-identifying TCs. We then investigate the change in genesis density between the 2069-2099 and 1984-2014 periods. No robust trend in TC genesis poleward of 30°N is found (Fig. 6.12), and so the original TC identification method is retained.

The TC identification method used here has been used in numerous studies based on reanalyses (Hodges et al. 2017; Baker et al. 2021) and climate models (e.g., Baker et al. 2022; Roberts et al. 2015; Vidale et al. 2021). It has been shown that PTC impacts over Europe in the present climate are similar whether this objective TC identification method, or objective track matching with observational data, are used (Sainsbury et al. 2020).

6.2.4. Recurvature, Europe Definitions and Regional Domains

Changes in TC statistics, recurving TC statistics, and Europe-impacting PTC statistics are considered in this study. A recurving TC is defined as a TC which enters a domain in the North Atlantic midlatitudes from 82°W-30°E, 36-70°N (as in Sainsbury et al. 2022). A Europe-impacting PTC is defined as a TC which enters a European domain defined as 10°W-30°E, 36-70°N (as used in Baker et al. 2021; Sainsbury et al. 2020, 2022b). The regions are constructed such that every Europe impacting PTC is a recurving TC by definition and are illustrated in Figure 6.1. PTCs can reach Europe with either a cold core or a low-level warm core (warm seclusion development, Baker et al. 2021; Dekker et al. 2018). In this study, both types are considered.

In section 6.3.2.2, we investigate North Atlantic TC genesis regionally. North Atlantic TCs are separated based on genesis into three regions: the Main Development Region (MDR, 0-20°N, 70°W-30°E), Subtropical Atlantic (SUB, 20-30°N, 82°W-30°E) and the western Atlantic comprising the Gulf of Mexico and the region south of the Caribbean (denoted WEST, vertices at (4°N,70°W), (4°N,90°W), (14°N,90°W), (14°N,100°W), (30°N,100°W), (30°N,82°W), (20°N,82°W) and (20°N,70°W)). These regions span the entire tropical North Atlantic, and all simulated TCs form in one of these regions. The boundaries of these regions are shown in Figure 6.7. It should be noted that metrics are conditioned in two different ways throughout the results section. For example, in Figures 6.5 and 6.9 metrics are presented which are conditional on cyclones reaching Europe (e.g., given that a set of cyclones reach Europe, what fraction are PTCs?), whereas in the rest of the manuscript metrics are conditioned on cyclones being TCs (e.g., given that a set of cyclones are TCs, what fraction reach Europe as PTCs?).

6.2.5. Environmental Field Analysis

Changes in large-scale environmental fields known to be associated with TC genesis and intensification are investigated in CMIP6 using the genesis potential index (GPI, Emanuel and Nolan 2004).

$$GPI = |10^5\eta|^{3/2}\left(\frac{H}{50}\right)^3\frac{V_{pot}}{70}(1+0.1V_{shear})^{-2}, \quad (6.1)$$

where η is the 850 hPa absolute vorticity, H is the relative humidity at 600 hPa, V_{shear} is the magnitude of the 250-850 hPa wind shear and V_{pot} is the potential intensity (PI) (Emanuel 1986), implemented using the tcPyPI python package (Gilford 2021). Fields are first re-gridded to a common resolution (1x1 degrees) to ensure comparability.

Deep layer steering flow is also used and is defined as in Colbert and Soden (2012). However, due to data availability, we use the 250 hPa field instead of the 200 hPa field.

6.3. Results

6.3.1. North Atlantic Tropical Cyclone Climatologies in Historical CMIP6 Simulations

In this section we examine the climatology and properties of the TCs simulated by each of the selected CMIP6 models. If we wish to learn something about how PTC impacts may change across Europe in the future, we need to understand whether these models are able to capture features of the observed TC climatology, and also identify any biases which may translate into biases in the projected changes in PTC statistics.

6.3.1.1. Spatial Statistics

Figure 6.1 shows the genesis density in the historical period for the five selected CMIP6 models (a-e) and ERA5 and HURDAT2 (f). Comparisons between HURDAT2 and ERA5/CMIP6 models should be made cautiously due to differences in how TCs are identified. For example, the cyclone detection and tracking scheme used in this study allows for the identification of TC precursors. Therefore, the genesis densities shown for the CMIP6 models and ERA5 represent the genesis density of the precursors to TCs, whereas HURDAT2 genesis density shows where these precursors developed into TCs. This explains the differences in genesis density between CMIP6/ERA5 and HURDAT2 over west Africa. The CMIP6 models, ERA5 and HURDAT2 typically show two regions of

genesis maxima: one centred between 0 and 30°W in the eastern tropical Atlantic, where the African Easterly Waves that act as TC precursors originate (Arnault and Roux 2011; Thorncroft and Hodges 2001), and a second to the western side of the basin. In ERA5 and HURDAT2, TC genesis is more of a continuum across the tropical Atlantic, whereas in the CMIP6 models (with the exception of CNRM) TC genesis is in two discrete regions. CNRM and HadGEM most closely match the spatial distribution of genesis seen during the same period in ERA5 and HURDAT2. Further information on the proportion of North Atlantic TCs forming in different subregions of the basin in CMIP6 and ERA5 can be found in Table 6.2. Additional analysis on 10 further CMIP6 models which did not meet our criteria (blue shaded boxes, Figure 6.11) showed very little (or no) genesis in the MDR, which is likely responsible for the low TC counts in these additional models (not shown). The cause(s) of the bias in TC activity in the MDR in these additional models is outside of the scope of this paper, but may be associated with insufficient horizontal resolution, differences in the representation of the large-scale circulation and tropical environment into which TCs are forming, and differences in the representation of TC seeds (frequency, intensity, and conversion rate).

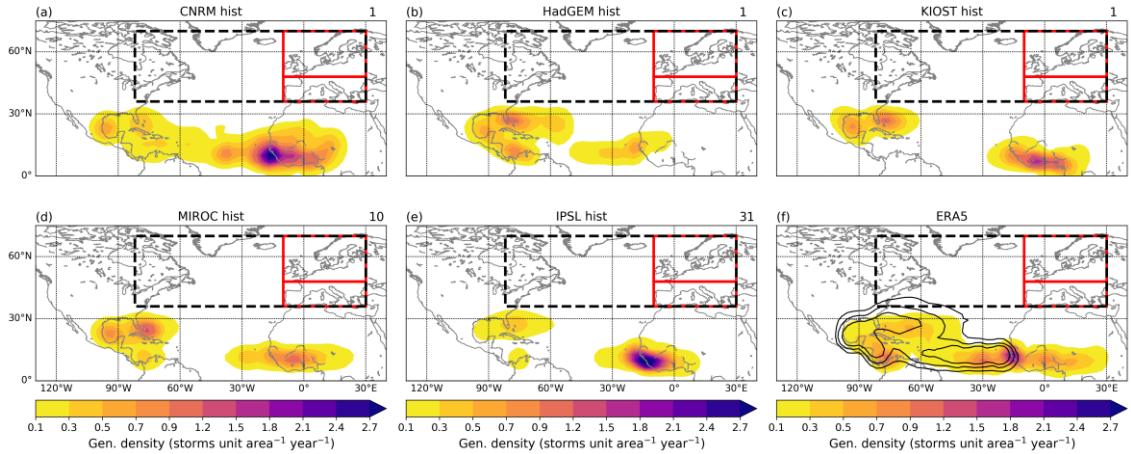

Figure 6.1. Genesis density (storms per unit area per year, where the unit area is equal to a spherical cap with a 5-degree radius) for the 1984-2014 period from the historical runs of 5 CMIP6 models (a-e), and ERA5 (filled) and HURDAT2 (black lines) (f). Only TCs forming during the North Atlantic hurricane season are considered. The number of ensemble members used is shown to the top right of each panel. Densities of less than 0.1 have been masked for clarity. HURDAT2 contours in (f) are 0.1, 0.3, 0.5 and 0.7 storms unit area^{-1} year^{-1}, where the unit area is equal to a spherical cap of 5-degree radius. Black dashed region represents the recurvature domain and red regions represent the Northern Europe (top), Southern Europe (bottom) and Europe (whole red region) domains.

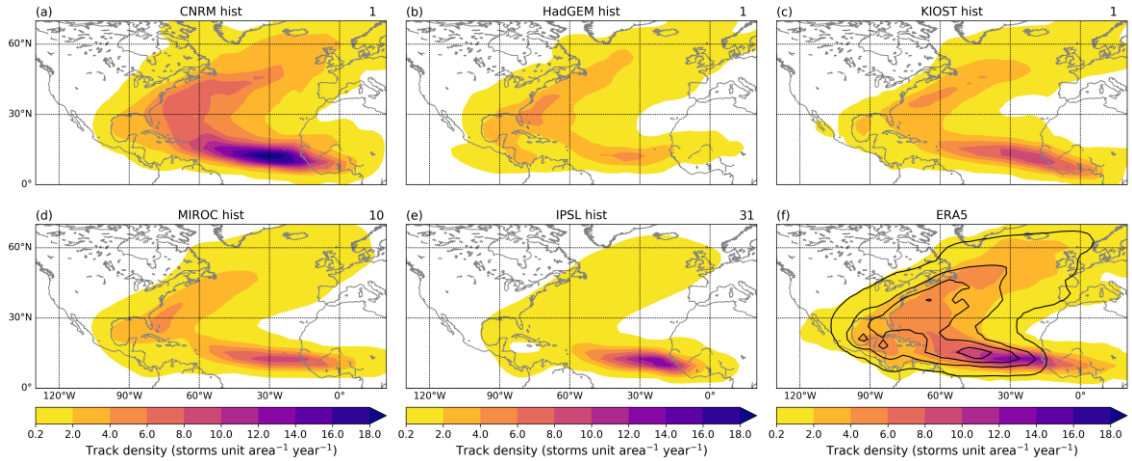

Figure 6.2. As in Figure 6.1, but for track density. Densities less than 0.2 have been masked for clarity. Black contours in (f) represent 0.2, 2.0, 4.0, 6.0 and 8.0 storms unit area^{-1} year^{-1}.

All of the models capture the maxima in track density in the Main Development Region (MDR) and the maxima in track density recurving around the US East Coast, heading towards Europe (as shown in Baker et al. 2021). As with genesis density (Figure 6.1), many of the models have two apparent storm tracks, one associated with storms originating in the MDR and one associated with storms originating further west in the basin. In all models except CNRM, track density decreases rapidly from east to west across the MDR, and this is particularly clear in IPSL (Fig. 6.2e). The lysis density (Figure 6.13) is greater in the MDR in KIOST, MIROC, and IPSL than it is in ERA5, indicating that in these models TCs forming in the MDR dissipate too quickly. This is particularly clear for IPSL, which shows almost all MDR TCs dissipating whilst still in the MDR, close to where they formed. MDR-forming TCs in ERA5 have a mean track length of ~9700 km and mean duration of ~16.5 days, compared to a mean track length of ~4200 km and a mean duration of 8.7 days in IPSL.

Coupled with the lack of genesis in the western MDR in these models (Figure 6.1), the track (Figure 6.2) and lysis (Figure 6.13) density plots suggests that conditions in the models are too hostile for TC genesis or intensification in this region. In particular, vertical wind shear in all models except CNRM is higher (~2-6 m s^{-1}) than ERA5 over the 1984-2014 period, with the biggest biases in the central and western MDR (Figure 6.14), consistent with previous studies (Han et al. 2022). Another possibility is that the conversion rate of seeds to TCs, which is sensitive to resolution, is too low in these models.

6.3.1.2. Seasonal Cycle

Figure 6.3 shows the seasonal cycle for the selected CMIP6 models and ERA5. TCs in HURDAT2 are identified later in their lifecycle than TCs tracked and identified objectively (sections 2.2, 2.3.2) in ERA5 and CMIP6 models. HURDAT2 data is therefore not included in Figure 6.3. CNRM has a bias towards early season North Atlantic TC activity (compared to ERA5), with a peak in August. This can also be seen in KIOST, but to a lesser extent. The other three CMIP6 models all show a peak in North Atlantic TC formation in September, the same as in ERA5. While the seasonal cycle is captured well by the models, all but CNRM underestimate North Atlantic TC frequency during hurricane season, with the largest underestimation found in HadGEM during the months of peak activity (August-October), consistent with too few simulated TCs originating in the MDR (Figs 6.1, 6.2). All models except the CNRM underestimate Europe-impacting PTC frequency (Fig. 6.3b) towards the beginning of the season (June – September). This is because in all models except CNRM, proportionally too few TCs originating in the MDR recurve (Table 6.2). As a result, there are less TCs reaching the midlatitudes; the region which often provides the baroclinicity to facilitate extratropical transition and future reintensification on approach to Europe. All selected CMIP6 models except KIOST have similar SST gradients along the midlatitude storm track to those found in ERA5 during hurricane season. In KIOST, SST gradients are slightly higher, which may be associated with the greater proportion of recurving TCs reaching Europe in the historical period (Table 6.1).

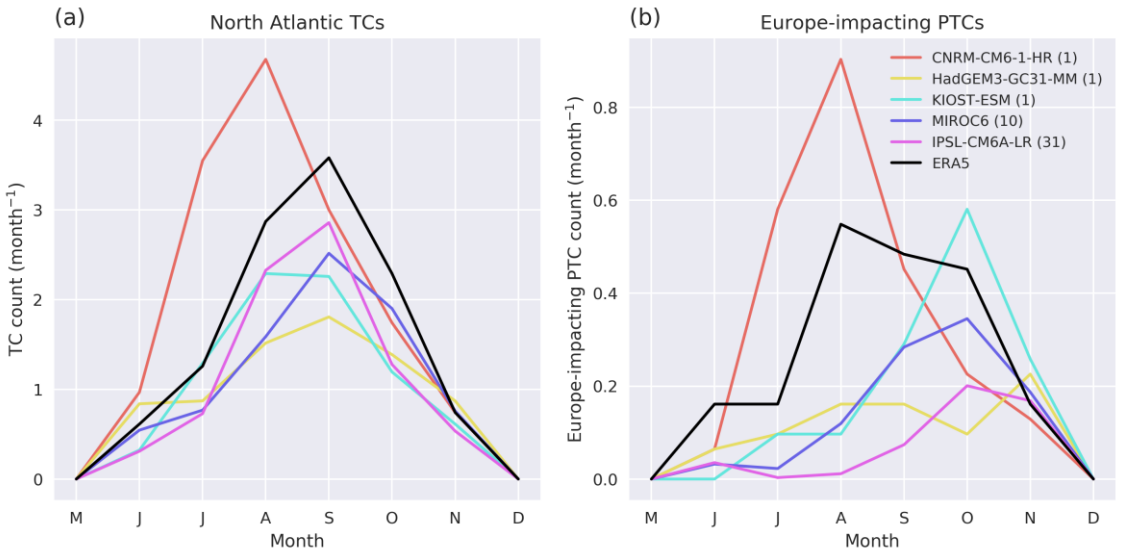

Figure 6.3. Seasonal cycle of North Atlantic TCs (a) and Europe-impacting PTCs (b) in the historical run (1984-2014) of 5 CMIP6 models (coloured lines) and ERA5 (same time period, black). Cyclones are binned by the month of genesis. TCs forming outside of hurricane season are not included in this study and so these months are set equal to zero. The number of ensemble members used for each model is shown in brackets in the key.

6.3.1.3. Lifetime Maximum Intensity

TC lifetime maximum intensity (LMI) distributions for the selected CMIP6 models are shown in Figure 6.4. All models use the same sampling frequency for wind speed (3hrPt). All selected CMIP6 models underestimate the mean TC LMI and are unable to simulate the strongest observed TCs. CNRM is able to simulate stronger TCs than the other CMIP6 models and ERA5, with some TCs approaching 50 m s^{-1} (category 3 on the Saffir-Simpson scale). MIROC is able to simulate storms with a similar intensity to ERA5, however is still biased towards weaker TCs. The other CMIP6 models are unable to simulate TCs with LMIs of hurricane force (33 m s^{-1}). The wind-pressure relationship (Fig. 6.15) also shows that TCs in ERA5 and CMIP6 models have wind speeds too low for a given sea level pressure (compared to HURDAT2), which is expected as low-resolution models tend to simulate larger TCs with a weaker pressure gradient.

The majority of TCs identified in the historical period of IPSL are extremely weak, with 10 m wind speeds less than tropical storm (17 m s^{-1}) strength. While IPSL does have positive wind shear biases and negative potential intensity biases compared with ERA5, these are no larger than for the other selected models (Fig. 6.14). The large peak in TC LMI between approximately 10 and 15 m s^{-1} in IPSL corresponds to TCs forming in the MDR. TC LMI values in the right-hand tail of the IPSL distribution correspond to TCs originating in the Gulf of Mexico and along the Gulf Stream (not shown). The TCs in IPSL forming in the Gulf of Mexico and along the Gulf stream are forming at higher latitudes (~25-30°N) than those in the MDR (~10-20°N). One (speculative) possibility is that TCs forming in the deep tropics (MDR) are purely diabatically driven, whereas those forming along the US East Coast derive a component of their energy from baroclinic sources (consistent with Fig. 1, Elsner et al. 1996; Kossin et al. 2010). Any issue with the parametrisation of diabatic fluxes in IPSL would therefore lead to MDR TCs which are much too weak but would not affect higher-latitude forming TCs as strongly, potentially explaining the difference. IPSL also uses a regular horizontal grid

(Boucher et al. 2020) and so effective resolution increases with latitude. Systems are likely to be larger in scale at higher latitudes, and hence better represented at this resolution than at lower latitudes (for example, in the MDR). This may also in part explain the better representation of TC intensity with latitude, but a dedicated study would be necessary to test these hypotheses and quantify their importance.

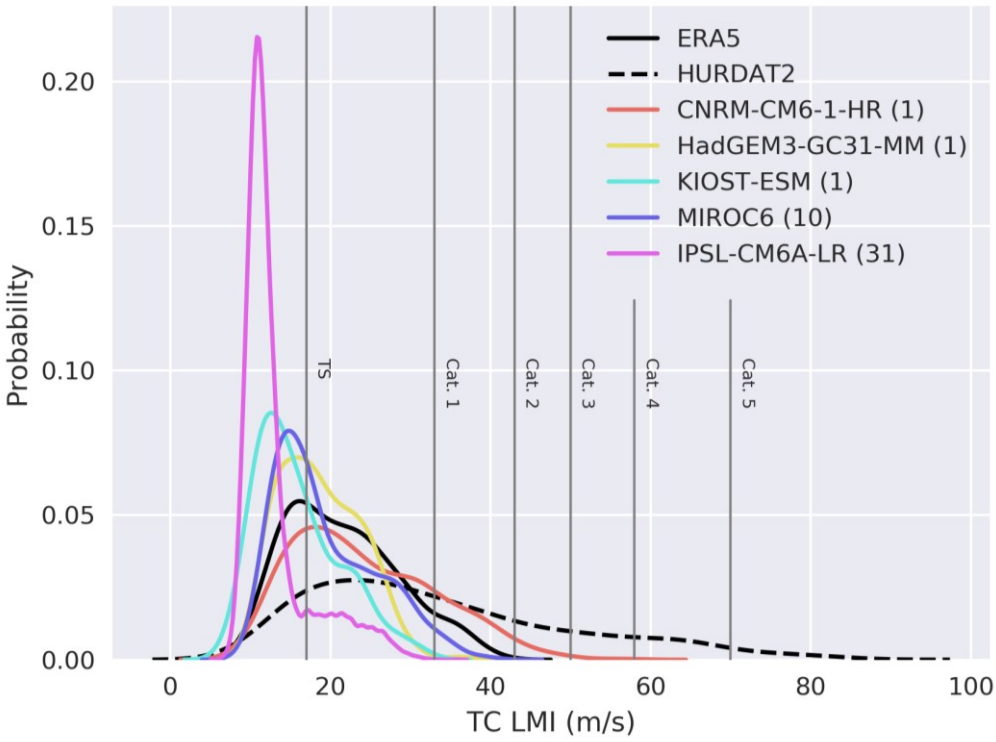

Figure 6.4. TC lifetime maximum intensity distributions for the historical (1984-2014) period for selected CMIP6 models, ERA5 (black, solid), and HURDAT2 (black, dashed). Only TCs forming during the North Atlantic hurricane season are considered. Densities are approximated as kernel density estimates. Vertical grey lines represent the different categories on the Saffir-Simpson scale. The number of ensemble members used for each model is shown in brackets in the key.

Despite clear model biases, the selected CMIP6 models represent many features of the observed TC climatology, with spatial patterns and frequencies in qualitative agreement with observations. TC frequency, seasonal cycle, and spatial distribution in these selected CMIP6 models are comparable to those found in higher-resolution modelling studies, such as Climate-SPHINX (Vidale et al. 2021), UPSCALE (Roberts et al. 2015) and HighResMIP-PRIMAVERA (Roberts et al. 2020b; Haarsma et al. 2016; Baker et al. 2022), which used the same tracking and identification scheme. However, many high-resolution climate models are able to simulate TCs with intensities greater than

50 m s^{-1} (Baker et al. 2021; Vidale et al. 2021), unlike all selected CMIP6 models except CNRM in this study. Many high-resolution models contain biases in their large-scale environment, but in most cases these biases are not consistent between models (Roberts et al. 2020a). This is also true for the selected CMIP6 models with the exception of vertical wind shear, which is too high in the MDR in all selected models except CNRM (Fig. 6.14). Improving model resolution does not systematically improve historical biases in the large-scale environmental fields correlated with TC genesis and intensification but does reduce historical biases in TC frequency and improves the spatial distribution of TCs, particularly in the MDR (Roberts et al. 2020a; Vidale et al. 2021; Baker et al. 2022). It is therefore possible that the lack of genesis in the western MDR in many of the selected CMIP6 models is the result of too much vertical wind shear and insufficient model resolution.

6.3.1.4. Recurving TC and Europe PTC Statistics

To gain insight into the projected changes in Europe-impacting PTCs, CMIP6 models must also capture the key features of the recurving TC, and Europe-impacting PTC climatologies. Previous work has shown that, to first order, TC activity governs recurving TC frequency (Sainsbury et al. 2022a). The selected CMIP6 models also capture the strong relationship between TC frequency and recurving TC frequency (Figure 6.16), highlighting that the models can capture the main driver of the interannual variability of recurving TCs, which may have important implications for European PTC risk.

A key feature of the observed PTC climatology is that PTC maximum intensities over Europe are on average, larger than those found for the broader class of midlatitude cyclones (MLCs, defined as all cyclones which are not PTCs) forming during hurricane season (Sainsbury et al. 2020). In Figure 6.5, we identify the maximum intensity associated with each PTC and MLC over Europe and subregions (Northern/Southern Europe, shown in Fig. 6.1) and investigate the fraction of cyclones in each intensity bin which are PTCs.

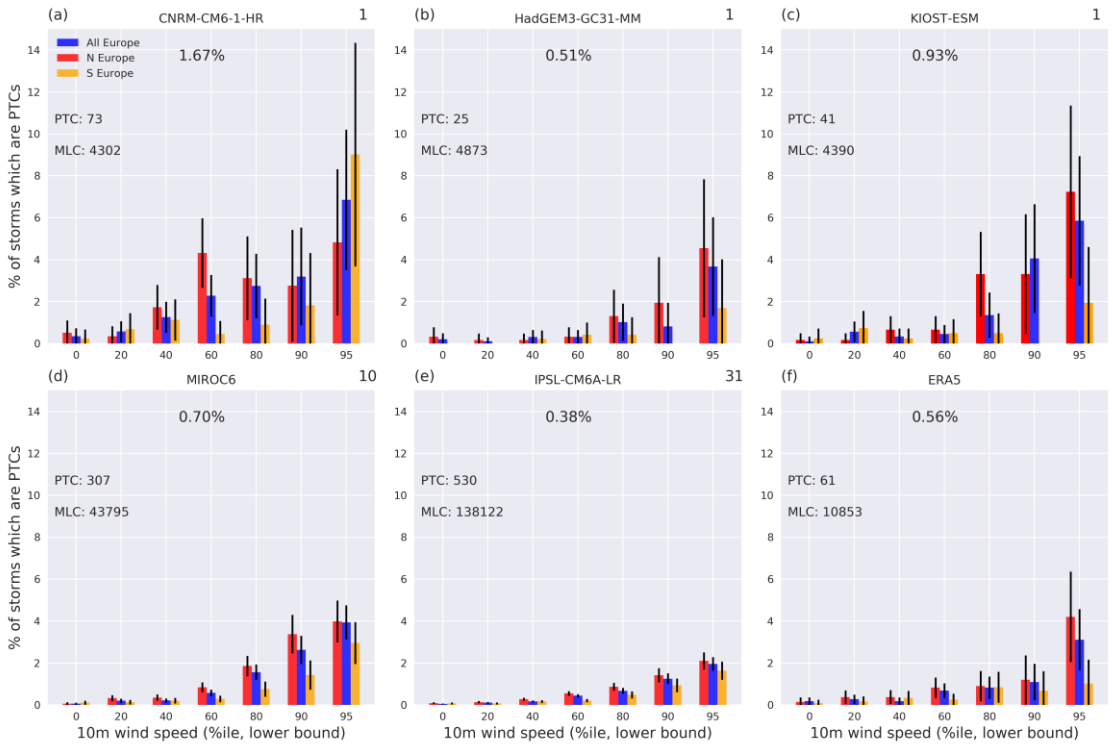

Figure 6.5. Fraction of hurricane-season-forming, Europe-impacting cyclones which are PTCs for CNRM (a), HadGEM (b), KIOST (c), MIROC (d), IPSL (e), and ERA5 (f), where cyclones are binned by their maximum 10 m wind speed over Europe (blue), Northern Europe (red) and Southern Europe (yellow) in the historical runs of the selected CMIP6 models (a-e). Northern Europe is defined as 48-70°N, 10°W-30°E, and Southern Europe is defined as 36-48°N, 10°W-30°E. The number of PTCs and MLCs impacting Europe (whole domain) during the North Atlantic hurricane season, and the percentage of cyclones impacting Europe (whole domain) during hurricane season which are PTCs, are shown in each panel. The number of ensemble members used for each model is shown to the upper-right of each panel. Vertical bars show the 95% binomial proportion confidence interval.

To ensure that the sample size remains reasonable across bins and across models, we bin the cyclones based on percentiles of the combined distribution. For each model, we combine the (Europe-impacting) PTC and MLC cyclone tracks over both time periods (historical and future) and calculate percentiles of this joint distribution of their maximum 10 m wind speeds over Europe. These percentiles are then used to bin the data. The bins therefore correspond to 0-20th, 20-40th, 40-60th, 60-80th, 80-90th, 90-95th and >95th percentiles.

In ERA5, only 0.56% of cyclones reaching Europe during the North Atlantic hurricane season are PTCs. However, when considering the highest intensity bin (>95th percentile), this fraction is 3.11%, over 5 times larger. While these numbers are

different to those found in Sainsbury et al. (2020) (~0.5% in the lowest intensity bin, ~9% in the highest intensity bin) due to differences in date range and the bins used to bin the data, the key point remains: There is an increasing trend in the fraction of cyclones which are PTCs with intensity. Despite being unable to simulate intense TCs, all five CMIP6 models capture the relationship between TC frequency and recurving TC frequency, and the disproportionate intensity associated with Europe-impacting PTCs. PTC and MLC counts for each bin can be found in Table 6.4.

6.3.2. Projected Changes in Europe-Impacting PTC Frequency

In this section we investigate the projected changes in Europe-impacting PTC counts. We consider the projected changes in three key components: **i)** Changes in basin-wide North Atlantic TC counts, **ii)** Changes in the likelihood that a North Atlantic TC will recurve, and **iii)** Changes in the likelihood that a recurving North Atlantic TC will reach Europe.

While some overlap exists, these three components are likely driven by different factors. Changes in basin-wide TC counts to an extent depend on how the large-scale environment (sea surface temperature, vertical wind shear, atmospheric moisture, etc.) and teleconnections (e.g., ENSO) change in the future (e.g., genesis potential index, Camargo 2013). Changes in likelihood of recurvature may depend on changes to the large-scale steering flow, changes in TC intensity (stronger TCs survive longer), changes in where TCs are forming (TCs in some regions are more prone to recurve than in other regions, Sainsbury et al. 2022), and changes to the large-scale environmental conditions in the subtropical Atlantic (more favourable conditions for TCs in the subtropics may lead to a larger proportion of TCs successfully making the transit from the tropics to the extratropics, Haarsma et al. 2013). Changes in the likelihood that a recurving TC will reach Europe may be related to changes in the midlatitude jet and the intensity of TCs (Haarsma 2021; Sainsbury et al. 2022b).

Europe-impacting PTC counts are therefore expressed as

$$N_{Europe} = N_{TC} F_{Rec} F_{Europe \mid Rec} , \tag{6.2}$$

where N_{Europe} is the number of Europe-impacting PTCs, N_{TC} is the number of North Atlantic TCs, F_{Rec} is the fraction of North Atlantic TCs which recurve (the likelihood of

recurvature), and $F_{Europe \mid Rec}$ is the fraction of recurving TCs which reach Europe (the likelihood that a recurving TC will reach Europe). Each term is calculated for the historical and future SSP5-85 projection for each model and shown (with the fractional changes) in Table 6.1.

All five selected models project a statistically significant (to 95%) decrease in North Atlantic TC frequency (N_{TC}) of 30-60% by the end of the 21st century. Four models also show an increase in the likelihood of recurvature (F_{Rec}), which is significant in HadGEM, MIROC and IPSL. HadGEM is the only model with a significant projected increase in $F_{Eur|Rec}$, and all other models have non-significant projected changes. Overall, there is no robust model response in Europe-impacting PTC frequency in the future (N_{Eur}), with CNRM projecting a significant decrease, MIROC projecting a significant increase, and the remaining models showing no significant change.

In all models except CNRM, the fractional decrease in TC counts is much larger than the fractional change in Europe-impacting PTC counts, with two models even projecting an increase in Europe-impacting PTC counts in the future. Therefore, in four of the five models, there is a projected increase in the proportion of North Atlantic TCs which reach Europe in the future (=$F_{Rec}\, F_{Eur|Rec}$), which is significant in MIROC and IPSL (Fig. 6.10a). In HadGEM, IPSL and MIROC the reduction in TC counts is offset by a projected increase in the likelihood of recurvature, highlighting that future TCs may be more likely to impact the heavily-populated US East Coast. The projected increase in F_{Rec} is consistent with the projected increase in potential intensity and projected decrease in vertical wind shear along the US East Coast (Figure 6.6). This result also supports previous studies which suggest that more favourable conditions in the subtropical North Atlantic will allow more TCs to survive the transit from the tropics to the extratropics in the future (Haarsma et al. 2013). The projected changes shown in Table 6.1 are not sensitive to whether all ensemble members are used, or whether only ensemble members common to both the historical and future periods (same realization, initialization, and physics) are used (Table 6.5). There is a large ensemble spread in the statistics presented in Table 2.1 in the MIROC and IPSL. However, the projected changes in North Atlantic TC frequency, likelihood of recurvature, and the proportion of North Atlantic TCs reaching Europe are considerably larger than the ensemble spread (Table 6.6). The analysis of Table 6.1 is also repeated for 10

additional CMIP6 ScenarioMIP models which did not meet our selection criteria but have sufficient data available for cyclone tracking and TC identification (Tables 6.7, 6.8). These additional models support the results in Table 6.1 and highlight the robustness of the projected changes in North Atlantic TC frequency, likelihood of recurvature, and proportion of TCs reaching Europe in CMIP6 simulations.

	N_{TC}			F_{Rec}			$F_{Eur\|Rec}$			N_{Eur}		
	Hist	SSP	Diff	Hist	SSP	Diff	Hist	SSP	Diff	Hist	SSP	Diff
CNRM	14.68	9.00	**-39%**	0.55	0.59	7%	0.29	0.24	-17%	2.35	1.29	**-45%**
HadGEM	7.29	4.35	**-40%**	0.46	0.61	**31%**	0.24	0.35	**49%**	0.81	0.94	16%
KIOST	7.97	5.19	**-35%**	0.41	0.40	-4%	0.40	0.50	24%	1.32	1.03	-22%
MIROC	8.07	5.53	**-31%**	0.43	0.68	**58%**	0.29	0.31	9%	0.99	1.17	**18%**
IPSL	8.04	3.16	**-61%**	0.20	0.42	**110%**	0.31	0.32	3%	0.49	0.42	-15%

Table 6.1. Counts of North Atlantic TCs, likelihood of recurvature, likelihood that a recurving TC will reach Europe, and counts of Europe-impacting PTCs for the historical (1984-2014) period and the future (2069-2099) period under the SSP5-85 scenario. Fractional changes shown under the 'Diff' columns. Bold values represent significance at the 95% level using a bootstrapping method. Shading represents the sign of the projected change.

6.3.2.1. Projected Change in the Number of North Atlantic TCs (N_{TC})

To investigate the significant projected decrease in North Atlantic TC counts (Table 6.1), the projected change in the genesis potential index and its terms (as calculated in section 6.2.5) during the North Atlantic hurricane season are calculated and shown in Figure 6.6. The historical biases in GPI and its terms for the selected CMIP6 models can be found in Figure 6.14. Although all models have some biases in GPI and comprising terms, the main similarity between the selected CMIP6 models is a positive wind shear bias in the MDR in all models except CNRM. Overall, the genesis potential index is projected to significantly increase along the US East Coast between approximately 30°N and 40°N (Fig. 6.6a-f). This indicates that in the future, TCs travelling through this region will be exposed to more favourable conditions for TCs, increasing the probability that they reach the recurvature domain. This is consistent with the projected increase in the likelihood of recurvature found in Table 6.1. In the selected models, the increase in GPI in this region is associated with a projected increase in potential intensity (PI, row 4) and a decrease in vertical wind shear (VWS, row 5), significant across all models.

While the projected changes in Figure 6.6 are consistent with an increased probability of recurvature, they do not help to explain the significant decrease in basin-wide TC counts towards the end of the century. Previous studies have shown that saturation deficit may be a better metric for TC genesis potential than relative humidity (Emanuel et al. 2008) and is projected to increase in the future (increasing hostility). Furthermore, it has been proposed that an increase in static stability may lead to a reduction in TC frequency (Bengtsson et al. 2007b; Sugi et al. 2002). These factors may help to explain why we see such a large projected decrease in TC counts in the North Atlantic despite an overall increase in the GPI.

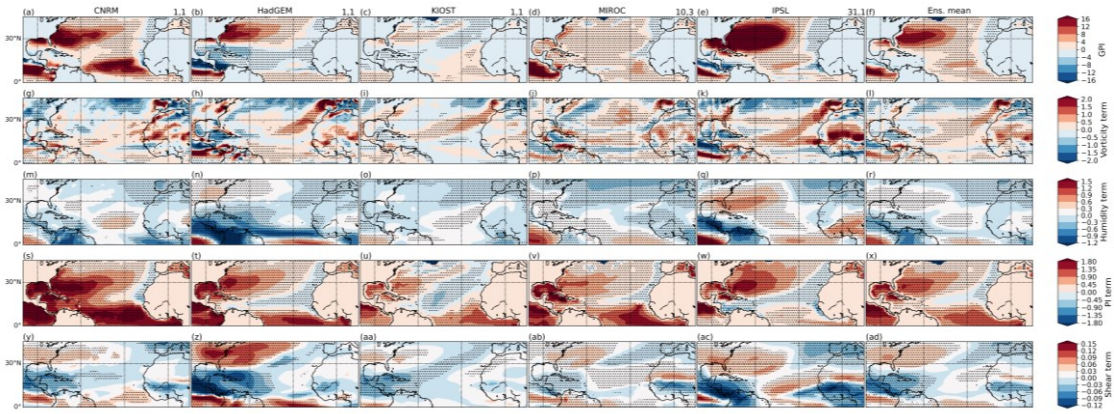

Figure 6.6. Projected change (future minus historical) in the GPI (top row) and the individual terms of the GPI equation (rows 2-4) for each of the selected CMIP6 models: vorticity term (second row), humidity term (third row), PI term (fourth row) and shear term (fifth row). Note that the vertical wind shear term is a function of the reciprocal of the wind shear, and so a positive difference indicates less vertical wind shear in the future. Number of ensemble members used for the historical and future periods are shown to the upper-right of each column (historical, future). Stippling represents statistical significance at the 95% level using Welch's t-test.

6.3.2.2. Projected Change in the Fraction of Recurving North Atlantic TCs (F_{Rec})

Table 6.1 shows a statistically significant increase in the likelihood of recurvature in 3 of the 5 models. Whether or not a TC recurves could depend on multiple factors (Sainsbury et al. 2022a): the location in which the TC forms, TC intensity (stronger TCs are more resilient to hostile conditions), and the steering flow (Colbert and Soden 2012). In this subsection, we aim to investigate which of these factors – if any – are responsible for the projected increase in F_{Rec}.

Projected increases in GPI along the US East Coast are consistent with the increased likelihood of recurvature. In this region, a reduction in wind shear is collocated with a projected increase in PI (Fig. 6.6s-ad). This is consistent with CMIP5 models (Camargo 2013) and indicates that future TCs traversing the US East Coast may retain TC-like conditions further poleward, increasing their likelihood of both making it to the midlatitudes (and being identified as recurving as a result), and potentially also reaching Europe. The projected increase in GPI along the US East Coast supports previous studies which suggest an increase in the latitude of TC LMI and an overall expansion of the tropical genesis region (Kossin et al. 2014; Haarsma 2021). However, all five models show an increase in GPI along the US East Coast, but only three models have a significant increase in F_{Rec}, indicating that other factors must also play a role.

Figure 6.7 shows the normalized TC track density for the historical and future periods, along with the difference (future minus historical). The track densities are normalized by dividing by the total number of TCs, so the differences show the geographical redistribution of North Atlantic TCs rather than the change in total number (N_{TC}).

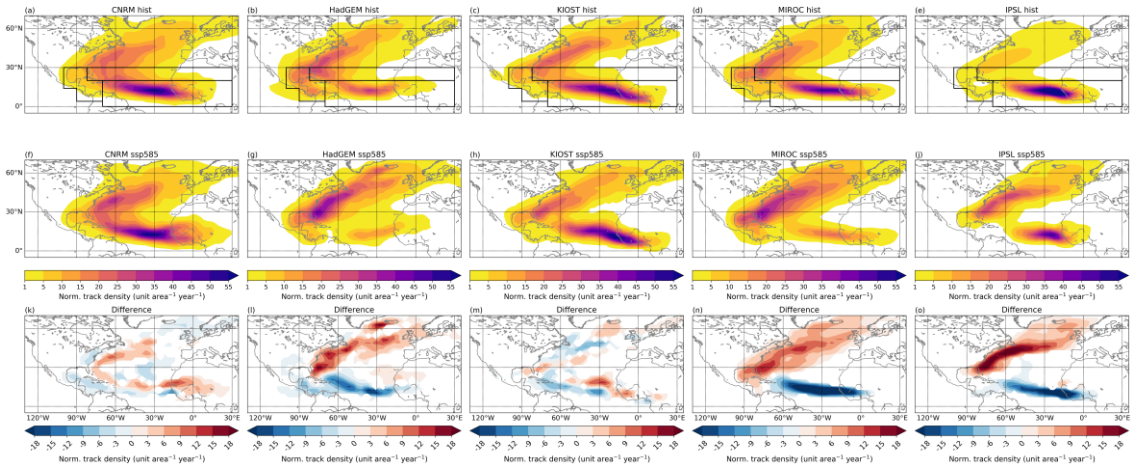

Figure 6.7. Normalized TC track density for the 5 selected CMIP6 models during the historical (top) period, towards the end of the century under SSP5-85 (middle) and the difference (future minus historical, bottom). Densities less than 1 have been masked for clarity. Black domains represent the boundaries of the MDR, SUB and WEST regions.

HadGEM, IPSL and MIROC have many similarities in normalized track density difference. There is proportionally less track density in the MDR and proportionally higher track density in the future along the East coast of the US heading towards Europe. The large decrease in normalized TC track density in the MDR indicates a

potential shift in genesis, away from the MDR towards the west of the North Atlantic, as confirmed by the normalized genesis densities (Fig. 6.18). To investigate this further, we separate the North Atlantic TCs based on genesis into three regions: the Main Development Region (MDR), Subtropical Atlantic (SUB), and western Atlantic (WEST). These regions are constructed such that all North Atlantic TCs form in one of these regions, and the boundaries for these regions can be found in section 6.2.4.

We decompose the likelihood of recurvature based on these three regions of genesis:

$$F_{Rec} = W_{MDR}F_{MDR} + W_{SUB}F_{SUB} + W_{WEST}F_{WEST}, \quad (6.3)$$

where W_i are weighting terms, representing the proportion of North Atlantic TCs which form in region i, and F_i represents the proportion of TCs forming in region i which recurve (i=MDR, SUB, WEST). The 6 terms on the right-hand side of equation 6.3 are calculated for the historical and future runs of the five selected CMIP6 models and are shown in Table 6.2.

HIST (1984-2014)	W_{MDR}	F_{MDR}	W_{SUB}	F_{SUB}	W_{WEST}	F_{WEST}
CNRM	0.77	0.54	0.11	0.69	0.12	0.54
HadGEM	0.34	0.14	0.31	0.83	0.35	0.46
KIOST	0.62	0.17	0.18	0.91	0.19	0.73
MIROC	0.52	0.19	0.21	0.86	0.26	0.55
IPSL	0.75	0.03	0.14	0.83	0.10	0.58
ERA5	0.62	0.46	0.19	0.75	0.19	0.33
SSP5-85 (2069-2099)	W_{MDR}	F_{MDR}	W_{SUB}	F_{SUB}	W_{WEST}	F_{WEST}
CNRM	0.76	0.54	0.16	0.78	0.08	0.68
HadGEM	0.17	0.22	0.42	0.74	0.41	0.64
KIOST	0.60	0.16	0.20	0.81	0.20	0.69
MIROC	0.25	0.32	0.33	0.90	0.41	0.72
IPSL	0.52	0.00	0.31	0.90	0.17	0.82
DIFF	W_{MDR}	F_{MDR}	W_{SUB}	F_{SUB}	W_{WEST}	F_{WEST}
CNRM	-1%	0%	**45%**	13%	**-33%**	26%
HadGEM	**-50%**	57%	**35%**	-11%	17%	**39%**
KIOST	-3%	-6%	11%	-11%	5%	-5%
MIROC	**-52%**	**66%**	**57%**	4%	**56%**	**30%**
IPSL	**-31%**	**-100%**	**111%**	8%	**71%**	**43%**

Table 6.2. Tabulated values of the terms of the right-hand side of equation 6.3 for the historical run (top), future run under SSP5-85 (middle) and the fractional change (bottom) for the five selected CMIP6 models. Bolded values represent significant fractional changes at the 95% level using a bootstrapping method. Shaded cells for the historical and future statistics show values which are greater (red) or less than (blue) the corresponding historical statistics in ERA5. Shaded difference represent the sign of the projected change.

Rows 2-6 of Table 6.2 highlight the significant bias historically of many of the models (all but CNRM) for recurvature of TCs originating in the MDR. Approximately 46% of MDR forming TCs recurve in ERA5, but this value is between 3% and 19% in four of the five models, with only CNRM correctly capturing this fraction. The three models which have a significant increase in F_{Rec}; HadGEM, MIROC and IPSL, all see a significant shift in proportional genesis away from the MDR towards the SUB and WEST regions. Due to the F_{MDR} bias in these models, the shift in genesis from the MDR to the other regions leads to an increase in F_{Rec}. A component of the projected increase in F_{Rec} is therefore likely a manifestation of model biases. To quantify the contribution of genesis shifts to the projected change in F_{Rec}, we split the change in F_{Rec} into three terms as described in the appendix (equation 6.7). Term 1 represents the contribution to the change in F_{Rec} caused by a change in the likelihood of recurvature within each region, and term 2 represents the contribution to the change in F_{Rec} caused by a shift in genesis location. Term 3 is the nonlinear combination of a shift in genesis location and a change in the likelihood of recurvature within each region. This term is usually small but is included for completeness.

Model	Term 1	Term 2	Term 3
CNRM	0.81	0.21	-0.02
HadGEM	0.42	**0.67 (0.28-1.81)**	-0.09
KIOST	1.84	-0.96	0.11
MIROC	**0.47 (0.31-0.59)**	**0.55 (0.47-0.67)**	-0.02
IPSL	0.07	**0.77 (0.61-1.02)**	**0.16 (0.05-0.24)**

Table 6.3. Contribution to projected change in F_{Rec} from terms 1 (second column), 2 (third column) and 3 (fourth column) of Equation 6.7. Bolded values represent significance at 95% using a bootstrapping method. For significant values, the 95% confidence interval is shown in brackets.

Term 2 dominates for the three models which have a significant increase in F_{Rec}, indicating a significant contribution to F_{Rec} from a shift in genesis location away from the MDR to the SUB and WEST regions in these three (and only these three) models. The projected change in GPI (Fig. 6.6) does not show a large increase in hostility in the MDR compared to other regions in the future. Changes in TC seeds have been shown to influence TC frequency (Vecchi et al. 2019), and so the shift in TC genesis away from the MDR could be the result of a projected decrease in the frequency or intensity of TC seeds in the MDR, or a change in the conversion rate of seeds into TCs. The results of Tables 6.2 and 6.3 are not sensitive to the exact position of the region boundaries (not shown).

While shifts in genesis explain most of the projected change in F_{Rec} in HadGEM, MIROC and IPSL, they do not explain all of the projected increase. To further investigate the projected changes in F_{Rec}, the relationship between projected TC LMI changes and projected F_{Rec} changes is explored in the MDR, WEST and SUB regions of the five selected models. Significant increases in TC LMI are found in the WEST region of HadGEM, MIROC and IPSL, and in the MDR in MIROC. A significant increase in F_{Rec} is also found in the same regions and models (Table 6.2). A significant relationship (Pearson's correlation coefficient of 0.52) is found between TC LMI changes and F_{Rec} changes across the five models (Figure 6.19), suggesting that projected increases in TC LMI may be associated with the projected increases in F_{Rec} in the HadGEM, MIROC and IPSL.

Figure 6.8 shows the change in the hurricane-season-mean deep layer steering flow (Colbert and Soden 2012). All models have a significantly weaker westerly flow between 30 and 40°N over the US East Coast corresponding to the region in which shear decreases in the future (Figure 6.6). Differences in the steering flow are very small in the tropics in all models except HadGEM. In HadGEM, the easterly flow in the western tropical Atlantic is reduced, with increased poleward flow in the subtropical North Atlantic. This difference in flow between the historical and future periods would suggest an increased likelihood for recurvature for TCs forming at a given latitude in the WEST region (as the TCs are not being steered as strongly westwards towards land), and an increase in the likelihood of recurvature in the MDR, where the slower easterly flow in the western MDR and stronger poleward flow in the subtropics may

aid recurvature. This is consistent with Table 6.2, which shows a significant increase in the likelihood of recurvature in the WEST region and a (non-significant) increase in the MDR.

Three of the five CMIP6 models project a significant increase in F_{Rec}. Section 6.3.2.2 suggests that a shift in genesis from the MDR towards the SUB and WEST regions is responsible for the majority of this projected increase, some of which is likely to be associated with historical model biases. In these three models, increases in TC LMI may also be associated with the projected increase in F_{Rec}, and in HadGEM, changes in the steering flow may also play a role. Reduction in vertical wind shear (VWS) and increases in PI (Figure 6.6), seen across the models, are also consistent with enhanced longevity, implying increased likelihood of recurvature.

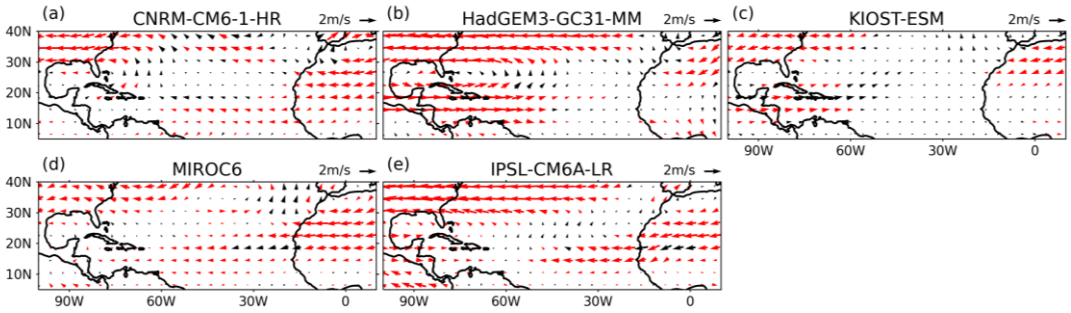

Figure 6.8. Difference (future minus historical) in the hurricane-season-averaged deep layer steering flow for the five selected CMIP6 models. Statistically significant differences between the future and historical period at the 95% level are shown in red and are calculated using Welch's t-test.

6.3.2.3. Projected Change in the Fraction of Recurving North Atlantic TCs which Reach Europe ($F_{Eur|Rec}$)

While 4 of the 5 CMIP6 models agree on the sign of the change in $F_{Eur|Rec}$, this projected increase is only significant in one model, HadGEM. This is associated with a shift in seasonality in HadGEM. In the future in this model, most recurving TCs interact with the midlatitudes later in the hurricane season, a result unique to HadGEM (not shown). A similar change in seasonality of extratropical transition was found across HighResMIP models (Baker et al. 2022). Climatologically, midlatitude baroclinicity increases throughout hurricane season and so in the future, many recurving TCs in HadGEM encounter a more favourable midlatitude environment. This suggests that

recurving TCs in HadGEM in the future are more likely to undergo extratropical reintensification, which has been shown to be linked to whether a recurving TC will reach Europe (Sainsbury et al. 2022b).

6.3.3. Projected Changes in Europe-Impacting PTC Intensity

In this section we investigate how the intensity of PTCs may change by the end of the century. Figure 6.9 shows the absolute number (per ensemble member) of Europe-impacting PTCs in each bin during the historical and future periods (bars), with the fractional change overlaid. CNRM and KIOST show both a decrease in the absolute number of strong Europe-impacting PTCs (Fig. 6.9a, e). IPSL and MIROC ensembles show an increase. HadGEM is mixed, with a decrease in the number of PTCs in the highest intensity bin but increases in the second and third highest intensity bins (Fig. 6.9b). The projected changes in Europe-impacting PTC intensity shown in Figure 6.9 are not significantly different if reproduced using only ensemble members common to both the historical and future periods (Figure 6.17).

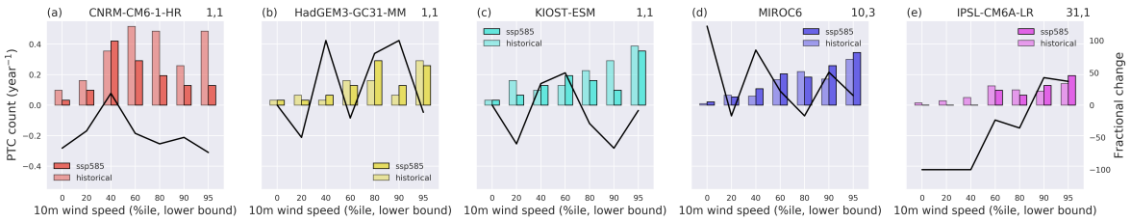

Figure 6.9. Bar plot showing the number of Europe-impacting PTCs (per ensemble member) in each intensity bin for the five selected CMIP6 models for the historical (1984-2014, lighter colours) period and towards the end of the century under the SSP5-85 scenario (2069-2099, darker colours). Fractional change in the counts in the future period compared to historical is shown as the black line corresponding to the right-hand side Y axis. Number of ensemble members used for the historical and future periods are shown to the upper right of each panel (historical, future).

In HadGEM, KIOST, MIROC and IPSL, the decrease in TC frequency basin-wide is considerably larger than the change in strong Europe-impacting PTCs. For example, MIROC has an increase in the number of strong Europe-impacting PTCs despite a 31% reduction in the number of North Atlantic TCs. This implies that the proportion of North Atlantic TCs which impact Europe as strong PTCs is projected to increase. This is illustrated in Figure 6.10, which shows the proportion of all North Atlantic TCs which reach Europe as strong PTCs (Fig. 6.10b) and very strong PTCs (Fig. 6.10c). Strong PTCs

are defined as PTCs which impact Europe with winds greater than the 90th percentile of the distribution of maximum winds over Europe during hurricane season (considering all PTCs and MLCs in the historical and future period). Very strong PTCs are PTCs which impact Europe with winds greater than the 95th percentile.

Four of the five models show an increase in the proportion of North Atlantic TCs which reach Europe as strong and very strong PTCs, and this difference is statistically significant in IPSL and MIROC. Our results therefore suggest that the future risk posed by PTCs to Europe may depend on how TC activity basin-wide changes in the future. If TC frequency decreases substantially (as suggested by this analysis), then the number of strong Europe-impacting PTCs is unlikely to change significantly. However, if TC frequency does not decrease much, or potentially increases, then Europe could be subject to significantly more strong PTCs in the future, as was found in Haarsma et al (2013).

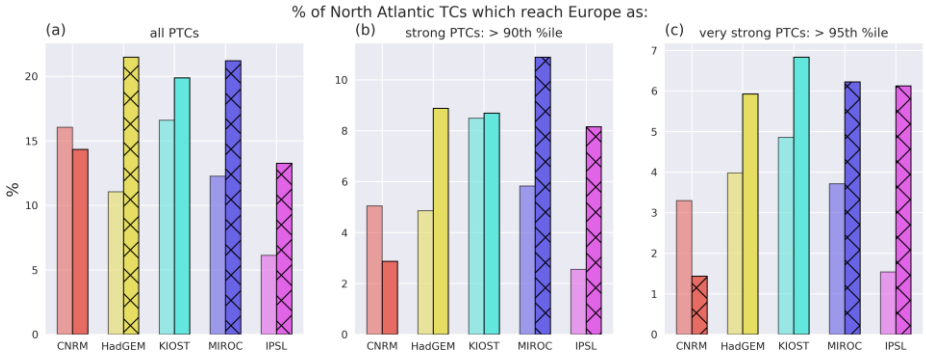

Figure 6.10. Bar charts showing the proportion of North Atlantic TCs which impact Europe as (a) PTCs, (b) strong PTCs (max winds > 90th percentile of the distribution of maximum winds over Europe) and (c) very strong PTCs (> 95th percentile). Lighter colours show the values for the historical period, darker bars for the future period. Hatching is overlaid in models where the projected change is significant to 95% using a bootstrapping method.

Haarsma et al. (2013) find a large increase in the frequency of hurricane force PTCs reaching Europe by the end of the century. The interpretation of Figures 6.9 and 6.10 does not change when using the regions (Norway, North Sea, West UK & Ireland, and Bay of Biscay) and season (August-October) used in Haarsma et al. (2013) (Figs 6.20-6.22). Despite using RCP 4.5, the prescribed SSTs used in Haarsma et al. (2013) are similar to the projected SST changes found in this study (not shown). The differences between Figure 6.20 and Figure 2f in Haarsma et al. (2013) could be caused by

different projected changes in North Atlantic TC counts (which were not investigated in their study), differences in model resolution, differences in TC identification methodology, or differences in model configuration (coupled vs atmosphere only).

6.4. Discussions and Conclusions

In this study, we have presented the first multi-model analysis of how Europe-impacting PTC frequency and intensity may change by 2100. Using a vorticity-based tracking scheme and objective TC identification method, we identify all North Atlantic TCs in five CMIP6 models in the historical (1984-2014) period, and the future (2069-2099) period under the SSP5-85 scenario, using all available ensemble members. These five models were selected from a wider sample of CMIP6 models based on their ability to simulate North Atlantic TC frequency compared to observations (Figure 6.11). While CMIP6 models do not have sufficient resolution to resolve all TC-related processes, the number of models and ensemble members allows us to investigate projected Europe-impacting PTC changes with a considerably larger TC sample size than available for previous studies. The key results are as follows:

- The five selected CMIP6 models are able to simulate many aspects of the North Atlantic TC climatology compared to observations. They capture the relationship between TC frequency and recurving TC frequency, and capture the disproportionate risk associated with PTCs compared to extratropical cyclones over Europe. However, the models still have many deficiencies. In particular, TCs forming in the MDR are too short lived and therefore unlikely to recurve, and TC intensity is significantly underestimated.
- No robust model response in Europe-impacting PTC frequency (overall, or as strong storms) is found in the future. This is because two competing factors – a decrease in North Atlantic TC frequency, and an increase in the proportion of TCs reaching Europe – are of approximately the same size.
- The projected decrease in North Atlantic TC frequency is statistically significant in all five models, with decreases of between 30 and 60% found by the end of the 21st century.
- The projected increase in the proportion of TCs reaching Europe is found in four of the five models and is associated with a projected increase in the

likelihood of recurvature. The increased likelihood of recurvature may be associated with a more favourable environment for TCs along the US East Coast, where wind shear is projected to decrease, and potential intensity is projected to increase in the future. This result is also consistent with previous studies which highlight that conditions between where TCs typically form and Europe are overall likely to become more favourable for tropical cyclogenesis in the future (Haarsma et al. 2013; Baatsen et al. 2015; Liu et al. 2017).

- The projected increase in the likelihood of recurvature in the North Atlantic is also associated with a shift in genesis, with proportionally less TCs forming in the MDR in the future, where model biases cause very few TCs to recurve.

Our results highlight the large uncertainty associated with projected changes in Europe-impacting PTC intensity and frequency. Even the model with the largest projected increase in intense Europe-impacting PTCs has a considerably lower increase than found in previous studies (Haarsma et al. 2013; Baatsen et al. 2015). The large uncertainties in the projected responses are anticipated – model uncertainties in TC genesis (Yamada et al. 2021; Yang et al. 2021; Vecchi et al. 2019; Camargo 2013; Ting et al. 2015), TC recurvature (Colbert and Soden 2012), TC intensity (Kossin et al. 2020) and midlatitude environment (for example, jet location and intensity, Harvey et al. 2020) could translate to model uncertainty in Europe-impacting PTCs due to the complex lifecycle of these systems.

Projected decreases in North Atlantic TC counts are found in many previous studies which explicitly track TCs (Roberts et al. 2015; Gualdi et al. 2008; Rathman et al. 2014), but not all (e.g., Bhatia et al. 2018). There are also physical arguments which support a decrease in TC activity due to an increase in static stability (e.g., Bengtsson et al. 2007; Sugi et al. 2002). However, other methods such as statistical and dynamical downscaling are more mixed in terms of the sign of the projected change (Emanuel 2021a, 2013; Jing et al. 2021), and there are often sensitivities to the tracking scheme when TCs are tracked explicitly (Roberts et al. 2020a). Previous studies have also suggested a broadening of weak TC circulations in the future (Sugi et al. 2020), which would result in future TCs having lower associated vorticity. As a result, tracking schemes which use a fixed vorticity threshold may capture a lower proportion of all model-simulated TCs in the future. The use of a percentile-based vorticity threshold

may alleviate this problem. It is therefore necessary to reduce the uncertainty associated with North Atlantic TC frequency projections before greater confidence in future European PTC risk can be achieved. This should involve further work on our theoretical understanding of what drives TC genesis, and further quantification of the uncertainty associated with different TC identification methods (e.g., Bourdin et al. 2022).

Model biases, particularly in the MDR, are likely to manifest in the future projections. Furthermore, TC LMI, which is not adequately captured by these models, has been shown to be associated with the likelihood of recurvature (Sainsbury et al. 2022a) and the likelihood that a recurving TC will reach Europe (Sainsbury et al. 2022b). The model deficiencies in TC intensity may therefore be contributing to the low bias in likelihood of recurvature across many of the models during the historical period. Additionally, there is a mismatch between climate model projections and observations of the zonal temperature gradient in the tropical Pacific, which has implications for North Atlantic vertical wind shear (Seager et al. 2019) and may therefore be important for TC genesis and for the projected change in the likelihood of recurvature of North Atlantic TCs. Additionally, CMIP6 models still contain biases in the representation of the North Atlantic storm track; likely related to biases in the location, intensity and variability of the North Atlantic jet (Harvey et al. 2020). Therefore, CMIP6 models must be used cautiously when investigating projected changes to TC recurvature or Europe PTC impacts in the future. Previous studies suggest that TCs will be more intense in the future (Knutson et al. 2010, 2019; Bhatia et al. 2018; Bender et al. 2010; Emanuel 2021a; Walsh et al. 2019), implying greater longevity and a greater probability of reaching Europe (Sainsbury et al. 2022b). Multi-model studies using high-resolution climate models, which are capable of better simulating the distribution of TC intensities, are therefore necessary to fully explore the projected changes in Europe-impacting PTCs.

6.5. Appendix

By splitting the North Atlantic basin into different spatial regions, the fraction of recurving North Atlantic TCs in the historical, H, and future, S, periods can be defined as:

$$F^H = \sum_i W_i^H F_i^H \ , \ F^S = \sum_i W_i^S F_i^S, \quad (6.4)$$

where i = MDR, SUB and WEST, W_i is the proportion of North Atlantic TCs forming in region i, and F_i represents the fraction of TCs forming in region i which recurve. The absolute change in the fraction of recurving TCs, $\Delta F = F^S - F^H$, can then be expressed as

$$\Delta F = \sum_i (W_i^S F_i^S - W_i^H F_i^H). \quad (6.5)$$

Replacing W_i^S with $W_i^H + \Delta W_i$ and F_i^S with $F_i^H + \Delta F_i$, rearranging and cancelling common terms allows ΔF to be expressed as three separate terms

$$\Delta F = \sum_i W_i^H \Delta F_i + \sum_i F_i^H \Delta W_i + \sum_i \Delta W_i \Delta F_i. \quad (6.6)$$

The relative contribution of each term can be investigated by dividing the right-hand side by ΔF, as shown in Table 6.3:

$$\sum_i \frac{W_i^H \Delta F_i}{\Delta F} + \sum_i \frac{F_i^H \Delta W_i}{\Delta F} + \sum_i \frac{\Delta W_i \Delta F_i}{\Delta F} = 1. \quad (6.7)$$

Acknowledgements

The authors thank Michiel Baatsen and an anonymous reviewer for their comments which greatly improved the clarity of this manuscript. E. Sainsbury was funded by the Natural Environment Research Council (NERC) via the SCENARIO Doctoral Training Partnership (Grant NE/S0077261/1) with additional CASE funding from BP. R.S., K.H., A.B., and L.S. are supported by the U. K. National Centre for Atmospheric Science (NCAS) at the University of Reading. A.B. acknowledges funding from the PRIMAVERA project received from the European Commission (Grant 641727 of the Horizon 2020 research program), and NERC funding through the North Atlantic Climate System Integrated Study (ACSIS) grant (NE/N018044/1). We thank Olivier Boucher and Thibaut Lurton (IPSL) for re-running the IPSL-CM6A-LR model to provide us the SSP5-85 scenario data needed to include the model in this study. The IPSL-CM6 experiments were performed using the HPC resources of TGCC under the allocation of 2021-A0100107732 (project gencmip6), provided by GENCI (Grand Equipment National de Calcul Intensif). This work benefited from French state aid, managed by the ANR under the “Investissements d’avenir” programme (reference ANR-11-IDEX-0004-17-EURE-

0006). S.B. is supported by public funding from the CEA and the EUR IPSL-Climate. L.S. and R.S. acknowledge funding from the NERC CANARI project (NE/W004984/1).

Data and Code Availability

HURDAT2 data can be downloaded from the NOAA's Hurricane Research Division

(https://www.aoml.noaa.gov/hrd/hurdat/). ERA5 data can be obtained from the Copernicus C3S Date store

(https://www.ecmwf.int/en/forecasts/datasets/reanalysis-datasets/era5). CMIP6 data can be obtained from the Earth System

Grid Federation (https://esgf.llnl.gov/). Potential Intensity is calculated using the tcPyPI Python package (Gilford 2021), available at https://github.com/dgilford/tcpyPI. TRACK can be downloaded from https://gitlab.act.reading.ac.uk/track/track, and version 1.5.2 is used for this study.

6.6. Supporting Information

6.6.1. CMIP6 Model Selection

The CMIP6 models used in the main manuscript were chosen from a large sample of CMIP6 models, based on their ability to simulate TCs in the North Atlantic. Figure 6.11 shows boxplots for North Atlantic TC frequency (hurricane season only), averaged over the entire historical run, for all the considered models. The green lines show the median, the box contains the interquartile range, and the maxima and minima are shown by the bars above and below the boxes. Between 1950 and 2014 (HURDAT2), there are approximately 12 TCs per year in the North Atlantic which have winds more than 17 m s^{-1}, and 6.4 hurricanes per year (winds > 33 m s^{-1}). These are labelled 'Ob_ts' and 'Obs_hurr' in Figure 6.11 respectively.

Based on Figure 6.11, we select all CMIP6 models which have a median annual North Atlantic TC frequency greater than the average number of hurricanes per year (6.4) in observations. Boxplots are coloured blue if SSP5-85 scenario data is also available, and

white if not. Of the 8 models which have a median TC frequency greater than 6.4 TCs per year, 5 of these models also have the high-frequency relative vorticity fields needed for tracking for the SSP5-85 scenario. These models are therefore retained for further analysis.

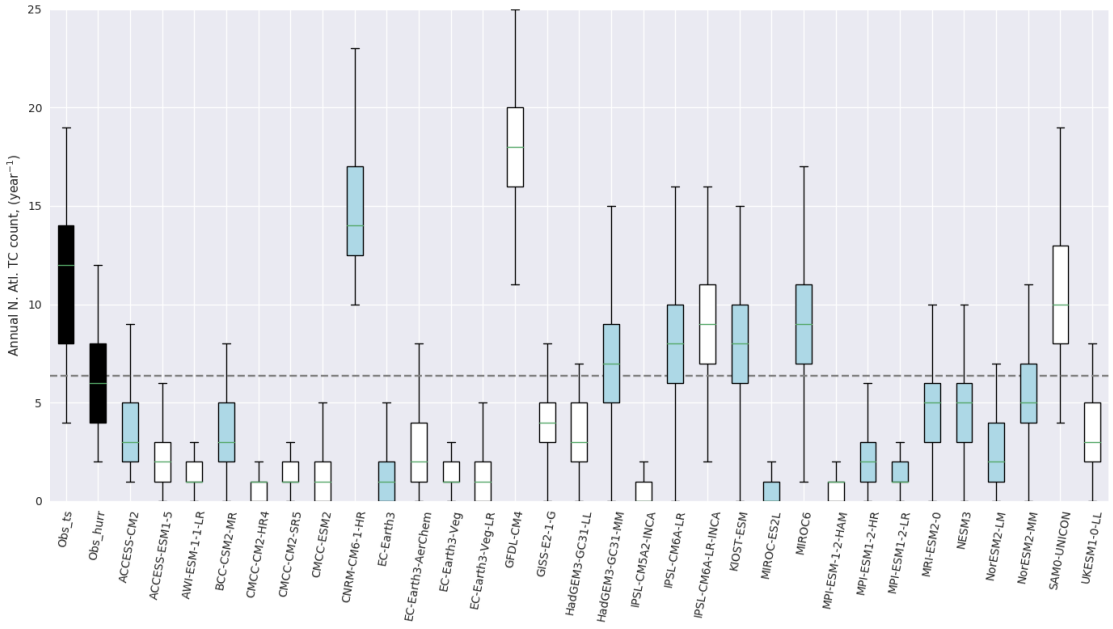

Figure 6.11. Boxplot showing the North Atlantic TC frequency (June 1st – Nov 30th), averaged over the entire historical run, for a selection of CMIP6 models and HURDAT2 (first two boxes, black). 'Obs_ts' represents all cyclones present in HURDAT2 with winds >= 17 m s^{-1}. 'Obs_hurr' represents all hurricanes (winds >= 33 m s^{-1}) present in HURDAT2. Grey horizontal line represents the threshold of 6.4 TCs per year used to select models for further analysis, which is the average number of hurricanes per year in HURDAT2 between 1950 and 2014. Blue boxes represent models which have sufficient data available for the SSP5-85 scenario to perform cyclone tracking and TC identification, and boxes which are not filled blue do not have sufficient SSP5-85 data available, and so cannot be considered in this study.

6.6.2. TC Identification Method

Objective TC identification methods such as used in Hodges et al. (2017) identify cyclone tracks as TCs if (among other things) they have a coherent vertical structure and a warm core, diagnosed using the vertical profile of relative vorticity. To achieve a balance between hit rate and false alarm rate, a latitude constraint is imposed such that the TC must have a genesis location equatorward of 30°N. In the present climate, this is quite suitable as most TCs forming in the North Atlantic basin form equatorward of 30°N (though there are notable exceptions, such as Ophelia in 2017). However,

climate change may extend the genesis region of TCs further polewards and eastwards (e.g., Haarsma et al. 2013), and so a 30°N threshold may lead to many future TCs being misidentified as non-tropical by virtue of where they form.

Figure 6.12 shows the genesis density for the 5 CMIP6 models in the historical (1984-2014) and future (2069-99) periods, along with the differences (future-historical). Here we identify the TCs using criteria in section 6.2.3, however the genesis constraint has been relaxed to 45°N, to investigate whether there is any model consensus for increased genesis of TC-like features between 30 and 45°N. Figure 6.12 shows no robust increase in TC genesis between 30 and 45°N, though there is some increase in the MIROC along the US East Coast. We therefore use a 30°N constraint throughout the main manuscript with confidence that we are not missing a large trend in subtropical TC genesis poleward of 30°N.

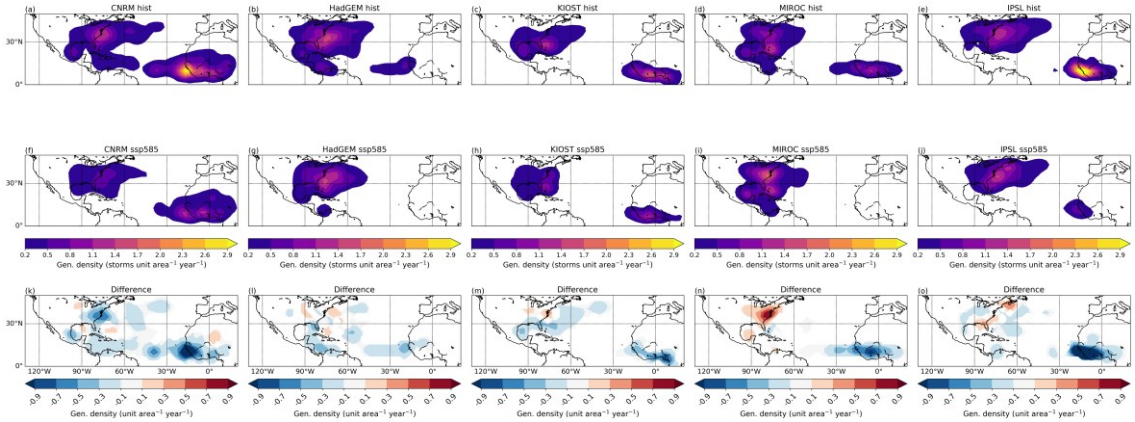

Figure 6.12. Genesis density for the historical (1984-2014, a-e) and future (2069-99, f-j) periods for the five selected CMIP6 models along with the differences (future-historical, k-o). TCs are identified using the criteria described in section 6.2.3, but the latitude constraint has been relaxed to 45˚N.

6.6.3. Historical Lysis Density

Figures 6.2 and 6.4 in the main manuscript indicate that the TCs forming in the Main Development Region in the IPSL model are weak, short-lived TCs. To investigate this further, a spatial map of the lysis density is created for the 5 models and ERA5, shown in Figure 6.13. There is a large region of non-zero lysis densities in the tropics, subtropics and midlatitudes in all the models and ERA5, highlighting the vast region in which TCs travel and dissipate. Many models (and ERA5) have their highest (or joint highest) lysis density values in the subtropics and midlatitudes. However, the IPSL is very different from the other models. In the IPSL, the highest lysis density values occur

in the MDR, very close to where the storms form. These TCs form on the west coast of Africa (Fig. 6.1), indicating that the storms are dissipating with little opportunity to move from their place of origin. This further indicates the severe bias in the MDR of the IPSL.

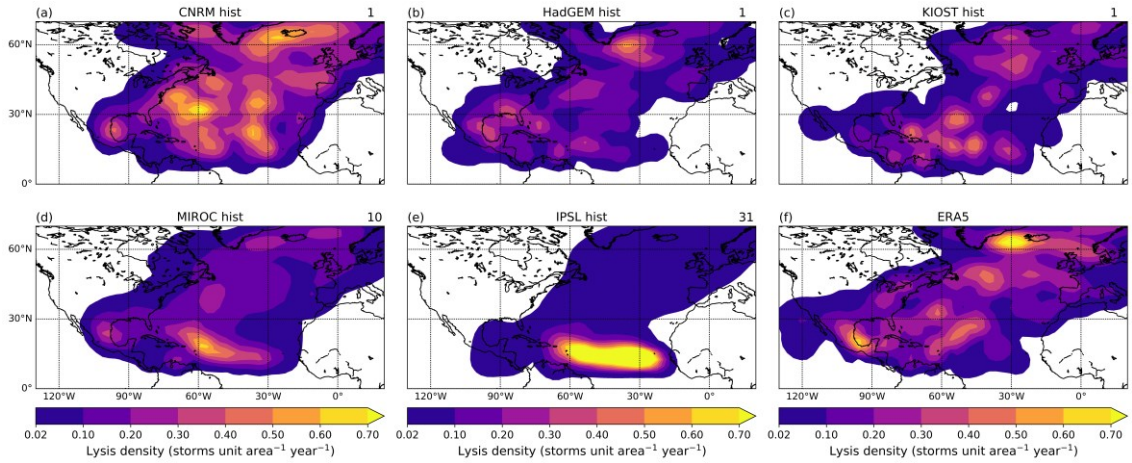

Figure 6.13. Lysis density (storms per unit area per year, where the unit area is equal to a spherical cap with a 5-degree radius) for the 1984-2015 period from the historical runs of 5 CMIP6 models (a-e) and ERA5 (f). All ensemble members are used where available. Densities less than 0.02 have been masked for clarity.

6.6.4. Historical GPI Bias

Figure 6.14 shows the bias in GPI (and individual terms) for the fully historical coupled runs from 1984-2014. Biases are calculated relative to ERA5. All models except CNRM have a negative GPI bias or no GPI bias (top row) in the Main Development Region. All models except the CNRM have too much wind shear in the western MDR, increasing hostility (row 5).

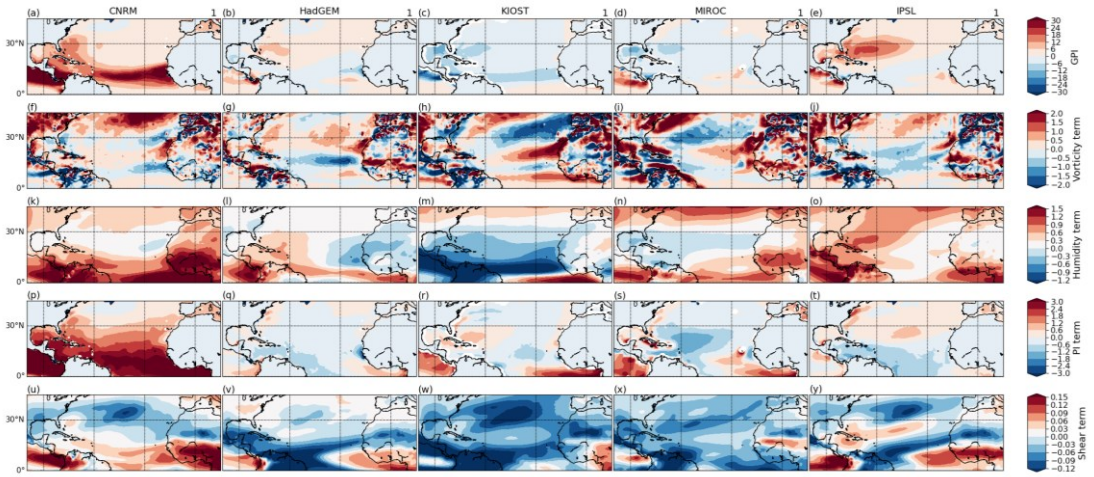

Figure 6.14. Bias (model minus ERA5) in GPI (top row) and the terms comprising GPI (rows 2-5). Data from 1984-2014 is used for ERA5 and the fully-coupled historical runs. Note that a positive bias in the shear terms means a low-bias in wind shear.

6.6.5. Wind-Pressure Relationship

The wind-pressure relationships for the warm-core part of the tracks (i.e., the part of the track at which the criteria in section 6.2.3 are satisfied) over the historical period is compared with ERA5 and HURDAT2 in Figure 6.15. The relationship between wind and pressure in TCs is well-established, and using one point for each TC, or all points for each TC, should not change the results. ERA5 and all of the CMIP6 models have a slope which is too steep, where cyclones do not reach the expected (from HURDAT2 observations) wind speeds for a given sea level pressure. The apparent intensity of the TCs is greater in terms of their sea level pressure than in terms of their maximum winds. This result has also been found in other reanalyses in previous studies (Hodges et al. 2017). This difference is smallest for CNRM, which simulates stronger TCs than the other 4 models. Despite this, in all 5 models (and ERA5), there is a clear relationship between wind and pressure in the tropical stage of the identified TCs, a feature present in observed TCs.

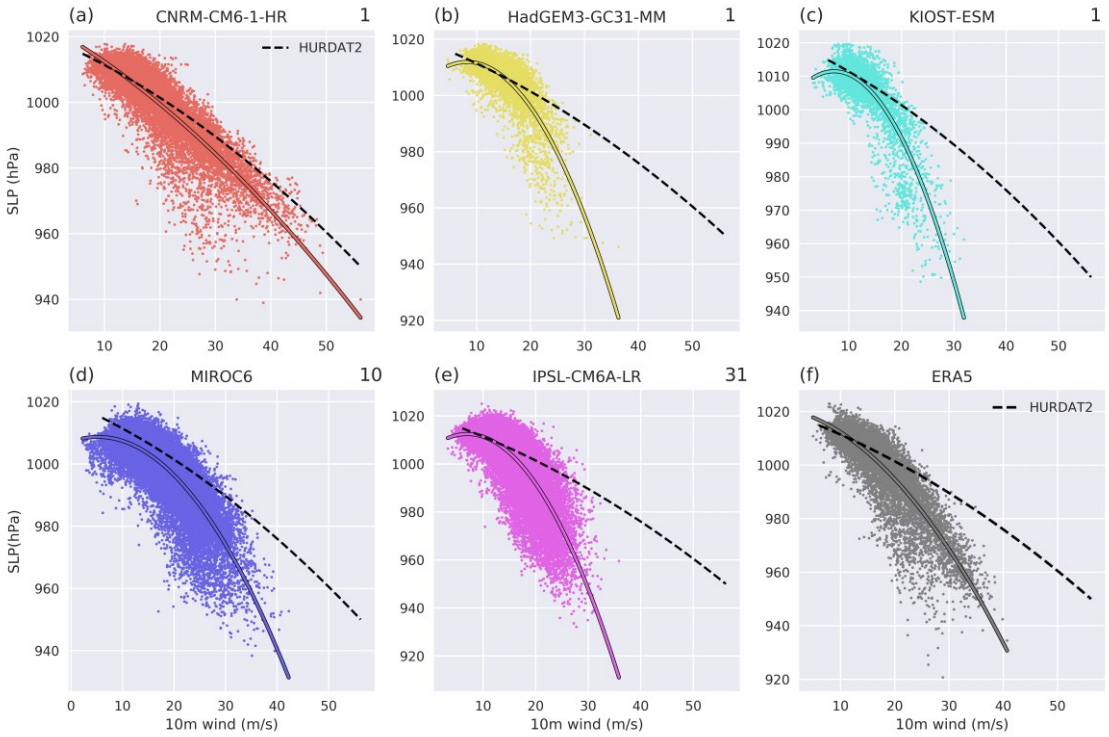

Figure 6.15. Wind-pressure relationship for the TCs (during their TC phase) for selected CMIP6 models (a-e) and ERA5 (grey, f). Coloured lines on each panel show a quadratic polynomial fit for each CMIP6 model and ERA5, dashed black line shows the quadratic polynomial fit for HURDAT2. The number of ensemble members used for each model is shown to the upper-right of each panel.

6.6.6. Relationship between TC Frequency and Recurving TC Frequency

To reach Europe as a PTC, a TC must first interact with the midlatitudes (i.e., enter the 'recurvature' domain shown in Figure 6.1). Previous work has shown that there is a strong relationship between TC activity and recurving TC activity (Sainsbury et al. 2022a). It is therefore important that CMIP6 models can capture this relationship, as it may have implications for the frequency of Europe-impacting PTCs. The ability of the selected CMIP6 models to capture this relationship is explored in Figure 6.16. In ERA5 (TCs identified using track matching with HURDAT2), there is a significant relationship between TC frequency and recurving TC frequency (top left panel, r=0.85). A strong relationship is also found in the CMIP6 models (correlations 0.61-0.76), which are statistically significant in all cases to the 95% level. CNRM, HadGEM and KIOST all have a slope like ERA5, whereas the IPSL and MIROC have a slope that is too shallow, indicating that too few TCs recurve in these two models.

Overall, all five CMIP6 models capture the relationship between TC frequency and recurving TC frequency despite TC intensity biases, indicating that the models can capture the main driver of the interannual variability of recurving TC frequency, which may have important implications for European PTC risk.

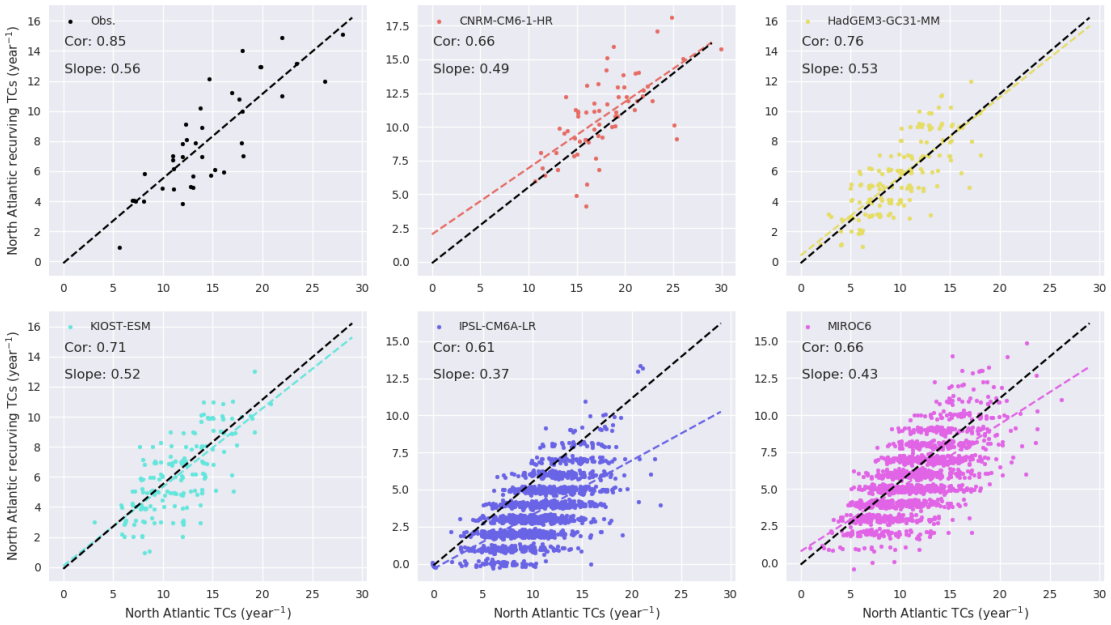

Figure 6.16. Relationship between TC frequency and recurving TC frequency in ERA5 (top left) and the five selected CMIP6 models. For ERA5, data from 1979-2018 is used. For the other models, all data from the fully-coupled historical runs are used (1950-2014 for CNRM, IPSL, 1850-2014 for HadGEM, KIOST, and MIROC). Random noise has been added to the data points so that all points can be seen, but the correlations and slopes are identified using the original data.

6.6.7. Figure 6.5 Cyclone Counts

Table 6.4 shows the PTC and MLC counts for each intensity bin in Figure 6.5. Note that these counts refer to the thole European domain (blue bars in Fig. 6.5).

% ile	CNRM		HadGEM		KIOST		MIROC		IPSL	
bins	PTC	MLC	PTC	MLC	PTC	MLC	PTC	MLC	PTC	MLC
0-20	3	872	2	978	1	885	5	8816	14	27717
20-40	5	870	1	978	5	881	18	8802	29	27701
40-60	11	864	3	977	3	883	19	8801	47	27683
60-80	20	855	3	976	4	882	51	8769	123	27607
80-90	12	425	5	485	6	437	69	4341	94	13771
90-95	7	212	2	243	9	213	58	2147	87	6845
95+	15	204	9	236	13	209	87	2119	136	6798

Table 6.4. Counts for the hurricane-season-forming, Europe-impacting PTCs and MLCs shown in Figure 6.5 (blue bars).

6.6.8. European-Impacting PTC Statistics: Consistent Ensemble Members, Ensemble Spread, and Additional CMIP6 Models

6.6.8.1. Consistent Ensemble Members

Finite computational resources force a compromise to be made between model resolution and length of simulation/number of ensemble members. In this work, we are using relatively coarse resolution models. This limitation is compensated by the large number of ensemble members available for some of the models, particularly during the historical period for the MIROC (10) and IPSL (31). However, data is not available for this many ensemble members in the future runs under the SSP5-85 scenario.

To ensure that the projected changes shown in the paper are not the result of different ensemble members being considered in the historical and future periods, we repeat the analysis, this time just considering the common ensemble members over the historical and future period. This is shown in Figure 6.17. CNRM, HadGEM and KIOST only have one ensemble member for the historical and future period and so see no change. However, for MIROC we only consider the first three ensemble members for the historical period (ensuring that a direct comparison can be drawn with the three ensemble members available for the future period). For IPSL, we only use the first ensemble member for the historical period, as this is the only ensemble member which is available for the future period under the SSP5-85 scenario.

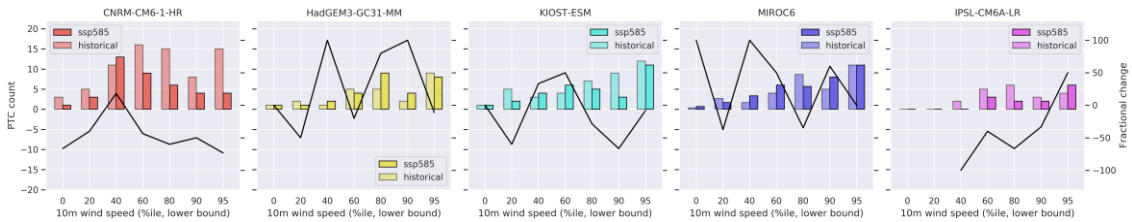

Figure 6.17. As in Figure 6.9, but only considering common ensemble members over the historical and future periods.

There are no changes to the data (and hence results) for the CNRM, HadGEM and KIOST. When just using common ensemble members, the projected change in the number of European-impacting PTCs in the highest intensity bin is smaller (fractional change down from +20% to +5%) in the MIROC and has increased for the IPSL (fractional change up to +50% from +40%). These changes are relatively small and do not alter the key result, which is that there is no robust model response in terms of European-impacting PTC intensity changes.

Table 6.5 shows the repeated analysis for Table 6.1, again only considering the common ensemble members. The results are largely unchanged. All fractional changes which were shown to be significant in Table 6.1 (except the increase in European-impacting PTC counts in the MIROC) are still significant when only considering common ensemble members, and therefore the robust responses seen in the models (reduction in North Atlantic TC count, increase in likelihood of recurvature) are not the result of differing ensemble sizes in the historical and future periods.

	N_{TC}			F_{Rec}			$F_{Eur\|Rec}$			N_{Eur}		
	Hist	SSP	Diff	Hist	SSP	Diff	Hist	SSP	Diff	Hist	SSP	Diff
CNRM	14.68	9.00	**-39%**	2.35	1.29	**-45%**	0.55	0.59	7%	0.29	0.24	-17%
HadGEM	7.29	4.35	**-40%**	0.81	0.94	16%	0.46	0.61	**31%**	0.24	0.35	**49%**
KIOST	7.97	5.19	**-35%**	1.32	1.03	-22%	0.41	0.40	-4%	0.40	0.50	24%
MIROC	8.37	5.53	**-34%**	1.08	1.17	8%	0.43	0.68	**58%**	0.30	0.31	3%
IPSL	8.84	3.16	**-64%**	0.65	0.42	-35%	0.20	0.42	**110%**	0.36	0.32	-11%

Table 6.5. As in Table 6.1, but only considering common ensemble members between the historical and future periods.

While there are some differences between results produced using all ensemble members and common ensemble members, they do not differ significantly, and they do not change the results of the paper.

6.6.8.2. Ensemble Spread

The analysis of section 6.8.8.1 shows that they key results of chapter 6 are not sensitive to whether or not common ensemble members are used between the historical and future periods. This subsection investigates the ensemble spread in the cyclone statistics from Table 6.1 in the two models for which multiple ensemble members are available, MIROC and IPSL.

Table 6.6 shows the cyclone statistics from Table 6.1, along with the proportion of TCs reaching Europe as PTCs (=$F_{Rec}F_{Eur|Rec}$) for the MIROC and IPSL. Instead of combining all ensemble members before the calculation of the statistics, here the statistics are calculated for each ensemble member individually and the minimum and maximum ensemble members are shown for each of the statistics.

While there is a large spread amongst ensemble members for MIROC and IPSL for both time periods, the ensemble spread is considerably smaller than the projected change in North Atlantic TC frequency (N_{TC}), the fraction of recurving TCs (F_{Rec}) and the fraction of North Atlantic TCs reaching Europe ($F_{Rec}F_{Eur|Rec}$).

	MIROC (10, 3)		IPSL (31, 1)	
	Hist	SSP	Hist	SSP
N_{TC}	(7.26, 8.29)	(5.23, 6.0)	(7.42, 8.84)	3.16
F_{Rec}	(0.37, 0.49)	(0.66, 0.71)	(0.16, 0.23)	0.42
$F_{Eur\|Rec}$	(0.23, 0.36)	(0.31, 0.32)	(0.18, 0.44)	0.32
N_{Eur}	(0.74, 1.29)	(1.06, 1.23)	(0.26, 0.65)	0.42
$F_{Rec}F_{Eur\|Rec}$	(0.09, 0.16)	(0.20, 0.23)	(0.03, 0.08)	0.13

Table 6.6. Values of the ensemble minimum and maximum (min, max) North Atlantic TC frequency (row 2), fraction of recurving TCs (row 3), fraction of recurving TCs reaching Europe (row 4), Europe-impacting PTC frequency (row 5) and fraction of North Atlantic TCs reaching Europe (row 6) for MIROC (columns 2, 3) and IPSL (columns 4, 5) in the historical and future simulations. The number of available ensemble members in MIROC and IPSL is given in brackets in row 1.

6.6.8.3. Additional CMIP6 Models

This subsection investigates the cyclone statistics shown in Table 6.1, along with the projected change in the fraction of North Atlantic TCs reaching Europe as PTCs, in 10 additional CMIP6 ScenarioMIP models for which sufficient data is available for cyclone tracking and TC identification. These additional models were not selected for use in the main manuscript as they do not simulate North Atlantic TC frequency reasonably compared to observations and reanalyses but are briefly investigated here with the aim of identifying any robust projected changes. TCs in the additional 10 CMIP6 models are identified using the same tracking and TC identification method. The same time periods (1984-2014, 2069-99) and future scenario (SSP5-85) are also used. The additional 10 CMIP6 models are shown in Figure 6.11 (blue shading).

The results of Table 6.7 are consistent with the results presented for the five selected models (Table 6.1). 9 of the 10 additional CMIP6 models project a significant decrease in North Atlantic TC frequency. All 10 models have a projected increase in the fraction of recurving TCs, significant in 4 models. The proportion of North Atlantic TCs reaching Europe as PTCs (Table 6.8) is projected to increase in 7 of the 10 additional models, significantly in 4. EC-Earth3 is a significant outlier compared to the wider model ensemble. In this model, North Atlantic TC frequency and the fraction of recurving TCs are both projected to increase, leading to a significant increase in projected Europe-impacting PTC frequency.

This additional analysis highlights the robust projected decrease in North Atlantic TC frequency, which is offset to some extent by an increase in the likelihood that a TC will reach Europe in CMIP6 models.

	N_{TC}			F_{Rec}			$F_{Eur\|Rec}$			N_{Eur}		
	Hist	SSP	Diff	Hist	SSP	Diff	Hist	SSP	Diff	Hist	SSP	Diff
ACCESS-CM2	104	49	**-53%**	0.41	0.71	**73%**	0.35	0.43	23%	15	15	0%
BCC-CSM2-MR	109	60	**-45%**	0.53	0.57	6%	0.34	0.29	-15%	20	10	**-50%**
EC-Earth3	45	65	**47%**	0.44	0.62	**41%**	0.32	0.37	14%	6.3	14.9	**133%**
MIROC-ES2L	16	4	**-73%**	0.31	0.75	139%	0.31	0	-100%	1.5	0	-100%
MPI-ESM1-2-HR	61	33	**-47%**	0.25	0.34	33%	0.30	0.32	7%	4.6	3.5	-25%
MPI-ESM1-2-LR	48	27	**-44%**	0.33	0.37	13%	0.34	0.34	-1%	5.4	3.4	**-40%**
MRI-ESM2-0	153	45	**-70%**	0.49	0.73	**51%**	0.30	0.39	30%	22.4	13	**-41%**
NESM3	146	74	**-49%**	0.46	0.69	**50%**	0.28	0.35	25%	19	18	-5%
NorESM2-LM	77	58	**-25%**	0.52	0.59	14%	0.40	0.44	9%	16	15	-6%
NorESM2-MM	169	73	**-57%**	0.49	0.52	7%	0.41	0.32	-24%	34	12	**-64%**

Table 6.7. As in Table 6.1, but for 10 additional (and poorer-performing with respect to North Atlantic TC frequency) CMIP6 ScenarioMIP models.

	Proportion of TCs reaching Europe (= $F_{Rec}F_{Eur|Rec}$)		
	Hist	SSP	Diff
ACCESS-CM2	0.14	0.31	**122%**
BCC-CSM2-MR	0.18	0.17	-9%
EC-Earth3	0.14	0.23	**61%**
MIROC-ES2L	0.10	0.0	-100%
MPI-ESM1-2-HR	0.08	0.11	42%
MPI-ESM1-2-LR	0.11	0.13	12%
MRI-ESM2-0	0.15	0.29	**97%**
NESM3	0.13	0.24	**87%**
NorESM2-LM	0.21	0.26	24%
NorESM2-MM	0.20	0.16	-18%

Table 6.8. Proportion of North Atlantic TCs reaching Europe in the historical (1984-2014) and future (2069-99) period under the SSP5-85 scenario (columns 2 and 3 respectively). Fractional change is shown in column 4. Bolded differences represent statistical significance at the 95% level using a bootstrap resampling method.

6.6.9. Normalized Genesis Density Changes

Figure 6.18 shows the change in the normalized genesis density in the five CMIP6 models. There is a robust model response for a shift in genesis (proportionally) away from the MDR towards the WEST and SUB regions. This difference is largest in the HadGEM, MIROC and IPSL - the three models in which there is the largest increase in the likelihood of recurvature - and is consistent with the results of Table 6.2.

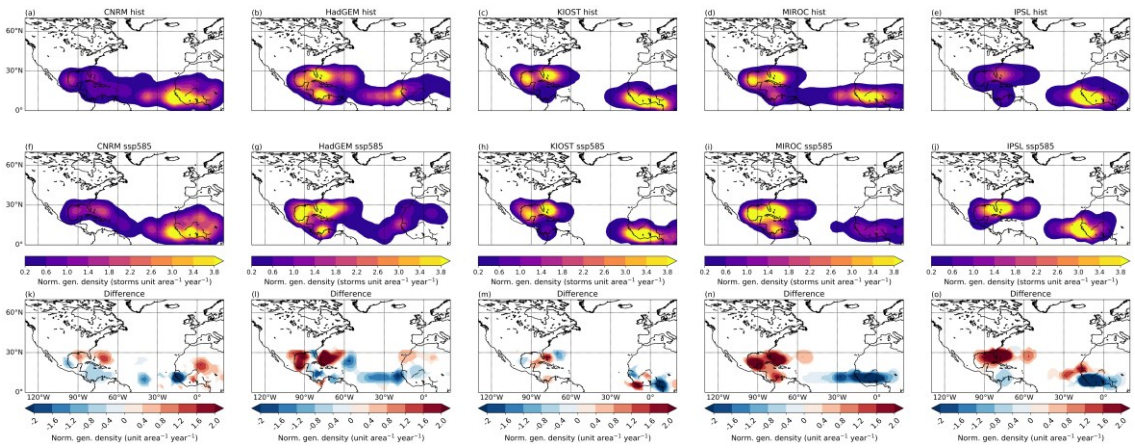

Figure 6.18. Normalized genesis density for the 5 selected CMIP6 models during the historical (top) period, towards the end of the century under SSP5-85 (middle), and the difference (future minus historical, bottom). Densities less than 0.2 have been masked for clarity.

6.6.10. TC LMI Changes

While shifts in genesis explain most of the projected change in F_{Rec} in HadGEM, MIROC and IPSL, they do not explain all of the projected increase. To further investigate the projected changes in F_{Rec}, the relationship between projected TC LMI changes and projected F_{Rec} changes is explored. Figure 6.19 shows the change in TC LMI for the 5 selected models, for each of the three regions in equation 6.3 and Table 6.2, along with a scatterplot of TC LMI changes against recurvature likelihood changes within the regions.

In the MDR, there is a large increase in the proportion of North Atlantic TCs which are strong (TC LMI > mean of the combined (historical + future) North Atlantic TC distribution) in MIROC. In the WEST region, this is also true for HadGEM, MIROC and IPSL. These are also the only four models/regions in our selection of CMIP6 models where there is a statistically significant increase in the likelihood of recurvature (Table 6.2). Figure 6.19d shows a strong relationship between TC LMI changes and changes in recurvature likelihood within regions. It is therefore possible that changes in TC LMI – particularly in the WEST regions of MIROC, HadGEM and IPSL, and MDR of MIROC – are associated with the projected increase in F_{Rec}. For Fig. 6.19d, the Pearson's correlation coefficient is 0.52 and is significant at the 95% level. However, it should be noted that this is only a correlation over 15 data points. It is not completely clear from the GPI (Fig. 6.6) why the TC LMI is seen to increase in the WEST regions in HadGEM and IPSL, and the MDR and WEST regions in MIROC.

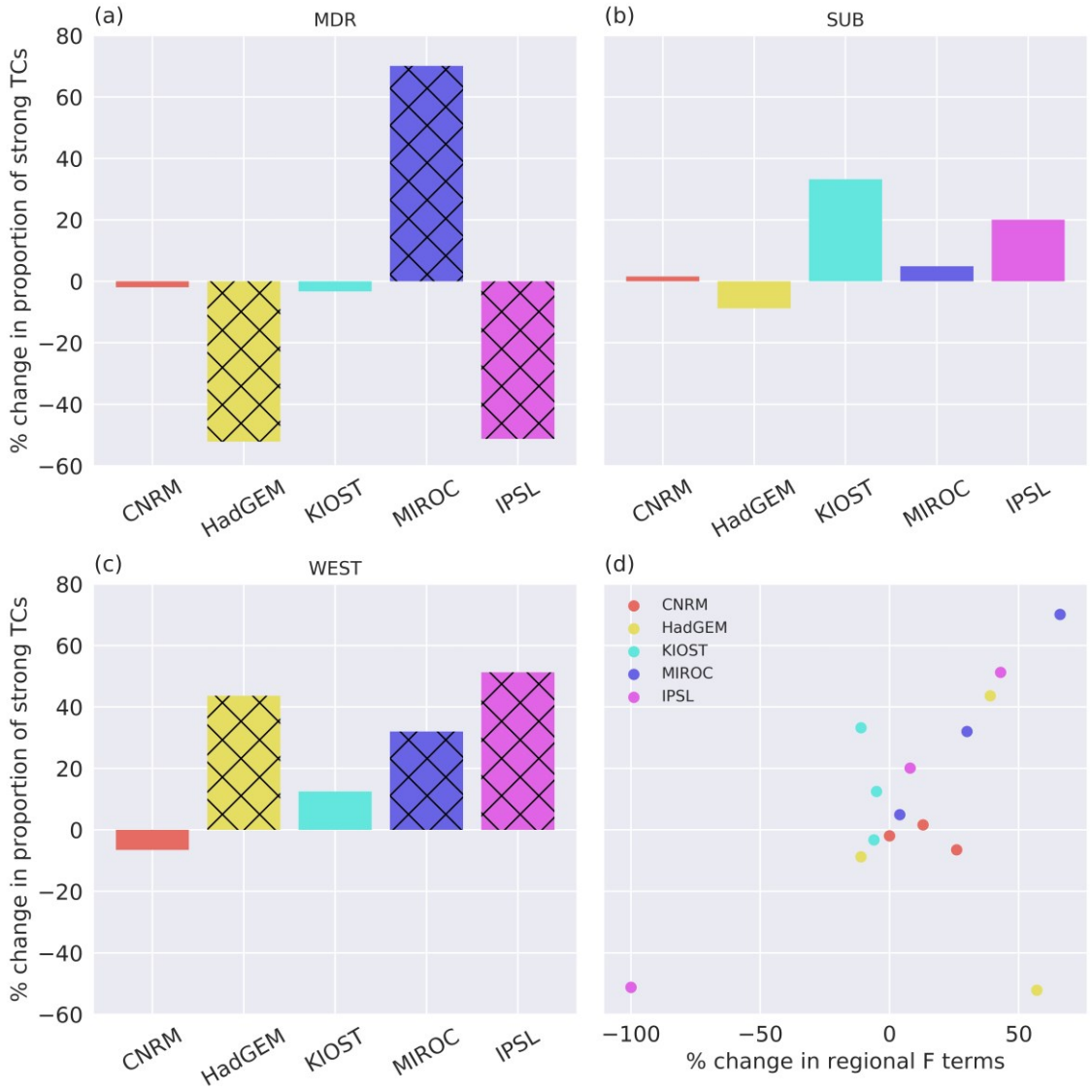

Figure 6.19. Bar charts showing the percentage change in the proportion of strong North Atlantic TCs (TCs which have a TC LMI greater than the mean of the combined (historical + future) distribution) in the MDR (a), SUB (b) and WEST (c) regions. (d) shows a scatterplot of the percentage change in the proportion of strong North Atlantic TCs against the percentage change in the F terms within the individual regions (columns 3, 5, and 7 of the bottom of Table 6.2). Hatching represents the models and regions in which the % change is significant to 95% using a bootstrapping method.

6.6.11. Comparison with Haarsma et al. (2013)

The only previous studies which investigate projected changes in Europe-impacting PTCs find a large increase in the number of high-intensity PTCs in the future (Haarsma et al. 2013, hereafter H13; Baatsen et al. 2015). None of the CMIP6 models investigated in this study show an increase as large as found in these previous studies

(driven by a very large decrease in TC counts basin-wide). However, the results presented in section 6.3.2. do not use the same methodology as used in H13.

To make our work as comparable as possible to H13, the analysis of Figures 6.9 and 6.10 are repeated with some methodological changes. As in H13, we only consider cyclones which impact Europe (Fig. 6.20) or form (Figs 6.21, 6.22) during August, September, and October. We also change the domain of interest to look at the same four regions which were used in H13: Norway (60-70°N, 0-15°E), North Sea (50-60°N, 3°W-8°E), Western UK and Ireland (50-60°N, 3-15°W) and the Gulf of Biscay (43-50°N, 0-15°W).

Due to the lower resolution of the CMIP6 models than used in H13, we cannot use the same intensity threshold of hurricane force (>33 m s^{-1}) winds. We instead just consider cyclones impacting each of the four regions in ASO which have maximum winds in the region greater than the 90th percentile of the combined (PTC+MLC, historical + future) distribution of cyclone maximum winds in the region. This gives us a similar PTC frequency as in H13 (Fig 2f therein).

Figure 6.20 shows mixed changes in the number of strong PTCs impacting each region in the future, though more regions and models project decreases than increases. Sample sizes are extremely small, as the Europe sub-regions are considerably smaller than the European domain used in the main manuscript. The result of Figure 6.20 is different from the result of H13, in which there was a substantial increase in strong PTCs in the future across three of these four regions. However, when considering the fraction of North Atlantic TCs forming in ASO which impact each of these regions (Figure 6.21 for all PTCs, Figure 6.22 for strong PTCs (> 90th percentile)), there's a general increase, in line with Figure 6.10 from the main manuscript. This suggests that in the future, North Atlantic TCs are more likely to reach these four regions of Europe, and future risk to these regions depends strongly on the projected change in basin-wide TC counts.

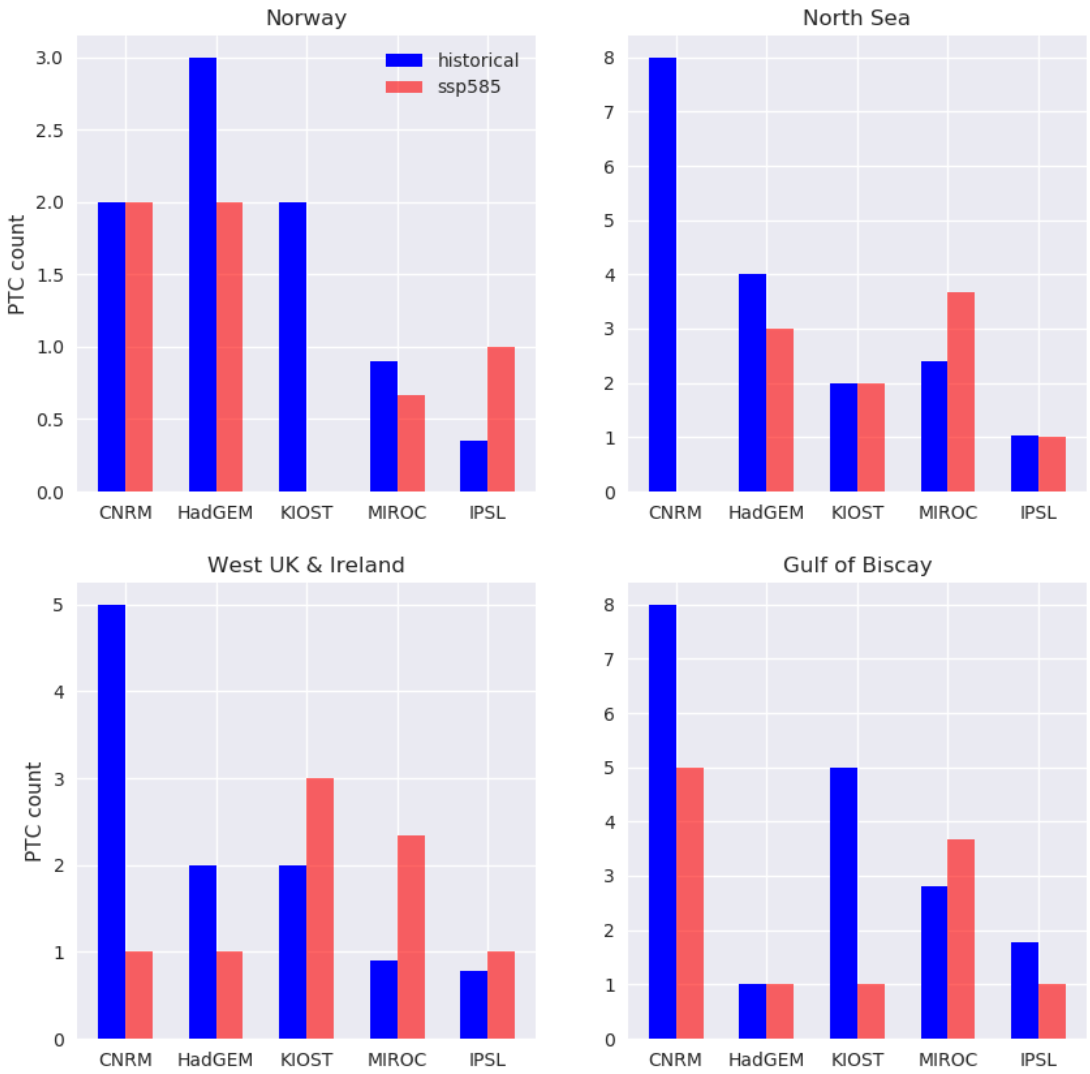

Figure 6.20. Number of strong PTCs (max wind in region > 90th percentile of combined distribution) impacting each of the four regions during Aug-Oct in the historical period (blue) and future period under the SSP5-85 scenario (red).

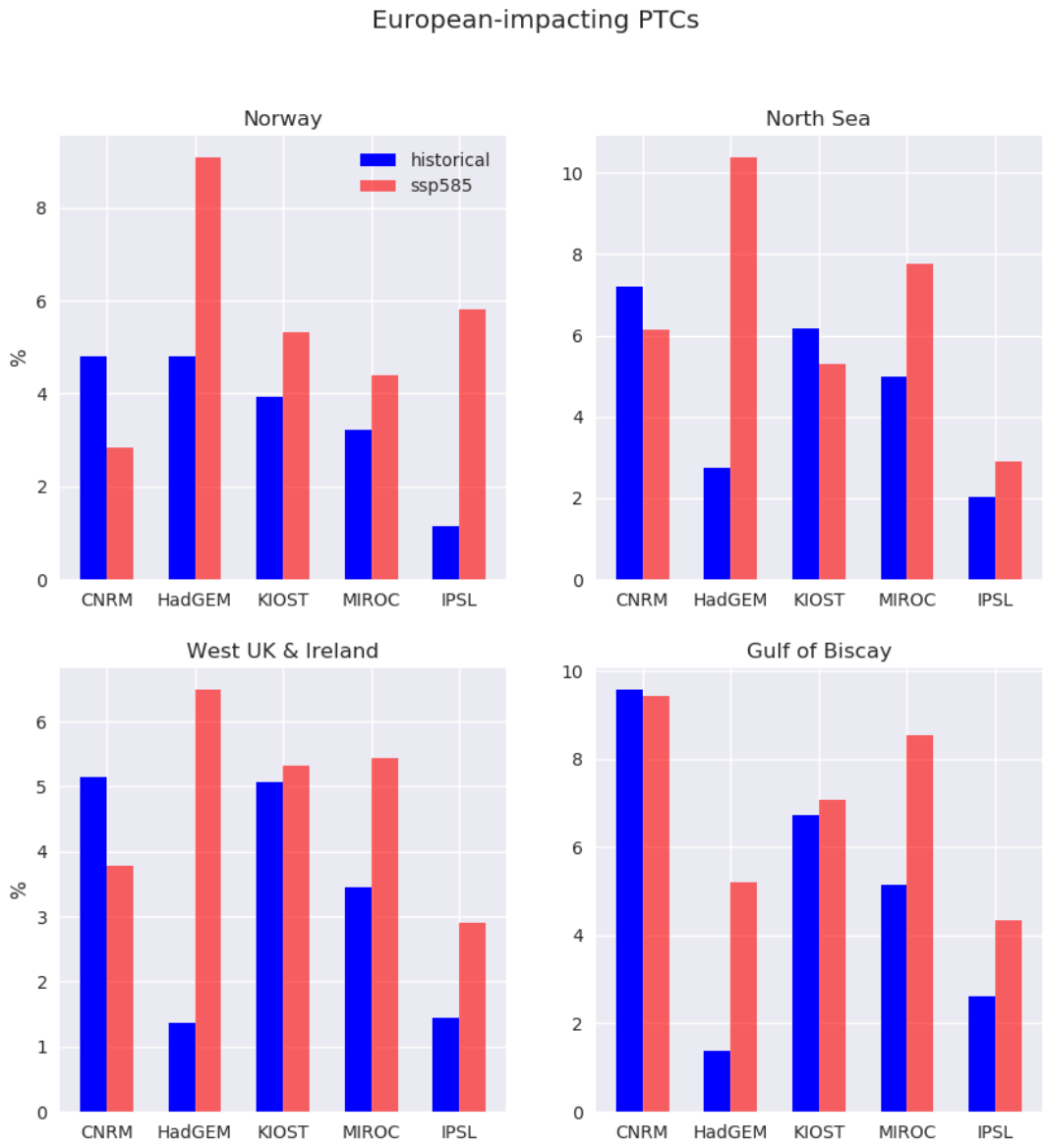

Figure 6.21. Fraction of North Atlantic TCs which impact the given four regions as PTCs, considering all North Atlantic TCs forming during August-October in the historical period (blue) and future period under the SSP5-85 scenario (red).

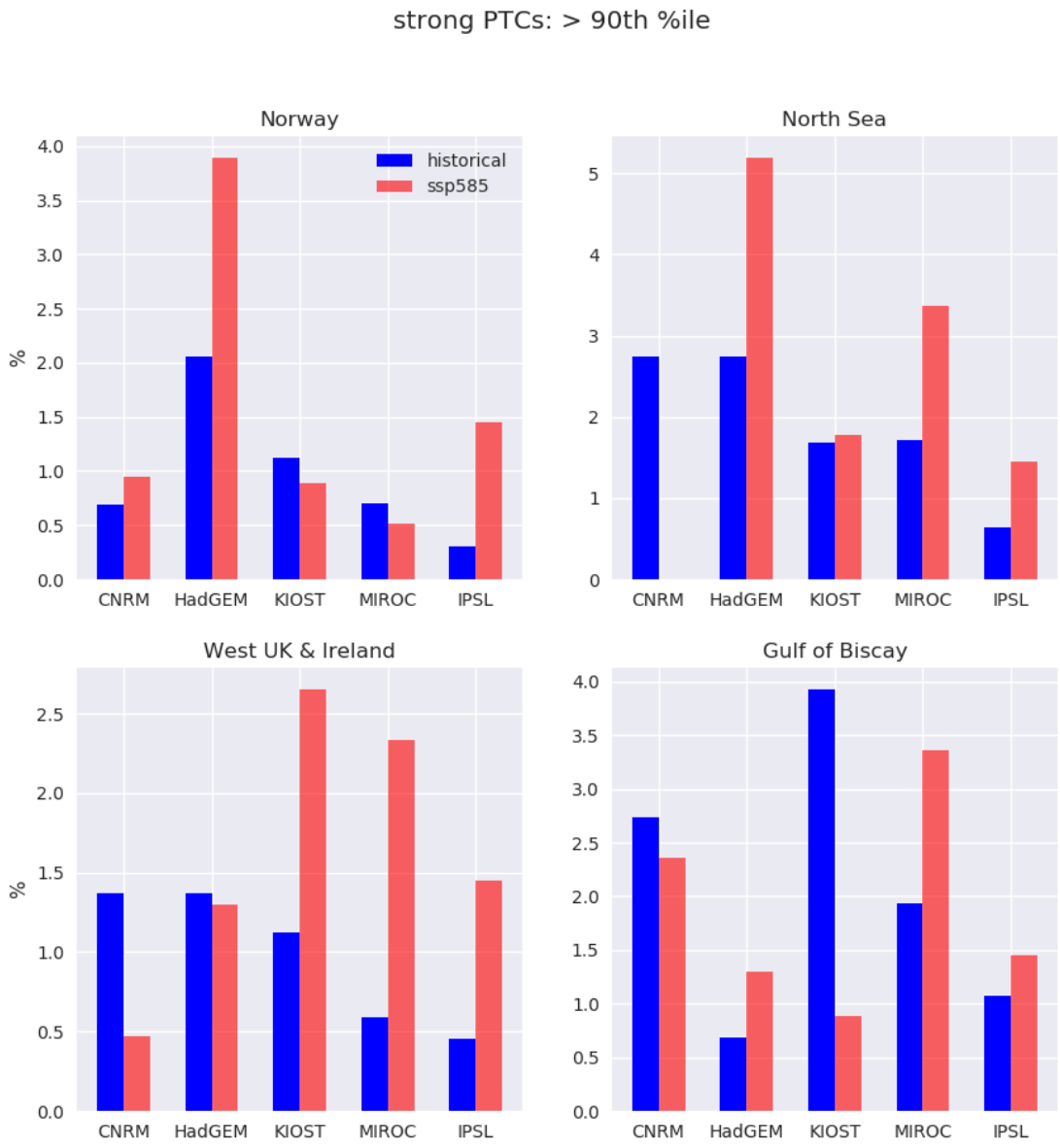

Figure 6.22. As in Figure 6.21 but considering the fraction of North Atlantic TCs which reach the four regions as strong PTCs (winds > 90th percentile of the max wind distribution in the region).

Chapter 7

Discussion and Conclusions

Post-tropical cyclones (PTCs) can produce high winds and heavy precipitation over Europe (Evans et al. 2017; Jones et al. 2003). They have been associated with wind speed records, loss of life, and large economic damage (e.g., Graham and Smart 2021). Despite often being associated with high-impact weather, few PTC studies with a European focus exist. Increases in computational power now permit climate models to run at high (<25 km) horizontal resolution, capturing the structure and lifecycle of tropical cyclones with increasing accuracy compared to observations. Studies using such climate models suggest an increase in PTC risk for Europe (Haarsma et al. 2013; Baatsen et al. 2015) due to an expansion of the tropical genesis area in the North Atlantic. However, high-resolution climate models are computationally expensive, and compromises are therefore made regarding the simulation length and number of ensemble members. As a result, previous studies using such models analyse only a small sample of PTCs and lack statistical significance.

This thesis aims to further our understanding of the hazards posed to Europe by PTCs, and the factors (environmental and cyclone-specific) governing their development, variability, and projected changes.

Section 7.1. provides an overview of the results and discusses the implications of the research chapters (3-6). Section 7.2 raises key questions that remain unanswered relating to Europe-impacting PTCs. This section also highlights further work which is necessary to fully contextualise the results presented in this thesis. Finally, section 7.3 describes the main conclusions of this thesis.

7.1. Summary and Discussion

7.1.1. How Important are Post-Tropical Cyclones for European Windstorm Risk?

The contribution of PTCs to high-intensity wind events over Europe during the North Atlantic hurricane season was investigated in chapter 3. Previous studies have highlighted the high-impact nature of PTCs for Europe from a case study perspective (Laurila et al. 2020; Rantanen et al. 2020), however their risk from a climatological

perspective has received less attention. Furthermore, high-resolution climate model studies suggest a large increase (~2-6 fold) in the frequency of hurricane-force (>33 m s^{-1}) PTCs over parts of Europe by the end of the century (Haarsma et al. 2013; Baatsen et al. 2015). To understand the implications of such a change in PTCs first requires an understanding of the risk they pose climatologically to Europe in the current climate.

The results presented in chapter 3 showed that PTCs have significantly higher 10 m wind speeds and lower sea level pressure than midlatitude cyclones (MLCs) when at their maximum intensity over Europe, when considering cyclones forming all year round, and when considering cyclones which formed during the North Atlantic hurricane season (June 1st – Nov 30th). The difference between the PTC and MLC maximum European wind speed distributions was larger for Northern Europe than for Southern Europe, with sample sizes considerably smaller over Southern Europe. PTCs are rare events, comprising approximately 1% of cyclones impacting Northern Europe during the North Atlantic hurricane season. Despite this rarity, PTCs are responsible for approximately 9% of the cyclones which reach Northern Europe with storm-force (>25 m s^{-1}) winds during hurricane season. Chapter 3 therefore showed that PTCs are disproportionately responsible for windstorm risk over Europe.

Previous studies suggest only small changes in the frequency and intensity of Europe-impacting MLCs in the future (Zappa et al. 2013; Priestley and Catto 2022). Chapter 3 therefore highlights the potential for a shift in European windstorm risk over the century, from primarily associated with MLCs in the current climate to increasingly also associated with PTCs towards the end of the century if the results of Haarsma et al. (2013) and Baatsen et al. (2015) are realised. This also highlights the possibility of a change in the seasonality of European windstorm risk, from primarily the winter months in the present climate where the risk is dominated by midlatitude cyclones, to increasingly the late summer and autumn months if PTC risk increases. This may lead to an extension of the months in which Europe typically experiences severe windstorms, or a future bimodal distribution of European windstorm risk, with a future peak during late hurricane season, alongside the existing peak in winter months.

Chapter 3 also provided a comparison of the three different methods to identify Europe-impacting PTCs presented in chapter 2. All three are methods for identifying

reanalysis cyclone tracks of PTCs: spatiotemporal track matching with observed TC tracks (section 2.3.1), a warm core test using the vertical profile of relative vorticity (section 2.3.2), and a thermal structure analysis using the cyclone phase space (Hart 2003) (section 2.3.3). All methods yield similar results. While the individual methods each have benefits and limitations, the key result that PTCs are disproportionately responsible for European windstorm risk is found using all three TC identification methods. This result provides justification for using the warm core test and cyclone phase space when identifying PTCs in datasets for which observed TC data is not available, such as in historically poorly-observed basins, and in future climate model simulations.

7.1.2. What Governs the Interannual Variability of Recurving North Atlantic Tropical Cyclones?

Recurving TCs – defined in chapter 4 as TCs which reach the midlatitudes – can cause extensive damage to the US East Coast and eastern Canada. In 2012, ex-hurricane Sandy impacted New York and surrounding areas, killing over 200 people and causing billions in damages (Blake et al. 2013). The recurvature of TCs is also a crucial stage of the lifecycle of all Europe-impacting PTCs. Furthermore, recurving TCs can amplify the midlatitude waveguide, causing a reduction in downstream midlatitude predictability in the following week (Keller et al. 2019) as well as causing downstream high-impact weather (Pohorsky et al. 2019; Grams and Blumer 2015). Given the risk recurving TCs pose to the US East Coast and Europe, and their implications for numerical weather prediction, it is important to understand what governs their interannual variability.

Results from chapter 4 showed that the genesis location plays a large role in the likelihood of recurvature. Most TCs forming in the subtropical North Atlantic (77%) recurve, whereas TCs forming in the western Atlantic (Gulf of Mexico and Caribbean Sea) rarely recurve (28%) due to frequent land interaction and subsequent dissipation. Approximately half of TCs forming in the Main Development Region (MDR) recurve, and recurving TCs which form in this region are found to be significantly stronger at their TC LMI than non-recurving TCs.

A multiple linear regression model built to predict recurving TC frequency based on TC activity in the MDR and subtropical North Atlantic explained over 75% of the variance

in recurving TC frequency. Stronger TCs were shown to be more likely to recurve than weak TCs. This could be because stronger TCs are more resilient to hostile midlatitude conditions that may exist on approach to the midlatitudes. For example, diabatic processes – which are often stronger in more intense TCs - can provide some resilience to the vertical misalignment of the TC circulation in the presence of high wind shear (Davis et al. 2007). It could also be because recurving TCs often (but not always) travel over the Gulf stream, allowing for continued intensification which is only possible because of recurvature. Conversely, only small (<0.5 m s^{-1}) differences in the seasonal mean (August-October) steering flow (Colbert and Soden 2012) and the westward extent of the North Atlantic Subtropical High (NASH) were found between years of high and low recurving TC frequency. A composite analysis showed that the westward extent of the NASH is slightly reduced during years of high recurving TC frequency originating in the MDR, and during these years slightly stronger poleward flow was present in the western subtropical North Atlantic. During years of high recurving TC frequency originating in the subtropical North Atlantic, a large-scale cyclonic flow anomaly was present in the subtropics. This is consistent with the reduced strength of the North Atlantic Oscillation which is weakly associated with increased higher-latitude TC genesis (Kossin et al. 2010). A steering flow index - defined as the regional average, meridional component of the seasonal mean steering flow in the western subtropical Atlantic - showed no significant relationship with recurving TC frequency.

The results presented in chapter 4 show that the interannual variability of recurving North Atlantic TCs is primarily governed by TC activity in the MDR and subtropical North Atlantic, with variability in the seasonal mean steering flow playing a smaller, secondary role. Given the lack of association between recurving TC frequency and the seasonal mean steering flow, the results suggest that seasonal forecasts of hurricane season activity – which are skilful prior to the start of hurricane season (Klotzbach et al. 2019) – could be used to give enhanced seasonal predictability to regions often impacted by recurving TCs, such as the US East Coast, Eastern Canada, and Europe.

7.1.3. Why do some Post-Tropical Cyclones Impact Europe?

While recurving TCs can have profound impacts along the US East Coast, they also have the opportunity to reach Europe if they undergo extratropical transition (ET) and

become embedded in the westerly midlatitude flow (Hart and Evans 2001). Case studies have highlighted a number of different lifecycles associated with Europe-impacting PTCs. Ex-hurricane Debby (Laurila et al. 2020) traversed the North Atlantic as a weak diabatic Rossby wave before rapidly reintensifying over Europe, bringing extreme winds to Finland. Ex-hurricane Katia maintained high intensity from the time of extratropical transition until it reached Scotland, aided by a phase-locked configuration between the transitioning TC and an upper-level trough (Grams and Blumer 2015). Ex-hurricane Ophelia was the easternmost major hurricane on record and maintained its hurricane status whilst taking a direct route to Europe.

Chapter 5 investigated why some PTCs reach Europe from a composite perspective. In particular, the importance of TC intensity and extratropical reintensification for Europe-impact likelihood were explored. PTCs which reach Europe recurve approximately 5 degrees further east in the basin, and complete ET significantly further polewards and eastwards. They also continue on a north-east trajectory after completing ET, allowing them to potentially interact with a more baroclinic environment than PTCs which do not impact Europe, which do not gain much latitude after ET.

It was also shown that PTCs reaching Europe have significantly stronger (~4-6 m s^{-1}) 10 m winds at their lifetime maximum intensity (LMI), throughout ET, and for a number of days post-transition. This result highlighted the possibility that strong TCs have enhanced resilience to hostile midlatitude conditions - such as decreasing sea surface temperatures and increasing vertical wind shear - which may increase cyclone longevity, and therefore the likelihood that the cyclone will reach Europe independently of the midlatitude flow configuration.

Furthermore, Europe-impacting PTCs were shown to be twice as likely to undergo extratropical reintensification after completing ET. Storm-centred composites showed that 24 hours prior to ET completion, PTCs which later reach Europe interact more strongly with an upstream trough in a significantly more baroclinic environment. This interaction may steer the cyclones on a northeast trajectory across a midlatitude jet streak located on the eastern flank of the trough. It is during the crossing of the jet streak that many PTCs reintensify. This is consistent with the cyclone-relative

atmospheric configuration surrounding reintensifying western North Pacific TCs (Harr et al. 2000a) which often develop into strong extratropical cyclones. During the 48-hour period centred on ET completion, PTCs that reach Europe are also collocated with greater low level temperature gradients in a region of higher Eady growth rates, develop a greater thermal asymmetry and contain a larger area of gale force winds. The weakest 20% of PTCs at ET onset were shown to be five times less likely to reach Europe than the strongest 20% of PTCs at ET onset. In addition, contingency table analysis showed that PTCs which were major hurricanes (TC LMI > 50 m s^{-1}), and PTCs which reintensify post-transition, were significantly more likely to reach Europe, highlighting two pathways through which PTCs may reach Europe.

The results of chapters 4 and 5 give insight into future European PTC risk. The strength of the relationship between recurving TC frequency and TC activity suggests that changes to recurving TC frequency are likely to depend on changes to TC activity in the North Atlantic, but may also depend on TC intensity changes, as stronger TCs are more likely to survive long enough to recurve. Previous studies suggest a decrease in North Atlantic TC frequency, although this projected reduction is mainly in weaker, short-lived TCs (Knutson et al. 2019) which have a low probability of recurvature. Coupled with more favourable conditions in the subtropical Atlantic for TCs (Haarsma et al. 2013) and an observed poleward shift in TC LMI (Kossin et al. 2014), future TCs may be more likely to recurve, though future changes in recurving TC frequency will depend on whether a reduction in TC frequency outweighs an increase in the likelihood of recurvature. Furthermore, the results of chapter 5 indicate that the strength of the TC, along with the configuration of the midlatitude environment into which the cyclone recurves, are key to understanding why some PTCs reach Europe. Climate change may lead to both an increase in TC LMI (Knutson et al. 2019) and a poleward shift in the latitude of TC LMI (Kossin et al. 2014). Given the importance of TC intensity for Europe-impact likelihood, this suggests a future increased risk to Europe. Conversely, whether PTCs interact with a jet streak and subsequently reintensify is also shown to be important, and many climate models indicate a poleward shift in the jet (Harvey et al. 2020). Changes in the likelihood that PTCs will reach Europe therefore depends on which of these competing factors is dominant.

7.1.4. Can Low-Resolution CMIP6 ScenarioMIP Models Provide Insight into Future European Post-Tropical Cyclone Risk?

Although intensity biases remain, high-resolution climate model simulations are representing TC structure with increasing accuracy, allowing for the study of how climate change may affect TCs and PTCs. Future European PTC risk studies are limited but suggest that a 2-6-fold increase in the frequency of hurricane force PTCs over parts of Europe by the end of the century is possible (Haarsma et al. 2013), with additional studies also highlighting the possible increased PTC risk to Europe (Jung and Lackmann 2021; Liu et al. 2017; Michaelis and Lackmann 2019). This may be the result of a poleward and eastward expansion of the region favourable for tropical cyclogenesis in the North Atlantic (Haarsma et al. 2013) and an increase in moisture availability, leading to more warm-seclusion cyclone types (Baatsen et al. 2015), which are typically stronger than cold-core cyclones (Dekker et al. 2018). Few studies exist on European PTC risk towards the end of the century, and those that do rely on a single climate model simulation, motivating the need for a multi-model study to assess the uncertainty surrounding future European PTC projections.

It is unknown whether CMIP6 models - which have lower resolution than climate models previously used to investigate ET (e.g., Baker et al. 2022; Liu et al. 2017) - can provide insight into future European PTC risk, given their coarse resolution and inability to accurately capture the structure and observed intensity spectrum associated with TCs (e.g., Vidale et al. 2021). The results of chapter 6 provide a critical analysis of CMIP6 model performance in terms of TC and PTC climatologies. It was found that a selection of CMIP6 models are able to capture the frequency, seasonal cycle, and spatial distribution of TCs well compared to reanalyses. These models also capture the disproportionate intensity associated with Europe-impacting PTCs compared with MLCs. However, biases in TC intensity were found across all models due to insufficient horizontal resolution, and the likelihood of recurvature for TCs forming in the MDR was found to be too small in four of the five models.

A significant reduction in TC activity of 30-60% is found across all five models, consistent with previous studies which explicitly track TCs (Knutson et al. 2010). Despite this decrease in TC activity, a proportional decrease in Europe-impacting PTCs

is not found due to a robust increase in the likelihood that a North Atlantic TC will reach Europe. The projected increase in the likelihood that TCs will reach Europe is largely driven by an increase in the likelihood of recurvature in the North Atlantic. In three models, this can be attributed to a shift in genesis away from the MDR, a region in which the models have a low bias for recurvature likelihood. In reality, a shift in genesis location as seen in these models would likely not lead to such a large increase in the likelihood of recurvature, and to an extent is a manifestation of model biases. There is model agreement for an increase in potential intensity along the US East Coast, driven by warming SSTs. This is collocated with a region in which vertical wind shear is projected to decrease. Many TCs that recurve (or begin to recurve) do so along this region, and these projected environmental changes may lead to more favourable conditions in the western subtropical North Atlantic, increasing the likelihood of recurvature.

The results presented in chapter 6 suggest an uncertain future for European PTC risk, with a projected reduction in North Atlantic TC activity crucially offsetting the projected increase in the likelihood that a North Atlantic TC will reach Europe. While many features of the TC and PTC climatology are well captured by the models, biases in recurvature likelihood in the MDR may lead to a bias in the projections which must also be considered in the interpretation of results. Additionally, CMIP6 models contain biases in the representation of the North Atlantic storm track and jet (Harvey et al. 2020), which may have implications for the trajectory and intensity of PTCs in the post-tropical stage of their lifecycle. This chapter highlights the biases that must be improved to enhance our confidence in climate model projections of the genesis and trajectory of TCs. It also provides a framework for evaluating projections of PTC risk in future generations of climate models.

Furthermore, there may be sensitivity to the TC identification method used, motivating the need for multi-model studies which use multiple methods of TC identification. Compared to IBTrACS, the TC identification method described in section 2.3.2 is found to have a higher probability of detection than other commonly-used TC identification methods, but also has a relatively high false alarm rate (Bourdin et al. 2022). Future work should consider the impact that the choice of TC identification method has on the resulting projections (such as in Roberts et al. 2020).

7.2. Future Work

The research conducted in chapters 3-6 highlight key questions for future research. These are discussed below.

- On average, Europe-impacting PTCs are considerably more intense than MLCs over Europe, but the cause of this difference is not understood. One possibility is that PTCs start reintensifying from a higher baseline intensity upon interacting with a favourable midlatitude environment than cyclones which form in the midlatitudes. TCs undergoing ET often advect warm, moist air poleward, which ascends slantwise upon interacting with a baroclinic zone and contributes to the formation of the warm conveyor belt. The convection and diabatic heating associated with this ascending air of tropical origin may have implications for the intensity of the cyclone downstream. Such diabatic processes may increase the likelihood of a warm seclusion developing. Previous studies have highlighted that preconditioning of the midlatitude environment - such as the advection of warm, moist air to the east of a recurving TC - may be important for reintensification of PTCs (Grams and Archambault 2016; Keller et al. 2019) . It would be of interest to investigate both of these hypotheses climatologically, with MLCs as a reference.
- Recurving TC frequency is strongly associated with TC activity in the Main Development Region and subtropical Atlantic. TC activity in the Main Development Region is well predicted using seasonal indices of environmental variables, but this is less true for TC activity in the subtropical Atlantic, which limits the applications of the results presented in chapter 4. Future work should investigate the drivers of subtropical Atlantic TC activity from a seasonal and subseasonal perspective. A weak association between TC activity in the subtropics and the NAO has been identified (Kossin et al. 2010; Elsner et al. 2000), but the importance of other factors, such as SSTs, TC seeds, and baroclinicity on TC activity in the subtropics need further quantifying.
- Recurving TCs which reintensify are more likely to reach Europe. In chapter 5 we showed that the intensity change occurs during the crossing of a midlatitude jet streak, however this was not demonstrated causally. The

contributions from the upper-level upstream trough, midlatitude jet streak, and any other sources to reintensification should be quantified to improve our understanding regarding the conditions under which a recurving TC may reach Europe.

- Further work is necessary to bridge the gap between recurving TC interannual variability and the factors which allow recurving TCs to reach Europe (chapters 4 and 5). This could be achieved by investigating recurving TC frequency and likelihood of recurving TCs reaching Europe on the subseasonal timescale. The Madden-Julian Oscillation, for example, has a relationship with TC activity in the North Atlantic (Klotzbach 2010; Manganello and Kinter 2021), and due to the strong relationship between TC activity and recurving TC activity may give some predictability for recurving TC activity. The MJO also has a relationship with the large-scale midlatitude circulation in the North Atlantic and Europe (Lee et al. 2019) via Rossby wave dynamics. The midlatitude circulation may affect the likelihood that a recurving TC will reach Europe (via reintensification). It may therefore be possible to identify subseasonal signals which highlight a decreased or increased likelihood of PTC risk to Europe via the MJO teleconnection.
- The results of chapter 6 show an increase in the likelihood that TCs will reach Europe, which is crucially offset by a reduction in North Atlantic TC frequency of 30-60%. Future work is therefore needed to quantify and reduce the uncertainty surrounding projected changes to North Atlantic TC activity. In particular, the uncertainty associated with the method used to diagnose TC activity (explicit tracking and identification, genesis indices, and downscaling approaches) must be quantified, along with the uncertainty associated with different implementations of TC identification methods (for example, the choice of humidity metric in genesis indices, and identification criteria - and their possible resolution dependence – in TC identification methods). Future work should focus on multi-model studies of high-resolution climate models, which better capture the structure and intensity of TCs. Future work may also benefit from the use of large ensembles – for example, the D4PDF (Mizuta et al. 2017) - which provide ample data to separate projected changes in TCs from

internal variability, but will not address model uncertainty and resolution issues.

- Although this work focusses on the North Atlantic and Europe, the framework provided by this thesis could be used to assess PTC risk, variability, and projected changes in other ocean basins in which TCs often complete ET, such as the Western North Pacific (Bieli et al. 2019a). Despite slightly different conditions compared to the North Atlantic, it may still be expected that stronger TCs, and TCs which reintensify post-ET are associated with greater longevity, and therefore may be important for PTC risk downstream of ET. Using cyclone tracking in conjunction with best track data and objective TC identification, PTC risk relative to the overall cyclone climatology should be investigated in regions which frequently see PTC impacts, and drivers of their interannual variability should be investigated. By splitting the lifecycle of TCs into TC genesis, recurvature, and post-ET evolution, the framework provided by chapter 6 could be used to assess future changes to PTC risk in other ocean basins.

7.3. Concluding Remarks

This thesis has provided climatological context for post-tropical cyclone risk and explored the variability associated with the recurvature and post-extratropical transition stages of their lifecycle, from a European perspective. Within this framework, future changes to Europe-impacting post-tropical cyclones were investigated in CMIP-class climate models. The key conclusions from this thesis are highlighted below.

- Despite being relatively rare events comprising less than 1% of cyclones to reach Northern Europe during the North Atlantic hurricane season, approximately 9% of cyclones which reach Northern Europe during hurricane season with storm-force (>25 m s^{-1}) winds are post-tropical cyclones. Post-tropical cyclones are therefore disproportionately responsible for European windstorm risk in the present climate.
- The interannual variability of recurving North Atlantic tropical cyclones is governed primarily by tropical cyclone activity in the Main Development Region

and subtropical Atlantic, with interannual variability in the seasonal mean steering flow playing a much smaller, secondary role.

- Post-tropical cyclones which were major hurricanes, and post-tropical cyclones which reintensify after completing extratropical transition, are significantly more likely to reach Europe than recurving tropical cyclones which were not major hurricanes, or do not reintensify after extratropical transition. Interaction with an upstream trough, which steers the cyclones across a midlatitude jet streak, is shown to be associated with reintensification and therefore an increased likelihood of reaching Europe.
- A selection of CMIP6 models capture the observed climatology of North Atlantic tropical cyclones well, and also capture the disproportionate risk associated with post-tropical cyclones across Europe. However, as expected, these models do not capture the full intensity distribution of tropical cyclones, and model biases remain. These models project a robust increase in the likelihood that a North Atlantic tropical cyclone will reach Europe, though this in part is likely due to the manifestation of model biases. The projected increased likelihood that a tropical cyclone will reach Europe is crucially offset by a significant reduction in North Atlantic tropical cyclone frequency of 30-60%. Future post-tropical cyclone risk to Europe therefore remains uncertain and depends on changes to tropical cyclone activity basin-wide.

This thesis presents evidence of the disproportionate risk associated with Europe-impacting post-tropical cyclones, identifies factors which may allow post-tropical cyclones to reach Europe, and highlights the uncertain future for Europe in terms of post-tropical cyclone risk. It is also shown that objective tropical cyclone identification can be used together with reanalyses and climate models to provide insight into post-tropical cyclone variability and future projections in the absence of observational data. However, reanalyses have tropical cyclone and post-tropical cyclone intensity biases, and different studies often use different tropical cyclone tracking and identification tools. An extension of best track datasets to include the full lifecycle of tropical cyclones using observational data would allow greater intercomparison between future post-tropical cyclone studies and would benefit the community.

Given their substantial impacts, it is important that the research community and funding bodies continue to focus on post-tropical cyclones. In particular, the large uncertainty in climate model projections implies that we need i) to keep improving climate models to better represent key processes related to tropical cyclone and post-tropical cyclone evolution, ii) monitor post-tropical cyclone frequency and intensity to detect any emerging trends, and iii) continue to improve our understanding of how post-tropical cyclones develop.

Bibliography

Agusti-Panareda, A., C. D. Thorncroft, G. C. Craig, and S. L. Gray, 2004: The extratropical transition of hurricane Irene (1999): A potential-vorticity perspective. *Q. J. R. Meteorol. Soc.*, **130**, 1047–1074, https://doi.org/10.1256/qj.02.140.

Aiyyer, A. R., and C. Thorncroft, 2006: Climatology of vertical wind shear over the tropical Atlantic. *J. Clim.*, **19**, 2969–2983, https://doi.org/10.1175/JCLI3685.1.

Andrews, M. B., and Coauthors, 2020: Historical Simulations With HadGEM3-GC3.1 for CMIP6. *J. Adv. Model. Earth Syst.*, **12**, https://doi.org/10.1029/2019MS001995.

Anfuso, G., C. Loureiro, M. Taaouati, T. Smyth, and D. Jackson, 2020: Spatial variability of beach impact from post-tropical cyclone Katia (2011) on Northern Ireland's North Coast. *Water*, **12**, 1–17, https://doi.org/10.3390/W12051380.

Anwender, D., P. A. Harr, and S. C. Jones, 2008: Predictability associated with the downstream impacts of the extratropical transition of tropical cyclones: Case studies. *Mon. Weather Rev.*, **136**, 3226–3247, https://doi.org/10.1175/2008MWR2249.1.

Archambault, H. M., L. F. Bosart, D. Keyser, and J. M. Cordeira, 2013: A climatological analysis of the extratropical flow response to recurving western north pacific tropical cyclones. *Mon. Weather Rev.*, **141**, 2325–2346, https://doi.org/10.1175/MWR-D-12-00257.1.

——, D. Keyser, L. F. Bosart, C. A. Davis, and J. M. Cordeira, 2015: A composite perspective of the extratropical flow response to recurving western North Pacific tropical cyclones. *Mon. Weather Rev.*, **143**, 1122–1141, https://doi.org/10.1175/MWR-D-14-00270.1.

Arias, P. A., and Coauthors, 2021: *Climate Change 2021: The Physical Science Basis. Contribution of Working Group 1 to the Sixth Assessment Report of the Intergovernmental Panel on Climate Change*. Cambridge University Press, 33–144 pp.

Arnault, J., and F. Roux, 2011: Characteristics of African easterly waves associated with tropical cyclogenesis in the Cape Verde Islands region in July-August-September of 2004-2008. *Atmos. Res.*, **100**, 61–82, https://doi.org/10.1016/j.atmosres.2010.12.028.

Arnott, J. M., J. L. Evans, and F. Chiaromonte, 2004: Characterization of extratropical transition using cluster analysis. *Mon. Weather Rev.*, **132**, 2916–2937,

https://doi.org/10.1175/MWR2836.1.

Atallah, E. H., and L. F. Bosart, 2003: The extratropical transition and precipitation distribution of hurricane Floyd (1999). *Mon. Weather Rev.*, **131**, 1063–1081, https://doi.org/10.1175/1520-0493(2003)131<1063:TETAPD>2.0.CO;2.

Avila, L. A., and J. Cangialosi, 2011: Tropical Cyclone Report - Hurricane Irene. 21–28.

Baatsen, M., R. J. Haarsma, A. J. Van Delden, and H. de Vries, 2015: Severe Autumn storms in future Western Europe with a warmer Atlantic Ocean. *Clim. Dyn.*, **45**, 949–964, https://doi.org/10.1007/s00382-014-2329-8.

Baker, A., and Coauthors, 2022: Extratropical transition of tropical cyclones in a multiresolution ensemble of atmosphere-only and fully coupled global climate models. *J. Clim.*, **35**, 5283–5306, https://doi.org/10.1175/JCLI-D-21-0801.1.

Baker, A. J., K. I. Hodges, R. K. H. Schiemann, and P. L. Vidale, 2021: Historical variability and lifecycles of North Atlantic midlatitude cyclones originating in the tropics. *J. Geophys. Res. Atmos.*, **126**, 1–46, https://doi.org/10.1029/2020jd033924.

Bell, B., and Coauthors, 2021: The ERA5 global reanalysis: Preliminary extension to 1950. *Q. J. R. Meteorol. Soc.*, 4186–4227, https://doi.org/10.1002/qj.4174.

Bender, M. A., T. R. Knutson, R. E. Tuleya, J. J. Sirutis, G. A. Vecchi, S. T. Garner, and I. M. Held, 2010: Modeled impact of anthropogenic warming on the frequency of intense Atlantic hurricanes. *Science (80-.).*, **327**, 454–458, https://doi.org/10.1126/science.1180568.

Bengtsson, L., K. I. Hodges, and M. Esch, 2007a: Tropical cyclones in a T159 resolution global climate model: Comparison with observations and re-analyses. *Tellus, Ser. A Dyn. Meteorol. Oceanogr.*, **59 A**, 396–416, https://doi.org/10.1111/j.1600-0870.2007.00236.x.

Bengtsson, L., K. I. Hodges, M. Esch, N. Keenlyside, L. Kornblueh, J. J. Luo, and T. Yamagata, 2007b: How may tropical cyclones change in a warmer climate? *Tellus, Ser. A Dyn. Meteorol. Oceanogr.*, **59 A**, 539–561, https://doi.org/10.1111/j.1600-0870.2007.00251.x.

Bhatia, K., A. Baker, G. Vecchi, H. Murakami, J. Kossin, P. Luigi, K. Hodges, and T. Knutson, 2020: An Environmental Explanation for the Recent Increase in Tropical Cyclone

Intensification. EGU General Assembly 2020, Ed., Online, 18644.

Bhatia, K. T., G. A. Vecchi, H. Murakami, S. D. Underwood, and J. P. Kossin, 2018: Projected Response of Tropical Cyclone Intensity and Intensification in a Global Climate Model. *J. Clim.*, **31**, 8281–8303, https://doi.org/10.1175/JCLI-D-17-0898.1.

Bieli, M., S. J. Camargo, A. H. Sobel, J. L. Evans, and T. Hall, 2019a: A global climatology of extratropical transition. Part I: Characteristics across basins. *J. Clim.*, **32**, 3557–3582, https://doi.org/10.1175/JCLI-D-17-0518.1.

——, ——, ——, ——, and ——, 2019b: A global climatology of extratropical transition. Part II: Statistical performance of the cyclone phase space. *J. Clim.*, **32**, 3583–3597, https://doi.org/10.1175/JCLI-D-18-0052.1.

——, A. H. Sobel, S. J. Camargo, H. Murakami, and G. A. Vecchi, 2020: Application of the Cyclone Phase Space to Extratropical Transition in a Global Climate Model. *J. Adv. Model. Earth Syst.*, **12**, https://doi.org/10.1029/2019MS001878.

Blake, E. S., T. B. Kimberlain, R. J. Berg, Cangia, J. P. Losi, and J. L. Beven II, 2013: Tropical cyclone report Hurricane Sandy (AL182012) 22 – 29 October 2012. *Natl. Weather Serv. Natl. Hurric. Cent.*, 1–157.

Boucher, O., and Coauthors, 2020: Presentation and evaluation of the IPSL-CM6A-LR climate model. *J. Adv. Model. Earth Syst.*, **12**, https://doi.org/10.1029/2019MS002010.

Boudreault, M., L. P. Caron, and S. J. Camargo, 2017: Reanalysis of climate influences on Atlantic tropical cyclone activity using cluster analysis. *J. Geophys. Res.*, **122**, 4258–4280, https://doi.org/10.1002/2016JD026103.

Bourdin, S., S. Fromang, W. Dulac, J. Cattiaux, and F. Chauvin, 2022: Intercomparison of Four Tropical Cyclones Detection Algorithms on ERA5. *preprint*, **2022**, 1–43, https://doi.org/10.5194/egusphere-2022-179.

Brannan, A. L., and J. M. Chagnon, 2020: A climatology of the extratropical flow response to recurving atlantic tropical cyclones. *Mon. Weather Rev.*, **148**, 541–558, https://doi.org/10.1175/MWR-D-19-0216.1.

Browning, K. A., 1998: Analysis of an ex-tropical cyclone after its reintensification as a warm-core extratropical cyclone. *Q. J. R. Meteorol. Soc.*, **124**, 2329–2356, https://doi.org/10.1256/smsqj.55107.

Camargo, S. J., 2013: Global and regional aspects of tropical cyclone activity in the CMIP5 models. *J. Clim.*, **26**, 9880–9902, https://doi.org/10.1175/JCLI-D-12-00549.1.

——, and A. A. Wing, 2016: Tropical cyclones in climate models. *Wiley Interdiscip. Rev. Clim. Chang.*, **7**, 211–237, https://doi.org/10.1002/wcc.373.

——, K. A. Emanuel, and A. H. Sobel, 2007a: Use of a genesis potential index to diagnose ENSO effects on tropical cyclone genesis. *J. Clim.*, **20**, 4819–4834, https://doi.org/10.1175/JCLI4282.1.

——, A. H. Sobel, A. G. Barnston, and K. A. Emanuel, 2007b: Tropical cyclone genesis potential index in climate models. *Tellus, Ser. A Dyn. Meteorol. Oceanogr.*, **59 A**, 428–443, https://doi.org/10.1111/j.1600-0870.2007.00238.x.

——, M. Ting, and Y. Kushnir, 2013: Influence of local and remote SST on North Atlantic tropical cyclone potential intensity. *Clim. Dyn.*, **40**, 1515–1529, https://doi.org/10.1007/s00382-012-1536-4.

Camp, J., M. Roberts, C. Maclachlan, E. Wallace, L. Hermanson, A. Brookshaw, A. Arribas, and A. A. Scaife, 2015: Seasonal forecasting of tropical storms using the Met Office GloSea5 seasonal forecast system. *Q. J. R. Meteorol. Soc.*, **141**, 2206–2219, https://doi.org/10.1002/qj.2516.

Caron, L. P., and C. G. Jones, 2012: Understanding and simulating the link between African easterly waves and Atlantic tropical cyclones using a regional climate model: The role of domain size and lateral boundary conditions. *Clim. Dyn.*, **39**, 113–135, https://doi.org/10.1007/s00382-011-1160-8.

Catto, J. L., L. C. Shaffrey, and K. I. Hodges, 2010: Can climate models capture the structure of extratropical cyclones? *J. Clim.*, **23**, 1621–1635, https://doi.org/10.1175/2009JCLI3318.1.

Chan, J. C. L., and W. M. Gray, 1982: Tropical Cyclone Movement and Surrounding Flow Relationships. *Mon. Weather Rev.*, **110**, 1354–1374.

Colbert, A. J., and B. J. Soden, 2012: Climatological variations in North Atlantic tropical cyclone tracks. *J. Clim.*, **25**, 657–673, https://doi.org/10.1175/JCLI-D-11-00034.1.

Dacre, H. F., M. K. Hawcroft, M. A. Stringer, and K. I. Hodges, 2012: An extratropical cyclone atlas a tool for illustrating cyclone structure and evolution characteristics. *Bull. Am.*

Meteorol. Soc., **93**, 1497–1502, https://doi.org/10.1175/BAMS-D-11-00164.1.

Datt, I., S. J. Camargo, A. H. Sobel, R. McTaggart-Cowan, and Z. Wang, 2022: An Investigation of Tropical Cyclone Development Pathways as an Indicator of Extratropical Transition. *J. Meteorol. Soc. Japan. Ser. II*, https://doi.org/10.2151/jmsj.2022-037.

Davis, C. A., S. C. Jones, and M. Riemer, 2008: Hurricane vortex dynamics during atlantic extratropical transition. *J. Atmos. Sci.*, **65**, 714–736, https://doi.org/10.1175/2007JAS2488.1.

Davis, C. A., 2018: Resolving Tropical Cyclone Intensity in Models. *Geophys. Res. Lett.*, **45**, 2082–2087, https://doi.org/10.1002/2017GL076966.

Dekker, M. M., R. J. Haarsma, H. de Vries, M. Baatsen, and A. J. va. Delden, 2018: Characteristics and development of European cyclones with tropical origin in reanalysis data. *Clim. Dyn.*, **50**, 445–455, https://doi.org/10.1007/s00382-017-3619-8.

Delgado, S., C. W. Landsea, and H. Willoughby, 2018: Reanalysis of the 1954-63 Atlantic Hurricane seasons. *J. Clim.*, **31**, 4177–4192, https://doi.org/10.1175/JCLI-D-15-0537.1.

Demirci, O., J. S. Tyo, and E. A. Ritchie, 2007: Spatial and spatiotemporal projection pursuit techniques to predict the extratropical transition of tropical cyclones. *IEEE Trans. Geosci. Remote Sens.*, **45**, 418–425, https://doi.org/10.1109/TGRS.2006.882251.

Eliassen, A., and E. Palm, 1961: On the transfer of energy in stationary moiuntain waves. *Geophys. Nor.*, **22**, 1–23.

Elsner, J. B., 2003: Tracking hurricanes. *Bull. Am. Meteorol. Soc.*, **84**, 353–356, https://doi.org/10.1175/BAMS-84-3-353.

——, G. S. Lehmiller, and T. B. Kimberlain, 1996: Objective Classification of Atlantic Hurricanes. *J. Clim.*, **9**, 2880–2889, https://doi.org/10.1175/1520-0442(1996)009<2880:OCOAH>2.0.CO;2.

Elsner, J. B., K. Liu, and B. Kocher, 2000: Spatial variations in major U.S. hurricane activity: Statistics and a physical mechanism. *J. Clim.*, **13**, 2293–2305, https://doi.org/10.1175/1520-0442(2000)013<2293:SVIMUS>2.0.CO;2.

Elsner, J. B., B. H. Bossak, and X. F. Niu, 2001: Secular changes to the ENSO-U.S. hurricane relationship. *Geophys. Res. Lett.*, **28**, 4123–4126, https://doi.org/10.1029/2001GL013669.

Emanuel, K., 2003: Tropical cyclones. *Annu. Rev. Earth Planet. Sci.*, **31**, 75–104, https://doi.org/10.1146/annurev.earth.31.100901.141259.

——, 2010: Tropical cyclone activity downscaled from NOAA-CIRES Reanalysis, 1908–1958. *J. Adv. Model. Earth Syst.*, **2**, https://doi.org/10.3894/james.2010.2.1.

——, 2021a: Response of global tropical cyclone activity to increasing CO2: Results from downscaling CMIP6 models. *J. Clim.*, **34**, 57–70, https://doi.org/10.1175/JCLI-D-20-0367.1.

——, 2021b: Atlantic tropical cyclones downscaled from climate reanalyses show increasing activity over past 150 years. *Nat. Commun.*, **12**, 1–8, https://doi.org/10.1038/s41467-021-27364-8.

——, and D. S. Nolan, 2004: Tropical Cyclone Activity and the Global Climate System. *26th Conference on Hurricanes and Tropical Meteorology*, 240–241.

Emanuel, K. A., 1986: An Air-Sea Interaction Theory for Tropical Cyclones. Part I: Steady-State Maintenance. *J. Atmos. Sci.*, **43**, 585–605, https://doi.org/10.1175/1520-0469(1986)043<0585:AASITF>2.0.CO;2.

——, 2013: Downscaling CMIP5 climate models shows increased tropical cyclone activity over the 21st century. *Proc. Natl. Acad. Sci. U. S. A.*, **110**, 12219–12224, https://doi.org/10.1073/pnas.1301293110.

——, R. Sundararajan, and J. Williams, 2008: Hurricanes and global warming. *Bull. Am. Meteorol. Soc.*, **89**, 347–368, https://doi.org/10.1175/BAMS-89-3-347.

Evans, C., and R. E. Hart, 2008: Analysis of the wind field evolution associated with the extratropical transition of Bonnie (1998). *Mon. Weather Rev.*, **136**, 2047–2065, https://doi.org/10.1175/2007MWR2051.1.

——, and Coauthors, 2017: The extratropical transition of tropical cyclones. Part I: Cyclone evolution and direct impacts. *Mon. Weather Rev.*, **145**, 4317–4344, https://doi.org/10.1175/MWR-D-17-0027.1.

Evans, J. L., and R. E. Hart, 2003: Objective indicators of the life cycle evolution of extratropical transition for Atlantic tropical cyclones. *Mon. Weather Rev.*, **131**, 909–925, https://doi.org/10.1175/1520-0493(2003)131<0909:OIOTLC>2.0.CO;2.

Eyring, V., S. Bony, G. A. Meehl, C. A. Senior, B. Stevens, R. J. Stouffer, and K. E. Taylor, 2016: Overview of the Coupled Model Intercomparison Project Phase 6 (CMIP6) experimental design and organization. *Geosci. Model Dev.*, **9**, 1937–1958, https://doi.org/10.5194/gmd-9-1937-2016.

Feng, X., N. P. Klingaman, and K. I. Hodges, 2021: Poleward migration of western North Pacific tropical cyclones related to changes in cyclone seasonality. *Nat. Commun.*, **12**, https://doi.org/10.1038/s41467-021-26369-7.

Foerster, A. M., M. M. Bell, P. A. Harr, and S. C. Jones, 2014: Observations of the Eyewall Structure of Typhoon Sinlaku (2008) during the Transformation Stage of Extratropical Transition. *Mon. Weather Rev.*, **142**, 3372–3392, https://doi.org/10.1175/MWR-D-13-00313.1.

Gelaro, R., and Coauthors, 2017: The modern-era retrospective analysis for research and applications, version 2 (MERRA-2). *J. Clim.*, **30**, 5419–5454, https://doi.org/10.1175/JCLI-D-16-0758.1.

Gilford, D. M., 2021: PyPI (v1.3): Tropical Cyclone Potential Intensity Calculations in Python. *Geosci. Model Dev.*, **14**, 2351–2369, https://doi.org/10.5194/gmd-14-2351-2021.

Graham, E., and D. Smart, 2021: 'Hurricane' Debbie – 60 years on: a fresh analysis. *Weather*, **76**, 284–292, https://doi.org/10.1002/wea.4051.

Gramcianinov, C. B., R. M. Campos, R. de Camargo, K. I. Hodges, C. Guedes Soares, and P. L. da Silva Dias, 2020: Analysis of Atlantic extratropical storm tracks characteristics in 41 years of ERA5 and CFSR/CFSv2 databases. *Ocean Eng.*, **216**, 108111, https://doi.org/10.1016/j.oceaneng.2020.108111.

Grams, C. M., and S. R. Blumer, 2015: European high-impact weather caused by the downstream response to the extratropical transition of North Atlantic Hurricane Katia (2011). *Geophys. Res. Lett.*, **42**, 8738–8748, https://doi.org/10.1002/2015GL066253.

——, and H. M. Archambault, 2016: The key role of diabatic outflow in amplifying the midlatitude flow: A representative case study of weather systems surrounding western North Pacific extratropical transition. *Mon. Weather Rev.*, **144**, 3847–3869, https://doi.org/10.1175/MWR-D-15-0419.1.

——, S. C. Jones, and C. A. Davis, 2013a: The impact of Typhoon Jangmi (2008) on the

midlatitude flow. Part II: Downstream evolution. *Q. J. R. Meteorol. Soc.*, **139**, 2165–2180, https://doi.org/10.1002/qj.2119.

——, ——, ——, P. A. Harr, and M. Weissmann, 2013b: The impact of Typhoon Jangmi (2008) on the midlatitude flow. Part I: Upper-level ridgebuilding and modification of the jet. *Q. J. R. Meteorol. Soc.*, **139**, 2148–2164, https://doi.org/10.1002/qj.2091.

——, S. T. K. Lang, and J. H. Keller, 2015: A quantitative assessment of the sensitivity of the downstream midlatitude flow response to extratropical transition of tropical cyclones. *Geophys. Res. Lett.*, **42**, 9521–9529, https://doi.org/10.1002/2015GL065764.

Gray, W. M., 1975: Tropical cyclone genesis and intensification. 121pp.

——, 1984: Atlantic seasonal hurricane frequency, Part I: El Nino and 30 mb Quasi-Biennial Oscillation influences. *Mon. Weather Rev.*, **112**, https://doi.org/10.1175/1520-0493(1984)112<1649:ASHFPI>2.0.CO;2.

Gualdi, S., E. Scoccimarro, and A. Navarra, 2008: Changes in Tropical Cyclone Activity due to Global Warming : Results from a High-Resolution Coupled General Circulation Model. *J. Clim.*, **21**, 5204–5228, https://doi.org/10.1175/2008JCLI1921.1.

Haarsma, R., 2021: European windstorm risk of post Tropical Cyclones and the impact of climate change. *Geophys. Res. Lett.*, https://doi.org/10.1029/2020gl091483.

Haarsma, R. J., J. F. B. Mitchell, and C. A. Senior, 1993: Tropical disturbances in a GCM. *Clim. Dyn.*, **8**, 247–257, https://doi.org/10.1007/BF00198619.

Haarsma, R. J., W. Hazeleger, C. Severijns, H. De Vries, A. Sterl, R. Bintanja, G. J. Van Oldenborgh, and H. W. Van Den Brink, 2013: More hurricanes to hit western Europe due to global warming. *Geophys. Res. Lett.*, **40**, 1783–1788, https://doi.org/10.1002/grl.50360.

——, and Coauthors, 2016: High Resolution Model Intercomparison Project (HighResMIP v1.0) for CMIP6. *Geosci. Model Dev.*, **9**, 4185–4208, https://doi.org/10.5194/gmd-9-4185-2016.

Hagen, A. B., D. Strahan-Sakoskie, and C. Luckett, 2012: A reanalysis of the 1944-53 atlantic hurricane seasons-the first decade of aircraft reconnaissance. *J. Clim.*, **25**, 4441–4460, https://doi.org/10.1175/JCLI-D-11-00419.1.

Han, Y., M. Z. Zhang, Z. Xu, and W. Guo, 2022: Assessing the performance of 33 CMIP6 models in simulating the large-scale environmental fields of tropical cyclones. *Clim. Dyn.*, **58**, 1683–1698, https://doi.org/10.1007/s00382-021-05986-4.

Harr, P. A., and R. L. Elsberry, 1995: Large-Scale Circulation Variability over the Tropical Western North Pacific. Part I: Spatial Patterns and Tropical Cyclone Characteristics. *Mon. Weather Rev.*, **123**, 1225–1446, https://doi.org/https://doi.org/10.1175/1520-0493(1995)123<1225:LSCVOT>2.0.CO;2.

Harr, P. A., R. L. Elsberry, and T. F. Hogan, 2000a: Extratropical transition of tropical cyclones over the Western North Pacific Part II: The impact of midlatitude circulation characteristics. *Mon. Weather Rev.*, **128**, 2634–2653, https://doi.org/10.1175/1520-0493(2000)128<2634:etotco>2.0.co;2.

——, ——, and ——, 2000b: Extratropical transition of tropical cyclones over the Western North Pacific Part I: Evolution of Structural Characteristics during the Transition Process. *Mon. Weather Rev.*, **128**, 2634–2653, https://doi.org/10.1175/1520-0493(2000)128<2634:etotco>2.0.co;2.

Harr, P. A., D. Anwender, and S. C. Jones, 2008: Predictability associated with the downstream impacts of the extratropical transition of tropical cyclones: Methodology and a case study of typhoon Nabi (2005). *Mon. Weather Rev.*, **136**, 3205–3225, https://doi.org/10.1175/2008MWR2248.1.

Hart, R. E., 2003: A Cyclone Phase Space Derived from Thermal Wind and Thermal Asymmetry. *Mon. Weather Rev.*, **131**, 585–616, https://doi.org/10.1175/1520-0493(2003)131<0585:ACPSDF>2.0.CO;2.

Hart, R. E., and J. L. Evans, 2001: A climatology of the extratropical transition of Atlantic tropical cyclones. *J. Clim.*, **14**, 546–564, https://doi.org/10.1175/1520-0442(2001)014<0546:ACOTET>2.0.CO;2.

Hart, R. E., J. L. Evans, and C. Evans, 2006: Synoptic composites of the extratropical transition life cycle of North Atlantic tropical cyclones: Factors determining posttransition evolution. *Mon. Weather Rev.*, **134**, 553–578, https://doi.org/10.1175/MWR3082.1.

Harvey, B. J., P. Cook, L. C. Shaffrey, and R. K. H. Schiemann, 2020: The Response of the Northern Hemisphere Storm Tracks and Jet Streams to Climate Change in the CMIP3 ,

CMIP5 , and CMIP6 Climate Models Journal of Geophysical Research : Atmospheres. *J. Geophys. Res. Atmos.*, **125**, 1–10, https://doi.org/10.1029/2020JD032701.

Hersbach, H., and Coauthors, 2020: The ERA5 global reanalysis. *Q. J. R. Meteorol. Soc.*, **146**, 1999–2049, https://doi.org/10.1002/qj.3803.

Hickney, K. R., and C. Connolly-Johnston, 2012: The Impact of Hurricane Debbie (1961) and Hurricane Charley (1986) on Ireland. *Adv. Hurric. Res. - Model. Meteorol. Prep. Impacts*, **1**, https://doi.org/10.5772/54039.

Hodges, K., A. Cobb, and P. L. Vidale, 2017: How well are tropical cyclones represented in reanalysis datasets? *J. Clim.*, **30**, 5243–5264, https://doi.org/10.1175/JCLI-D-16-0557.1.

Hodges, K. I., 1994: A general method for tracking analysis and its application to meteorological data. *Mon. Weather Rev.*, **122**, 2573–2586, https://doi.org/10.1175/1520-0493(1994)122<2573:AGMFTA>2.0.CO;2.

——, 1995: Feature Tracking on the Unit Sphere. *Mon. Weather Rev.*, **123**, 3458–3465, https://doi.org/10.1175/1520-0493(1995)123<3458:ftotus>2.0.co;2.

——, 1996: Spherical nonparametric estimators applied to the UGAMP model integration for AMIP. *Mon. Weather Rev.*, **124**, 2914–2932, https://doi.org/10.1175/1520-0493(1996)124<2914:SNEATT>2.0.CO;2.

——, 1999: Adaptive constraints for feature tracking. *Mon. Weather Rev.*, **127**, 1362–1373, https://doi.org/10.1175/1520-0493(1999)127<1362:acfft>2.0.co;2.

Hodges, K. I., and R. Emerton, 2015: The prediction of Northern Hemisphere tropical cyclone extended life cycles by the ECMWF ensemble and deterministic prediction systems. Part I: Tropical cyclone stage. *Mon. Weather Rev.*, **143**, 5091–5114, https://doi.org/10.1175/MWR-D-13-00385.1.

Hoskins, B. J., and P. J. Valdes, 1990: On the Existence of Storm-Tracks. *J. Atmos. Sci.*, **47**, 1854–1864, https://doi.org/https://doi.org/10.1175/1520-0469(1990)047<1854:OTEOST>2.0.CO;2.

J. B. Elsner, C. P. S., 1993: Improving Extended-Range Seasonal Predictions of Intense Atlantic Hurricane Activity. *Weather Forecast.*, **8**, 345–351, https://doi.org/10.1175/1520-0434(1993)008,0345: IERSPO.2.0.CO;2.

Jing, R., N. Lin, K. A. Emanuel, G. A. Vecchi, and T. R. Knutson, 2021: A Comparison of Tropical Cyclone Projections in a High-Resolution Global Climate Model and from Downscaling by Statistical and Statistical-Deterministic Methods. *J. Clim.*, **34**, 9349–9364, https://doi.org/10.1175/JCLI-D-21-0071.1.

Jones, S. C., and Coauthors, 2003: The extratropical transition of tropical cyclones: Forecast challenges, current understanding, and future directions. *Weather Forecast.*, **18**, 1052–1092, https://doi.org/10.1175/1520-0434(2003)018<1052:TETOTC>2.0.CO;2.

Jung, C., and G. M. Lackmann, 2019: Extratropical Transition of Hurricane Irene (2011) in a Changing Climate. *J. Clim.*, **32**, 4847–4871, https://doi.org/10.1175/jcli-d-18-0558.1.

——, and ——, 2021: The response of extratropical transition of tropical cyclones to climate change: Quasi-idealized numerical experiments. *J. Clim.*, **34**, 4361–4381, https://doi.org/10.1175/JCLI-D-20-0543.1.

Keller, J. H., 2017: Amplification of the downstream wave train during extratropical transition: Sensitivity studies. *Mon. Weather Rev.*, **145**, 1529–1548, https://doi.org/10.1175/MWR-D-16-0193.1.

——, and Coauthors, 2019: The extratropical transition of tropical cyclones. Part II: Interaction with the midlatitude flow, downstream impacts, and implications for predictability. *Mon. Weather Rev.*, **147**, 1077–1106, https://doi.org/10.1175/MWR-D-17-0329.1.

Kelly, P., L. R. Leung, K. Balaguru, W. Xu, B. Mapes, and B. Soden, 2018: Shape of Atlantic Tropical Cyclone Tracks and the Indian Monsoon. *Geophys. Res. Lett.*, **45**, 10,746-10,755, https://doi.org/10.1029/2018GL080098.

Klein, P. M., P. A. Harr, and R. L. Elsberry, 2000: Extratropical transition of western North Pacific tropical cyclones: An overview and conceptual model of the transformation stage. *Weather Forecast.*, **15**, 373–395, https://doi.org/10.1175/1520-0434(2000)015<0373:ETOWNP>2.0.CO;2.

Klein, P. M., P. A. Harr, and R. L. Elsberry, 2002: Extratropical transition of western North Pacific tropical cyclones: Midlatitude and tropical cyclone contributions to reintensification. *Mon. Weather Rev.*, **130**, 2240–2259, https://doi.org/10.1175/1520-0493(2002)130<2240:ETOWNP>2.0.CO;2.

Klotzbach, P., and Coauthors, 2019: Seasonal Tropical Cyclone Forecasting. *Trop. Cyclone Res. Rev.*, **8**, 134–149, https://doi.org/10.6057/2019TCRR03.03.

Klotzbach, P. J., 2007: Revised prediction of seasonal Atlantic basin tropical cyclone activity from 1 August. *Weather Forecast.*, **22**, 937–949, https://doi.org/10.1175/WAF1045.1.

——, 2010: On the Madden-Julian oscillation-atlantic hurricane relationship. *J. Clim.*, **23**, 282–293, https://doi.org/10.1175/2009JCLI2978.1.

——, 2014: Prediction of seasonal Atlantic basin accumulated cyclone energy from 1 July. *Weather Forecast.*, **29**, 115–121, https://doi.org/10.1175/WAF-D-13-00073.1.

Klotzbach, P. J., M. A. Saunders, G. D. Bell, and E. S. Blake, 2017: North Atlantic seasonal hurricane prediction: underlying science and an evaluation of statistical models. *Clim. Extrem. Patterns Mech. Geophys. Monogr.*, **226**, 315–328, https://doi.org/10.1002/9781119068020.

Knaff, J. A., 1997: Implications of summertime sea level pressure anomalies in the tropical Atlantic region. *J. Clim.*, **10**, 789–804, https://doi.org/10.1175/1520-0442(1997)010<0789:IOSSLP>2.0.CO;2.

Knapp, K. R., M. C. Kruk, D. H. Levinson, H. J. Diamond, and C. J. Neumann, 2010: The international best track archive for climate stewardship (IBTrACS). *Bull. Am. Meteorol. Soc.*, **91**, 363–376, https://doi.org/10.1175/2009BAMS2755.1.

Knutson, T., and Coauthors, 2019: Tropical cyclones and climate change assessment. Part II: Projected Response to Anthropogenic Warming. *Bull. Am. Meteorol. Soc.*, **100**, 1987–2007, https://doi.org/10.1175/BAMS-D-18-0189.1.

Knutson, T. R., and Coauthors, 2010: tropical cyclones and climate change. *Nat. Geosci.*, **3**, 157–163, https://doi.org/10.1038/ngeo779.

Kofron, D. E., E. A. Ritchie, and J. S. Tyo, 2010: Determination of a consistent time for the extratropical transition of tropical cyclones. Part I: Examination of existing methods for finding "ET Time." *Mon. Weather Rev.*, **138**, 4328–4343, https://doi.org/10.1175/2010MWR3180.1.

Kossin, J. P., S. J. Camargo, and M. Sitkowski, 2010: Climate modulation of north atlantic hurricane tracks. *J. Clim.*, **23**, 3057–3076, https://doi.org/10.1175/2010JCLI3497.1.

——, K. A. Emanuel, and G. A. Vecchi, 2014: The poleward migration of the location of tropical cyclone maximum intensity. *Nature*, **509**, 349–352, https://doi.org/10.1038/nature13278.

——, K. R. Knapp, T. L. Olander, and C. S. Velden, 2020: Global increase in major tropical cyclone exceedance probability over the past four decades. *Proc. Natl. Acad. Sci. U. S. A.*, **117**, https://doi.org/10.1073/pnas.2021573117.

Kozar, M. E., M. E. Mann, S. J. Camargo, J. P. Kossin, and J. L. Evans, 2012: Stratified statistical models of North Atlantic basin-wide and regional tropical cyclone counts. *J. Geophys. Res. Atmos.*, **117**, 1–13, https://doi.org/10.1029/2011JD017170.

Landsea, C. W., 1993: A CLimatology of Intense (or Major) Atlantic Hurricanes. *Mon. Weather Rev.*, **121**, 1703–1713, https://doi.org/https://doi.org/10.1175/1520-0493(1993)121%3C1703:ACOIMA%3E2.0.CO;2.

——, and J. L. Franklin, 2013: Atlantic hurricane database uncertainty and presentation of a new database format. *Mon. Weather Rev.*, **141**, 3576–3592, https://doi.org/10.1175/MWR-D-12-00254.1.

——, R. A. Pielke Jr., A. M. Mestas-Nunez, and J. A. Knaff, 1999: Atlantic Basin Hurricanes: Indices of Climatic Changes. *Clim. Change*, **42**, 89–129.

——, G. A. Vecchi, L. Bengtsson, and T. R. Knutson, 2010: Impact of duration thresholds on Atlantic tropical cyclone counts. *J. Clim.*, **23**, 2508–2519, https://doi.org/10.1175/2009JCLI3034.1.

Laurila, T. K., V. A. Sinclair, and H. Gregow, 2020: The Extratropical Transition of Hurricane Debby (1982) and the Subsequent Development of an Intense Windstorm over Finland. *Mon. Weather Rev.*, **148**, 377–401, https://doi.org/10.1175/mwr-d-19-0035.1.

Lawrence, M. B., 1996: Tropical Cyclone Report: Hurricane Lili.

Lee, C. Y., S. J. Camargo, F. Vitart, A. H. Sobel, J. Camp, S. Wang, M. K. Tippett, and Q. Yang, 2020: Subseasonal predictions of tropical cyclone occurrence and ace in the s2s dataset. *Weather Forecast.*, **35**, 921–938, https://doi.org/10.1175/WAF-D-19-0217.1.

Lee, R. W., S. J. Woolnough, A. J. Charlton-Perez, and F. Vitart, 2019: ENSO Modulation of MJO Teleconnections to the North Atlantic and Europe. *Geophys. Res. Lett.*, **46**, 13535–13545, https://doi.org/10.1029/2019GL084683.

Liu, M., G. A. Vecchi, J. A. Smith, and H. Murakami, 2017: The present-day simulation and twenty-first-century projection of the climatology of extratropical transition in the North Atlantic. *J. Clim.*, **30**, 2739–2756, https://doi.org/10.1175/JCLI-D-16-0352.1.

Liu, M., G. A. Vecchi, J. A. Smith, H. Murakami, R. Gudgel, and X. Yang, 2018: Towards Dynamical Seasonal Forecast of Extratropical Transition in the North Atlantic. *Geophys. Res. Lett.*, **45**, 12,602-12,609, https://doi.org/10.1029/2018GL079451.

——, L. Yang, J. A. Smith, and G. A. Vecchi, 2020: Response of Extreme Rainfall for Landfalling Tropical Cyclones Undergoing Extratropical Transition to Projected Climate Change: Hurricane Irene (2011). *Earth's Futur.*, **8**, 1–13, https://doi.org/10.1029/2019EF001360.

Longshore, D., 2008: *Encyclopedia of hurricanes, typhoons, and cyclones*. Second. Checkmark Publishing, 480 pp.

Manganello, J. V., and J. L. Kinter, 2021: Modulation of mid-Atlantic tropical cyclone landfalls by the Madden-Julian Oscillation. *Weather Clim. Extrem.*, **34**, 100387, https://doi.org/10.1016/j.wace.2021.100387.

——, and Coauthors, 2012: Tropical cyclone climatology in a 10-km global atmospheric GCM: Toward weather-resolving climate modeling. *J. Clim.*, **25**, 3867–3893, https://doi.org/10.1175/JCLI-D-11-00346.1.

McTaggart-Cowan, R., J. R. Gyakum, and M. K. Yau, 2001: Sensitivity testing of extratropical transitions using potential vorticity inversions to modify initial conditions: Hurricane earl case study. *Mon. Weather Rev.*, **129**, 1617–1636, https://doi.org/10.1175/1520-0493(2001)129<1617:STOETU>2.0.CO;2.

——, ——, and ——, 2003: The influence of the downstream state on extratropical transition: Hurricane Earl (1998) case study. *Mon. Weather Rev.*, **131**, 1910–1929, https://doi.org/10.1175//2589.1.

——, ——, and ——, 2004: The impact of tropical remnants on extratropical cyclogenesis: Case study of Hurricanes Danielle and Earl (1998). *Mon. Weather Rev.*, **132**, 1933–1951, https://doi.org/10.1175/1520-0493(2004)132<1933:TIOTRO>2.0.CO;2.

Menkes, C. E., M. Lengaigne, P. Marchesiello, N. C. Jourdain, E. M. Vincent, J. Lefèvre, F. Chauvin, and J. F. Royer, 2012: Comparison of tropical cyclogenesis indices on seasonal to interannual timescales. *Clim. Dyn.*, **38**, 301–321, https://doi.org/10.1007/s00382-

011-1126-x.

Met Éireann, 1961: Exceptional Weather Events - Hurricane Debbie, September 1961.

——, 1986: Exceptional Weather Events - Hurricane Charley, August 1986.

Michaelis, A. C., and G. M. Lackmann, 2019: Climatological changes in the extratropical transition of tropical cyclones in high-resolution global simulations. *J. Clim.*, **32**, 8733–8753, https://doi.org/10.1175/JCLI-D-19-0259.1.

Mizuta, R., and Coauthors, 2017: Over 5,000 years of ensemble future climate simulations by 60-km global and 20-km regional atmospheric models. *Bull. Am. Meteorol. Soc.*, **98**, 1383–1398, https://doi.org/10.1175/BAMS-D-16-0099.1.

Mokhov, I. I., E. M. Dobryshman, and M. E. Makarova, 2014: Transformation of tropical cyclones into extratropical: The tendencies of 1970-2012. *Dokl. Earth Sci.*, **454**, 59–63, https://doi.org/10.1134/S1028334X14010127.

Molod, A., L. Takacs, M. Suarez, and J. Bacmeister, 2015: Development of the GEOS-5 atmospheric general circulation model: Evolution from MERRA to MERRA2. *Geosci. Model Dev.*, **8**, 1339–1356, https://doi.org/10.5194/gmd-8-1339-2015.

Moore, P., 2021: An analysis of storm Ophelia which struck Ireland on 16 October 2017. *Weather*, **76**, 301–306, https://doi.org/10.1002/wea.3978.

Murakami, H., 2014: Tropical cyclones in reanalysis data sets. *Geophys. Res. Lett.*, **41**, 2133–2141, https://doi.org/https://doi.org/10.1002/2014GL059519.

——, and Coauthors, 2016a: Seasonal forecasts of major hurricanes and landfalling tropical cyclones using a high-resolution GFDL coupled climate model. *J. Clim.*, **29**, 7977–7989, https://doi.org/10.1175/JCLI-D-16-0233.1.

——, G. Villarini, G. A. Vecchi, W. Zhang, and R. Gudgel, 2016b: Statistical-dynamical seasonal forecast of north atlantic and U.S. landfalling tropical cyclones using the high-resolution GFDL FLOR coupled model. *Mon. Weather Rev.*, **144**, 2101–2123, https://doi.org/10.1175/MWR-D-15-0308.1.

Pak, G., and Coauthors, 2021: Korea Institute of Ocean Science and Technology Earth System Model and Its Simulation Characteristics. *Ocean Sci. J.*, **56**, 18–45, https://doi.org/10.1007/s12601-021-00001-7.

Palmén, E., 1958: Vertical Circulation and Release of Kinetic Energy during the Development of Hurricane Hazel into an Extratropical Storm. *Tellus*, **10**, 1–13, https://doi.org/10.3402/tellusa.v10i1.9222.

Pantillon, F., J. P. Chaboureau, and E. Richard, 2015: Remote impact of North Atlantic hurricanes on the Mediterranean during episodes of intense rainfall in autumn 2012. *Q. J. R. Meteorol. Soc.*, **141**, 967–978, https://doi.org/10.1002/qj.2419.

——, ——, and ——, 2016: Vortex–vortex interaction between Hurricane Nadine (2012) and an Atlantic cut-off dropping the predictability over the Mediterranean. *Q. J. R. Meteorol. Soc.*, **142**, 419–432, https://doi.org/10.1002/qj.2635.

Pantillon, F. P., J. P. Chaboureau -Pierre, P. J. Mascart, and C. Lac, 2013: Predictability of a mediterranean tropical-like storm downstream of the extratropical transition of Hurricane Helene (2006). *Mon. Weather Rev.*, **141**, 1943–1962, https://doi.org/10.1175/MWR-D-12-00164.1.

Pohorsky, R., M. Röthlisberger, C. M. Grams, J. Riboldi, and O. Martius, 2019: The climatological impact of recurving North Atlantic tropical cyclones on downstream extreme precipitation events. *Mon. Weather Rev.*, **147**, 1513–1532, https://doi.org/10.1175/MWR-D-18-0195.1.

Priestley, M. D. K., and J. L. Catto, 2022: Future changes in the extratropical storm tracks and cyclone intensity, wind speed, and structure. *Weather Clim. Dyn.*, **3**, 337–360, https://doi.org/https://doi.org/10.5194/wcd-3-337-2022.

Quinting, J. F., and S. C. Jones, 2016: On the impact of tropical cyclones on Rossby wave packets: A climatological perspective. *Mon. Weather Rev.*, **144**, 2021–2048, https://doi.org/10.1175/MWR-D-14-00298.1.

——, M. M. Bell, P. A. Harr, and S. C. Jones, 2014: Structural characteristics of T-PARC typhoon sinlaku during its extratropical transition. *Mon. Weather Rev.*, **142**, 1945–1961, https://doi.org/10.1175/MWR-D-13-00306.1.

Rantanen, M., J. Räisänen, V. A. Sinclair, J. Lento, and H. Järvinen, 2020: The extratropical transition of Hurricane Ophelia (2017) as diagnosed with a generalized omega equation and vorticity equation. *Tellus, Ser. A Dyn. Meteorol. Oceanogr.*, **72**, 1–26, https://doi.org/10.1080/16000870.2020.1721215.

Rappaport, E. N., and Coauthors, 2009: Advances and challenges at the national hurricane center. *Weather Forecast.*, **24**, 395–419, https://doi.org/10.1175/2008WAF2222128.1.

Rathman, N. M., S. Yang, and E. Kaas, 2014: Tropical cyclones in enhanced resolution CMIP5 experiments. *Clim. Dyn.*, **42**, 665–681, https://doi.org/10.1007/s00382-013-1818-5.

Riboldi, J., M. Röthlisberger, and C. M. Grams, 2018: Rossby wave initiation by recurving tropical cyclones in the western North Pacific. *Mon. Weather Rev.*, **146**, 1283–1301, https://doi.org/10.1175/MWR-D-17-0219.1.

——, C. M. Grams, M. Riemer, and H. M. Archambault, 2019: A phase locking perspective on Rossby wave amplification and atmospheric blocking downstream of recurving western North Pacific tropical cyclones. *Mon. Weather Rev.*, **147**, 567–589, https://doi.org/10.1175/MWR-D-18-0271.1.

Riemer, M., and S. C. Jones, 2010: The downstream impact of tropical cyclones on a developing baroclinic wave in idealized scenarios of extratropical transition. *Q. J. R. Meteorol. Soc.*, **136**, 617–637, https://doi.org/10.1002/qj.605.

——, and ——, 2014: Interaction of a tropical cyclone with a high-amplitude, midlatitude wave pattern: Waviness analysis, trough deformation and track bifurcation. *Q. J. R. Meteorol. Soc.*, **140**, 1362–1376, https://doi.org/10.1002/qj.2221.

——, ——, and C. A. Davis, 2008: The impact of extratropical transition on the downstream flow: An idealized modelling studywith a straight jet. *Q. J. R. Meteorol. Soc.*, **134**, 69–91, https://doi.org/10.1002/qj.189.

Ritchie, E. A., and R. L. Elsberry, 2001: Simulations of the transformation stage of the extratropical transition of tropical cyclones. *Mon. Weather Rev.*, **129**, 1462–1480, https://doi.org/10.1175/1520-0493(2001)129<1462:SOTTSO>2.0.CO;2.

Roberts, M. J., and Coauthors, 2015: Tropical cyclones in the UPSCALE ensemble of high-resolution global climate models. *J. Clim.*, **28**, 574–596, https://doi.org/10.1175/JCLI-D-14-00131.1.

Roberts, M. J., and Coauthors, 2020a: Projected Future Changes in Tropical Cyclones Using the CMIP6 HighResMIP Multimodel Ensemble. *Geophys. Res. Lett.*, **47**, 1–12, https://doi.org/10.1029/2020GL088662.

——, and Coauthors, 2020b: Impact of model resolution on tropical cyclone simulation using

the HighResMIP-PRIMAVERA multimodel ensemble. *J. Clim.*, **33**, 2557–2583, https://doi.org/10.1175/JCLI-D-19-0639.1.

Russell, J. O., A. Aiyyer, J. D. White, and W. Hannah, 2017: Revisiting the connection between African Easterly Waves and Atlantic tropical cyclogenesis. *Geophys. Res. Lett.*, **44**, 587–595, https://doi.org/10.1002/2016GL071236.

Sainsbury, E. M., R. K. H. Schiemann, K. I. Hodges, L. C. Shaffrey, A. J. Baker, and K. T. Bhatia, 2020: How Important Are Post-Tropical Cyclones for European Windstorm Risk? *Geophys. Res. Lett.*, **47**, https://doi.org/10.1029/2020GL089853.

——, R. K. H. Schiemann, K. I. Hodges, A. J. Baker, L. C. Shaffrey, and K. T. Bhatia, 2022a: What Governs the Interannual Variability of Recurving North Atlantic Tropical Cyclones? *J. Clim.*, **35**, 3627–3641, https://doi.org/10.1175/jcli-d-21-0712.1.

——, R. K. H. Schiemann, K. I. Hodges, A. J. Baker, L. C. Shaffrey, and K. T. Bhatia, 2022b: Why do some Post-Tropical Cyclones impact Europe ? *Mon. Weather Rev.*,.

——, R. K. H. Schiemann, K. I. Hodges, A. J. Baker, L. C. Shaffrey, K. T. Bhatia, and S. Bourdin, 2022c: Can low-resolution CMIP6 ScenarioMIP models provide insight into future European Post-Tropical Cyclone risk ? *Weather Clim. Dyn.*, https://doi.org/https://doi.org/10.5194/wcd-2022-46.

Sardeshmukh, P. D., and B. J. Hoskins, 1984: Spatial Smoothing on the Sphere. *Mon. Weather Rev.*, **112**, 2524–2529, https://doi.org/https://doi.org/10.1175/1520-0493(1984)112<2524:SSOTS>2.0.CO;2.

Sarro, G., and C. Evans, 2022: An Updated Investigation of Post-Transformation Intensity, Structural, and Durational Extremes for Extratropically Transitioning North Atlantic Tropical Cyclones. *Mon. Weather Rev.*, https://doi.org/https://doi.org/10.1175/MWR-D-22-0088.1.

Saunders, M. A., P. J. Klotzbach, and A. S. R. Lea, 2017: Replicating annual North Atlantic hurricane activity 1878-2012 from environmental variables. *J. Geophys. Res.*, **122**, 6284–6297, https://doi.org/10.1002/2017JD026492.

Seager, R., M. Cane, N. Henderson, D. E. Lee, R. Abernathey, and H. Zhang, 2019: Strengthening tropical Pacific zonal sea surface temperature gradient consistent with rising greenhouse gases. *Nat. Clim. Chang.*, **9**, 517–522,

https://doi.org/10.1038/s41558-019-0505-x.

Semmler, T., S. Varghese, R. McGrath, P. Nolan, S. Wang, P. Lynch, and C. O'Dowd, 2008a: Regional climate model simulations of North Atlantic cyclones: Frequency and intensity changes. *Clim. Res.*, **36**, 1–16, https://doi.org/10.3354/cr00732.

——, ——, ——, ——, ——, ——, and ——, 2008b: Regional model simulation of North Atlantic cyclones: Present climate and idealized response to increased sea surface temperature. *J. Geophys. Res. Atmos.*, **113**, 1–16, https://doi.org/10.1029/2006JD008213.

Shapiro, M. A.; Keyser, D., 1990: Fronts, jet streams and the tropopause. 167–191.

Smart, D., and E. Graham, 2021: Downscaling the ERA5 reanalysis for ' Hurricane ' Debbie (1961): evidence of both cold-conveyor belt and sting jets. *Weather*, **76**, 292–294, https://doi.org/10.1002/wea.4057.

Stewart, S., 2012: Tropical Cyclone Report: Hurricane Katia (AL122011). **1**, 20.

Stewart, S. R., 2018: Tropical Cyclone Report: Hurricane Ophelia. 1–32, https://doi.org/AL142016.

Studholme, J., K. I. Hodges, and C. M. Brierley, 2015: Objective determination of the extratropical transition of tropical cyclones in the Northern Hemisphere. *Tellus, Ser. A Dyn. Meteorol. Oceanogr.*, **67**, https://doi.org/10.3402/tellusa.v67.24474.

——, A. V. Fedorov, S. K. Gulev, K. Emanuel, and K. Hodges, 2022: Poleward expansion of tropical cyclone latitudes in warming climates. *Nat. Geosci.*, **15**, 14–28, https://doi.org/10.1038/s41561-021-00859-1.

Sugi, M., A. Noda, and N. Sato, 2002: Influence of the global warming on tropical cyclone climatology an experiment with the JMA global model. *J. Meteorol. Soc. Japan*, **80**, 249–272, https://doi.org/10.2151/jmsj.80.249.

——, Y. Yamada, K. Yoshida, R. Mizuta, M. Nakano, C. Kodama, and M. Satoh, 2020: Future Changes in the Global Frequency of Tropical Cyclone Seeds. *Sci. Online Lett. Atmos.*, **16**, 70–74, https://doi.org/10.2151/sola.2020-012.

Tatebe, H., and Coauthors, 2018: Description and basic evaluation of simulated mean state, internal variability, and climate sensitivity in MIROC6. *Geosci. Model Dev.*, 1–92,

https://doi.org/10.5194/gmd-2018-155.

Thorncroft, C., and S. C. Jones, 2000: The extratropical transitions of Hurricanes Felix and Iris in 1995. *Mon. Weather Rev.*, **128**, 947–972, https://doi.org/10.1175/1520-0493(2000)128<0947:TETOHF>2.0.CO;2.

Thorncroft, C., and K. Hodges, 2001: African easterly wave variability and its relationship to Atlantic tropical cyclone activity. *J. Clim.*, **14**, 1166–1179, https://doi.org/10.1175/1520-0442(2001)014<1166:AEWVAI>2.0.CO;2.

Ting, M., S. J. Camargo, C. Li, and Y. Kushnir, 2015: Natural and Forced North Atlantic Hurricane Potential Intensity Change in CMIP5 Models*. *J. Clim.*, **28**, 3926–3942, https://doi.org/10.1175/jcli-d-14-00520.1.

Torn, R. D., and G. J. Hakim, 2015: Comparison of wave packets associated with extratropical transition and winter cyclones. *Mon. Weather Rev.*, **143**, 1782–1803, https://doi.org/10.1175/MWR-D-14-00006.1.

Ullrich, P. A., C. M. Zarzycki, E. E. McClenny, M. C. Pinheiro, A. M. Stansfield, and K. A. Reed, 2021: TempestExtremes v2.1: A community framework for feature detection, tracking, and analysis in large datasets. *Geosci. Model Dev.*, **14**, 5023–5048, https://doi.org/10.5194/gmd-14-5023-2021.

Varlas, G., A. Papadopoulos, and P. Katsafados, 2019: An analysis of the synoptic and dynamical characteristics of hurricane Sandy (2012). *Meteorol. Atmos. Phys.*, **131**, 443–453, https://doi.org/10.1007/s00703-017-0577-y.

Vecchi, G. A., M. Zhao, H. Wang, G. Villarini, A. Rosati, A. Kumar, I. M. Held, and R. Gudgel, 2011: Statistical-dynamical predictions of seasonal North Atlantic hurricane activity. *Mon. Weather Rev.*, **139**, 1070–1082, https://doi.org/10.1175/2010MWR3499.1.

Vecchi, G. A., and Coauthors, 2014: On the seasonal forecasting of regional tropical cyclone activity. *J. Clim.*, **27**, 7994–8016, https://doi.org/10.1175/JCLI-D-14-00158.1.

Vecchi, G. A., and Coauthors, 2019: Tropical cyclone sensitivities to CO2 doubling: roles of atmospheric resolution, synoptic variability and background climate changes. *Clim. Dyn.*, **53**, 5999–6033, https://doi.org/10.1007/s00382-019-04913-y.

——, C. Landsea, W. Zhang, G. Villarini, and T. Knutson, 2021: Changes in Atlantic major hurricane frequency since the late-19th century. *Nat. Commun.*, **12**, 1–9,

https://doi.org/10.1038/s41467-021-24268-5.

Vidale, P. L., and Coauthors, 2021: Impact of stochastic physics and model resolution on the simulation of Tropical Cyclones in climate GCMs. *J. Clim.*, 1–85, https://doi.org/10.1175/jcli-d-20-0507.1.

Villarini, G., and G. A. Vecchi, 2012: Twenty-first-century projections of North Atlantic tropical storms from CMIP5 models. *Nat. Clim. Chang.*, **2**, 604–607, https://doi.org/10.1038/nclimate1530.

Voldoire, A., and Coauthors, 2019: Evaluation of CMIP6 DECK Experiments With CNRM-CM6-1. *J. Adv. Model. Earth Syst.*, **11**, 2177–2213, https://doi.org/10.1029/2019MS001683.

Walsh, K., S. J. Camargo, T. R. Knutson, J. P. Kossin, T.-C. Lee, H. Murakami, and C. M. Patricola, 2019: Tropical cyclones and climate change. *Trop. Cyclone Res. Rev.*, **8**, 240–250, https://doi.org/10.1016/j.tcrr.2020.01.004.

Walsh, K. J. E., and Coauthors, 2015: Hurricanes and climate: The U.S. Clivar working group on hurricanes. *Bull. Am. Meteorol. Soc.*, **96**, 997–1017, https://doi.org/10.1175/BAMS-D-13-00242.1.

Wang, B., X. Li, and L. Wu, 1997: Direction of hurricane beta drift in horizontally sheared flows. *J. Atmos. Sci.*, **54**, 1462–1471, https://doi.org/10.1175/1520-0469(1997)054<1462:DOHBDI>2.0.CO;2.

Wang, B., Y. Wang, and L. Wu, 1998: Dynamics in tropical cyclone motion : A review. *Chinese J. Atmos. Sci.*, **22**.

Wheeler, D., R. García-Herrera, J. M. Vaquero, M. Chenoweth, and C. J. Mock, 2009: Reconstructing the trajectory of the August 1680 hurricane from contemporary records. *Bull. Am. Meteorol. Soc.*, **90**, 971–978, https://doi.org/10.1175/2009BAMS2649.1.

Wilks, D. S., 2016: "The Stippling Shows Statistically Significant Grid Points." *Bull. Am. Meteorol. Soc.*, **97**, 2263–2274.

Wood, K. M., and E. A. Ritchie, 2014: A 40-year climatology of extratropical transition in the Eastern North Pacific. *J. Clim.*, **27**, 5999–6015, https://doi.org/10.1175/JCLI-D-13-00645.1.

Yamada, Y., and Coauthors, 2021: Evaluation of the contribution of tropical cyclone seeds to

changes in tropical cyclone frequency due to global warming in high-resolution multi-model ensemble simulations. *Prog. Earth Planet. Sci.*, **8**.

Yang, W., T.-L. Hsieh, and G. A. Vecchi, 2021: Hurricane annual cycle controlled by both seeds and genesis probability. *Proc. Natl. Acad. Sci. U. S. A.*, **118**, 1–5, https://doi.org/10.1073/pnas.2108397118/-/DCSupplemental.y.

Zappa, G., L. C. Shaffrey, K. I. Hodges, P. G. Sansom, and D. B. Stephenson, 2013: A multimodel assessment of future projections of north atlantic and european extratropical cyclones in the CMIP5 climate models. *J. Clim.*, **26**, 5846–5862, https://doi.org/10.1175/JCLI-D-12-00573.1.

Zarzycki, C. M., D. R. Thatcher, and C. Joblonowski, 2017: Objective Tropical Cyclone Extratropical Transition Detection in High-Resolution Reanalysis and Climate Model data. *J. Adv. Model. Earth Syst.*, **9**, 130–148, https://doi.org/https://doi.org/10.1002/2016MS000775.